43328 1613

OSM

OFFICE OF SURFACE MINING

RECLAMATION AND ENFORCEMENT

TECHNICAL REPORT/1994

INVESTIGATION OF DAMAGE TO STRUCTURES IN THE McCUTCHANVILLE-DAYLIGHT AREA OF SOUTHWESTERN INDIANA

Volume 3 of 3

Part VII: Experimental and Analytical Studies of the Vibration Response of Residential Structures Due to Surface Mine Blasting.

Part VIII: Dynamic Soil Property Testing and Analysis of Soil Properties, Daylight and McCutchanville, Indiana.

Part IX: Environmental Conditions Related to Geology, Soils, and Precipitation, McCutchanville and Daylight, Vanderburgh County, Indiana.

US Department of Interior
Office of Surface Mining
Reclamation and Enforcement

Kenneth K. Eltschlager
Mining/Explosives Engineer
3 Parkway Center
Pittsburgh, PA 15220

Phone 412.937.2169
Fax 412.937.3012
Keltschl@osmre.gov

U.S. Department of the Interior

Office of Surface Mining Reclamation and Enforcement

Part VII

Experimental and Analytical Studies of the Vibration Response of Residential Structures Due to Surface Mine Blasting.

DEPARTMENT OF THE ARMY
WATERWAYS EXPERIMENT STATION, CORPS OF ENGINEERS
3909 HALLS FERRY ROAD
VICKSBURG, MISSISSIPPI 39180-6199

REPLY TO
ATTENTION OF

May 12, 1994

Structural Mechanics Division
Structures Laboratory

Mr. Peter Michael (COTR)
U.S. Department of the Interior
Office of Surface Mining
Reclamation and Enforcement
Ten Parkway Center
Pittsburgh, Pennsylvania 15220

Dear Mr. Michael:

Reference draft report, U.S. Army Engineer Waterways Experiment Station, dated January 1994, Subject: "Experimental and Analytical Studies of the Vibration Response of Residential Structures Due to Surface Mine Blasting." Included are changes and additional comments to Figure 4.23, prepared under the Interagency Agreement No. EF68-IA91-13796, "Field and Laboratory Evaluation of Potential Causative Factors of Structural Damages in Daylight/McCutchanville, IN."

A replacement figure (enclosure 1) is provided for Figures 22 and 4.23 of Parts I and VII, respectively, of the Draft Final Report on Indiana Blasting Investigation. Added to the figure were the results for 2- and 5-percent damping response and the linear predictions for the three cases (undamped, 2 percent, and 5 percent). Also, the labeling for the middle critical tensile strain (CTS) line was corrected to "Max computed CTS from Figure 2.22 for Concrete Masonry Units."

The 2- and 5-percent damping results were obtained by:

a. Computing the linear-elastic response spectrum for the N-S component of the 10 April 1992 event (enclosure 2) recorded at the free-field location near the one-story study house. Shown in enclosure 3 is the linear-elastic response spectrum.

b. Computing the ratios of the 2- and 5-percent response spectra to the undamped response spectrum. These ratios are the fractions of reduction. Enclosure 4 shows the response reductions in percentages.

Questions were asked about the constraints and the response of the linear-elastic finite-element (FE) model of a part of a

free-standing brick wall. Motions were applied to the base of the FE model and were constrained to the plane of the model. Therefore, the response of the wall was that of a shear wall. The model assumes homogeneity of the linear-elastic material for the brick wall model. As described in the draft report, this is a reasonable conservative model which will provide upper bound results. There are several refinements one could make to the model for future efforts: account for tie stiffnesses normal to the plane of the brick wall veneer, contact with soffit, and attachment around windows and doors; an extension to a three-dimensional model as a separate shell surrounding the structural framing with all the previous details; plan validation tests; and incorporate nonlinear effects.

The conclusions drawn from Figure 4.23 or Figure 22 are changed as follows: Realistic damping values for houses are between 2 and 5 percent. The value of 2 percent is a realistic upper bound and reduces the undamped results by 66 percent. For this damping value, the model predicts strain values in the brick veneer to exceed 5.8 millionths for ground velocities of 0.4 in./sec and greater. The strain of 5.8 millionths is a design value and represents the lowest value at which the material tensile capacity may be exceeded. These predicted values are less than the peak strains reported by Stagg et al (1984), as shown in enclosure 1. As stated in the report, some peak strains occurred across cracks and may represent displacements of the wall and not material strains. These peak strains exceed the upper bound of tensile capacity of mortar of a brick veneer wall, thus, indicating tensile failure of the material. Therefore, based on the results of a simple conservative analysis and the reported data, one cannot rule out the possibility of having structural responses which exceed the tensile capacity of the mortar in a brick veneer wall.

For comments, questions, or additional information, please contact me at telephone No. (601) 634-2714.

Sincerely,

Vincent P. Chiarito

Vincent P. Chiarito
Research Structural Engineer

Enclosures

Copy Furnished:

Dr. Paul F. Hadala

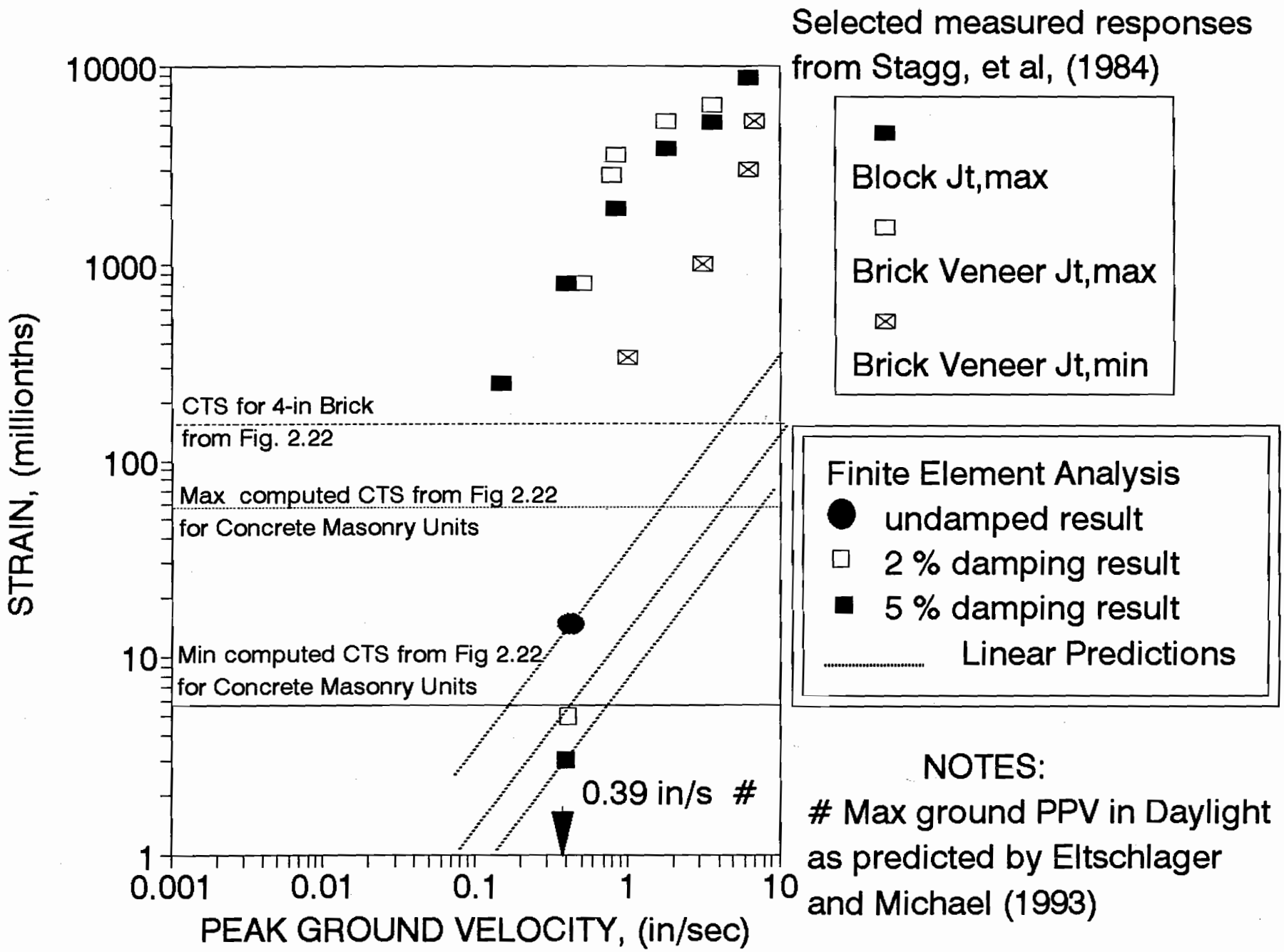
Selected measured responses
from Stagg, et al, (1984)
Block Jt,max
Brick Veneer Jt,max
Brick Veneer Jt,min
10000
1000
100
10
1
STRAIN, (millionths)
CTS for 4-in Brick
from Fig. 2.22
Max computed CTS from Fig 2.22
for Concrete Masonry Units
Min computed CTS from Fig 2.22
for Concrete Masonry Units
0.39 in/s #
0.001
0.01
0.1
1
10
PEAK GROUND VELOCITY, (in/sec)
Finite Element Analysis
undamped result
2 % damping result
5 % damping result
Linear Predictions
NOTES:
Max ground PPV in Daylight
as predicted by Eltschlager
and Michael (1993)

10 April 1992 Event, N-S component

Free-Field location at One-Story Study House

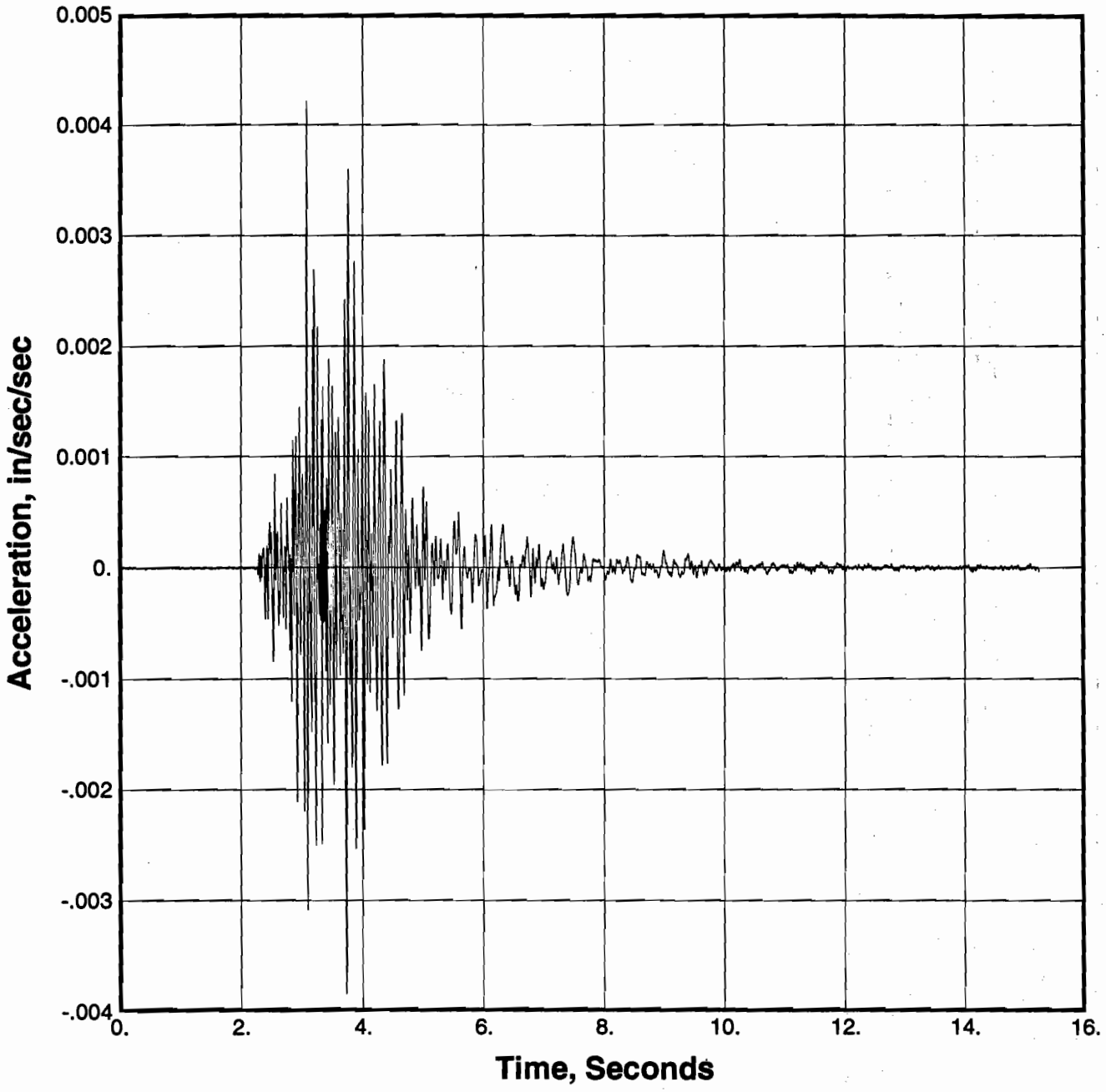

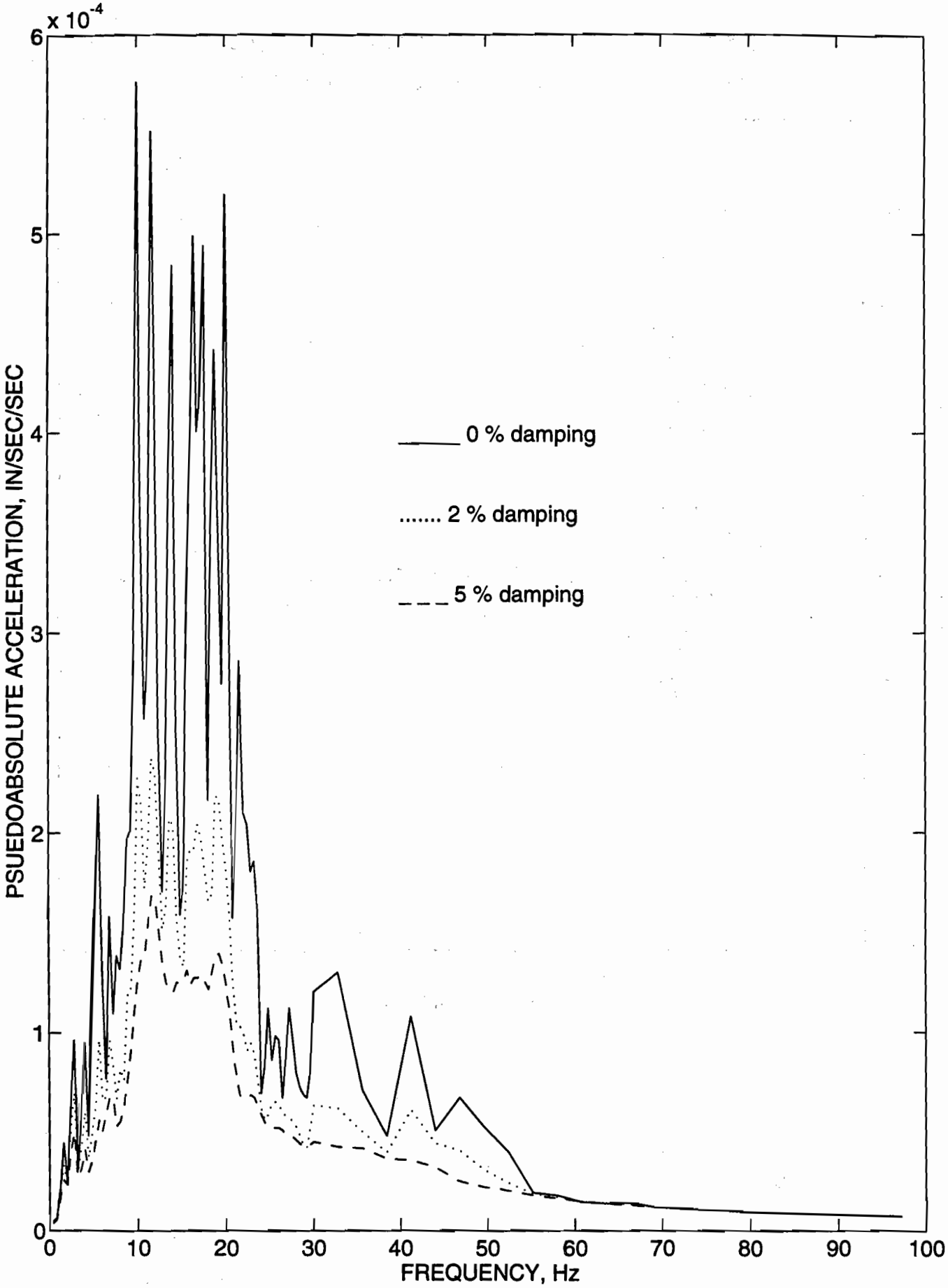
x 10^-4
6
5
4
3
2
1
0
PSUEDOABSOLUTE ACCELERATION, IN/SEC/SEC
0 % damping
2 % damping
5 % damping
0
10
20
30
40
50
60
70
80
90
100
FREQUENCY, Hz

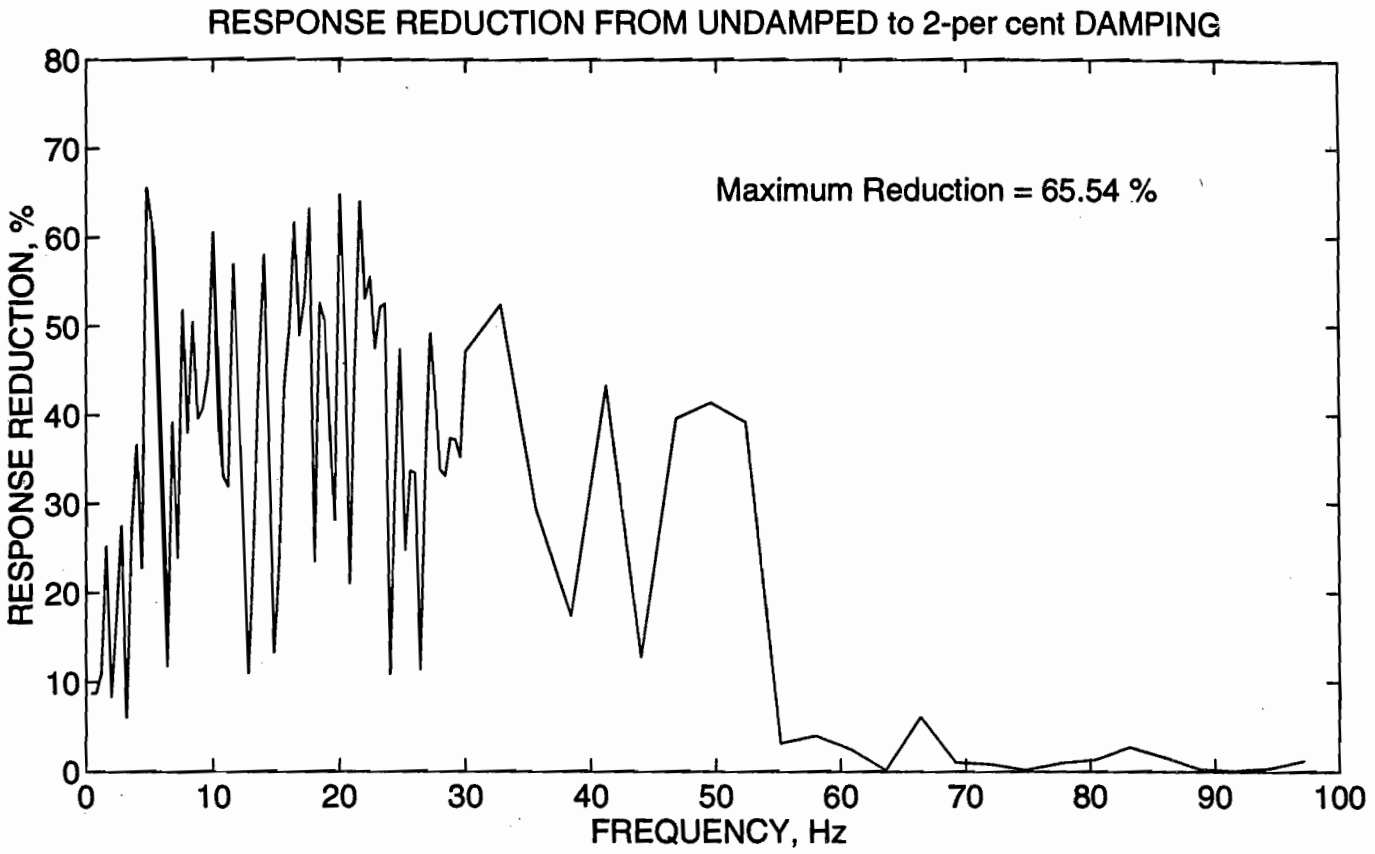
RESPONSE REDUCTION FROM UNDAMPED to 2-per cent DAMPING
Maximum Reduction = 65.54 %
RESPONSE REDUCTION, %
FREQUENCY, Hz
0
10
20
30
40
50
60
70
80
90
100

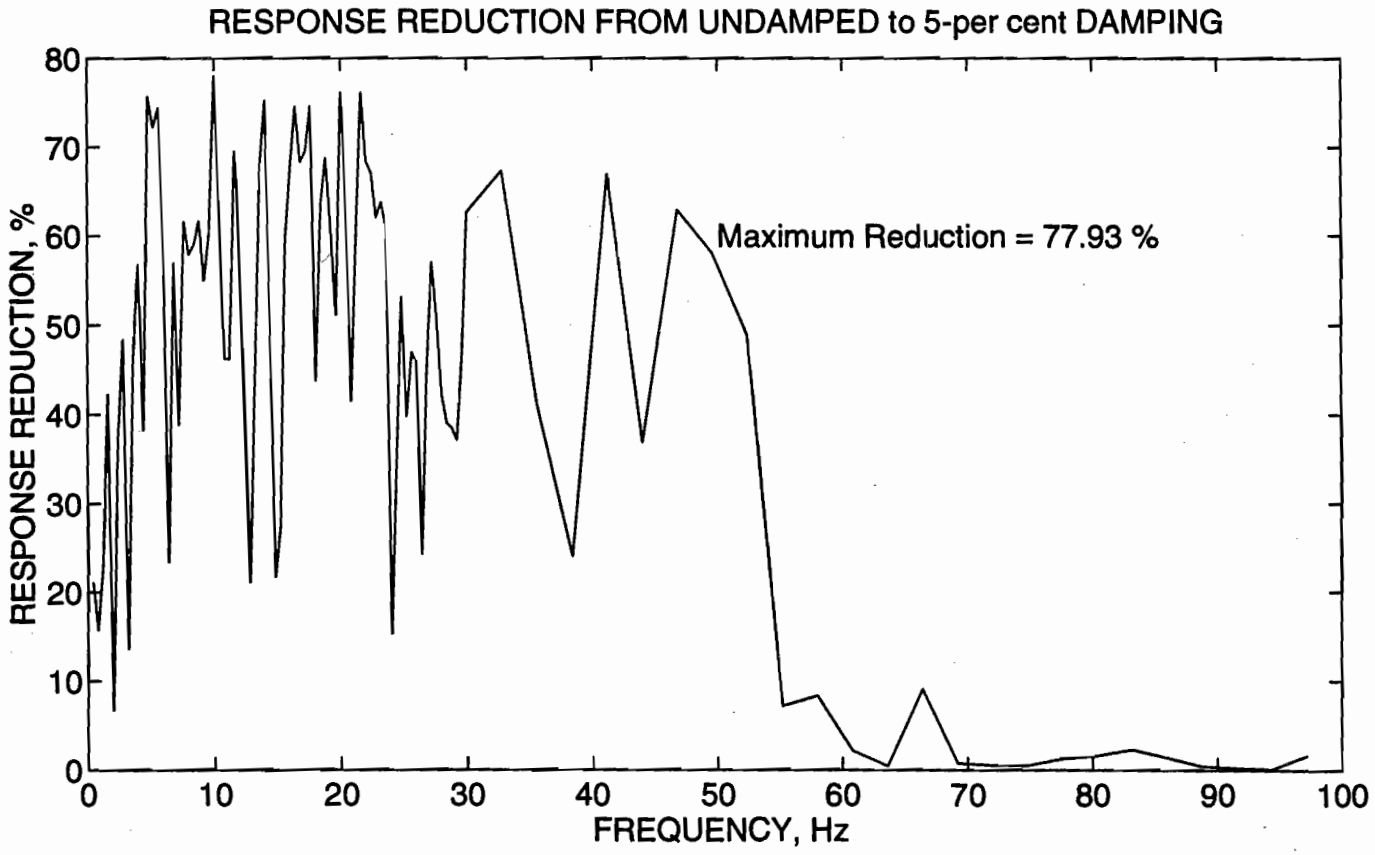
RESPONSE REDUCTION FROM UNDAMPED to 5-per cent DAMPING
Maximum Reduction = 77.93 %
RESPONSE REDUCTION, %
FREQUENCY, Hz
0
10
20
30
40
50
60
70
80
90
100

THE OFFICE OF SURFACE MINING RECLAMATION AND ENFORCEMENT CONSIDERS THIS DOCUMENT FINAL UNDER THE TERMS OF THE INTERAGENCY AGREEMENT EF68IA91-13796. AS OF THIS PRINTING, THE DOCUMENT HAS NOT BEEN PUBLISHED BY THE U.S. ARMY CORPS OF ENGINEERS, WATERWAYS EXPERIMENT STATION AND, THEREFORE, IS STILL LISTED AS "DRAFT" ON THE COVER SHEET (FOLLOWING PAGE).

DRAFT

TECHNICAL REPORT SL-93-

EXPERIMENTAL AND ANALYTICAL STUDIES OF THE VIBRATION RESPONSE OF RESIDENTIAL STRUCTURES DUE TO SURFACE MINE BLASTING

By

Vincent P. Chiarito and Robert L. Hall, PhD

DEPARTMENT OF THE ARMY
Waterways Experiment Station, Corps of Engineers
PO Box 631, Vicksburg, Mississipi 39180-0631

January 1994

Approved for public release; distribution is unlimited.

Prepared for The Office of Surface Mining
Reclamation and Enforcement
U.S. Department of the Interior

DRAFT

CONTENTS

PREFACE

The field experimental and numerical modeling studies of the vibrations of residential structures due to explosive detonations to support surface mining were conducted during the period October 1991 through August 1992 for the U.S. Department of the Interior, Office of Surface Mining, under Interagency Agreement EF68-IA91-13796, "Field and Laboratory Evaluation of Potential Causative Factors of Structural Damages in Daylight/McCutchanville, IN". The Contracting Officer's Technical Representative was Mr. Peter Michael.

The experimental and numerical studies were planned and conducted by the Structures Laboratory (SL) at the U.S. Army Engineer Waterways Experiment Station (WES) under the direct supervision of Mr. Vincent P. Chiarito, Structural Mechanics Division (SMD). Mr. Steve Shore, SMD, SL, assisted with planning, supervising, and performing the initial field investigations from October to December 1991. Dr. Cary Cox, Instrumentation Services Division (ISD), provided data acquisition and data reduction/management support for all aspects of the field investigations. Dr. Cox also authored Appendix B. Mr. Joe Ables, ISD, was the senior electronics technician responsible for operation of the data acquisition system, shaker tests, and assisting with the development of the remote data acquisition system during the period 12 March through 15 April 1992. Mr. Michael Goodwin, ISD, assisted Mr. Ables with the data acquisition. Messrs. Ables' and Goodwin's efforts are greatly appreciated. Mr. Robert E. Walker, Applied Research Associates Vicksburg, MS, was under contract to WES from December 1991 through August 1992 for technical consultation concerning various aspects of the vibration tests, data acquisition, and data analyses. Mr. Tommy Bevins, Ms. Sharon Garner, and Dr. Mostafiz Chowdhury (SMD) conducted the finite-element analyses. Mses. Vicky H. Smith and Jennifer Bennett (SMD)

assisted with report preparation of tables, contents, and figures. Drs. Robert L. Hall (Chief, Structural Analysis Group (SAG), SMD) and Sammy A. Kiger, (West Virginia University) provided valuable assistance and many technical discussions concerning various aspects of the project.

Dynamic soil property tests and related soils analyses conducted by WES under this Interagency Agreement were accomplished by Drs. Paul F. Hadala and Richard W. Peterson of the Geotechnical Laboratory, WES. Their work is documented in a separate report entitled "Dynamic Soil Property Testing and Analysis of Soil Properties - Daylight and McCutchanville, Indiana," dated January 1993.

The project was under the supervision of Mr. Bryant Mather, Director, SL; Mr. J. T. Ballard, Assistant Director, SL; Dr. Jimmy P. Balsara, Chief, SMD; Dr. Hall, Chief, SAG, SMD. Acknowledged are all others whose help was extremely important to the success of the experimental study during the test.

At the time of publication of this report, Director of WES was Dr. Robert W. Whalin. Commander and Deputy Director was COL Bruce K. Howard.

EXPERIMENTAL AND ANALYTICAL STUDIES OF THE VIBRATION RESPONSE OF RESIDENTIAL STRUCTURES DUE TO SURFACE MINE BLASTING

CHAPTER 1: INTRODUCTION

1. This report documents experimental and analytical studies on the effects of vibration response of residential structures due to surface mine blasting. This chapter describes the background of the problem, lists the objectives, and describes the scope of efforts reported in each chapter.

Background

2. The U.S. Department of Interior, Office of Surface Mining Reclamation and Enforcement (OSM) received a request from the Indiana Department of Natural Resources (IDNR) to investigate claims of damage to buildings due to blasting conducted for surface mining operations. Residents of Daylight and McCutchanville (near Evansville), Vanderburgh County, Indiana, reported these claims. Acting through its Eastern Support Center, OSM supported investigations to study the potential of vibrations from the Ayrshire Mine (owned by the AMAX Coal Company) to cause damages to residential structures in the Daylight and McCutchanville area. The study area included Daylight, McCutchanville, and a control area that was assumed unaffected by any surface mining operations. A vicinity map shows Vanderburgh County and Evansville in the State of Indiana in Figure 1.1[1].

3. In 1973, the AMAX Coal Company began mining operations in Warrick County (the neighboring county to the east). The Ayrshire Mine progressed from the eastern boundary of the permit

---

[1]All figures are presented in order after the text of each chapter.

to within 3.5 miles (5.6 km) east of McCutchanville and 2 miles (3.2 km) east of Daylight. In March of 1988, cast blasting was initiated, and since that date complaints have increased. The Ayrshire Mine is the focal point of blasting complaints in the study area. Figure 1.2 shows the mine blast locations in the vicinity of Daylight and McCutchanville, IN. The area labeled "AMAX COAL CO." is the Ayrshire Mine east of McCutchanville and Daylight. The unnumbered symbols represent locations of blasts from 1988 through 1992. The numbered symbols (small solid triangles) represent locations of compliance monitoring stations. Approximately 10 percent of the residents, at distances of 1.5 to 7 miles (2.4 to 11.2 km) from the Ayrshire Mine, claim damages to their homes were caused by blasting. Significant and widespread occurrences of structural damage in the study area were documented.

4. The U.S. Bureau of Mines (USBM) (Siskind et al. 1990) investigated seven homes near Evansville, IN, from November 1989 to January 1990, monitoring the effects of vibration and airblast from nearby surface mining. They conducted pre- and post-blast crack inspections along with measuring ground vibrations, airblasts, and dynamic structural response due to blasting and other sources such as nearby aircraft operations and human activity within the homes. Also, the USBM quantified settlement of the foundation and subsidence of the embankment through level loop surveys. These results, along with a year's worth of state and coal company historical data, were analyzed to determine if measurements recorded in the seven study homes were consistent with past studies which provided regulatory criteria. Measured vibration levels at these seven homes were significantly below the regulatory limit. None of the blasts during this study produced significant changes in the 45 inspection areas within the study homes. The USBM concluded that structural damage in the homes was probably due to movements in the local expansive clay or other mechanisms resulting from drainage and slope conditions.

5. To address issues identified by in-house and interagency reviews of OSM investigations up to and including the USBM study, an Interagency Agreement between OSM and the U.S. Army Engineer Waterways Experiment (WES) was established. Pertinent details of this agreement, "Field and Laboratory Evaluation of Potential Causative Factors of Structural Damages in Daylight/ McCutchanville, IN," Contract No. EF68IA91-13796, are presented in Appendix A.

6. Personnel from the WES, USBM, and the U.S. Geological Survey (USGS) conducted a preliminary field reconnaissance and review of pertinent available information in February 1991 (Chiarito 1991). From this study a number of experimental, analytical, and computational tasks were defined to address the issues referred to in Paragraph 5. A one-story and a two-story house were selected for testing and analysis.

Objectives

7. This study addresses and resolves these issues:

a. Are there ground vibrations at very low frequencies (down to 0.5 Hz) that are capable of causing structural damage?

b. Do airblasts produce adverse structural response in the study area?

c. Certain types of structural damages, observed by some investigators, appear to have been caused by lateral forces. If so, what are the relative contributions of blast-induced ground vibrations/airblasts, earthquakes, and wind to this force?

d. Can observed damage be ascribed to fatigue induced by the repetitive exposure of structures to ground vibrations and/or airblasts?

e. Do alternative mechanisms (inadequate foundations, slope/soil movement) contribute to the observed damages?

Scope

8. To address the issues stated previously in the objectives, WES planned and conducted a comprehensive experimental and analytical investigation. In addition to WES, USBM and USGS participated in various aspects of this study. The general approach for the investigation was to conduct forced-vibration tests on a one-story and a two-story house located in the study area. From these tests, dynamic response characteristics such as natural frequencies, vibrating deflection shapes at natural frequencies (normal modes), and structural damping were determined. Also, vibration tests were used to develop, refine, and validate the finite-element models used in the structural analyses of the study houses. Next, the structural responses of the study houses were monitored along with free-field ground motion and airblast pressure during times when mine blasting operations were in progress. Ground motions recorded during mine blasting were used as forcing functions to drive the finite-element models of the study houses. Maximum stresses from the dynamic structural analyses were compared with accepted structural damage criteria.

9. Differential foundation settlements required to cause cracking in basement floor slabs were predicted from static analyses. Also, total earth pressures and vertical house loads were applied to basement walls to determine resulting stresses and the potential for cracking. Finally, the potential for fatigue damage was investigated based on comparing the cyclic characteristics and duration of measured structural motions and relevant historical case histories of fatigue studies. Specific tasks accomplished in this study in order of presentation in this report are:

a. Chapter 2: Field tests procedures, equipment, instrumentation, and measurements are discussed in this section.

The reasons for and importance of field tests measurements are presented along with the concept for selecting one-story and two-story study houses.

b. Chapter 3: Static structural analyses are used to predict vertical wall loads on footings and the resulting settlements are determined based on recommended procedures presented by Hadala (1993). These foundation settlements are then compared to levels of differential settlement which should cause cracking in a yield-line pattern in basement floor slabs. Next, basement walls are analyzed for lateral loads resulting from total earth pressures and loads resulting from the house structure. The analyses provide some information about levels of stress on the house due to lateral loads on basement walls and settlement of the foundation.

c. Chapter 4: Dynamic finite-element analyses are conducted for the one-story and two-story houses subjected to maximum ground motions and airblasts due to surface mine blasting. Maximum stress levels in critical structural components of the houses are compared to relevant damage criteria. Damage levels are classified according to Table 1.1 (Dowding, 1985) which lists the description for threshold, minor, and major damage classifications. These three classifications are used throughout this report when describing observed or potential damage as resulting from each aspect of this study. Threshold damage, as further discussed in this report, also includes exceedence of the tensile capacity of a material. This may not necessarily result in a visible crack.

d. Chapter 5: The potential for damage due to fatigue is discussed in this section. Measured stress levels, frequency, and duration along with free field ground motion are evaluated based on a fatigue criteron. Field test results are compared to results from historical case histories.

e. Chapter 6: Conclusions relating to threshold, minor, or major structural damage from fatigue, low frequency response,

airblast, lateral vibratory loads, and alternate damage mechanisms are presented in this section.

Table 1.1
Comparison of Damage Classification in Probabilistic Study (Dowding 1985)

Description	Study	Uniform Classification
Loosening of paint Small plaster cracks at joints between construction elements Lengthening of old cracks	Threshold Dvorak (1962) Edwards and Northwood 1960) Northwood et al. (1963) Minor Thoenen and Windes (1942)	Threshold
Loosening and falling of plaster Cracks in masonry around openings near partitions Hairline to 3-mm (0-1/8 in.) cracks Fall of loose mortar	Minor Dvorak (1962) Edwards and Northwood (1960) Northwood et al. (1963) Jensen and Rietman (1978) Langfors et al. (1958) Major Thoenen and Windes (1942)	Minor
Cracks of several millimeters in walls Rupture of opening vaults Structural weakening Fall of masonry (e.g. chimneys) Load support ability affected	Major Dvorak (1962) Edwards and Northwood (1960) Northwood et al. (1963) Langfors et al. (1958)	Major

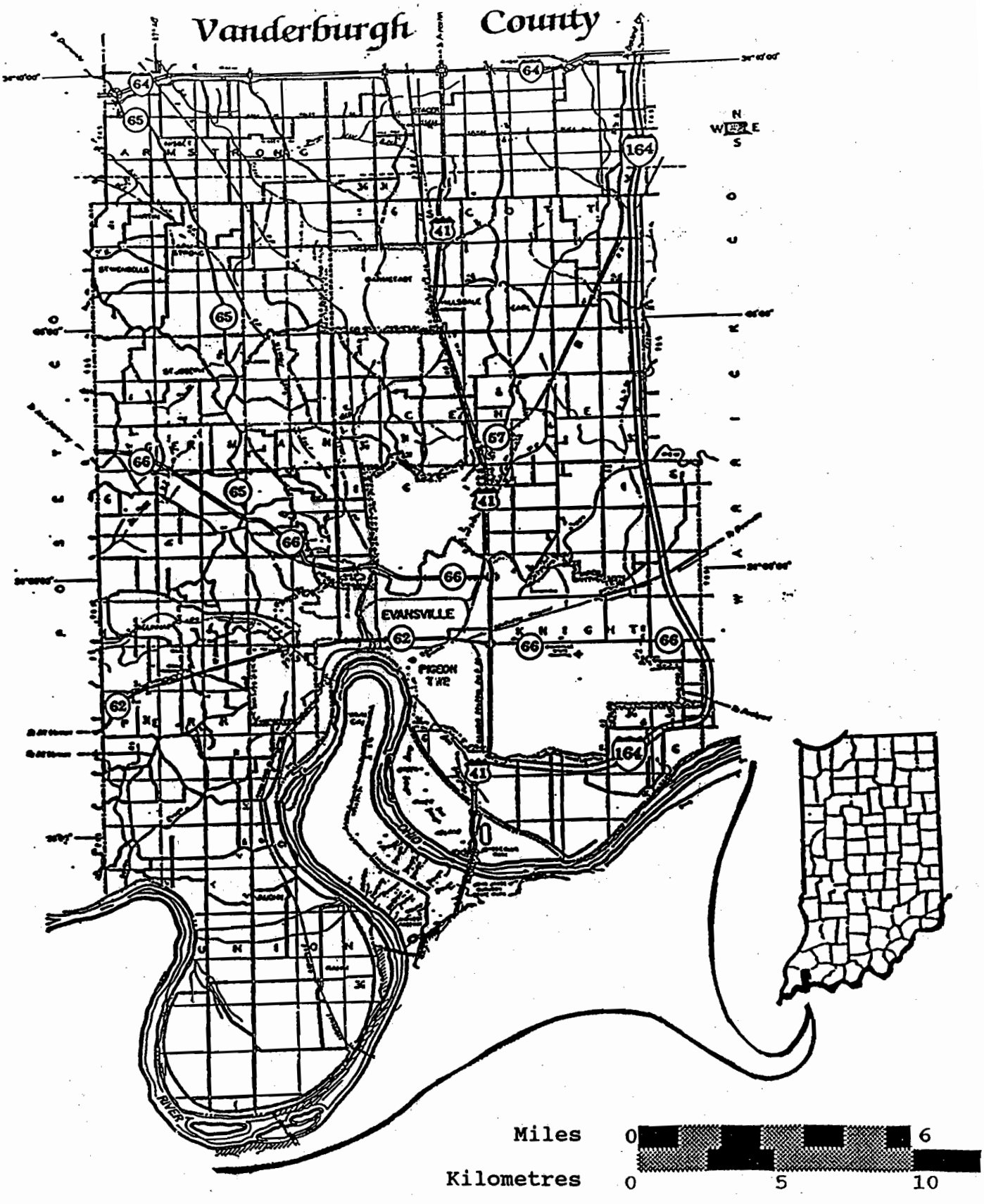

Figure 1.1 Vicinity map showing Vanderburgh County and Evansville, IN

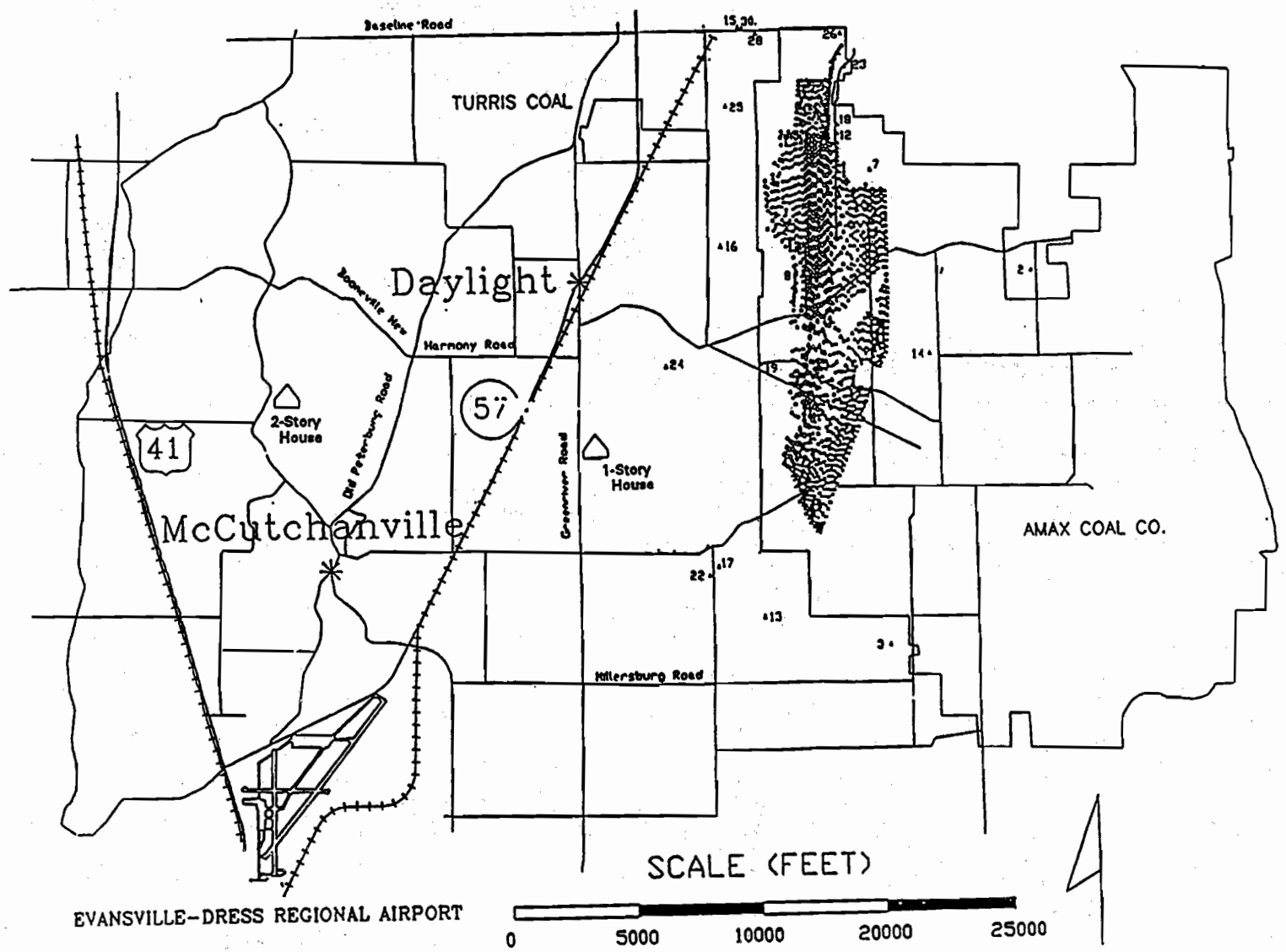

Figure 1.2. Study area, mine blast locations (1988-1992), and compliance monitoring stations

CHAPTER 2: FIELD TESTS

General

10. Field tests were conducted to record actual data for evaluating ground motion and airblast effects on house responses. Ground motion data were recorded using seismic accelerometers with flat frequency response down to 0.5 Hz. Dynamic responses of one- and two-story houses were recorded from a broad range of loading conditions including: blast events, wind, overhead aircraft, and controlled forced excitations. Airblast measurements were recorded at the one-story house for correlation with house responses. Prior to field mobilization, a rehearsal house near WES was used to check out procedures and calibrate equipment and data acquisition systems.

11. Initially, to gather field data, two house sites were visited during 2 weeks from 1 December to 12 December 1991, and vibration responses were monitored during anticipated blast events. Only two blast events were recorded in this time, but many more samples were subsequently obtained using a remote instrumentation system during the 5 weeks from 12 March to 15 April 1993.

Test Procedure

12. To properly prepare for the field tests, a vacant house in Vicksburg, MS, was used to check out the experimental procedures. This house was a one-story, wood-frame, brick veneer structure. The test house was made available for 2 weeks in November 1991 through the City of Vicksburg, MS. The excitation and data recording systems were evaluated by placing accelerometers on the house and recording vibrations due to various excitations.

13. Modal tests using an electrodynamic inertial mass exciter (shaker) were allowed by owners of the one-story study

house in Daylight, IN, to identify overall and component dynamic properties of the structure. Modal testing using a shaker was not allowed on the two-story house in McCutchanville, IN. These data were recorded to determine energy levels of frequency vibrations down to 0.5 Hz and interrelationships between exterior dynamic loadings at frequencies from 0.5 to 50 Hz and structural responses. The measurements involved an instrumentation setup with 14 channels of data acquisition from 2 pressure gages and 12 accelerometers. The pressure gages were mounted so at least one airblast measurement was obtained at the house and another at the location of the free-field ground motion station.

14. Forced-vibration studies are used to determine dynamic properties describing the vibration modes of the structures and structural systems. This type of testing has been used quite extensively for modal testing and system analysis and identification, and in many earthquake engineering studies (e.g. Clough and Penzien 1975, Newmark and Hall 1970, Bendat and Piersol 1980, Chiarito and Fagerburg 1988, Duron 1987, Duron and Hall 1988, Ewins 1984).

15. Passive or ambient types of vibration are caused by wind, minor earthquake motions, or any other naturally occurring or unintentional energy sources. A blast event is considered an ambient event because no direct electronic measurement of ground acceleration or other characteristics of energy input to the ground are recorded at the source. To obtain accurate ambient vibration response data, a very large number of ensembles (averages) in the frequency domain are required. Thus, it was planned to measure as many separate and independent blast responses of the study houses as possible. Normal (Guassian) statistical distribution of the random vibration response is assumed and, therefore, more ensembles reduce the random error of the measured amplitude response. Ambient response data are useful for checking consistency of forced vibration results among different excitation methods. Damping values were estimated

using the Half-Power (Bandwidth) Method (Bendat and Piersol 1980).

16. In addition to the measurements obtained in December 1991, a remote instrumentation setup was used from 12 March to 15 April 1992. All vibrations were recorded in a range from 0.5 to 50 Hz. A summary of all blast events that occurred during this study is given in Table 2.1, and the free-field peak-particle velocities that were recorded during several blast events are given in Table 2.2.

17. During the modal testing the frequency response functions (FRF) from input-output excitation-response relationship of a house system are measured. The FRF is defined by the processed Fourier transforms of the output divided by the processed Fourier transform of the input. Modal analysis extracts the system information from these measured FRFs. This system information includes the parameters defining the modes of vibration.

18. A mathematical formulation of the modes of vibration in the Laplace domain can be completely defined by the transfer function. The details of this mathematical formulation can be found in several references (e.g. see Ewins 1984, Bendat and Piersol 1980, Harris and Crede 1976, Paz 1985, or the technical notes by Hewlett Packard).

19. Estimates based on the formula 0.1 x N (see UBC code, 1989), where N = number of stories, indicate that the first natural periods of one-story and two-story buildings are, respectively, 0.1 and 0.2 sec (corresponding to frequencies of 10 and 5 cycles per sec (Hz)) (UBC CODE 1989, Clough and Penzien 1975, Newmark and Rosenblueth 1971, and Paz 1985). Thus, an excitation for modal tests was planned to cover the frequency range from at least 1 Hz to 25 Hz during modal tests.

Test Equipment

20. The setup for conducting the nondestructive tests

included input excitations, seismic accelerometers for response measurements (output), signal conditioning, and data acquisition. The excitations were provided by three inputs: a shaker, an instrumented hammer, and blast events.

21. While the input excitation was recorded during forced-vibration tests, it was necessary to record, simultaneously, the response of the one-story house at strategic locations. For this study, seismic accelerometers with built-in amplifiers were used. These are very sensitive accelerometers with a useful frequency range covering 0.3 to 100 Hz, with maximum sensitivities ranging from 100 to 1,000 volts per g (1 g equals 9.8 metres per second per second (m/s^2)). Several measurement locations on the house were required to describe adequately at least the first three flexural modes and the first torsional mode. Figure 2.1 shows a schematic of the approximate locations for measuring the responses of the study houses. Accelerometers were placed at a total of 10 locations. The accelerometers were primarily oriented to monitor the horizontal response motions of the houses during ambient or forced vibrations. From 30 March through 15 April at the one-story house, vertical response measurements were monitored at two of these locations.

22. The vibration instrumentation and recording system consisted of a data acquisition system analog-to-digital converter installed in an IBM-compatible 386, 25-MHz portable computer. Signal conditioning included continuous variable gain amplifiers, tracking filters and anti-alias filters. Acquisition of additional data was provided by a portable two-channel FFT analyzer. The software, MATLAB, was used to process the stored time domain data. MATLAB has numerical and graphical tools to manipulate matrices, perform frequency analysis, plot graphs, or use many other mathematical functions (The MathWorks, Inc. 1990). More details and a diagram of the data acquisition and reduction system are included in Appendix B.

23. Impact or transient input methods were used to obtain

information on house response characteristics. Typically, an instrumented hammer ranging from a few ounces (grams) to several pounds (kilograms) is used to strike a structure. A variety of impact tips (such as soft rubber and hard plastic) can be attached to control the length of the forced pulse applied to the structure. The softer the impact tip, the longer the force pulse and the more input energy is concentrated to the lower frequency response. The number of repeated "hammer" hits required depends on the energy needed to excite the responses of interest.

One-Story House

24. The one-story house selected for this study is located in Daylight as shown in Figure 1.2 and was included as part of a previous investigation (Chiarito 1991). The one-story house has a wood frame with brick veneer. The house is rectangular in plan (Figures 2.2 through 2.5) and is approximately 16 years old. The long direction of the house is approximately perpendicular to the advancing mine (parallel to the pit). This house has a full dugout basement except beneath the garage and part of the kitchen. The basement walls are unreinforced masonry blocks (UMB) and are founded on concrete footings. It is not known whether the footings or the basement floor slab are reinforced. The owners have reported that tables, the floor, and hanging lights have shaken, and the garage doors and window screens have rattled during specific blasts. The owners reported that they have felt effects of the blasts since the early 1980's. Dust generated from the mining activities was noticed by the owners near the house after several blasts. The house is approximately 1-1/2 miles (2.4 km) from the existing pit.

25. Damage observed included visible cracks near all the corners of the house in the brick veneer, diagonal cracks near windows and door openings and staircase-type cracks in the interior UMB basement walls. The owners reported the increase of "nail pops" from 280 in June 1989 to over 959 as of February

1991. Not all of the nail pops completely broke the surface or pulled out of the wallboard. Some nail pops were observed as cracks formed in the plaster coatings over the wallboard nail heads.

26. During the December 1991 field tests (Figure 2.6), the biaxial accelerations and horizontal responses at each corner were measured at the attic floor level (or ceiling level of the main floor). However, free-field measurements were not attempted during the December efforts. Response of the house was recorded due to one blast event of 7 December 1991, at approximately 1010 hours CST. This blast event was a cast blast (Pattern 271).

27. While preparing for the blast events, many other ambient responses were recorded. Table 2.3 lists test data other than blast events recorded at the one-story house.

28. Because of the lack of blast data and missing data during the first series of shaker tests, additional shaker tests were performed and instrumentation layouts (Figure 2.7 through 2.11) were selected for remote, long-term measurements of ambient responses over a period of approximately 5 weeks (from 12 March to 15 April 1992). Also, recordings of as many blasts and other ambient responses as possible were attempted. Airblast was measured near the house and at the free-field location.

29. During the remote recording period, data from 18 blast events (Table 2.2) were recorded.

Two-Story House

30. The two-story house (Figure 2.12) selected for this study is located in McCutchanville as shown in Figure 1.2. The two-story house is a wood-frame structure with brick veneer from the first floor to the second floor ceiling. The age of the house is unknown. In plan, the house is rectangular with a two-car garage. There was no visible exterior damage observed but a few visible cracks on interior walls and brick near the fireplace were observed. Figures 2.13 through 2.15 show the dimensions of

the house. Figure 2.16 shows the instrumentation layout. Typical instrumentation located in the attic and second floor of the house along with the data acquisition system are shown in Figures 2.17-2.19. Table 2.4 lists all of the recorded tests on the two-story house. Detailed house plans were not available, so all dimensions and construction details had to be estimated or measured on site.

31. During the December 1991 field tests the response of the house was recorded during one blast event of 6 December 1991, at approximately 1022 hours CST. Free-field measurements were not made. Airblast measurements were attempted but not obtained.

Field Tests Results

32. Results from the field tests were generally of good quality and are contained in Appendix C. The Appendix is subdivided into five parts. Part 1 consists of typical free-field and one-story house acceleration-time and frequency histories and spectrum from conventional blast. Part 2 is typical data for cast blast. Conventional and cast blasts are identified by pattern Numbers 101 and 121, and 252 and 271, respectively, in Table 2.1. Peak particle velocities (PPV) of measured structural response at the one-story house ranged from 0.005 to 0.05 in./sec. The PPV of measured structural response for the only blast event monitored at the two-story house was 0.01 in./sec. Part 3 is the airblast measured at distant (free-field) and near locations to the one-story house for conventional blast. The data show airblast arrival at 7 to 10 seconds after the arrival of the ground motion. Peak airblast pressures measured were less than 1×10^{-3} psi. Peak pressures measured from wind were the same order of magnitude. Parts 4 and 5 are frequency plots of averages of 9 and 20 shots, respectively. The nine ensembles used for the analysis presented in Part 4 are from the nine conventional blast events (pattern Type 121) between

27 March and 14 April, inclusively (refer to Tables 2.1 and 2.2). The 20 ensembles of Part 5 include all blast events listed in Table 2.2 (which include the nine ensembles of Part 4). The transfer function gives the amplification factors by averaging the ratios of the vibration responses measured at locations on the house to the ground vibrations measured at the free-field locations. The amplication factors ranged from 2 to 6. By averaging the results of several blast events, random errors of the amplitude estimates of the amplification factors are reduced. Parts 6 and 7 contain forced vibration test data for the one-story house and hammer test data for the two-story house. First natural frequencies from these data were 7.5 Hz and 6.0 Hz for the one- and two-story house, respectively.

33. Amplification factors are approximately 1.0 below 4Hz. These results show that low-frequency ground vibrations below 4 Hz produce no amplified responses in the houses. Above 4 Hz the houses begin to show some amplification of ground motion. The largest, or more significant, amplifications occur at frequency ranges from 7 to 15 Hz. There are isolated cases where amplifications occur above 15 Hz. Therefore, at ground vibrations below 4 Hz, the houses tend to respond as rigid bodies moving with the ground and developing no internal stresses due to relative dynamic movements.

34. The measured acceleration shown in Figure 2.20 is for the gages shown in Figure 2.9 which were located above and below the first floor, where cracks were observed in other houses in the study area. This figure shows the phase relationship between the two accelerometers. The data indicate an in-phase relationship although there is amplification up the wall. Because there is no significant out-of-phase relative motion there is no discernable relative movement across the potential crack area.

Comparisons to Previous Field Tests and Data

35. Data from previous field tests have been documented by Stagg et al. (1984) and Dowding (1985). Figures 2.21 and 2.22 summarize the relationship between peak ground motions to material strains. Critical tensile strain levels are shown for wallboard, plaster, and masonry block joints. The lower range of ground motion includes values recorded during this study; values lower than 0.01 in./sec were measured.

36. Figure 2.21 shows selected maximum values of strain versus peak ground velocity for wallboard and plaster, and wallboard tape joint for the test house reported in Stagg et al. (1984). The frequency content of the specific data points shown in Figures 2.21 and 2.22 are not known. However, spectra are shown in Stagg et al. (1984) for two specific shots at various locations in their test house. The spectra by Stagg et al. appear comparable to the estimated autospectral density function shown in Appendix C. The symbols "+" and "x" are measured values of maximum strain for wallboard and plaster, and wallboard tape joint, respectively. The data shown by the "+" symbols include responses measured at locations on wallboard or on plaster on wallboard. It is not noted, however, by Stagg et al. (1984) which data are for wallboard or plaster. The data show that the maximum measured strain of the wallboard tape joint has about the same maximum response as the wallboard and plaster on wallboard. The symbol "-" denotes selected measured values of minimum strain for both materials.

37. Critical tensile strain (CTS) levels are indicated for wallboard and plaster on wallboard; (all values taken from Siskind et al. (1980) and Stagg et al. (1984)). The CTS levels represent the strain threshold for when the material strength is exceeded for static tensile loads. The CTS levels due to static loads are conservative and may be increased for dynamic loads because of strain rate enhancements. It was noted by Stagg et al. (1984) that the kitchen-living room area was coated with a

3/16-in. veneer plaster. The CTS for wallboard is higher than the CTS for plaster as seen in Figure 2.21. Because of the relatively thin coating, one expects that the maximum strain measured on the plaster to approximately equal the maximum strain measured on the wallboard at the same location. The plaster CTS level was derived by tests on plaster beams. In Figure 2.21 comparisons indicate that the maximum strain responses of wallboard, wallboard joints, and plaster on wallboard are less than all the CTS levels at 0.39 in./sec and below. Therefore, one would not expect to see evidence of threshold damage for wallboard, wallboard joints, or plaster on wallboard if the peak ground velocities were less than 2.0 in./sec.

38. Figure 2.22 shows maximum values of strain versus peak ground velocity for block joint and brick veneer joint for the test house reported in Stagg et al. (1984). The solid and open box symbols are selected maximum values of strain response for the block and brick veneer joint, respectively. These maximum values were selected from Figures 35 and 36 found in the report by Stagg et al. (1984). The description of these data does not indicate levels of damage, but simply presents maximum response strains versus maximum ground velocities. Stagg et al. (1984) reported that in brick or block walls visible cracking occurred after measuring displacements from 0.01 mm to 0.1 mm, which corresponds to strains of 770 μin./in. to 7,700 μin./in. across joint widths of 13 mm. Cracks generally occur in the mortar joints and, therefore, decrease strains and increase damping resulting in the bricks and block not cracking. In the notes footnoted by "*" the range marked indicates the upper range of ground motions reported by Siskind, Crum, and Plis (1990).

39. The range of computed critical tensile strain values for UMB joints was computed from the range of allowable flexural tension stresses and the modulus of elasticity for 1500- and 2000-psi concrete masonry units (ACI 530-88/ASCE 5-88). Typical values for the modulus of elasticity for types N and M or S mortars for 1500- and 2000-psi strength units are presented in

Table 2.5. These values represent an estimate of what materials were used to construct the houses in McCutchanville and Daylight. The two values shaded in Table 2.5 are the lower and upper bound values chosen for the modulus of elasticity of concrete masonry block units. Table 2.6 lists allowable flexural tension (in psi) values for concrete masonry for portland cement/lime, and masonry cement and air entrained portland cement/lime mortar. These values were excerpted from Table 6.3.1.1 of ACI 530-88/ASCE 5-88. The values range from 14 to 82 psi.

40. To compute a range of CTS for concrete masonry units the values in Table 2.6 are divided by the lowest and the highest value from Table 2.5 (in the shaded cells). Table 2.7 presents the resulting range of computed critical tensile strains for concrete masonry units shown in Figure 2.22. The two shaded cells of Table 2.7 show the range of computed CTS of the material as 6.4 to 54.7 millionths (or 6.4×10^{-6} to 54.7×10^{-6} in./in.). These CTS levels using ACI values are conservative since they were developed to be used for design and they contain some inherent factor of safety. As with the plaster, the values are for static loads and may be increased for dynamic loads. To justify these higher levels the material would have to be tested at strain rates resulting from measured ground motions. In Figure 2.22 the comparisons indicate that the maximum strain response block and brick veneer joints exceed all the CTS levels at 0.39 in./sec. Therefore, one could expect to see evidence of threshold damage of block and veneer joints somewhere (not necessarily everywhere) if the peak ground velocities equalled or exceeded 0.13 in./sec. This level of threshold damage would not affect the ultimate load-carrying capacity of the wall.

41. During communications with Siskind and Stagg (1994) it was revealed that some data in Figures 33-37 from Stagg et al (1984) - aka RI 8896 - were measured strains across prexisting cracks. Thus, the strain measurements reported include material

strains combined with displacements of the crack openings. Since the minimum critical tensile strains reported in Figure 2.22 are for the material only, Siskind and Stagg think that their data should not be used in these comparisons. If Siskind's and Stagg's experiment had been conducted on a completely uncracked wall, their strain measurements would only contain material strains and would directly compare to strains based on elastic material properties. The fact that cracks existed in Siskind's and Stagg's experiments is consistent with Figure 2.22 which indicates all their reported peak data are above the critical tensile strain limits. The data reported by Stagg et al. (1984), from which the maximum values were selected, contain much scatter. The lower bounds for peak ground velocity less than 1 in. per second is almost zero. It is important to note that the maximum values reported in Figure 2.22 display a consistent relationship between strains and peak ground velocity. This consistent relationship would allow an engineer to make meaningful interpretation of brick or block wall response for peak ground velocities between about .3 to 8 in./sec. which includes peak ground motions important for this study.

42. Figure 2.23 shows the fitted line of measured PPV versus strain of a 9-in.-thick concrete wall (the PPV and strains were measured at the center of the wall (Crawford and Ward 1965)). In Figure 2.23 this is compared to a critical response point computed by Dowding (1985) and the static critical tensile strain computed from the modulus of rupture and the initial elastic modulus for 3000-psi strength concrete.

43. According to Dowding (1985) at least 5.9 in./sec of material response (through wave propagation) is required for cracking to occur of plain concrete beams subjected to hammer impacts in the tests he discusses. This would correspond to threshold damage. The line fitted by Crawford and Ward indicates no threshold damage observed until the velocity of the concrete wall reached 10 in./sec. The static CTS level is reasonably close to the strains required to cause threshold damage in

concrete. Thus, one would not expect any evidence of threshold damage in concrete unless the material response exceeded 5.9 in./sec.

44. Since concrete is used mostly just for slabs and footings in house construction and is in contact with the ground, the PPV of slabs and footings could approximate the maximum ground velocity. Then, one would not expect to see evidence of threshold damage in concrete at peak ground velocities of 0.39 in./sec or less.

45. Table 2.8 summarizes the CTS for materials of concern for this study.

46. Street et al. (1988) reported peak ground velocities from the June 10, 1987, Illinois earthquake to be .44 in./sec. These peak ground velocities are greater than any maximum ground velocity measured in Daylight or McCutchanville or the maximum peak velocity predicted by Eltschlager and Michael (1993).

Table 2.1
Summary of All Blast Events During WES Field Study

Date	Time	Pattern	PF	TOTLB	Burden	Spacing	HOLEDEP	HOLES
12-03-91	1440	271	1.13	108990	21	23	71	76
12-06-91	1022	271	1.08	129240	21	26	77	77
12-07-91	1011	271	1.29	115990	22	22	65	77
03-12-92	1305	121	0.24	6120	30	30	32	24
03-13-92	1120	251	0.90	48152	21	22	53	59
03-14-92	1124	251	1.19	48285	20	22	64	39
03-14-92	1140	251	1.21	25740	20	22	65	20
03-16-92	1058	501	0.67	26550	15	15	16	295
03-18-92	1120	252	1.11	79827	22	23	65	59
03-18-92	1422	252	1.21	79186	22	22	62	59
03-19-92	1431	501	0.69	13635	15	15	13	182
03-20-92	1022	121	0.16	8820	30	30	27	60
03-21-92	1530	501	0.68	13884	15	15	14	171
03-23-92	0915	501	0.56	13884	15	15	16	186
03-23-92	1005	501	0.68	765	15	15	15	9
03-23-92	1503	252	1.33	70980	20	21	58	59
03-24-92	1527	252	1.29	58522	20	20	52	59
03-26-92	1542	252	1.15	54288	20	20	54	59

Table 2.1 (Concluded)
Summary of All Blast Events During WES Field Study

Date	Time	Pattern	PF	TOTLB	Burden	Spacing	HOLEDEP	HOLES
03-27-92	1052	252	0.97	36315	20	20	54	47
03-27-92	1106	252	0.77	26640	19	20	52	47
03-27-92	1451	121	0.26	26550	30	30	52	59
03-30-92	0926	121	0.25	9830	30	30	30	40
03-30-92	1519	121	0.13	5400	30	30	27	47
03-31-92	1405	121	0.09	6210	30	30	27	80
04-01-92	0935	501	0.16	6003	20	20	10	261
04-02-92	1447	501	0.17	4623	20	20	9	201
04-03-92	0919	501	0.16	3588	20	20	10	156
04-03-92	1411	121	0.25	9000	30	30	55	20
04-07-92	1428	121	0.25	10800	30	30	54	24
04-09-92	0956	121	0.22	36130	30	30	62	80
04-10-92	1355	121	0.20	34200	30	30	66	76
04-13-92	1149	121	0.21	23400	30	30	65	52
04-14-92	1010	101	0.09	2499	30	30	14	57
04-14-92	1026	121	0.10	2345	30	30	12	57
04-15-92	1257	501	0.11	2478	30	30	12	58
04-15-92	1303	501	0.07	1195	30	30	10	51

Table 2.2
Maximum Free-Field Peak-Particle Velocities (PPV) from Recorded Blast Events

Date	Time	TOTLB	MAX PPV (in./sec) (N-S)	(E-W)*	$(N-S)_s$	(E-W)**	Type
12-06-91	1022	129240			~0.01	+	271
12-07-91	1011	115990			0.03		271
(Remote recording begins)							
03-12-92	1305	6120	0.01	0.01	0.03	0.05	121
03-20-92	1022	8820	0.02	0.01	0.04	0.10	121
03-26-92	1542	54288	0.01	0.01	0.05	0.05	252
03-27-92	1052	36315	0.01	0.01	0.02	0.05	252
03-27-92	1106	26640	0.01	0.01	0.02	0.05	252
03-27-92	1451	26550	0.01	0.01	0.02	0.05	121
03-30-92	0926	9830	0.01	0.01	0.02	0.05	121
03-30-92	1519	5400	0.01	0.01	0.02	0.05	121
03-31-92	1405	6210	0.01	0.01	0.02	0.05	121
04-03-92	1411	9000	0.006	0.005	0.01	0.015	501
04-07-92	1428	10800	0.003	0.005	0.005	0.01	121
04-09-92	0956	36130	0.01	0.01	0.03	0.04	121
04-10-92	1355	34200	0.02	0.01	0.04	0.04	121
04-13-92	1149	23400	0.02	0.015	0.04	0.04	121
04-14-92	1010	2499	0.01	0.01	0.04	0.04	101
04-14-92	1026	2345	0.01	0.01	0.04	0.04	121
04-15-92	1257	2478	0.01	0.01	0.04	0.04	501
04-15-92	1303	1195	0.01	0.01	0.04	0.04	501
(Remote recording ends)							

Notes:
* (N-S), (E-W) indicate maximum ground peak particle velocity in inches per second in the N-S and the E-W directions, respectively.
** $(N-S)_s$, $(E-W)_s$ indicate maximum peak particle velocity in inches per second in the N-S and the E-W directions of the stu house, respectively.
+ Only event recorded at the two-story study house; all other events were recorded at the one-story study house.

Table 2.3
Summary of Selected Recorded Tests Other than Blasts at the One-Story House

Date	Time	Description	Remarks
7 Dec 91	1145	Ambient Test	----
7 Dec 91	1250	Ambient Test	----
7 Dec 91	1310	Hammer Test	----
7 Dec 91	1330	Hammer Test	----
7 Dec 91	1345	Hammer Test	----
7 Dec 91	1400	Hammer Test	----
7 Dec 91	1410	Hammer Test	----
7 Dec 91	1450	Hammer Test	----
7 Dec 91	1505	Hammer Test	Airplane at 30 sec.
8 Dec 91	1010	Ambient Test	----
8 Dec 91	1030	Ambient Test	Exchanged 1 & 2 and 3 & 4; 15 and 16 off-line
8 Dec 91	1125	Ambient Test	----
8 Dec 91	1310	Ambient Test	Airplane test
8 Dec 91	1400	Ambient Test	----
8 Dec 91	1445	Forced-Vibration Test	Sine sweep from 1.8-4 Hz
8 Dec 91	1515	Forced-Vibration Test	Sine sweep from 3-25 Hz
8 Dec 91	1535	Forced-Vibration Test	Sine sweep from 2-25 Hz (16 CAL value wrong)
9 Dec 91	1120	Ambient Test	Jet flew over
9 Dec 91	1145	Ambient Test	Large farm tractor at beginning

Table 2.4
Summary of All Recorded Tests at the Two-Story House

Date	Time	Description	Remarks
5 Dec 91	0920	Data Check	Check data CH 1-12 at house 1
5 Dec 91	1251	Ambient Test	----
5 Dec 91	1312	Ambient Test	----
5 Dec 91	1620	Hammer Test	Hammer longitudinal SW corner
5 Dec 91	1630	Hammer Test	Hammer transverse SW corner
6 Dec 91	0931	Ambient Test	New sign on some CAL values
6 Dec 91	0955	Ambient Test	----
6 Dec 91	1015	Ambient Test	Increased A/D CAL's by 10
6 Dec 91	1105	Ambient Test	Moved 15 & 16 to center of house
6 Dec 91	1150	Ambient Test	Moved 15 & 16 to front SW corner (15 now -1)
6 Dec 91	1235	Ambient Test	Moved 15, 16, 17 & 18 to floor of second floor
6 Dec 91	1425	Hammer Test	Changed 4 to gain of 20 instead of 50
6 Dec 91	1455	Hammer Test	Hammer in SW corner of house
6 Dec 91	1500	Hammer Test	Gages moved to back of house
6 Dec 91	1600	Hammer Test	Hammer in NW corner of house
6 Dec 91	1630	Ambient Test	Changed CAL factor back to 10 cm A/D
6 Dec 91	1720	Ambient Test	Decreased gain on 15 by factor of 10 (cd 14 & 18); looking at vertical on 15 & 18 (master bedroom and back bedroom)
6 Dec 91	1020	Blast Event	Changed to 50 Hz filters instead of 100 Hz

Table 2.5 Concrete Masonry (Excerpted From Table 5.5.1.3 in ACI 530-88/ASCE 5-88)

Net area compressive strength of units, psi	Modulus of Elasticity E_m, psi x 10^6	
	Type N Mortar	Type M or S mortar
2000	1.8	2.2
1500	1.5	1.6

Table 2.6 Allowable Flexural Tension, psi, for Concrete Masonry (Excerpted From Table 6.3.1.1 in ACI 530-88/ASCE 5-88)

Concrete masonry		Mortar types			
		Portland cement/lime		Masonry cement and air entrained portland cement/lime mortar	
		M or S	N	M or S	N
Normal to bed joints	Solid units	40	30	30	22
	Hollow units	25	19	19	14
	Fully grouted units	68	58	51	44
Parallel to bed joints in running bond masonry	Solid units	80	60	60	45
	Hollow units	50	38	38	28
	Fully grouted units	82	70	61	46

Table 2.7
Computed Critical Tensile Strains for Concrete Masonry Units, Millionths (in./in. x 10^{-6})

Concrete masonry		Mortar types			
		Portland cement/lime		Masonry cement and air entrained portland cement/lime mortar	
		M or S	N	M or S	N
Normal to bed joints	Solid units	18.2	13.7	13.7	10.0
		26.7	20.0	20.0	14.7
	Hollow Units	11.4	8.6	8.6	6.4
		16.7	12.7	12.7	9.3
	Fully grouted units	30.9	26.4	23.2	20.0
		45.3	38.7	34.0	29.3
Parallel to bed joints in running bond masonry	Solid units	36.4	27.3	27.3	20.5
		53.3	40.0	40.0	30.0
	Hollow units	22.7	17.3	17.3	12.7
		33.3	25.3	25.3	18.7
	Fully grouted units	37.3	31.8	27.7	20.9
		54.7	46.7	40.7	30.7

Table 2.8 Summary of Critical Tensile Strains for Materials		
Material	Critical Tensile Strain (CTS), ($x10^{-6}$ in/in)	Comments
Plaster	246 - 1754	Computed from mechanical properties of plaster found in literature reported in Table 1 of Leigh (1974)
	462	Computed from test value reported in Table 1 of Leigh (1974)
	260 - 460	Range of data from Table A-1 of Stagg, et al (1984). Value of 260 results from failure at 10,000 cycles with no prestrain.
Gypsum core	130	For 5/8" wallboard with paper laminate removed. Data from Table A-1 of Stagg, et al (1984)
	340	For 5/8" wallboard - cited as core failure. Data from Table A-1 of Stagg, et al (1984)
Wallboard	1045	For initial paper failure of 1/2" wallboard test samples. Mean of yield values from Table A-3 of Stagg, et al (1984)
Concrete	132	Static CTS computed from modulus of rupture value (ACI 318-89)
	50	CTS computed by Dowding (1985) for impact tests on curing concrete prisms
	100	CTS measured by Crawford and Ward (1965) at 10 in/s on 9-in concrete wall
Brick	160	Lowest CTS reported in Table A-7 of Stagg, et al (1984) for 4-in brick wall
Block joint	110	Reported in Table A-7 of Stagg, et al (1984)
	300	Reported by Crawford and Ward (1965) on 8-in block wall across joints at 3 in/s.
	6.4 - 54.7	Design values of CTS range computed from allowable flexural tension and modulus of elasticity for 1500- and 2000-psi concrete masonry units (ACI 530-88/ASCE 5-88)

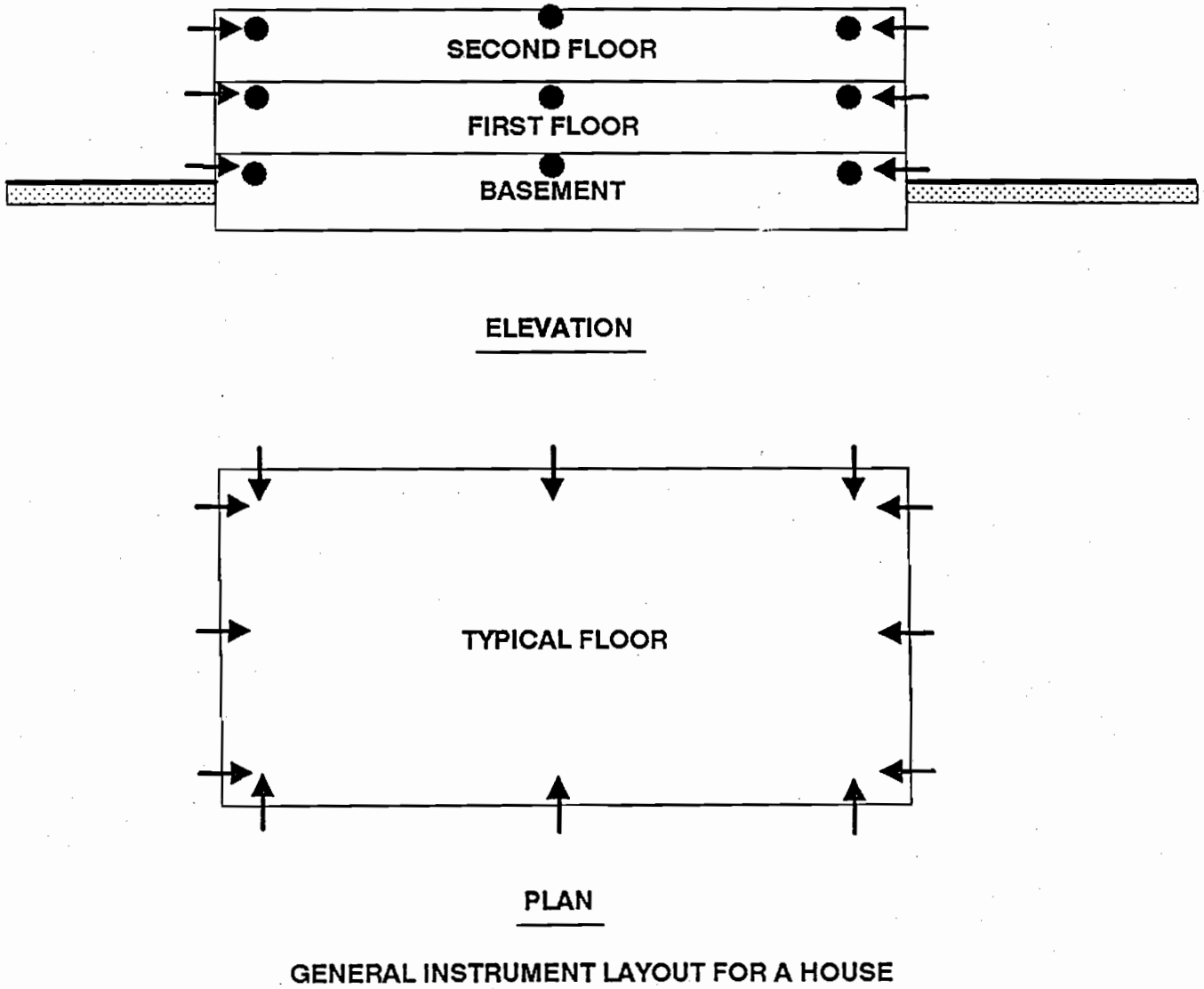

Figure 2.1 Schematic of approximate instrument locations for measuring structural motions

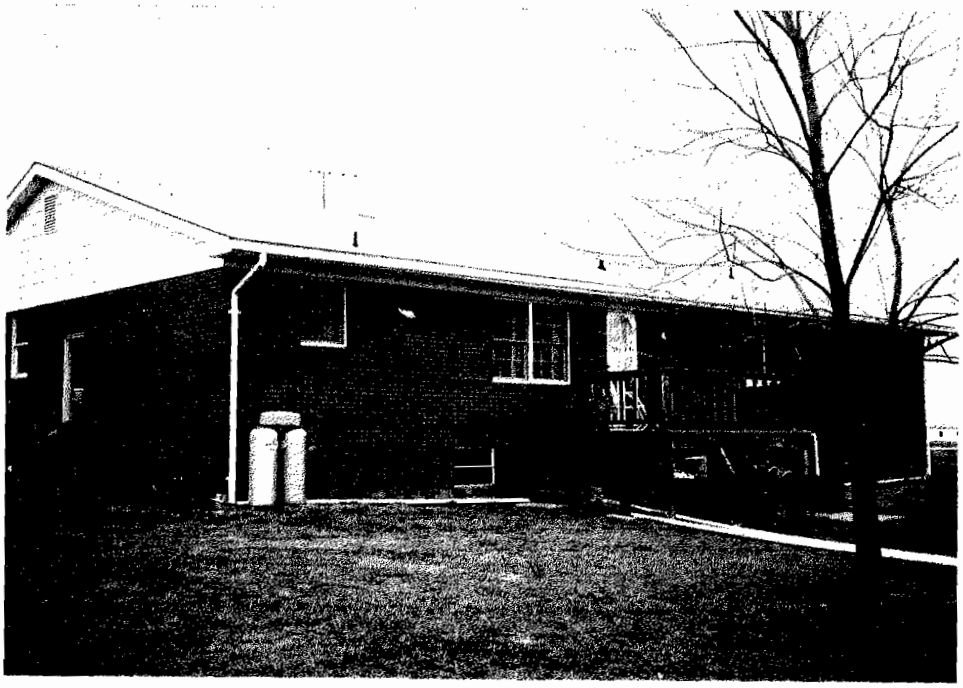

Figure 2.2 Back elevation view of one-story house

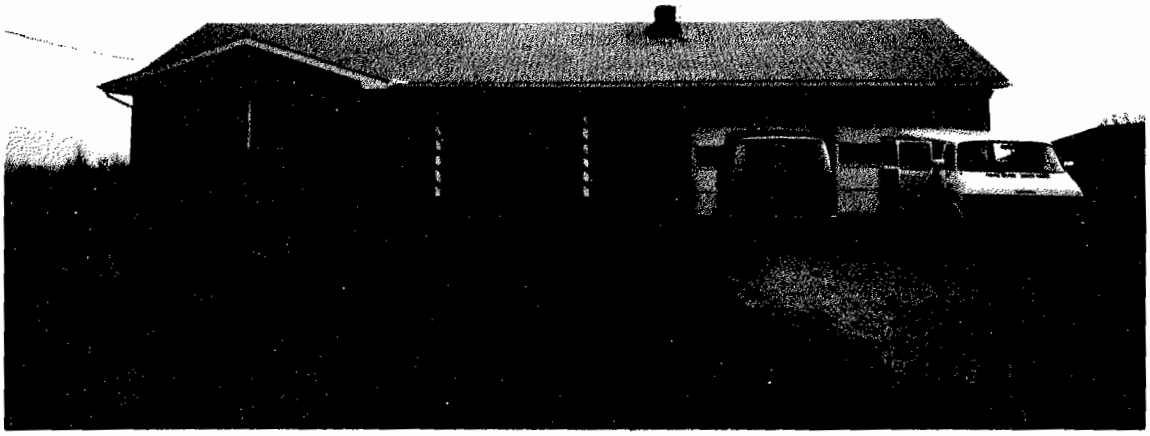

Figure 2.3 Front elevation view of one-story house

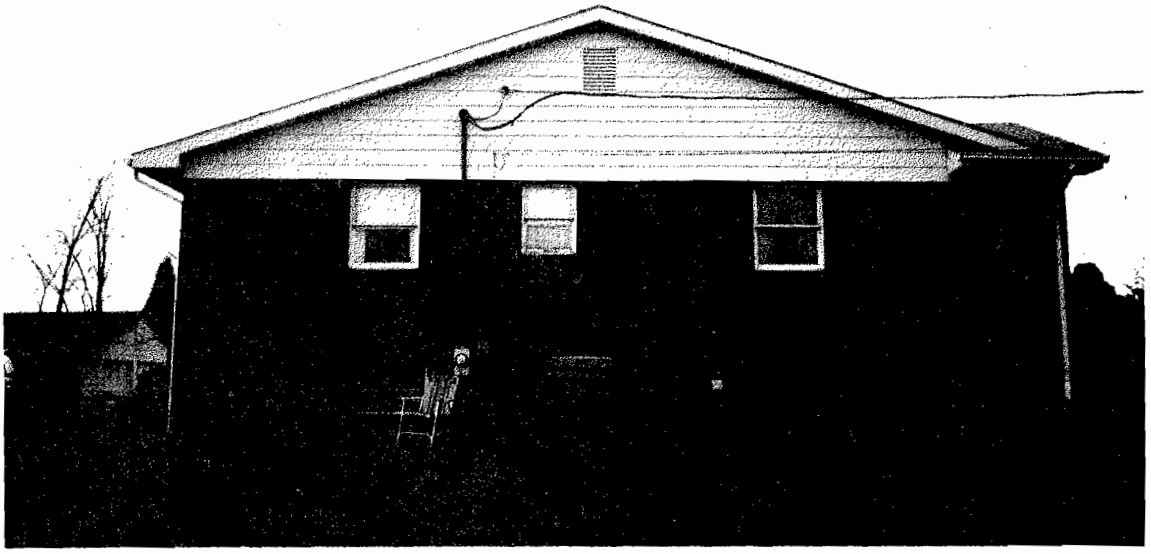

Figure 2.4 North elevation view of one-story house

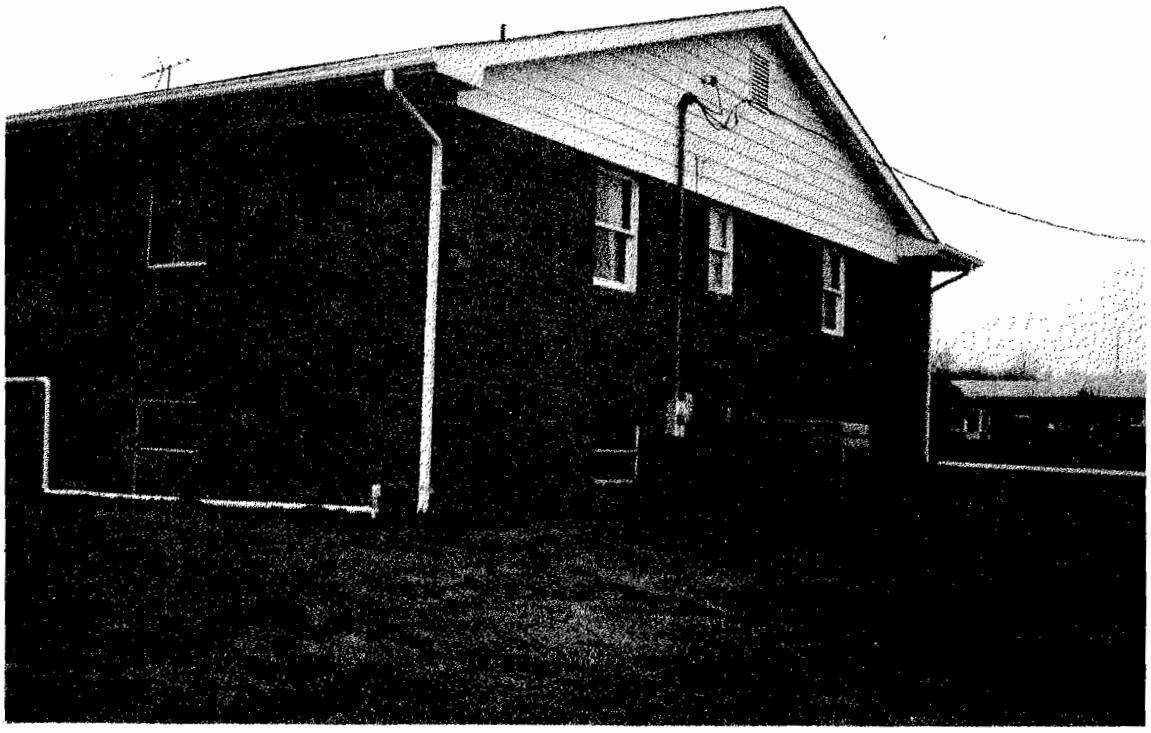

Figure 2.5 Northeast elevation view of one-story house

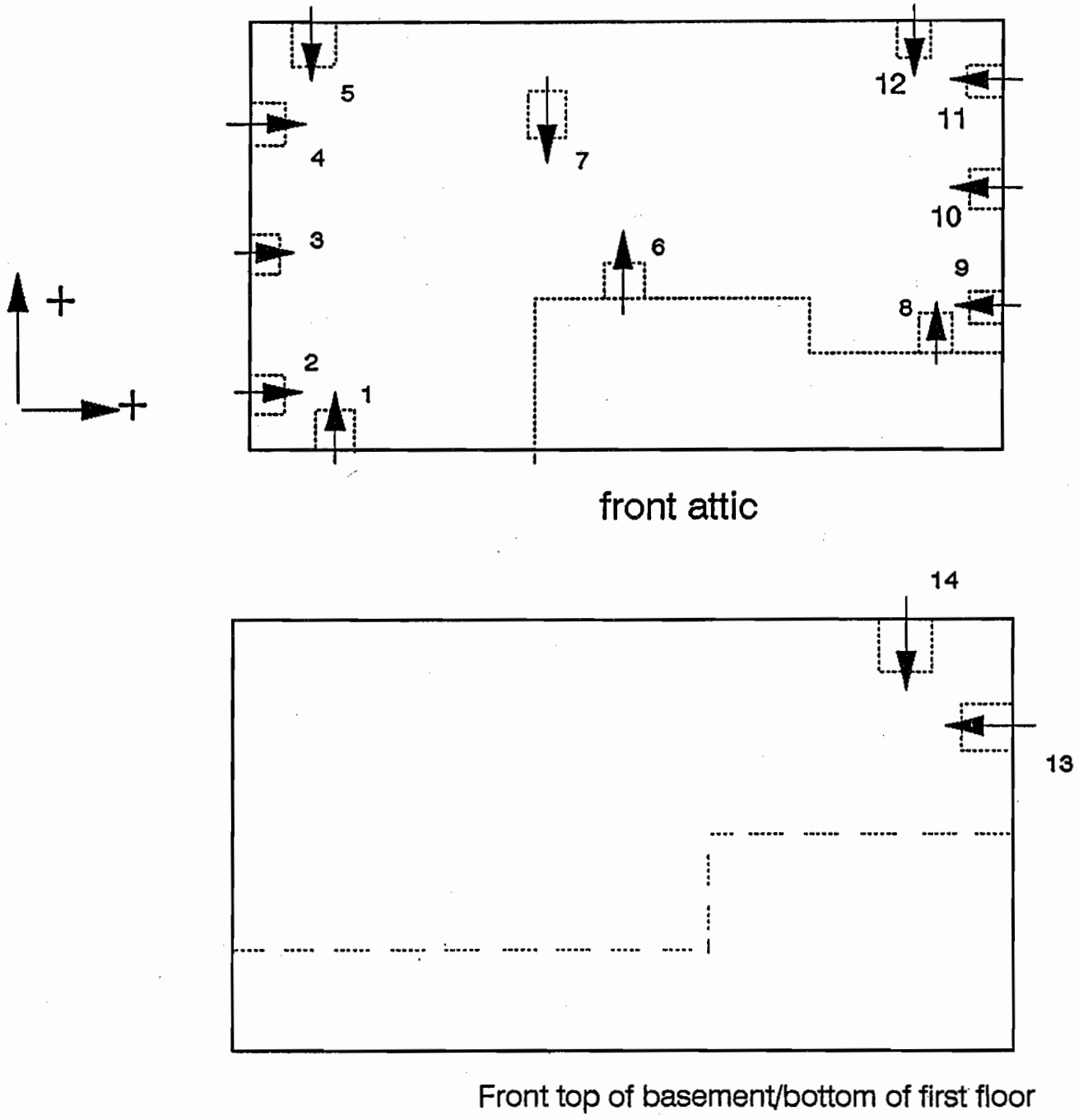

Figure 2.6 Accelerometer locations for data acquisition during 6-7 December 1991

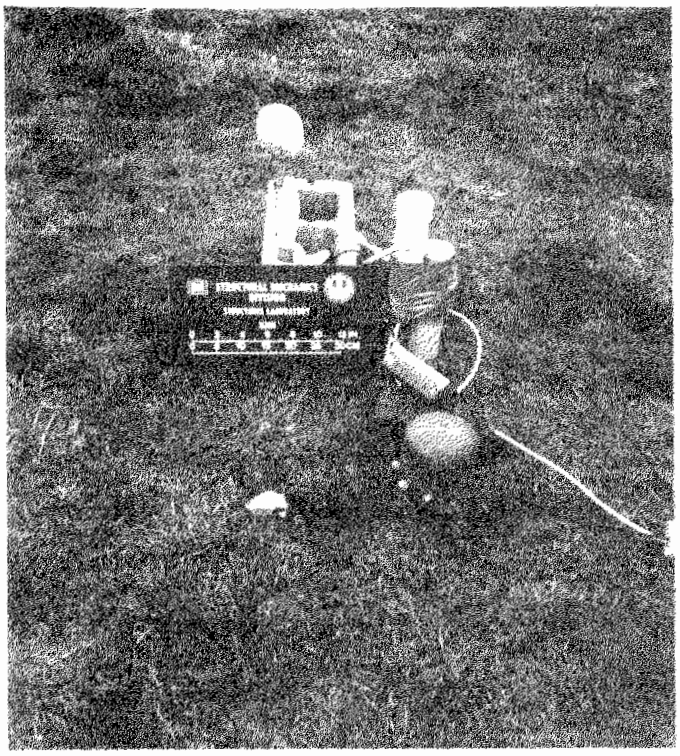

Figure 2.7 Closeup view of the "free-field" instrumentation

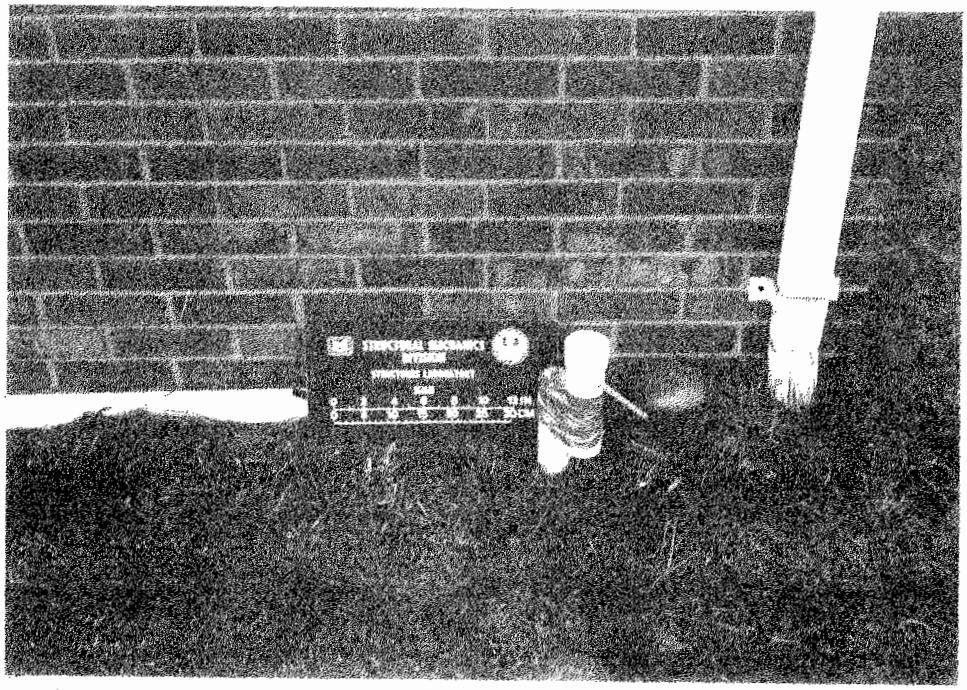

Figure 2.8 Closeup view of the ground instrumentation in the vicinity of the northeast corner of the one-story house

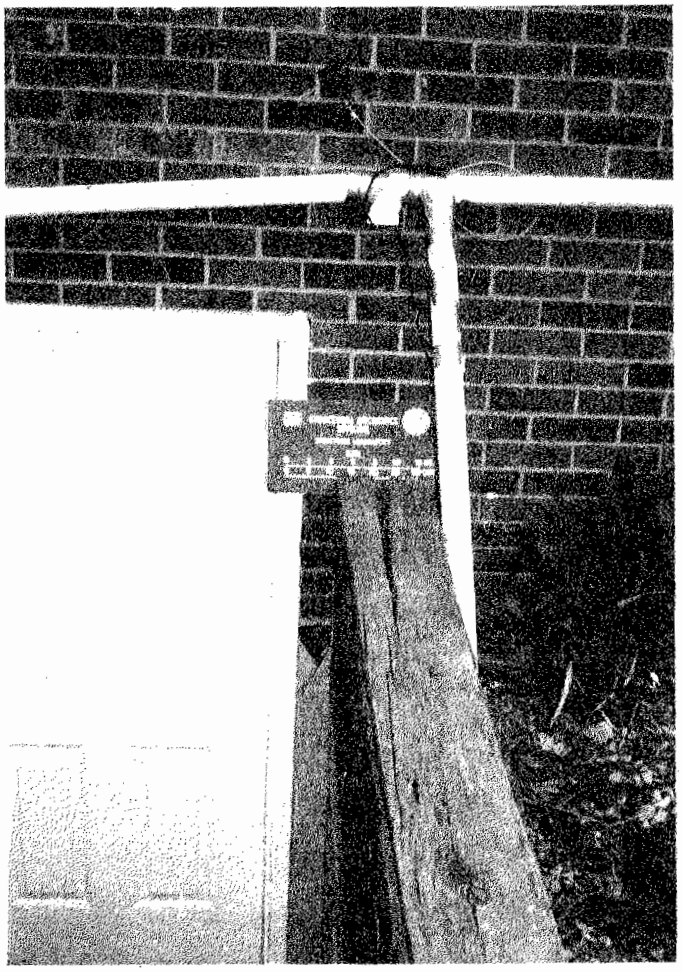

Figure 2.9 View of horizontal exterior accelerometer locations on the east wall above and below the first floor level (top accelerometer is on the exterior face of the brick veneer; bottom accelerometer is on the exterior face of the block of the basement wall)

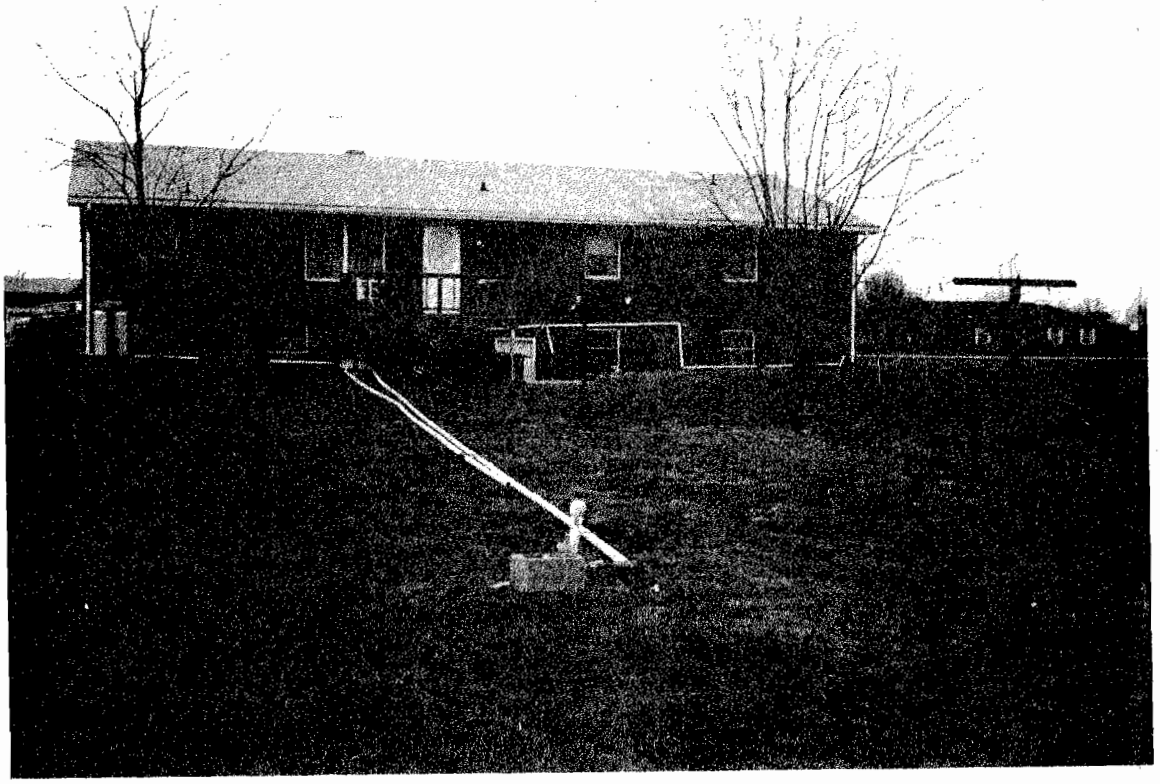

Figure 2.10 Perspective views of the "free-field" instrumentation

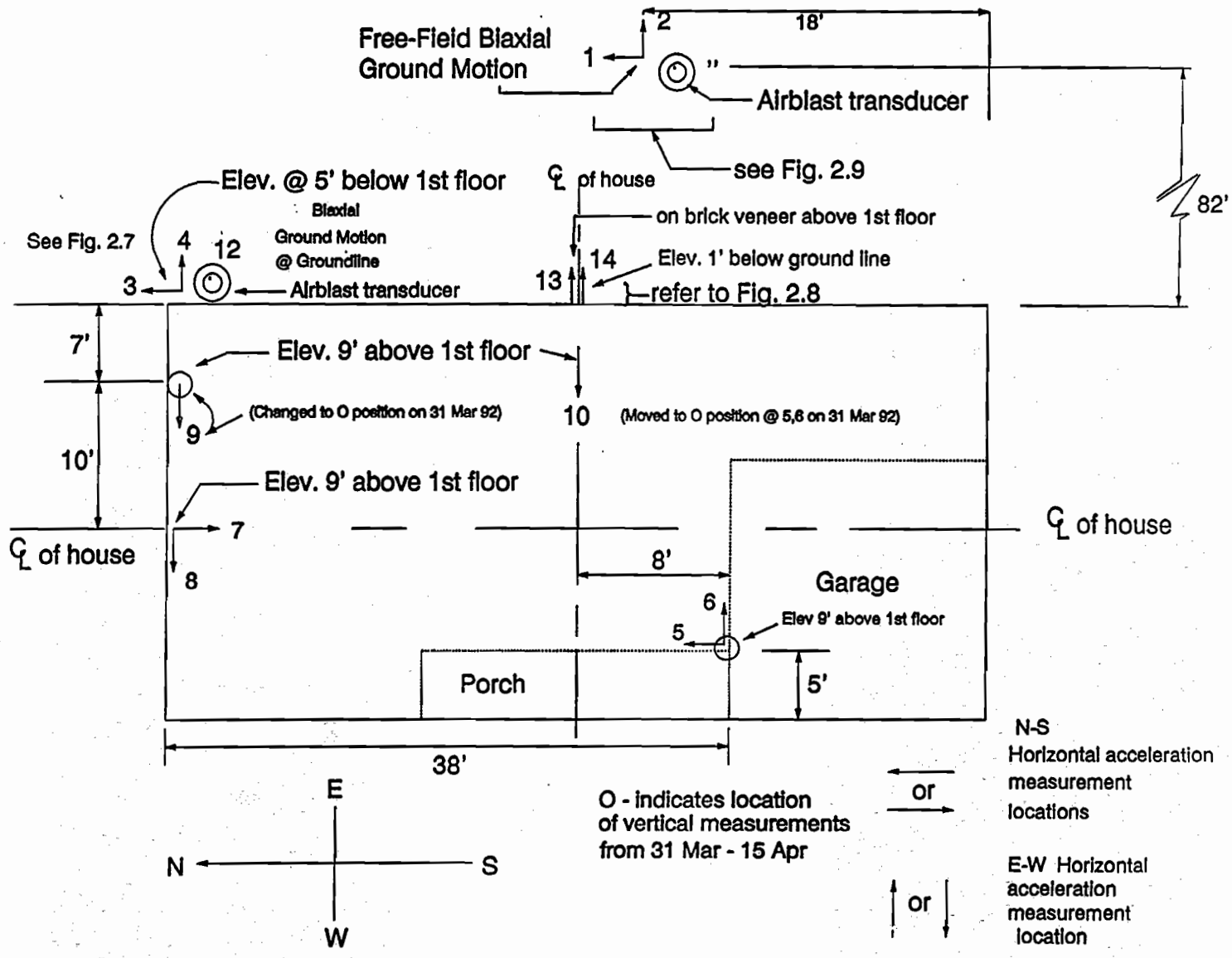

Figure 2.11 Location of instrumentation in one-story house from 12 March to 15 April 1992

a. Front elevation view

b. Back elevation view

Figure 2.12 Two-story house

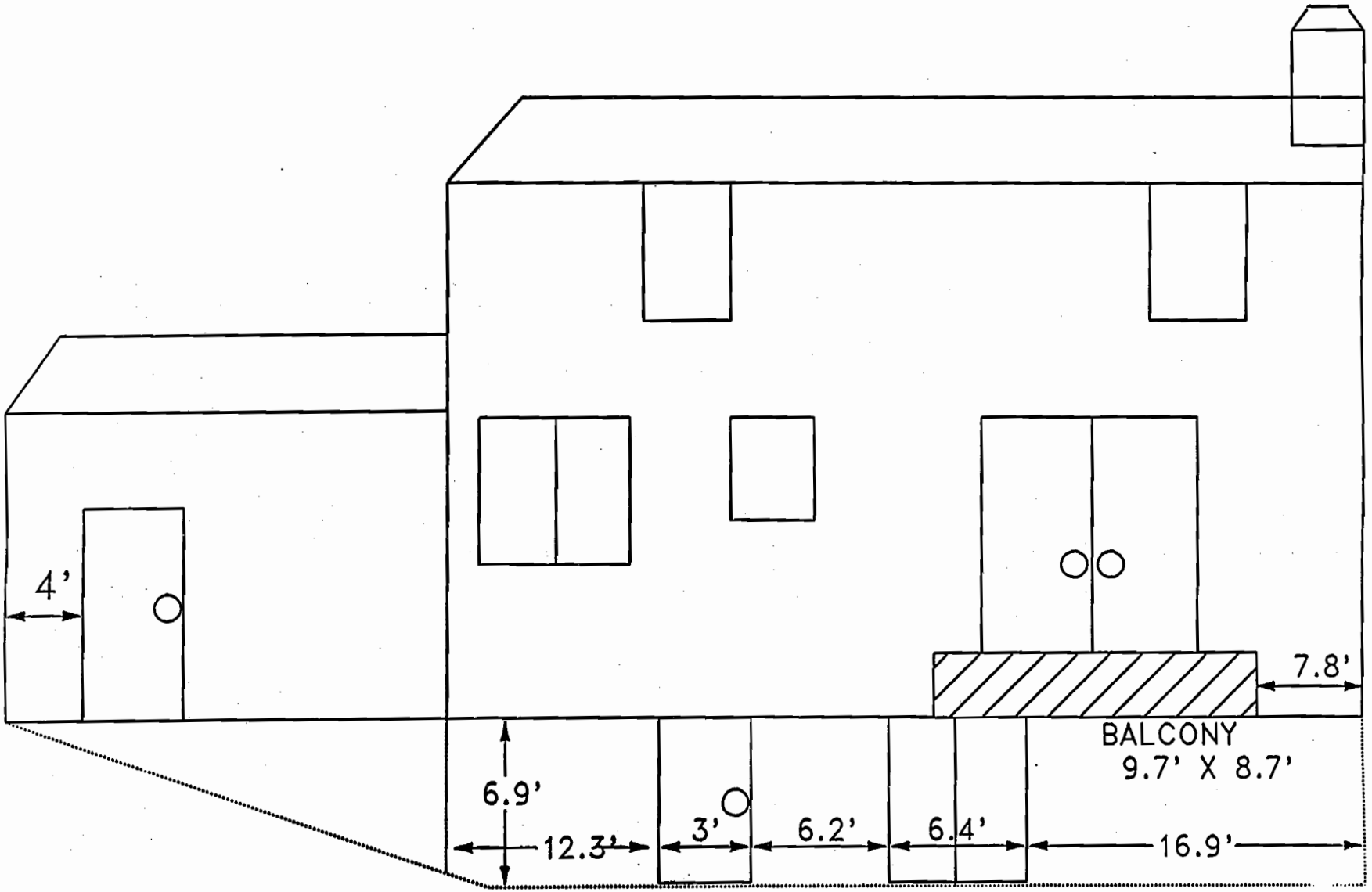

Figure 2.13 Schematic and dimensions of back elevation of the two-story house

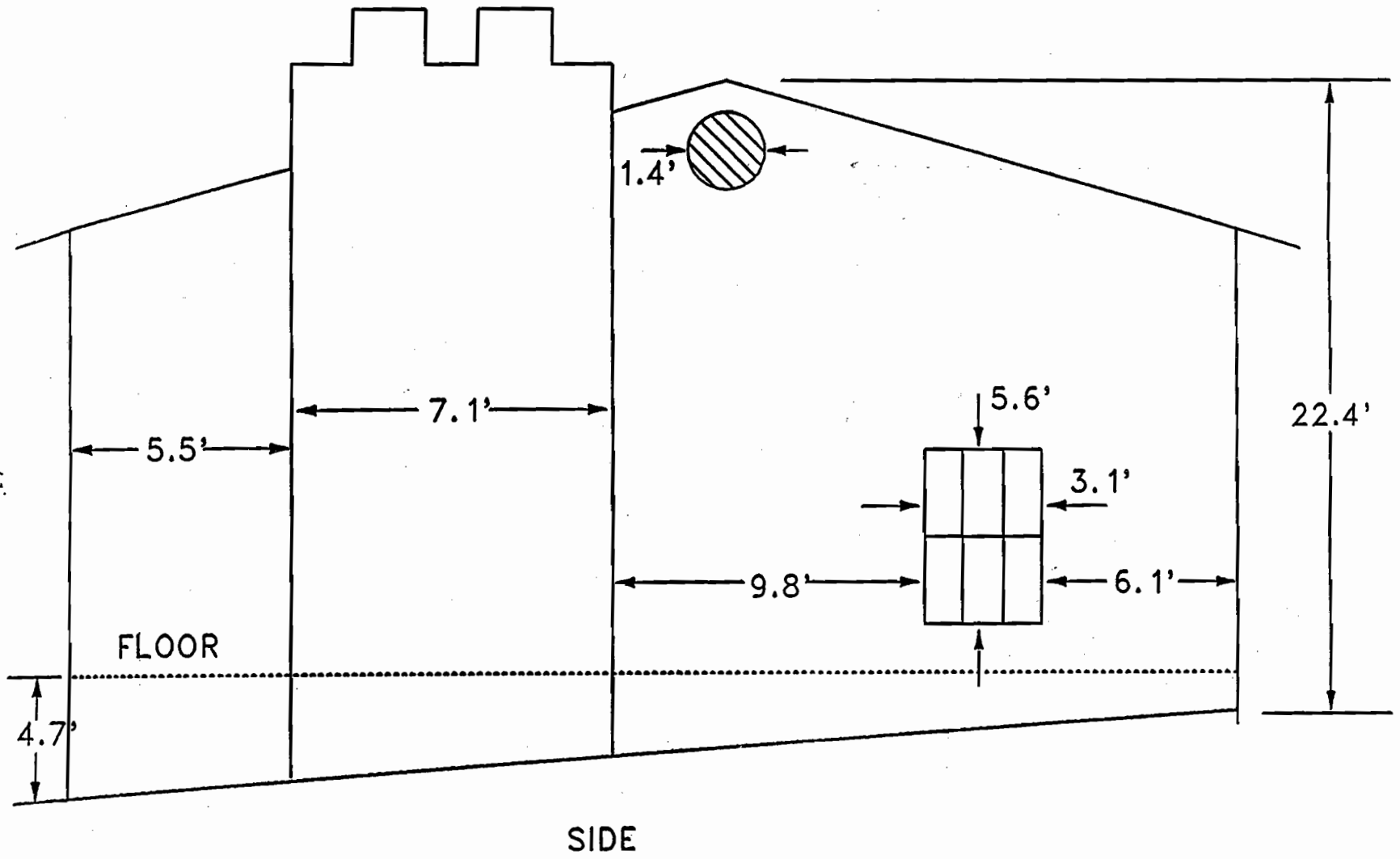

Figure 2.14 Schematic and dimensions of elevation of chimney side of the two-story house

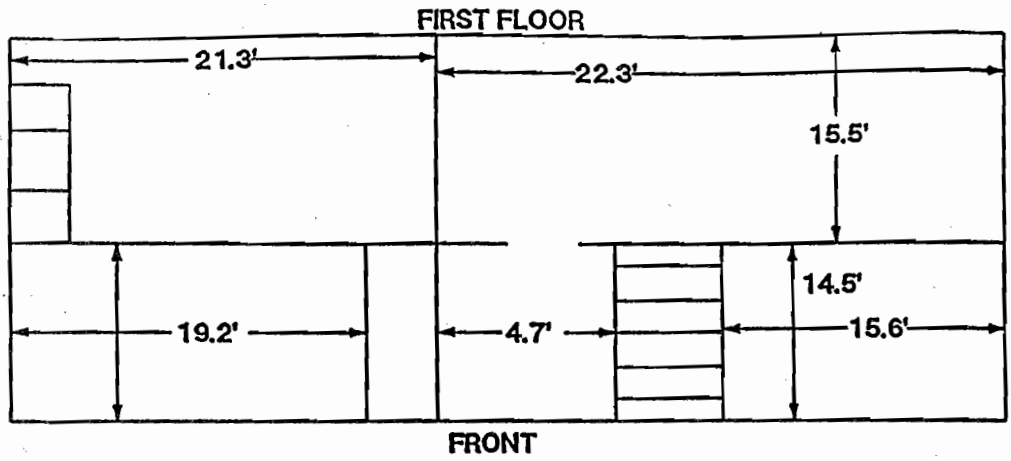

Figure 2.15a

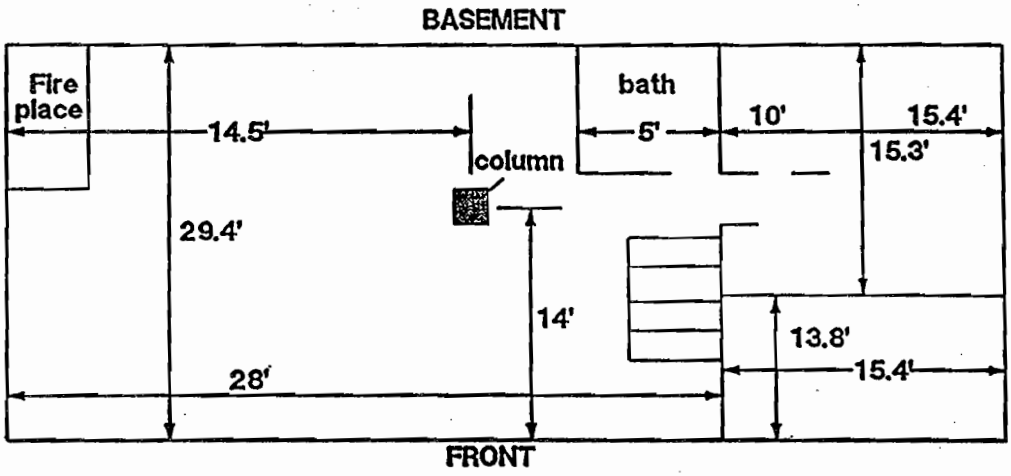

Figure 2.15b

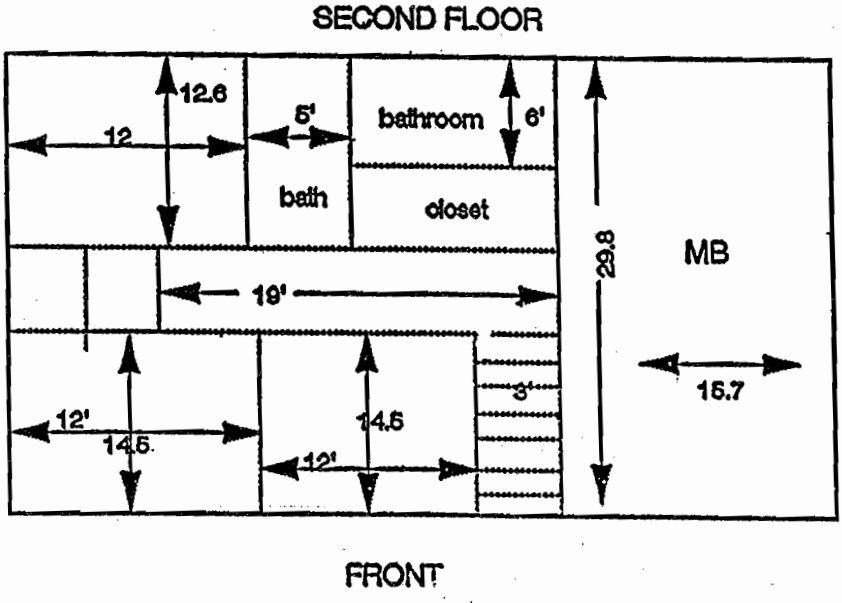

Figure 2.15c

Figure 2.15 Dimensions of second floor plan of the two-story house

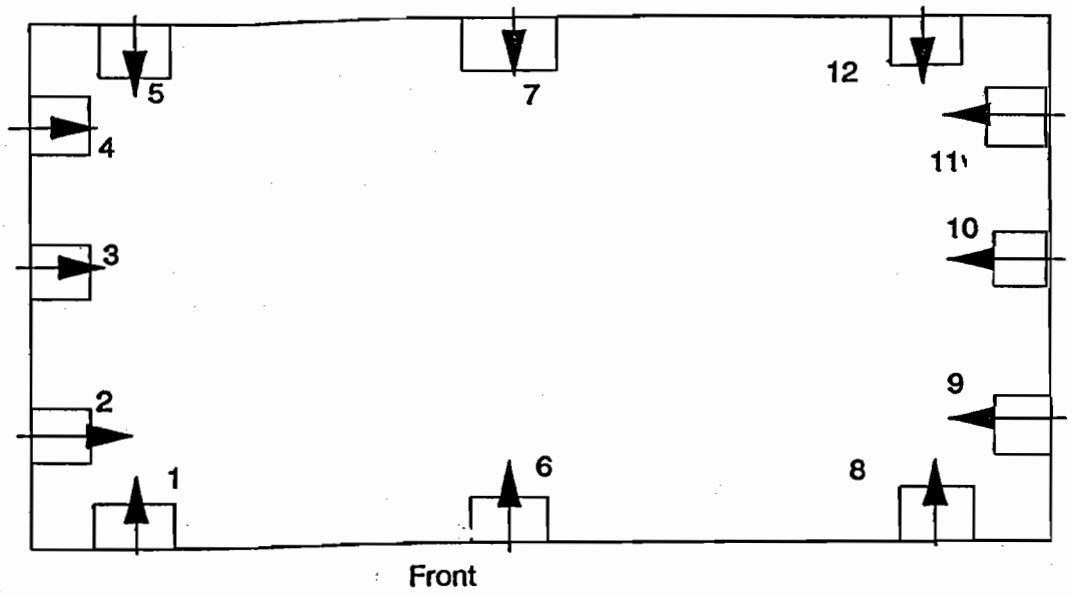

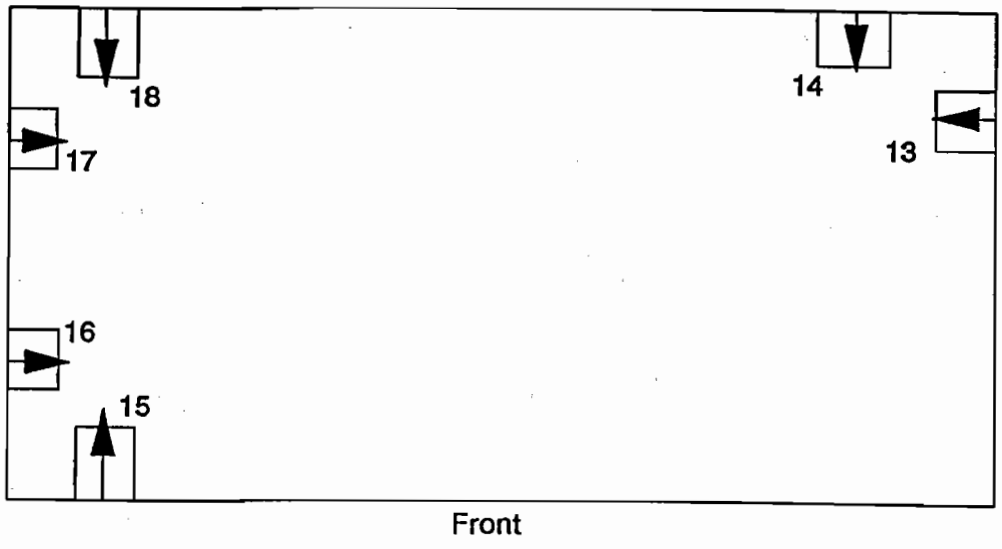

Figure 2.16 Instrumentation layout for two-story house. Arrows denote horizontal measuring orientations. Numbers indicate channel number.

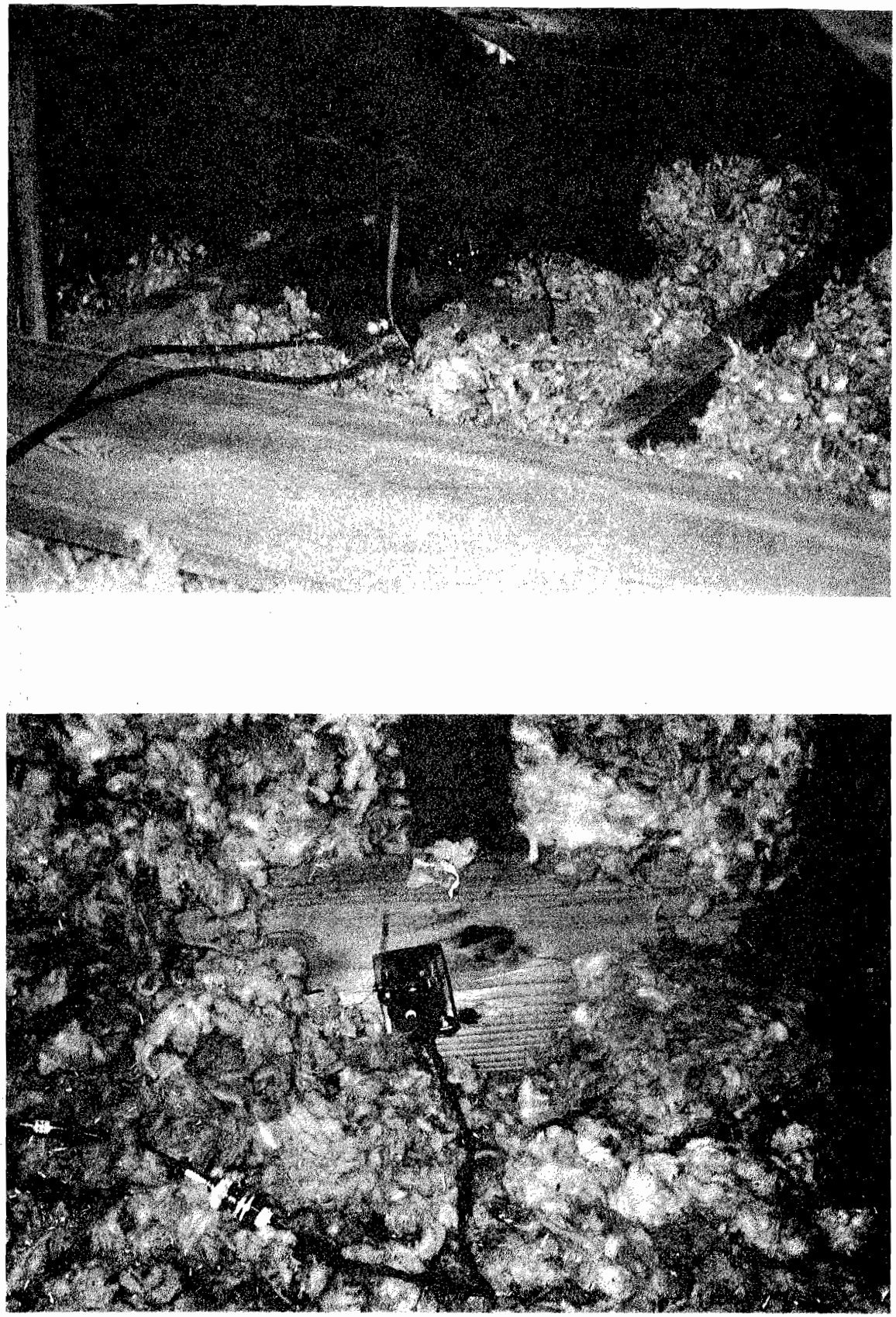

Figure 2.17 Accelerometers located in the attic of the two-story house for horizontal response measurements

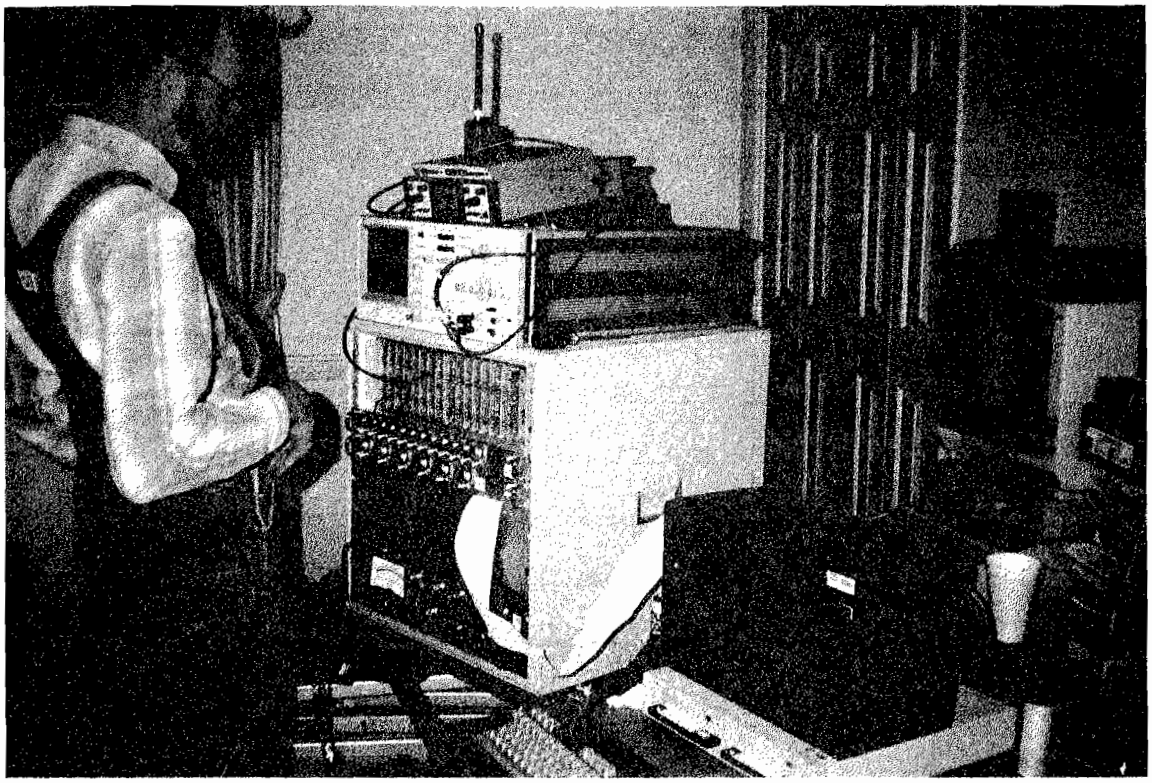

Figure 2.18 View of data acquisition setup at two-story house

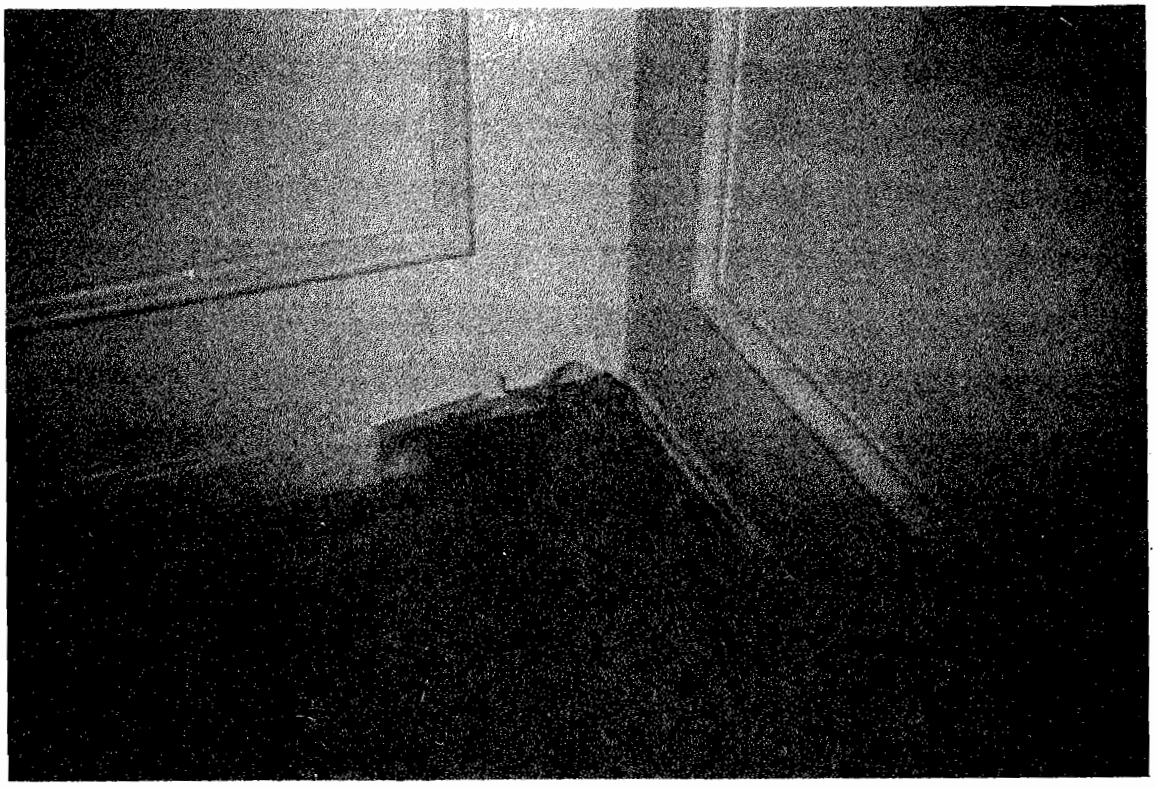

Figure 2.19 View of typical horizontal biaxial accelerometer array for second floor

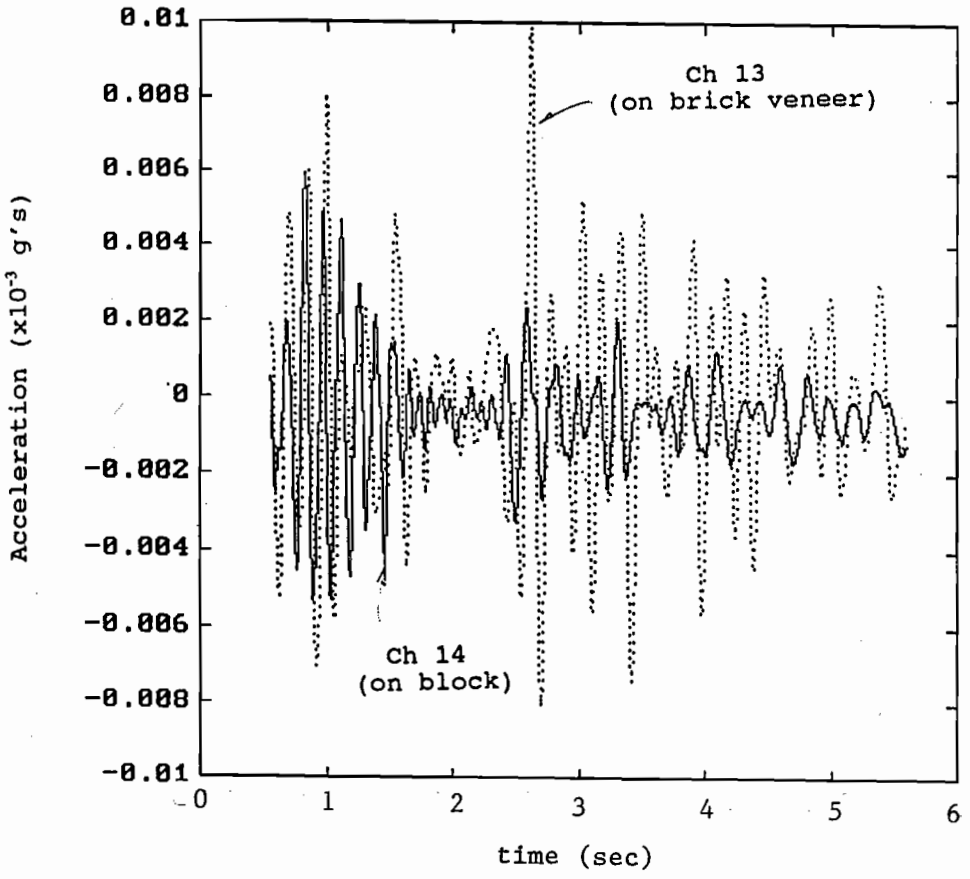

Figure 2.20 Comparison of horizontal response above and below reported locations of horizontal crack

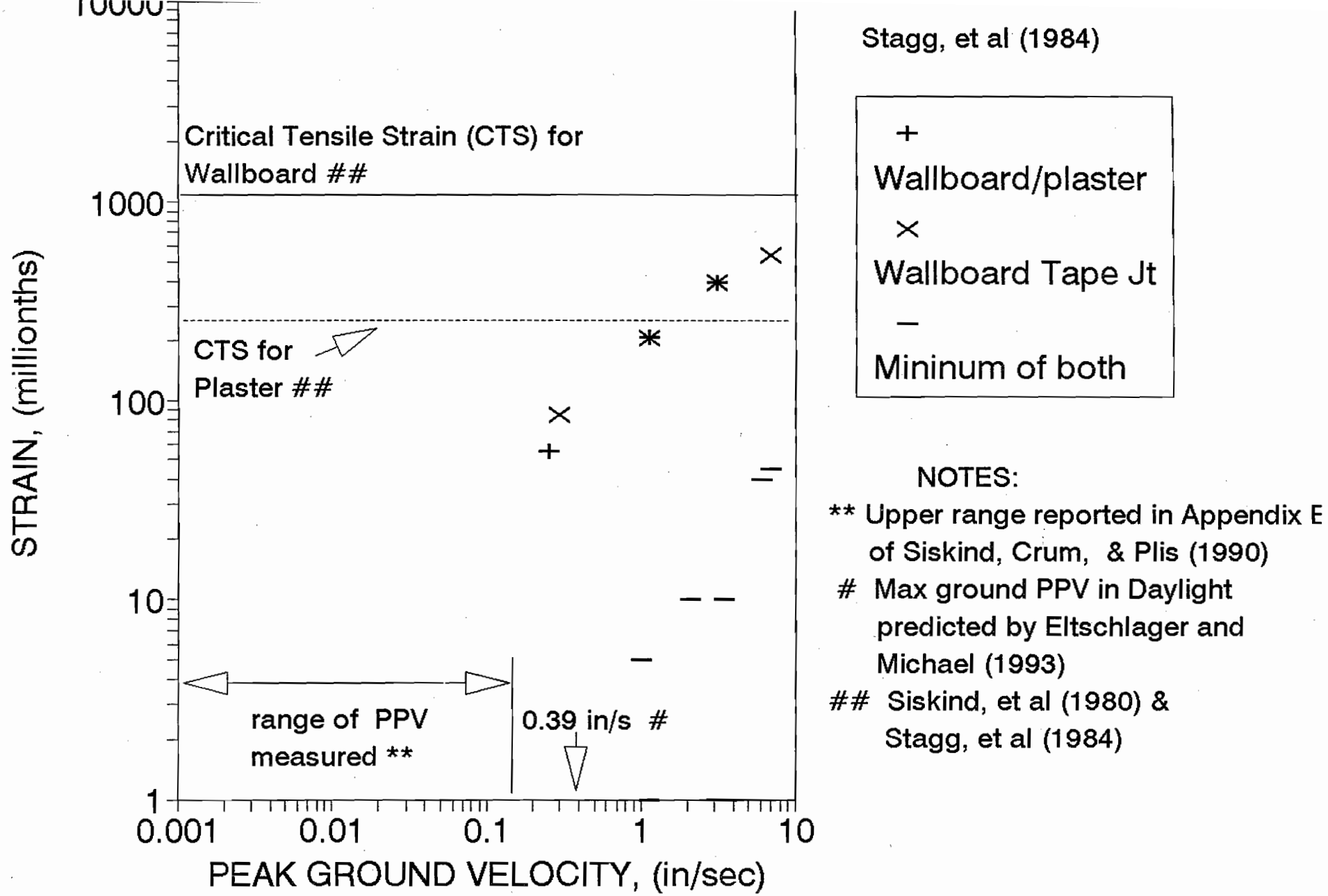

NOTES:

** Upper range reported in Appendix E of Siskind, Crum, & Plis (1990)

Max ground PPV in Daylight predicted by Eltschlager and Michael (1993)

Siskind, et al (1980) & Stagg, et al (1984)

Figure 2.21 Strain versus peak ground velocity for wallboard, plaster, and wallboard tape joint

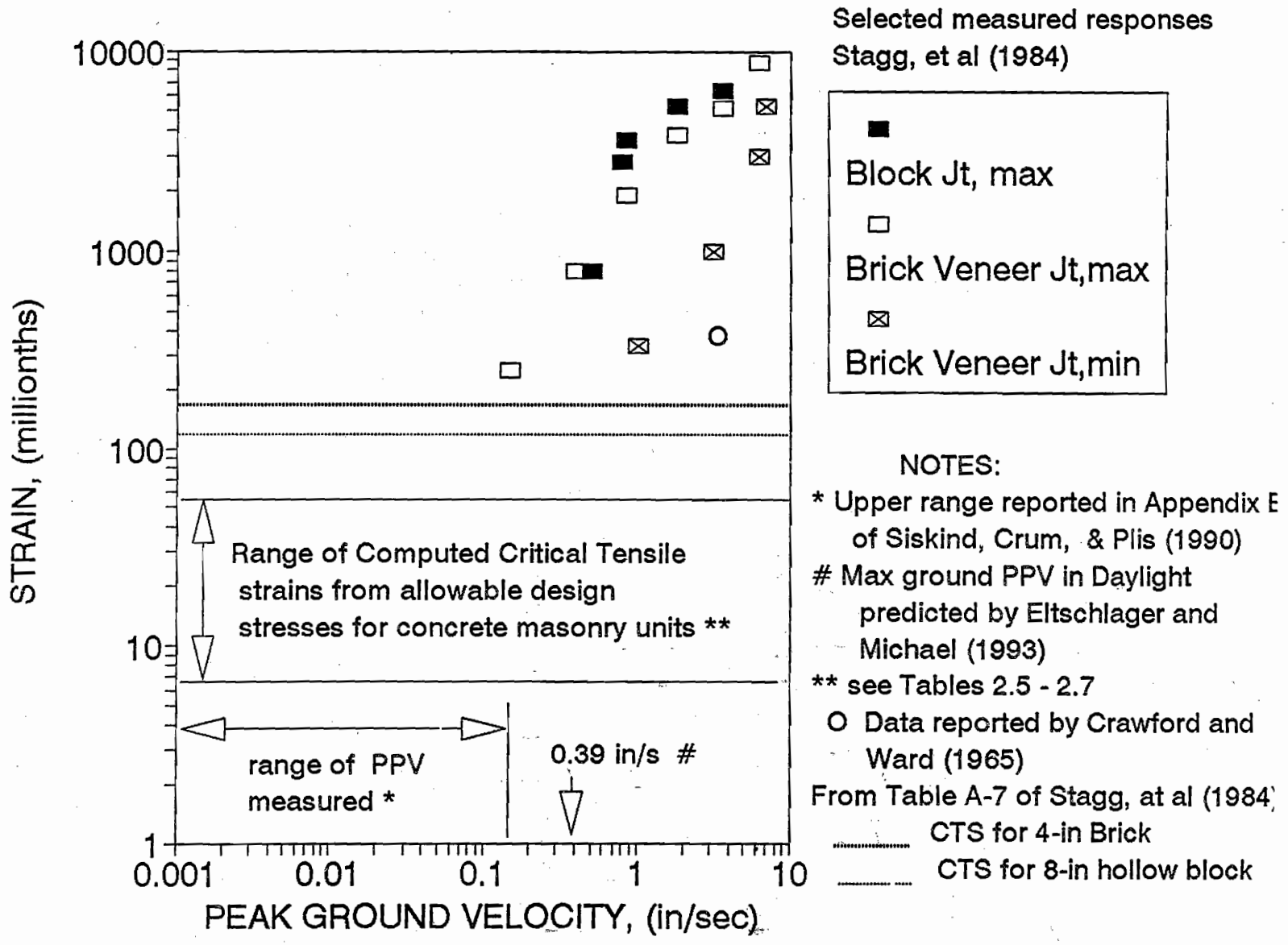

Figure 2.22 Strain versus peak ground velocity for block joint and brick veneer joint

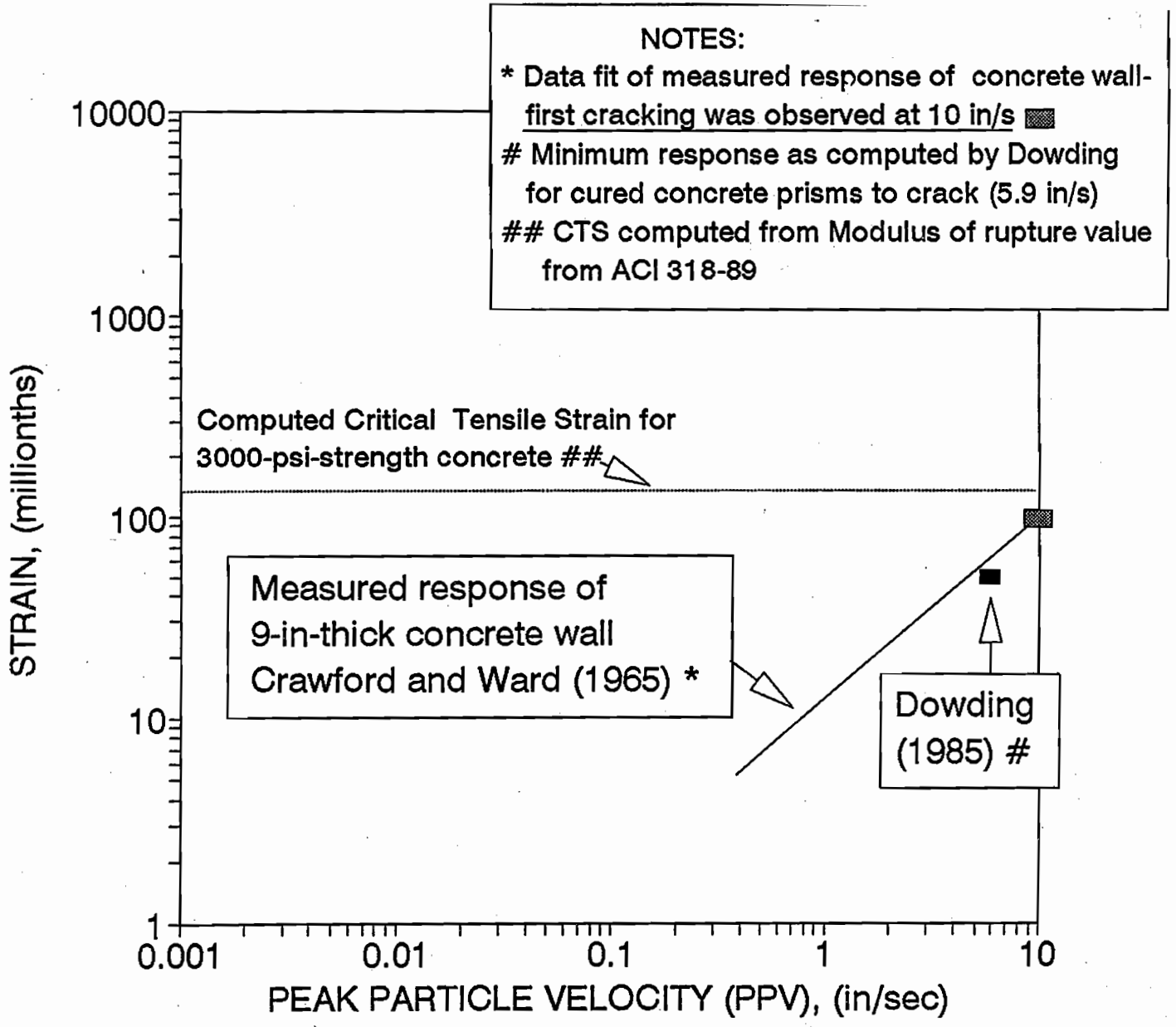

Figure 2.23 Strain versus peak particle velocity for unreinforced concrete

CHAPTER 3: STATIC ANALYSES OF SLABS AND WALLS

General

47. Simplified engineering analyses were formulated for explaining the occurrance of cracks and movements observed in houses during a 1991 field study (Chiarito 1991). In order to investigate the potential for cracking in the floor slabs due to relative settlement of the footings, displacements required to cause cracking were determined. These required displacements were then compared with observed foundation displacements. The walls were analyzed as flexural members under static loads resulting from expected soil pressures and house loads. The resulting stresses were then compared with tensile stresses which can cause cracking in blocks or mortar joints. These analyses were used to determine an initial state of stress for idealized UMB walls and unreinforced concrete basement slab houses before any mine-blast ground motions occur.

Slabs

48. The normal loads for a floor slab are developed by the soil in contact with the bottom of the slab and due to settlement of the footings. The cross section of the one-story house used in estimating footing loads is shown in Figure 3.1. Footing loads for a two-story house are approximately 40 to 50 percent more than the footing loads for a one-story house. Settlements of a two-story house would increase essentially linearly for the magnitudes of footing loads (Hadala and Petersen 1993).

49. Displacements of an idealized slab section are used to assess the likelihood of yield-line cracking in slabs similar to those observed in basements. The results from Appendix D show that about 0.7 to 1.2 in. of displacement are required to cause cracking in an unreinforced concrete slab assuming a tensile strength of 411 psi. Figure 3.2 shows examples of scatter in the

tensile strengths of concrete (Mlakar, Vitayaudom, and Cole 1984). These data indicate tensile strength can vary from 230 to 400 psi which indicates cracking from 0.7 in. of displacement.

50. Appendix D presents the simplified static calculations. A slice of the floor slab was treated as a beam. This is a satisfactory assumption for the floor slabs that had long cracks generally extending from one end to the other. As the footings settle, vertical soil pressures develop under the flexible slab. This results in a relative displaced shape as shown as a dotted line in Figure 3.3. The static deflection in the slab occurs downward at contact with footings and relatively upward at the center of the slab. The results show that the observed settlements of 1 in. at some houses (not at the study houses) visited in 1991 (Chiarito 1991) are more than sufficient to cause cracking in the floors.

Walls

51. Hadala and Peterson (1993) provided bounding values for lateral earth pressures on basement walls, and included values for active pressure, passive pressure, and confined swell pressures in expansive clays. Using estimates of the tensile strength of the block and mortar of the walls (American Concrete Institute and American Society of Civil Engineers 1988) the potential for the onset of cracking in the walls was evaluated using values for bounding values for lateral earth pressures acting on vertical walls. These calculations are presented in Appendix D.

52. Appendix D shows that the values of maximum tensile stresses on the interior basement block wall vary from 19.8 psi to 220 psi. Based on approximate tensile strength capacities of the mortar (the "weak link" between blocks), ranging from about 14 to 82 psi (ACI/ASCE Standard, 1988) (see Table 2.6 in Chapter 2) it is expected that cracking could occur in the mortar joints for static soil loads alone.

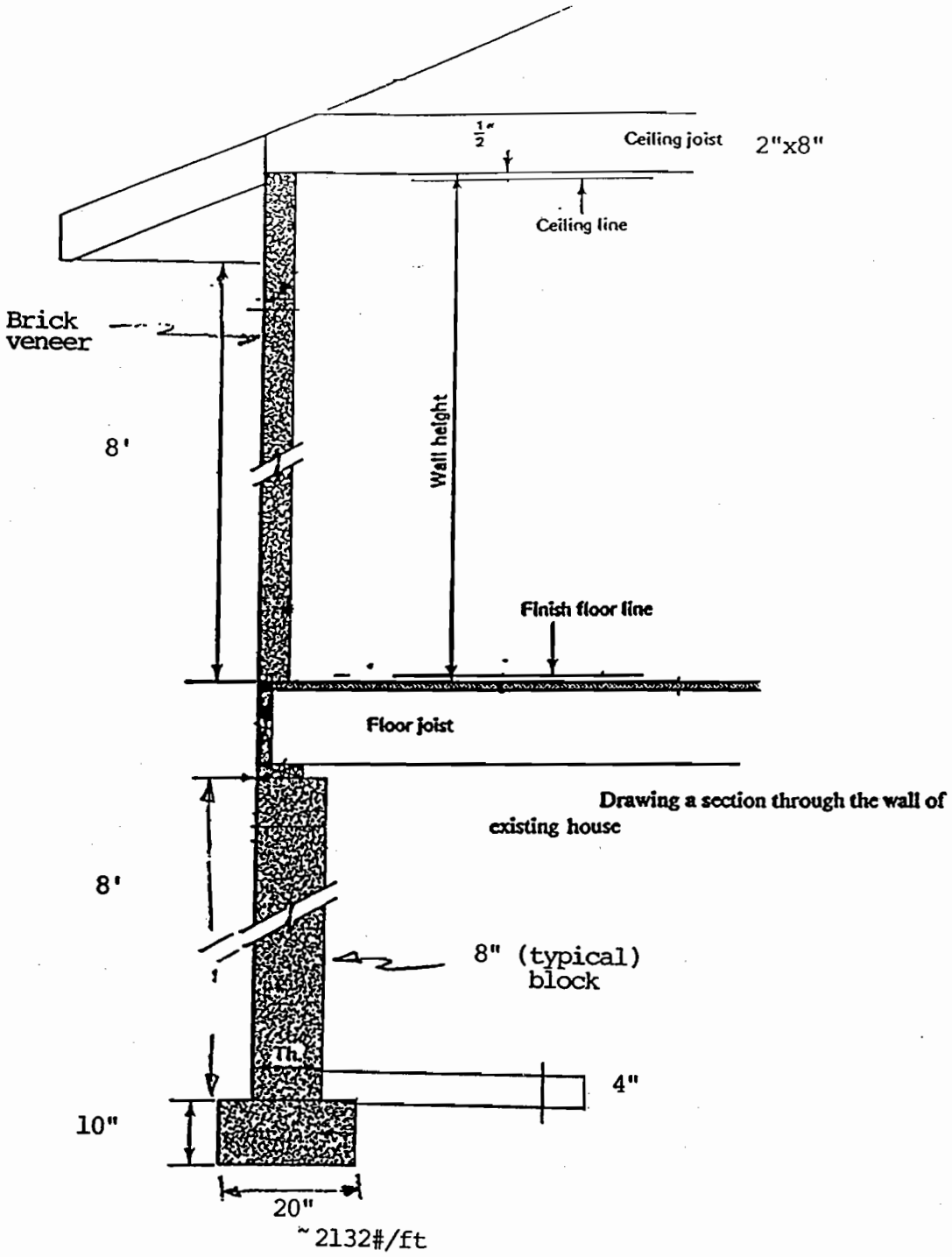

Figure 3.1 Idealized cross section of the one-story house for estimating footings loads

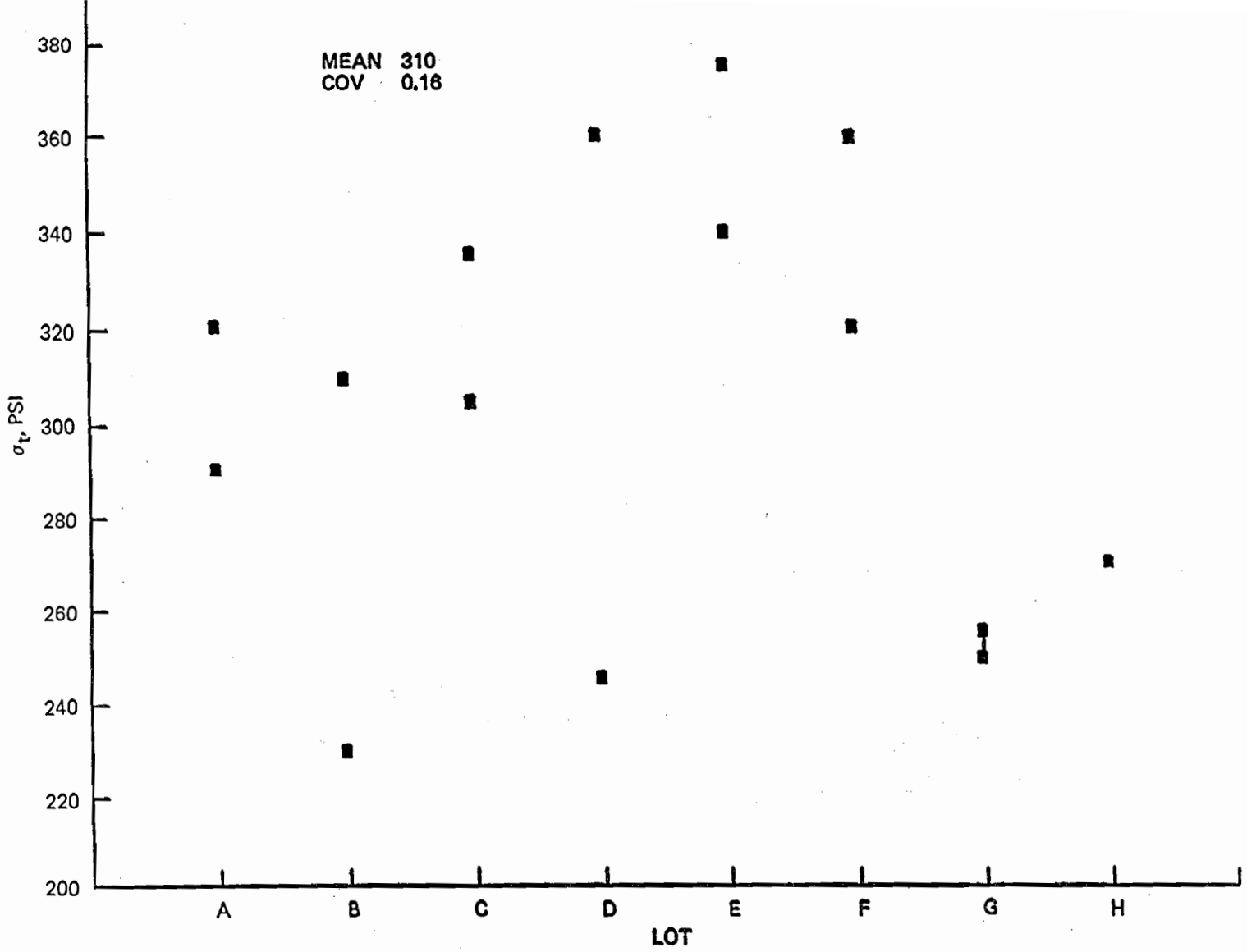

Figure 3.2 Tensile strength of control concrete cylinders (Mlakar, Cole, and Vita-Udom, 1984)

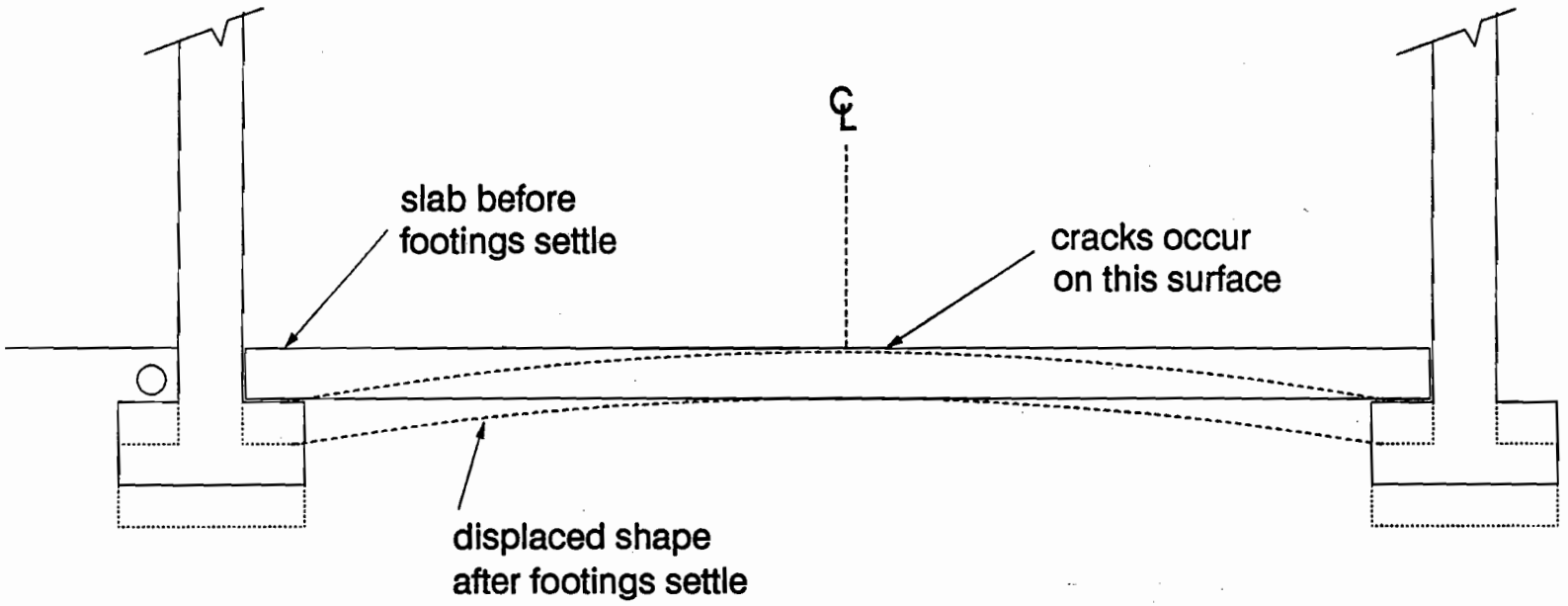

Figure 3.3 Idealized displaced shape of concrete slab after footings settle. Tension occurs on top surface. Amplitude of displaced shape is exaggerated to illustrate

CHAPTER 4: FINITE-ELEMENT ANALYSIS

53. The objective of the numerical studies described in this chapter is to determine structural stresses in the study houses due to ground motions as a result of mine-blast operations. To determine the total state of stress for an elastic structural member, the level of static stresses reported in Chapter 3 are added vectorally to the dynamic stresses reported in this chapter.

General

54. Although the finite-element (FE) method has been in commercial use since the late 1950's, many engineering disciplines are just realizing the benefits of the technique and determining that there are no other methods of analysis available to answer many of today's structural analyses problems. The FE method has been used quite extensively for predicting the response of structures due to transient, harmonic, and random base motions (Bathe 1982). In the FE method, the equations of motion describing the response of the structure are solved numerically. The structure is subdivided into elements and nodes where degrees of freedom are specified. Each degree of freedom has an associated mass, damping, and stiffness which can be represented in matrix notation by the following set of simultaneous equations:

$$[M]\{\ddot{x}\}+[C]\{\dot{x}\}+[K]\{x\} = \{f(t)\}$$

$f(t)$ = dynamic forcing function.
$[K]$ = stiffness matrix.
$[C]$ = damping matrix.
$[M]$ = mass matrix.
$\{\ddot{x}\}$ = nodal acceleration.
$\{\dot{x}\}$ = nodal velocity.
$\{x\}$ = nodal displacement.

55. In analyzing a structure by the FE method, the structure is reduced into a simple assemblage of nodes which are connected with discrete elements, called finite elements (see Figure 4.1). Physical problems modeled by finite elements are defined completely by specifying: (a) the geometric shapes, (b) the material properties, (c) the boundary conditions, and (d the applied loads. The mass, damping, and stiffness assigned to each element are dependent on the material properties and structural dimensions of the structure under study. The nodes i a three-dimensional structural model can have up to 6 degrees of freedom. The degrees of freedom represent displacements in the coordinate x, y, and z directions and rotations about each of these coordinate axes.

56. Since the FE method results in the development of a mathematical model, this model must be calibrated and verified before interpreting the results. The verification of the structure elements that are used has been through stringent quality-assurance tests to ensure that the mathematical formulations are accurately reproduced with the current computer code. The FE codes used in these studies are the ABAQUS and ADINA codes and have been certified by the National Regulation Commission for quality assurances. The model of the single-story house was calibrated with the modal test conducted with the force vibration test. The two-story house was then constructed using the elements developed for the single-story house.

Element Properties

57. The main structural elements of the single- and two-story houses, i.e., walls, roofs, and floors are made up of composite elements. A typical wall section, as in Figure 4.2, consists of a 2-by-4 stud with plywood or black board attached to the exterior face and gypsum board attached to the interior face. The 2-by-4 studs are placed on 16-in. centers. This composite element can be regarded as an I-beam with 16-in. flanges and a

.5-in. web. The I-beam shape is approximated with a uniform thickness shell element. The thickness of the uniform shell element is computed to give the same moment of inertia as the composite element. The uniform thickness element will then have the same flexural rigidity as the actual composite element. Uniformly thick elements modeling the plywood and wood-beam construction were also developed for the roof and floors. The effectiveness of using this method is demonstrated by comparing the FE result with the experimental results of Kasal (1992). The static response computed by the use of uniform shell elements agreed well with the test results of a wood-frame stud wall loaded by axial forces and pressure (Chowdhury 1993) (Figure 4.3).

58. The time-history analyses were conducted using the Rayleigh damping procedure. Five percent damping for all modes was assumed for the calculations of the Rayleigh damping coefficient.

59. The calibration of the single-story house was accomplished by comparing the first mode shape and frequency of the FE model with the corresponding mode shapes and frequencies of the single-story house obtained from the modal tests. The FE model of the single-story house is made up of shell elements. The mass of the bricks is added to the horizontal degrees of freedom for the nodes in the exterior part of the walls. It is assumed here that the vertical inertial motion of the brick veneer acts independently of the structural wall element. The brick veneer transmits the vertical inertial force directly to its base support. The response of brick veneer is determined with another FE model. The values of the modulus of elasticity of the elements, which affect the stiffness, were varied to develop wall elements to match the dynamic characteristics of the modal tests of the one-story house. This model results in a natural frequency of 10.2 Hz which compares favorably with a measured value of 7.5 Hz. These same wall elements were then used to model the two-story house.

60. These FE models reproduce overall structural motions such as torsion (twisting in place), side-sway in strong and we axes, and higher-order vibration modes. A selected ground-moti record, which is an actual record with amplitudes scaled to a peak velocity of 0.39 in./sec, is used to perform an elastic dynamic analysis of a residential structure to determine interna stresses. The peak velocity of 0.39 in./sec was selected based on recommendations from OSM (Eltschlager and Michael 1993).

61. This model represents only the basic dynamic response of these structures. Some interior walls, cabinets, and other elements of the houses are not modeled and have different dynami characteristics than those main structural elements modeled within this report. Houses have been designed primarily on past experience using simple structural materials (i.e., wood, wallboard, sheetrock, etc.). Houses are not designed using structural mechanics in the way that reinforced concrete and steel structures are designed. This design and construction practice for houses results in complex structures which present very difficult problems in terms of structural stress analysis. This is due mainly to the presence of uncertainties (random variations) in material uses, connections, boundary conditions, and construction practices. Abrupt changes in geometry and stiffness in elevation and plan can also greatly affect the dynamic response of a structure. It was noted that several structures in the study area had significant abrupt geometry changes that would be expected to influence dynamic responses. Relatively uniform structures were selected for analysis in order that the selected structures would be as representative as possible of typical houses in the study area. Uniform structures reduce variables in the FE model and allow for more reliable modal testing. Thus, the one- and two-story study houses were chosen because of uniformity in shape and construction.

62. The use of the FE procedure for this evaluation is simply to develop a representative multi-degree-of-freedom model.

This allows for the evaluation of structures which responds dynamically in more than a single mode of vibration. The comparison between the actual one-story house modal test and the corresponding FE modal response provides information on the validity of using this numerical tool.

Dynamic Responses of Brick Veneer

63. The dynamic responses of the brick veneer are modeled using the FE grid. The field test demonstrated that the brick veneer will respond independently of the interior walls and is only loosely coupled to the wall as indicated by the modeling of the exterior wall.

64. The wall was modeled using 4 rows of thick shell elements and was 62 ft long by 8 ft high. All edges except the base were unsupported. The vertical and lateral acceleration records were applied to base nodes as boundary conditions, and no damping was included. This model was developed to determine the dynamic characteristics of a free-standing brick wall which is conservative in that it will have higher stresses than a wall in an existing house because of the strength added by loose coupling with house and rigid support at corners.

65. The model results (Figure 4.4) indicate maximum principal strain of 15 x 10^{-6} in./in. (30 psi) near the footings. Field investigations have demonstrated that the mortar joints of either brick or block are the weakest structural element in this structural system. Figure 2.22 demonstrates that brick and block joints behave similarly for maximum measured responses. Also, mortar in brick and block walls is similar and has critical tensile strains ranging from 6.4 to 300 x 10^{-6} in./in. (12.8 to 60.0 psi) (see Table 2.8). Predicted response exceeds the mininum of the the range of strength. Therefore, mine blasting

could result in cracks in mortar.[1]

One-Story House

66. The one-story house FE model is used to represent a typical model for a single-story house subjected to dynamic ground motions generated from mine-blasting operations. Dynami time-history analyses are performed in order to determine the magnitude and distribution of stress which could be caused by mine-blasting operations.

67. From the modal tests as described in Chapter 2, it wa determined that the first mode of the one-story house is approximately 7.5 Hz. The FE model of this structure is shown Figure 4.1. This figure shows the boundary conditions which represent the foundation (indicated by arrows) and the overall geometry of the house (showing the boundary of the shell elements). The elements are shell elements with 6 degrees-of-freedom per node (5 degrees-of-freedom is used for nodes which have no boundary conditions, no attached elements, and whose connecting elements have similar surface normals). Figure 4.5 presents the FE results of the first natural mode shape of the house with a corresponding frequency of 10.24 Hz. This frequenc is the upper-bound limit for the house. An increase in the computed natural frequency over the measured frequency occurs du to an overestimation of the boundary stiffnesses. A detailed model for the soil-structure interaction and the rotational stiffnesses for joints connecting the floor-roof-wall system would provide a more accurate dynamic system response for the house. A lower bound frequency estimate of the house when the bottom of the walls had boundary conditions, allowing unrestrained motion, shows that the natural frequency falls to

[1] For concrete masonry depending on the mortar type (portland cement /lime or masonry cement and air-entrained portland cement/lime mortar), see Table 6.3.1.1 of ACI 530-88/ASCE 5-88.

less than 1 Hz, which is much below the experimental value of 7.5 Hz. This indicates that the measured 7.5 Hz frequency lies between the lower and upper limits of the FE model. The first mode generally found for typical single-story residences is a side-sway motion about the long axes with frequency from 7 to 10 Hz (Dowding 1985). The modal analysis indicates that the house has dynamic characteristics consistent with previous studies.

68. The FE model computes stresses, strains, velocities, acceleration, and displacements at the numerical integration points within each element on both interior and exterior sides of the walls of each time-step of the time-history analysis. Figure 4.6 displays the principal stress contour plot at the time of peak response for the exterior wall. This plot provides information regarding the principal stress distribution and the location of highest stress concentrations due to the prescribed base motion. For instance, Node 83 (see Figure 4.7) on the garage wall has the highest stress and Node 711 on the front face of the house has the second highest stress in the structure. The time of peak response for a nodal point was chosen by examining the stress time-history that has the highest stress magnitude (for example, time-history plot in Figure 4.8 for Node 711 shows the time for peak response). Figure 4.9 displays the arrow plots of the maximum principal stresses for the exterior walls. This Figure can be used to identify the potential crack pattern on the wall surface due to the applied blast-induced ground motion. Figures 4.7, 4.8, and 4.10 display the principal stress time-history plot for Nodes 83, 711, and 1328, respectively, for the exterior wall which produces stress levels of primary interest for this study. The absolute maximum principal stresses for Nodes 83, 711, and 1328 occur at about 2.95 sec after the arrival of ground motions. The principal stress values are used for determining maximum tensile and compressive stresses, which can cause structural damage. For this study, the tensile stresses (psmax) are the stresses of interest since the material strength

for tensile stresses are less than that for compressive stresse The stresses of interest for each time-history plot are the average of the six highest tensile stress six peaks. This is done because a single spike of a large magnitude will not necessarily cause structural damage. The average of several peaks provides a better estimate of stresses which can be used t measure the structural damage from a linear-elastic analysis.

69. The dynamic amplification factor (DAF) of the model, a ratio of output response (such as displacement) to the corresponding input, is computed for the house to determine the magnification of responses as a result of base motion and compar it with that of the experimental results. FE analysis provides DAF of 4.88. The DAF as obtained from the experimental forced-response analysis ranged from 2.0 to 6.0. This agreement furthe validates the confidence of the analytical study adopted in this investigation.

70. The FE model of the one-story residential structure indicates a maximum stress level of about 55 psi at the garage wall (an upper limit), and less than 1 psi at the center of the walls from mine-blasting ground motions. The FE model reproduce the first experimental mode shape which validates the numerical model for this study. The stress level from these studies indicates the interior wall will experience no damage from mine blast since the gypsum wallboard has a tensile strength of about 170 to 250 psi (Stagg, Siskind, Stevens, Dowding 1984).

Two-Story House

71. The two-story house model is used to represent a typical response of a two-story residence subjected to dynamic ground motions generated from mine-blasting operations. Dynamic analyses are performed in order to determine the magnitude and distribution of stresses. The two-story house is constructed using the wall elements developed for the single-story house.

72. Since there was not a modal test performed on the two-

story house, the same structural elements developed for the one-story house (i.e., modulus of elasticity, mass, thickness, and Poisson's ratio) are used to construct the FE model of the two-story house. The elements are shell elements with 6 degrees-of-freedom per node (5 degrees-of-freedom is used for nodes which have no boundary conditions, no attached elements, and whose connecting elements have similar surface normals). The time-history representing ground-induced motions from the mine blasting is the same as used for the one-story house. Figure 4.11 displays the FE model used for these analyses.

73. As with the one-story house, the first step of the dynamic analysis of the two-story house was to determine the natural modes and frequencies of the model. The first mode is shown in Figure 4.12 and has a corresponding frequency of 23.7 Hz. The first mode generally found for typical two-story houses is a side-sway motion about the long axes with a frequency of 5 to 10 Hz. The addition of the garage adds considerable stiffness to the dynamic response which results in a more complex first mode of the house responding at a higher frequency.

74. Figures 4.13 and 4.14 display stress vector plots during the time of peak response. These Figures indicate highest stresses at the corners of the windows. These stresses at the corners are commonly encountered in FE analyses due to numerical singularities in dealing with sharp corners resulting from the hole in the grid, such as windows. Due to these problems these stresses are usually considered artifacts of the model and are ignored.

75. However, Figures 4.13 and 4.14 do provide important information pertinent to this study. These figures indicate the magnitude of stresses and stress patterns caused by blast-induced ground motions. These stress patterns also indicate a potential crack pattern (if stresses exceed the material strengths) on the exterior wall surface as shown in Figure 4.15.

76. Stress at each time-step can also be used to generate stress time-histories as shown in Figures 4.16 and 4.17. Time-

histories recorded at a location in the middle of the wall are shown in Figure 4.18. Figure 4.16 displays the stresses in the coordinate x, y, and z directions at a representative point in the middle of the wall. Figure 4.19 displays the principal stress time-history. The principal stress values are used for determining maximum tensile and compressive stresses, which can cause structural damage. For this study, the tensile stresses (psmax) are the stresses of interest since the material strength for tensile stresses is less than that for compressive stresses. The time-histories indicate several peak values which must be considered in determining stress values of interest. The stresses of concern for each time-history plot are the average of the highest six peaks.

77. Figure 4.20 displays the lateral velocities and Figure 4.21 displays the vertical velocities at the location shown in Figure 4.18. The average of the six maximum peaks indicates a lateral velocity of 0.0018 in./sec which is 1.5 times greater than the lateral velocity of the ground motions. The 1.5 increase in lateral velocity corresponds to a dynamic amplification factor of 1.5.

78. The FE model of the two-story residential structure indicates a stress level of about 2 psi in the center wall away from corners and windows, and 45 psi below the windows. As with the one-story house, no damage was predicted since the stress values are below the strength capacity of the gypsum wallboard and plaster.

Comparison with Field Test

79. Figure 4.22 displays peak strains vs. peak ground velocity for wallboards while Figure 4.23 displays the envelope of peak strains vs peak ground velocity for block joints and brick veneer joints (Stagg et al. 1984). For the input velocity of 0.39 in./sec, the FE calculated strains in the wallboard and brick veneer joints for single-story house are shown.

80. The FE strains for wallboard are consistent with previous studies and below the CTS at a maximum ground velocity of 0.39 in/sec. Since the finite element analysis is linear elastic, the linear prediction is obtained simply by scaling the finite element result proportionately to any selected peak ground velocity divided by 0.39 in./sec (the scaled maximum amplitude of the selected ground motion). The resulting linear prediction is shown (Figure 4.22) by the inclined and dotted line through the finite element result. The correlation between the FE strain and the studies by Stagg et al. (1984) further verify the FE results and verify that study houses respond in the same manner as houses in previous studies.

81. Figure 4.23 shows selected maximum responses of block joints and selected maximum and minimum responses for brick veneer joints measured by Stagg (Stagg et al. 1984). The FE result for the maximum response of a brick wall (from the Section "Dynamic Responses of Brick Veneer") is shown as the solid oval using the scaled selected ground motion for a peak ground velocity of 0.39 in./sec. Again, the FE analysis is linear elastic so the linear prediction is obtained by scaling the finite element result proportionately to any selected peak ground velocity divided by 0.39 in./sec (the scaled maximum amplitude of the selected ground motion). The resulting linear prediction is shown by the inclined and dotted line through the finite element result.

82. The recorded brick and block response by Stagg et al. (1984) is above the highest level of CTS which indicates the possibility of cracking of the mortar joints. Also, Figure 4.23 shows a linear prediction based on fitting a line through the minimum recorded data. This fit exceeds the calculated response of a simple elastic model of a brick wall. Again, the recorded brick and block response includes strain resulting from the opening of cracks. The largest difference occurs at high peak ground velocities because of the increase of nonlinear behavior of the cracks. Differences are due to the simplicity of FE

modeling corners and the interaction with the framing members. However, even the conservative FE model predicts strain levels above the minimum computed CTS. This analysis leads to the same conclusion based on the recorded brick and block response data. This suggests that threshold damage of block and brick veneer joints may occur if the peak ground velocities equal or exceed 0.13 in./sec. The level of threshold material damage would not affect the ultimate load-carrying capacity of the block or brick wall.

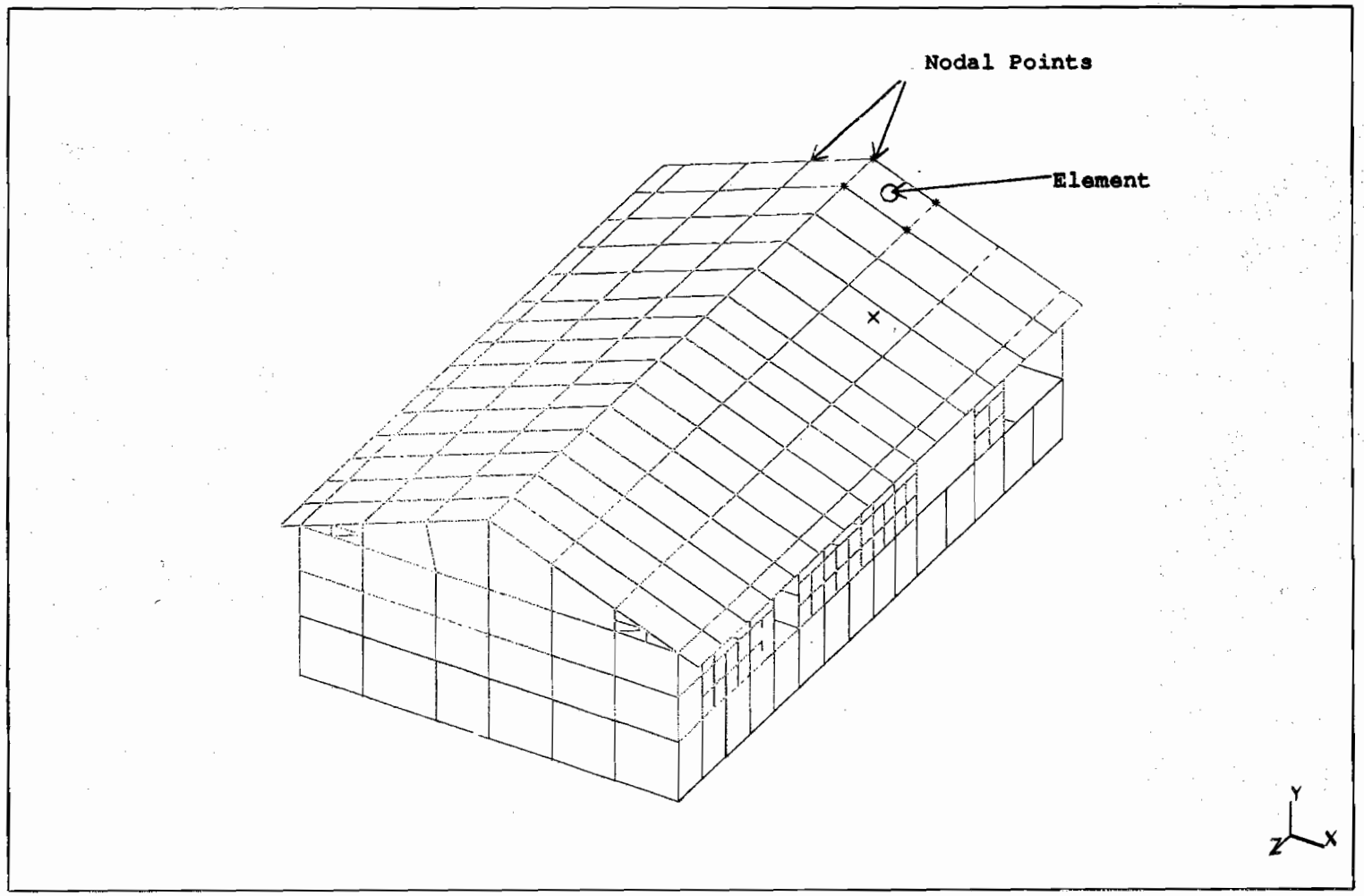

Figure 4.1 Finite-element grid of single-story house

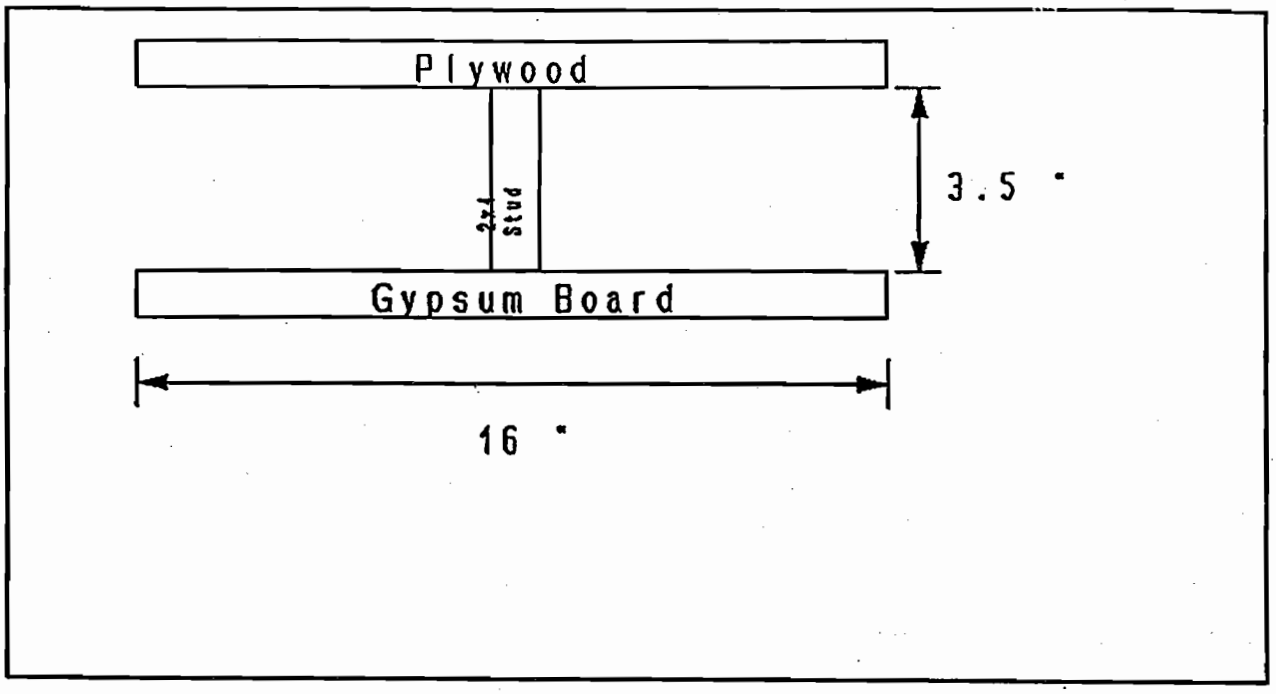

Figure 4.2 A typical wall section for the single-story house

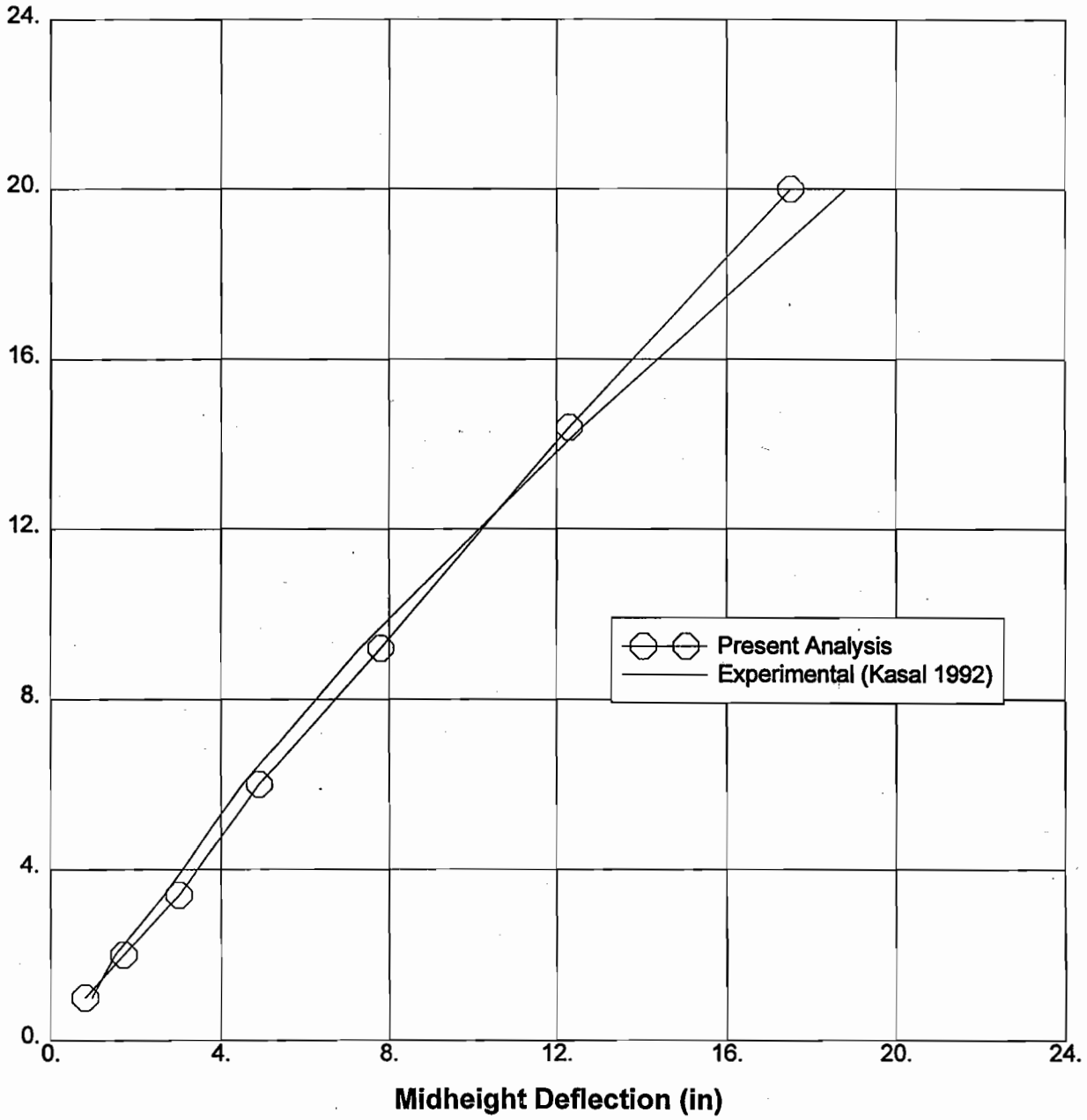

Figure 4.3 Experimental (Kasal, 1992) and analytical results for wall

Time=2.92 Seconds
Brick E=2.E6 psi

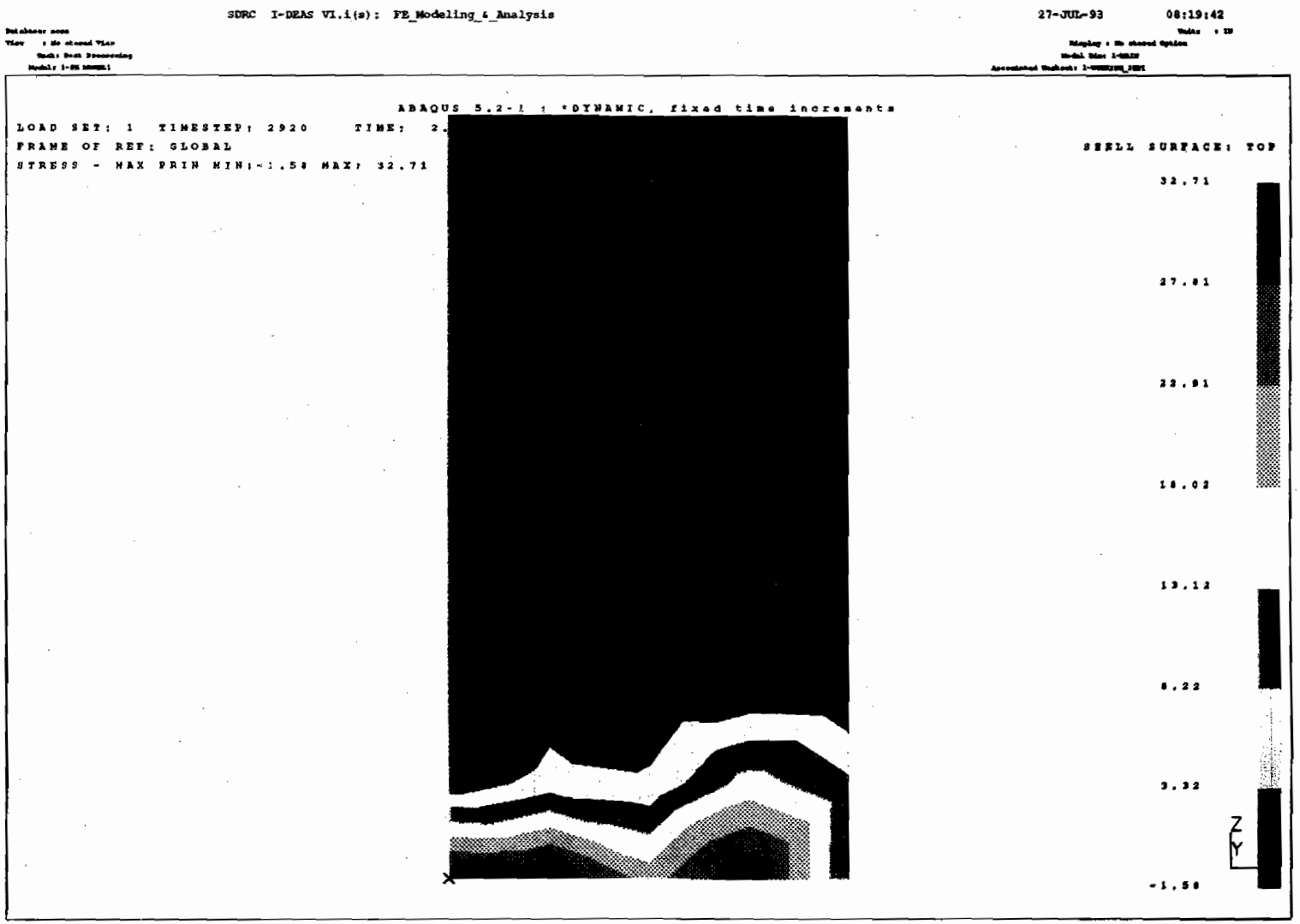

Figure 4.4 Maximum principle stress at 2.92 seconds, brick veneer wall

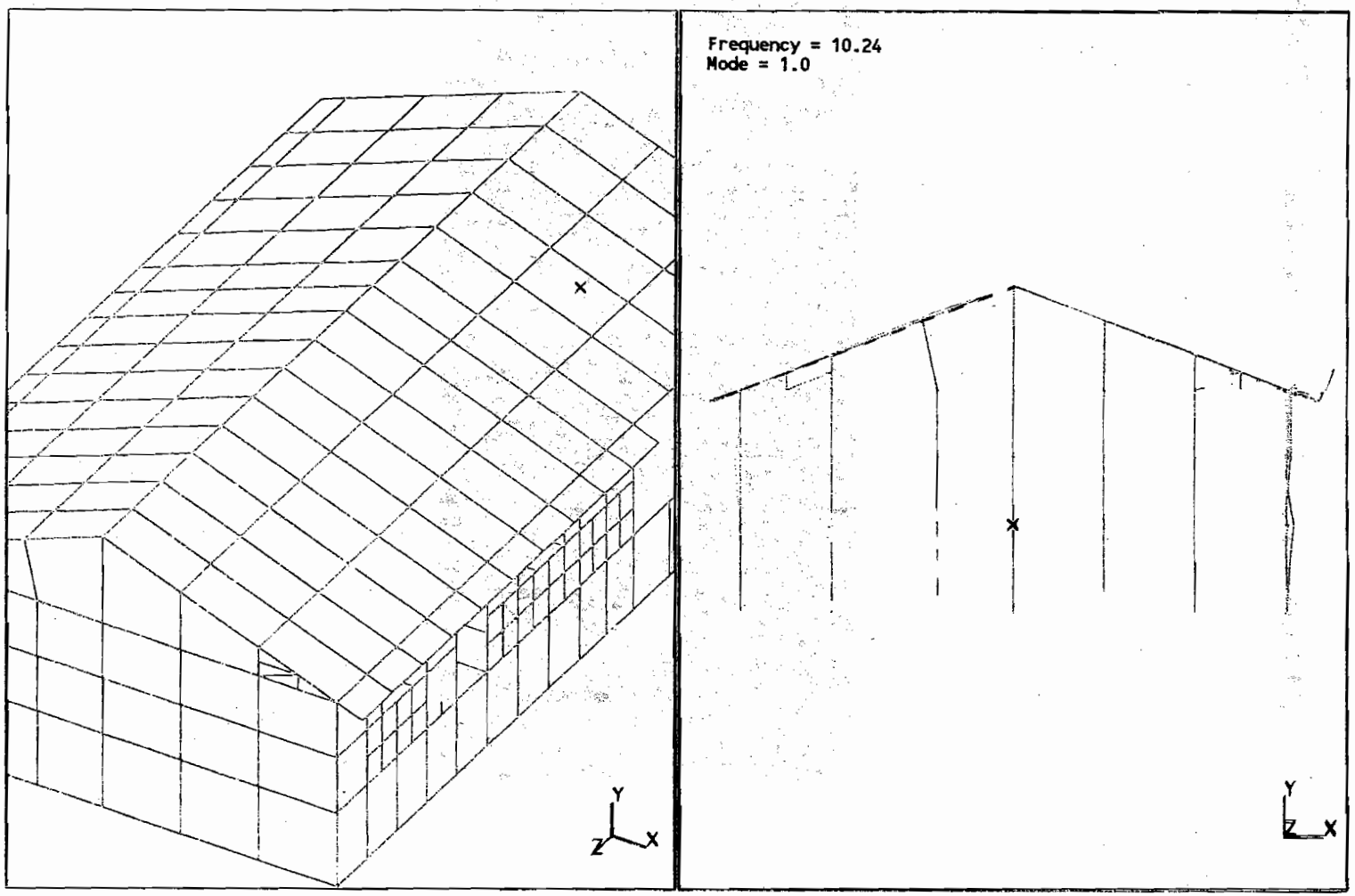

Figure 4.5 First mode shape of the single-story house

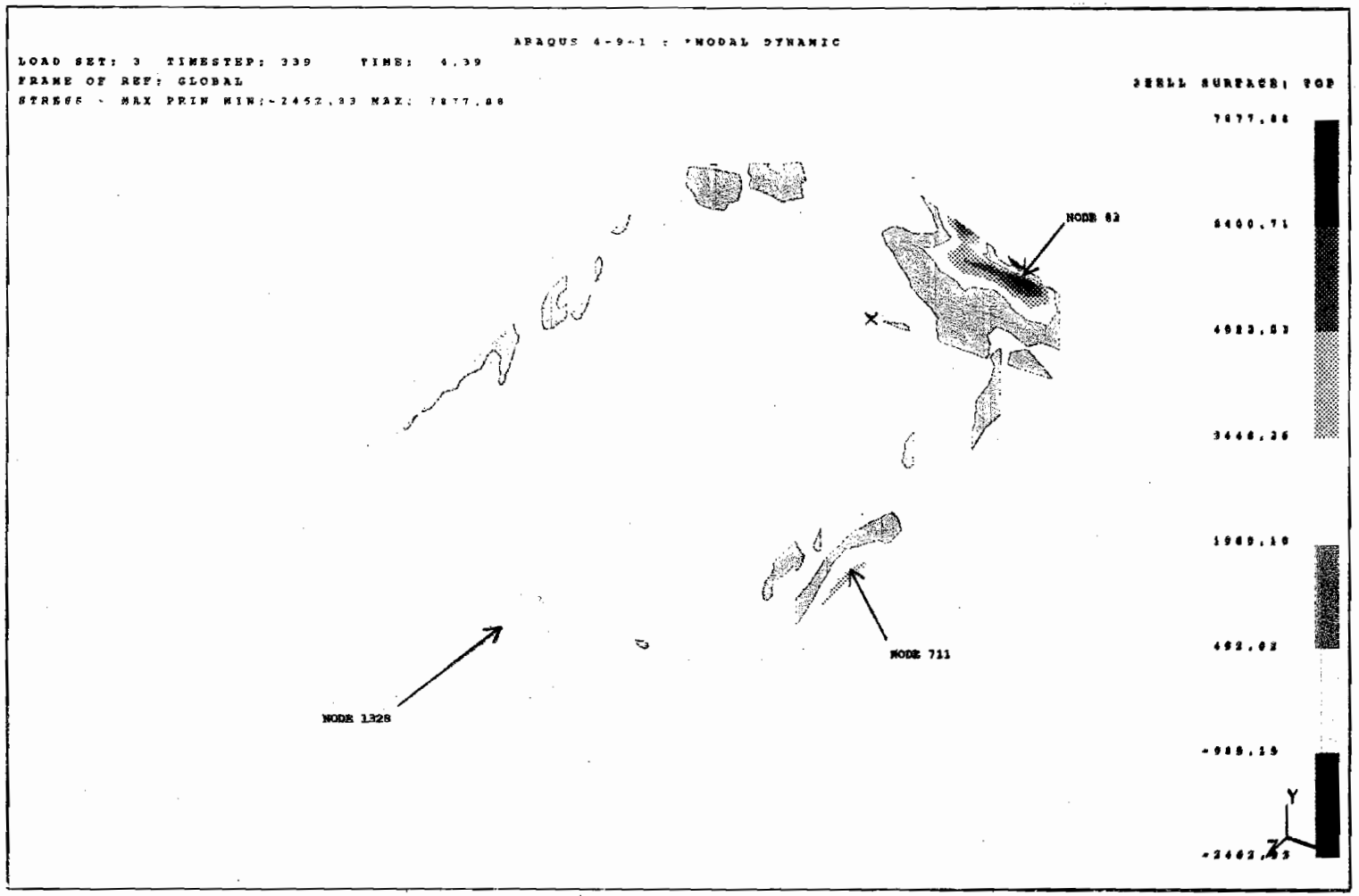

Figure 4.6 Principal stress-vector plot (in psf) on exterior wall of the single-story house (FE results)

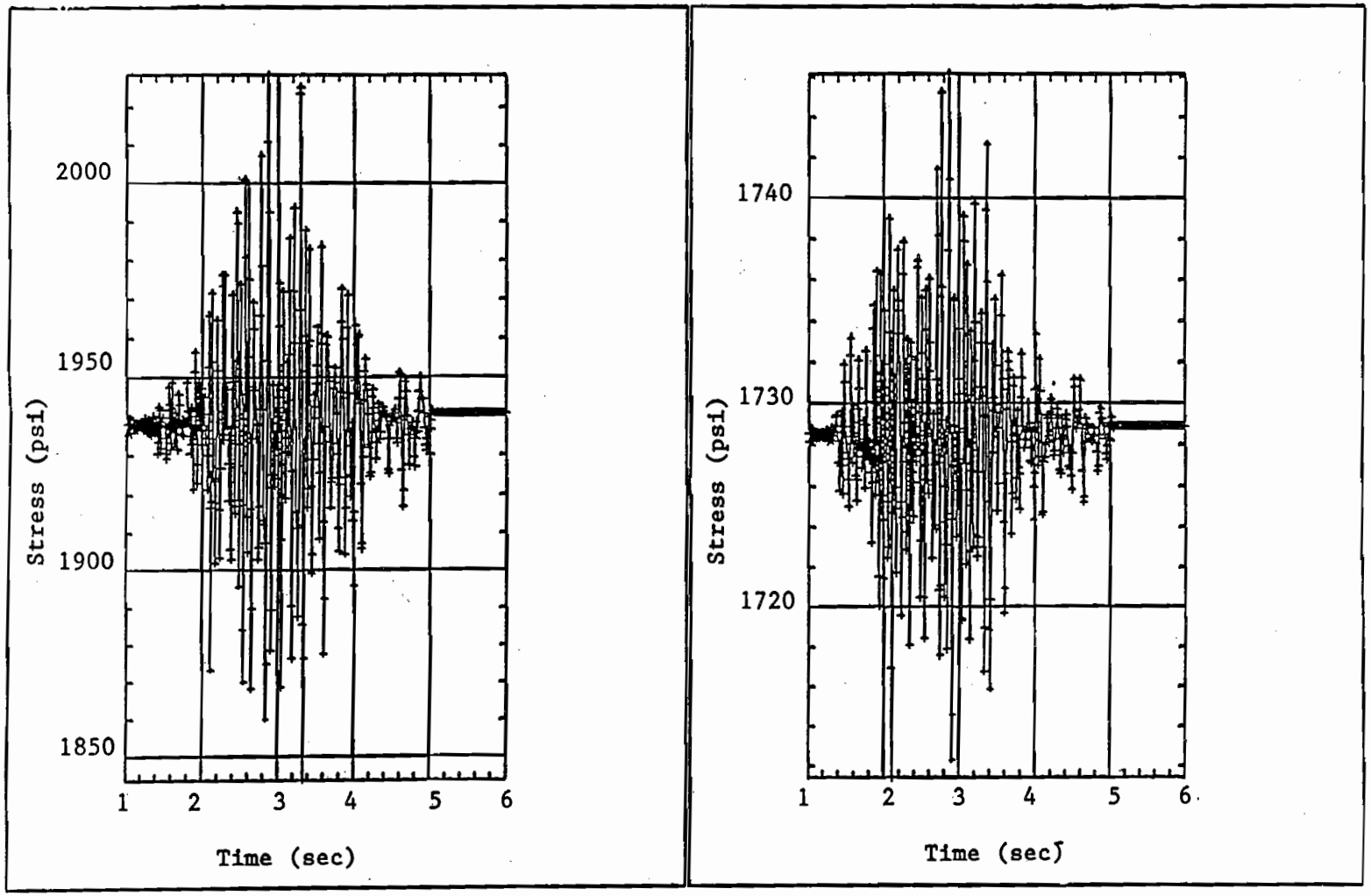

Figure 4.7 Maximum and minimum principal stress for Node 83

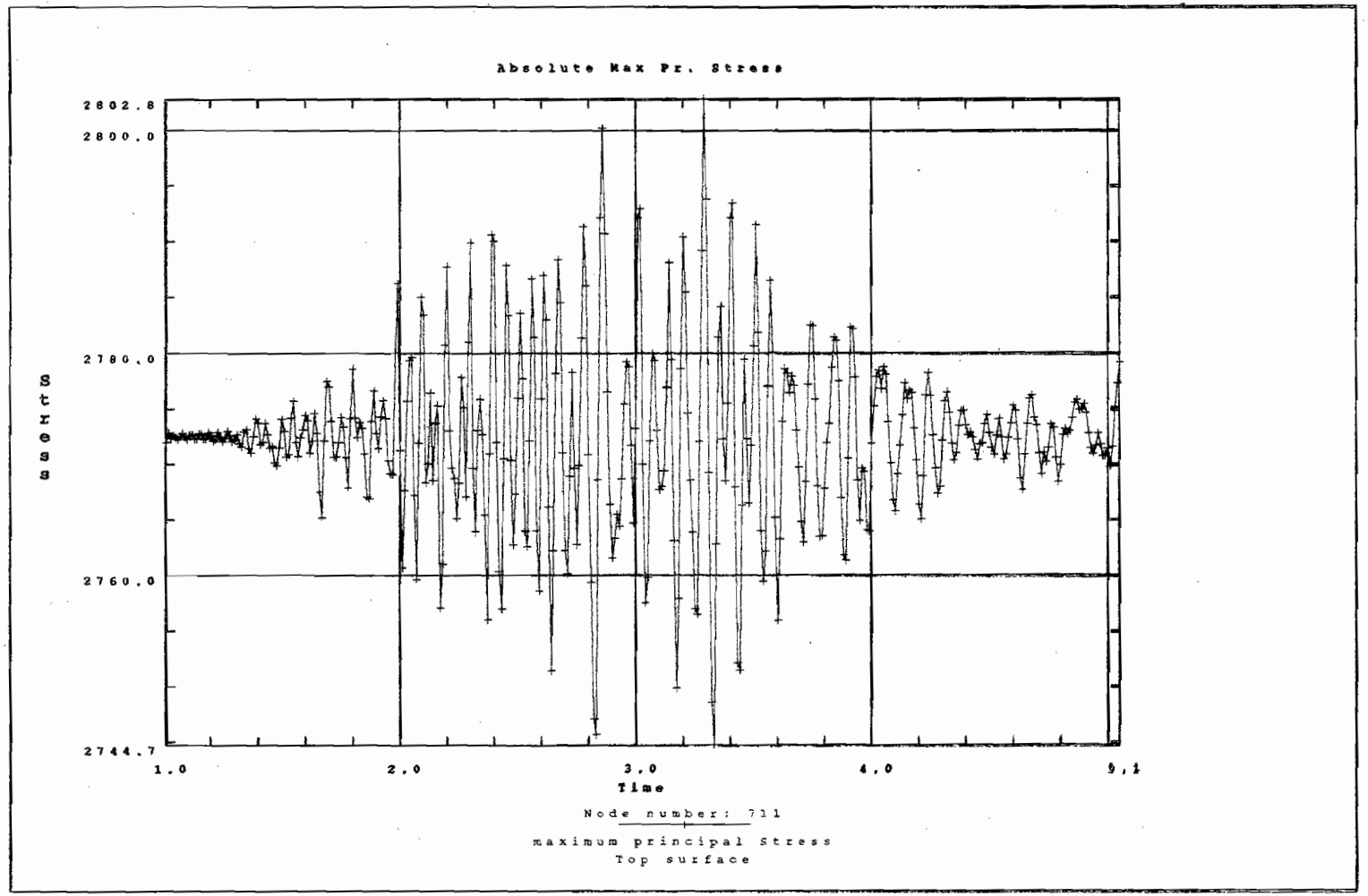

Figure 4.8 Principal stress time-history for the single-story house (FE results in psf)

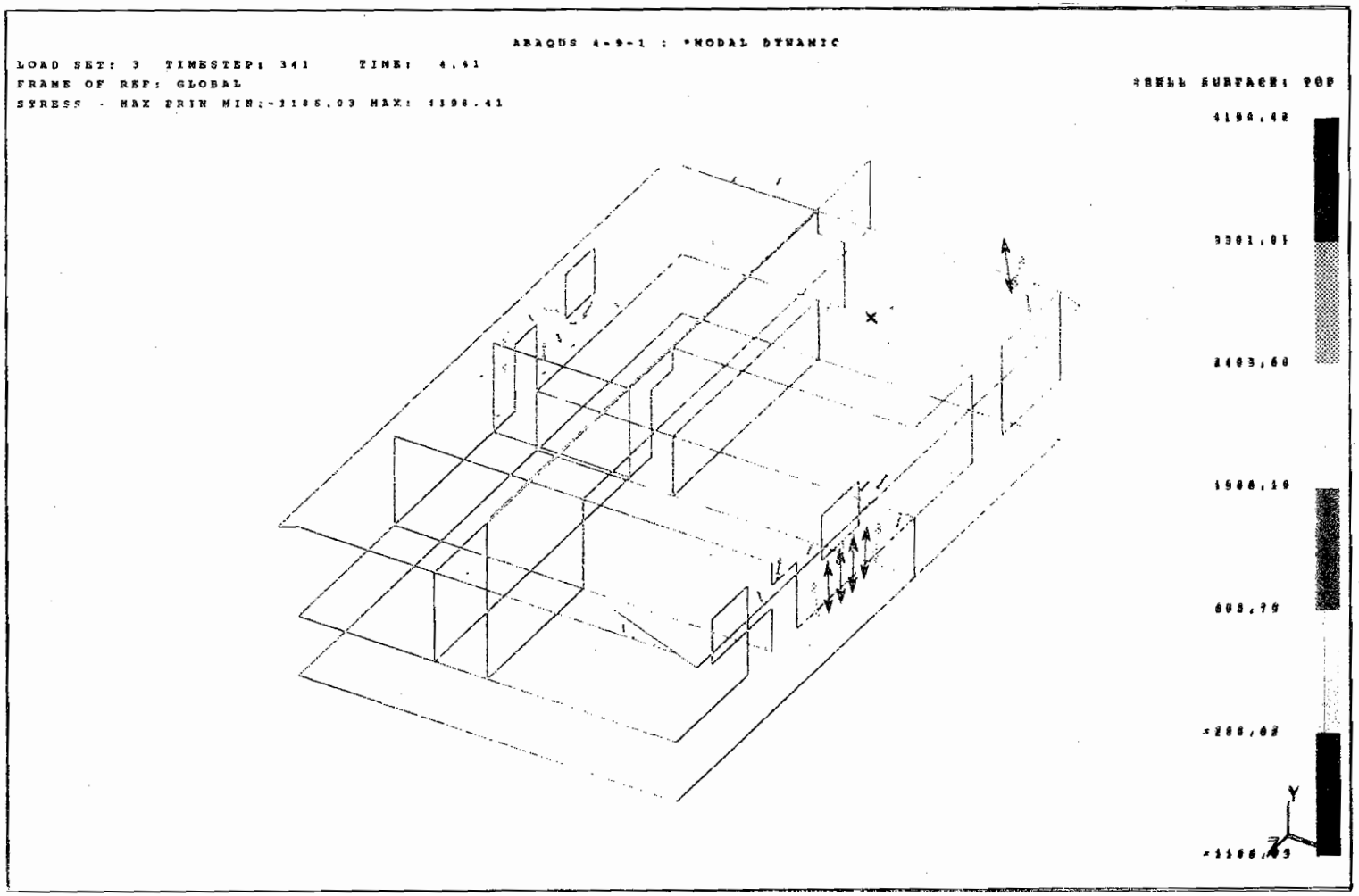

Figure 4.9 Potential crack-pattern on exterior wall of the single-story house

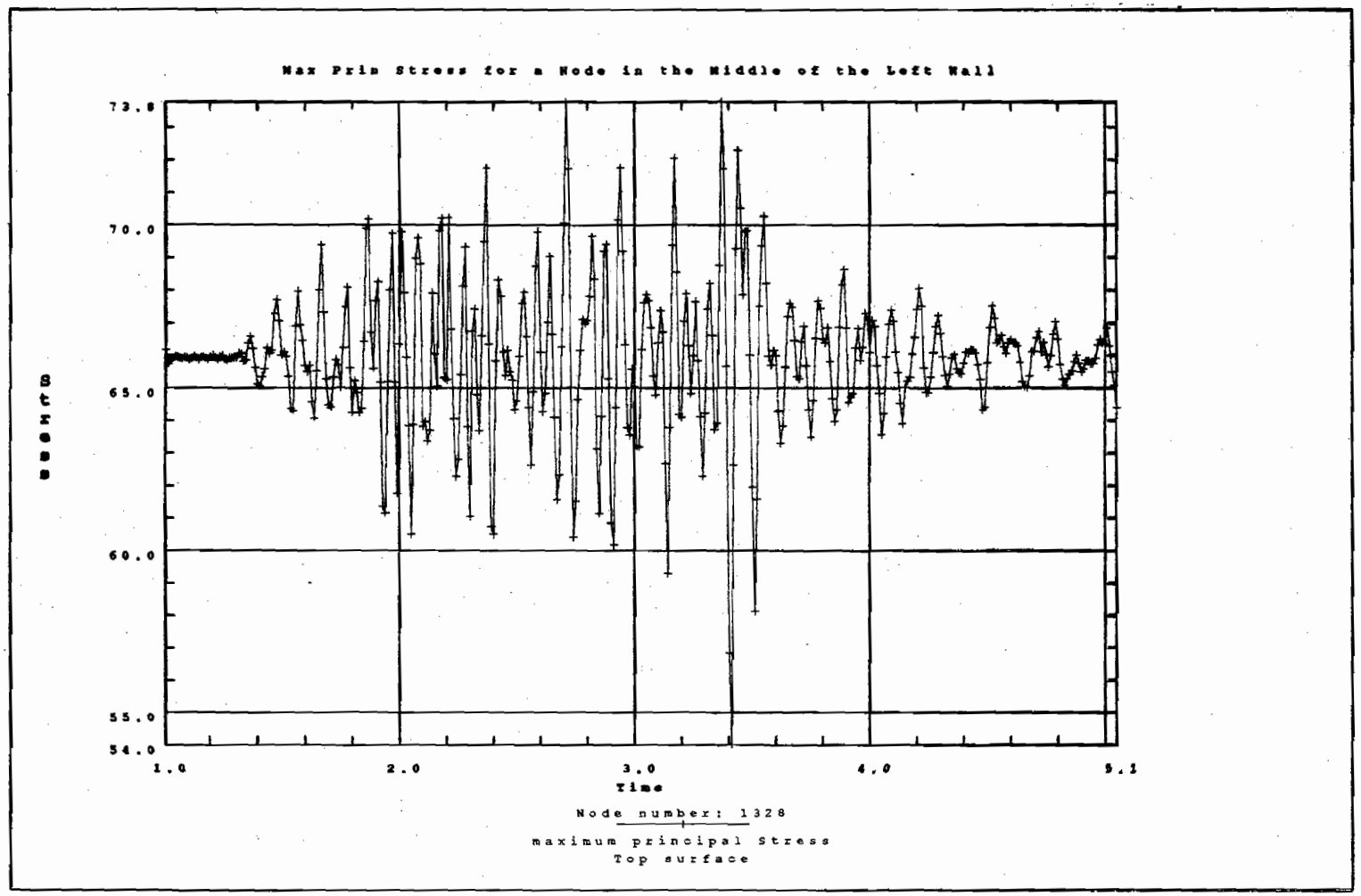

Figure 4.10 Principal stress time-history for middle of exterior wall of single-story house (FE results in psf)

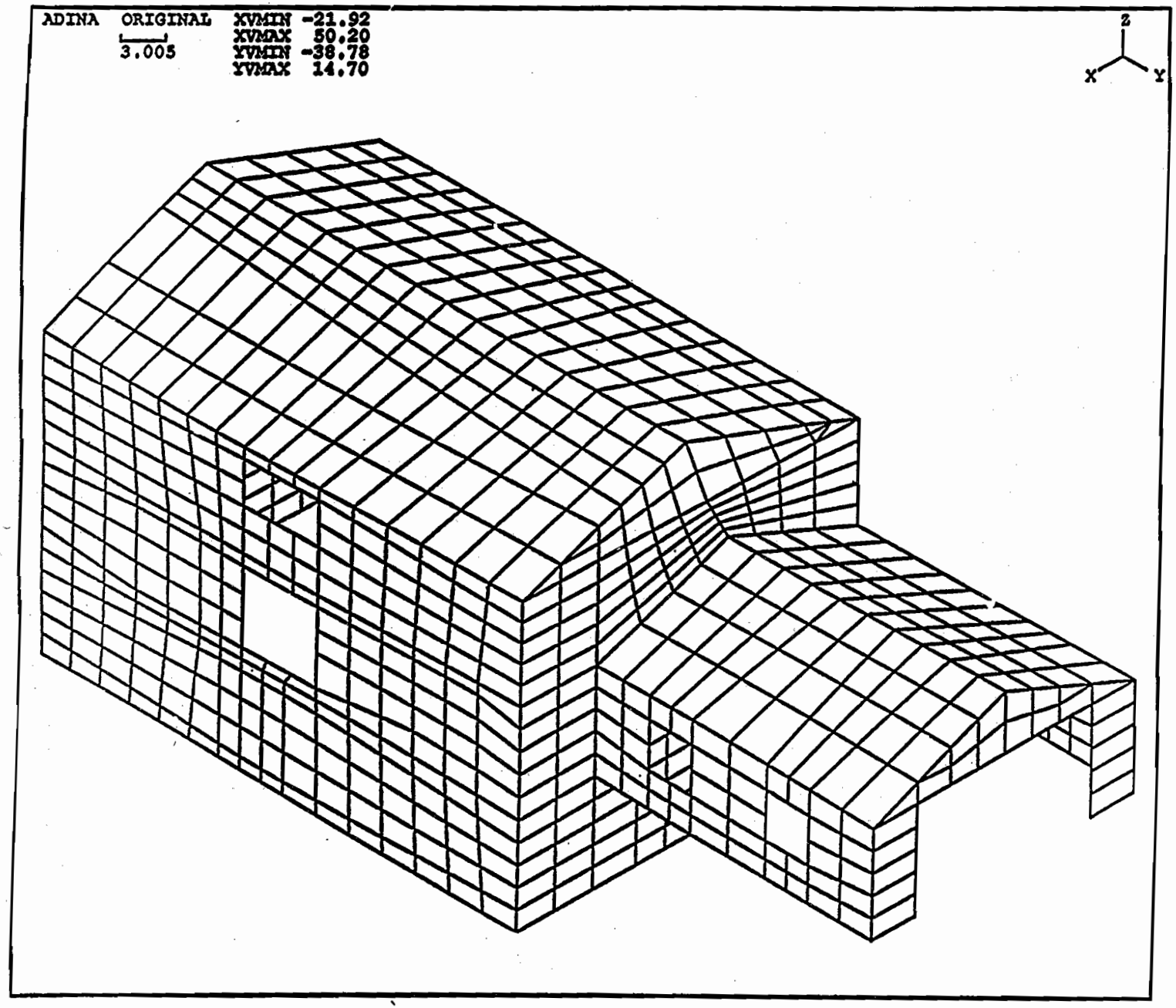

Figure 4.11 Finite-element grid of two-story house

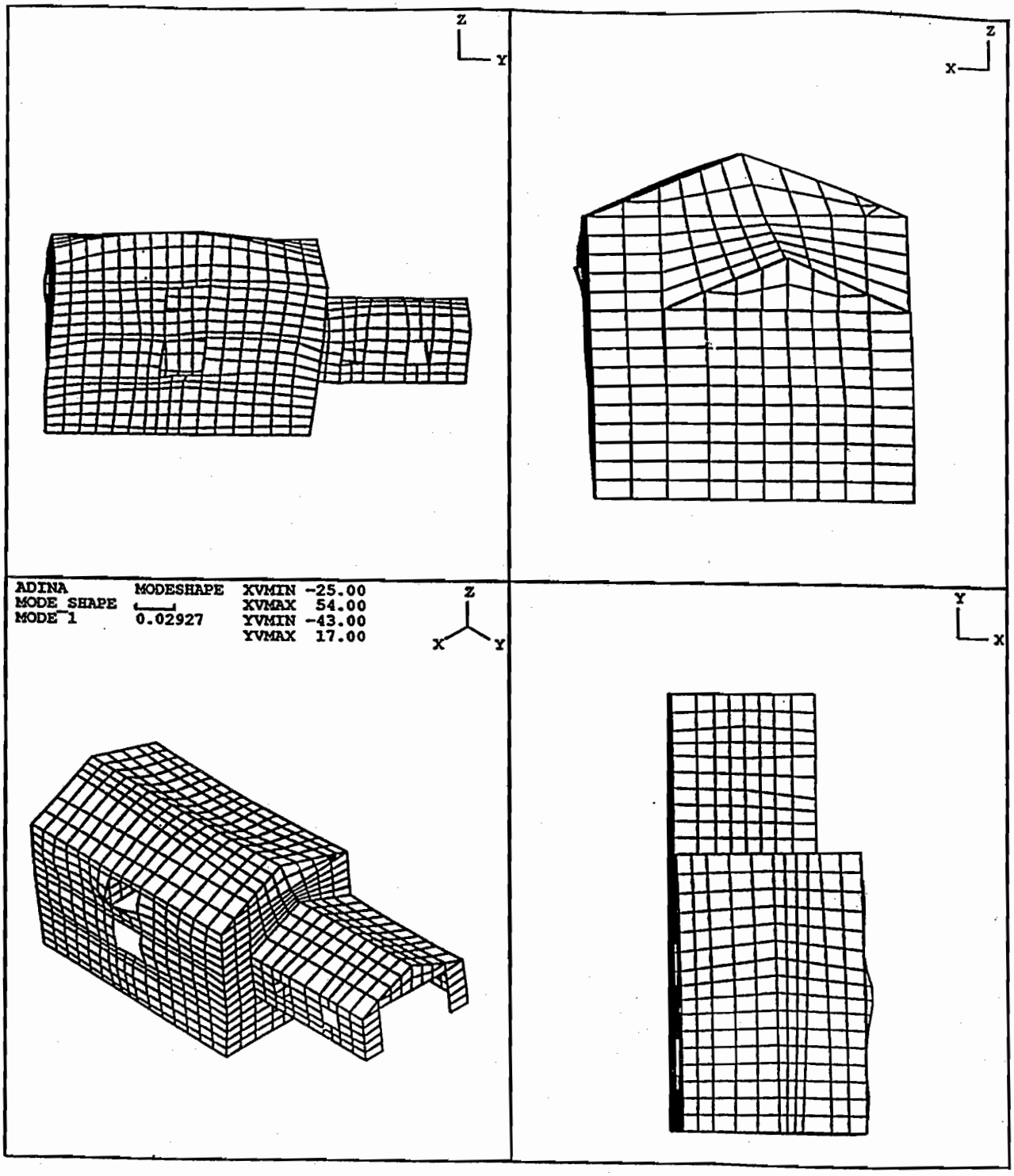

Figure 4.12 First mode shape of the two-story house

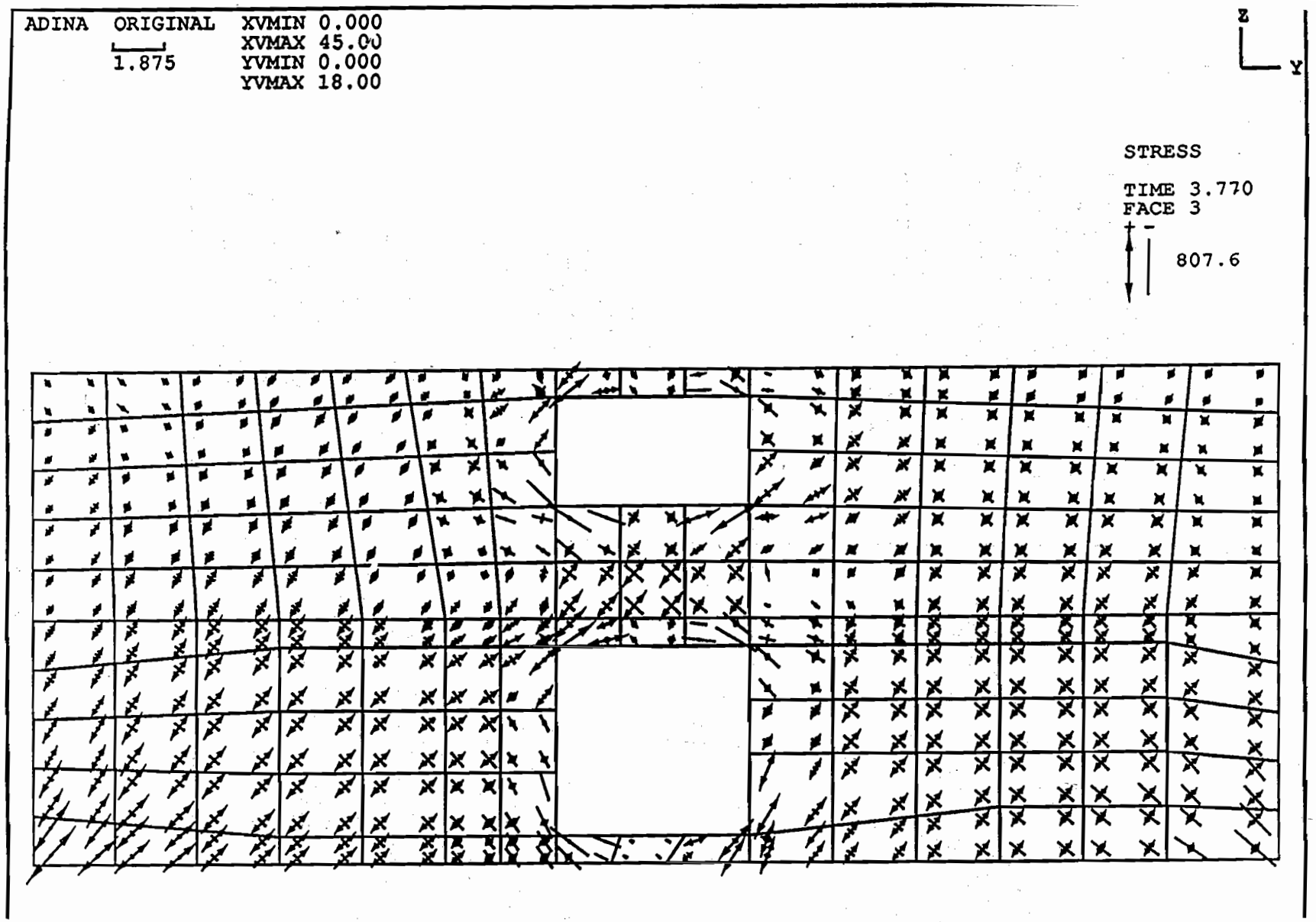

Figure 4.13 Principal stress-vector plot on exterior wall of the two-story house (FE results)

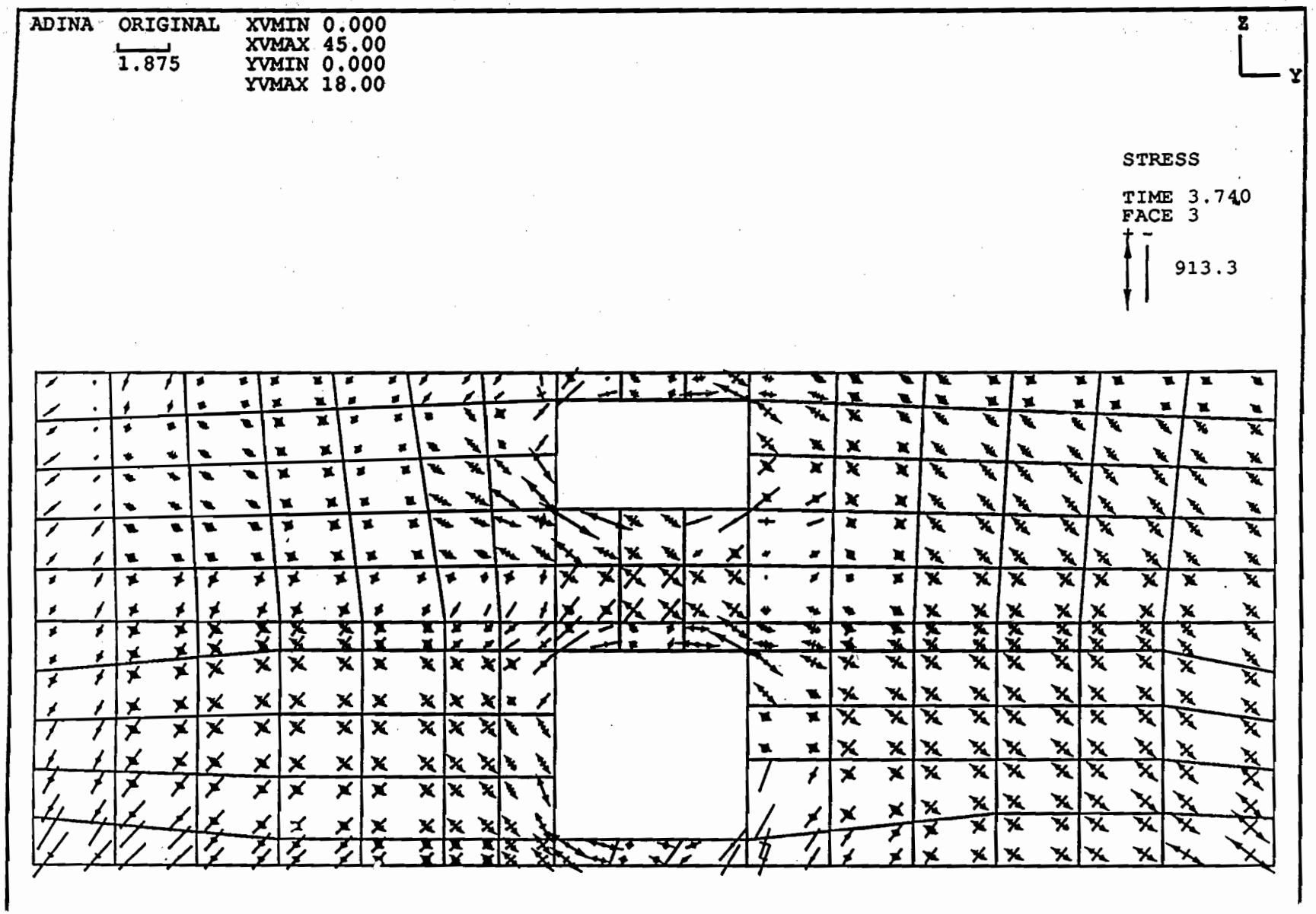

Figure 4.14 Principal stress-vector plot on interior walls of the two-story house (FE results)

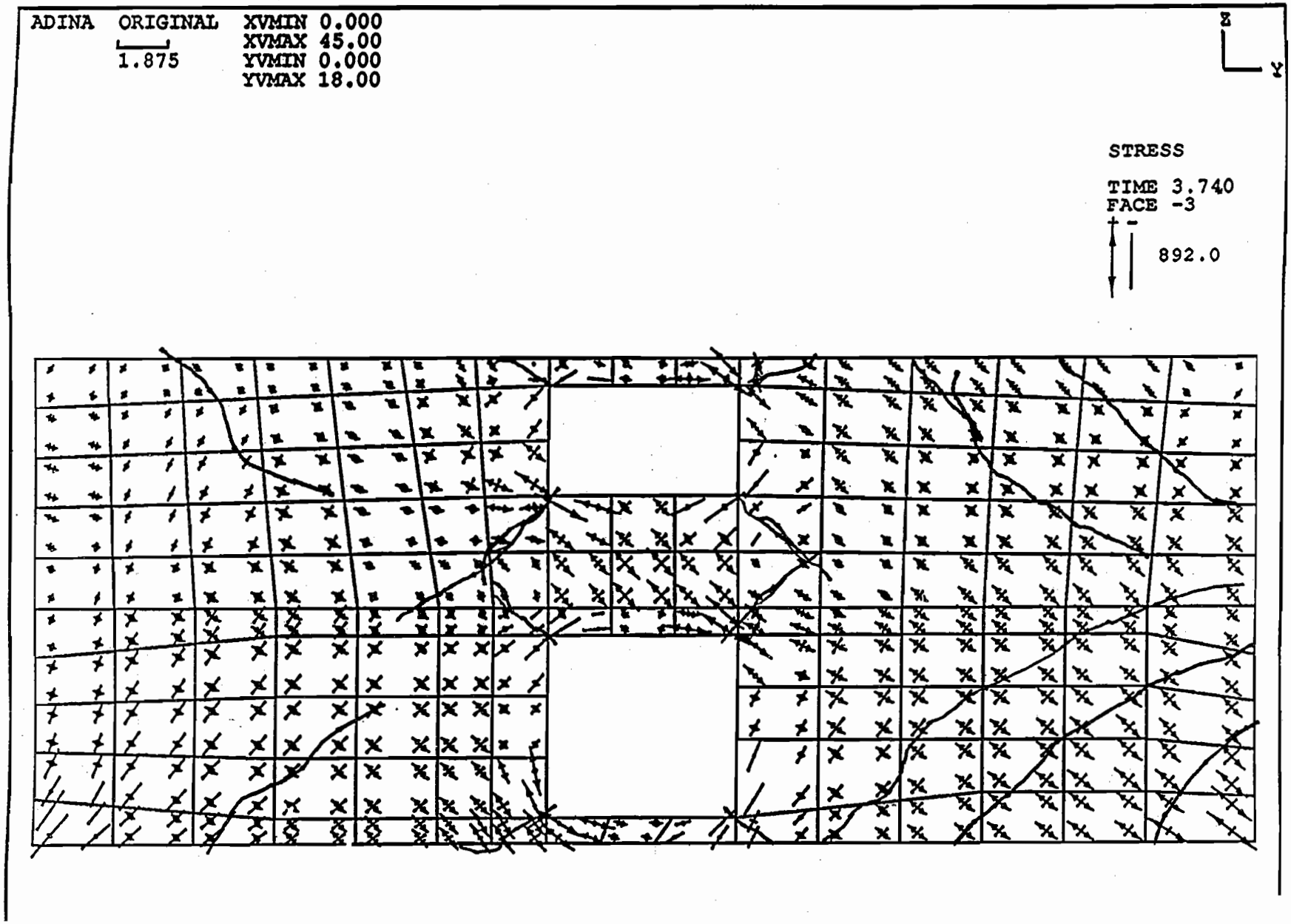

Figure 4.15 Potential crack-pattern on exterior wall of the two-story house

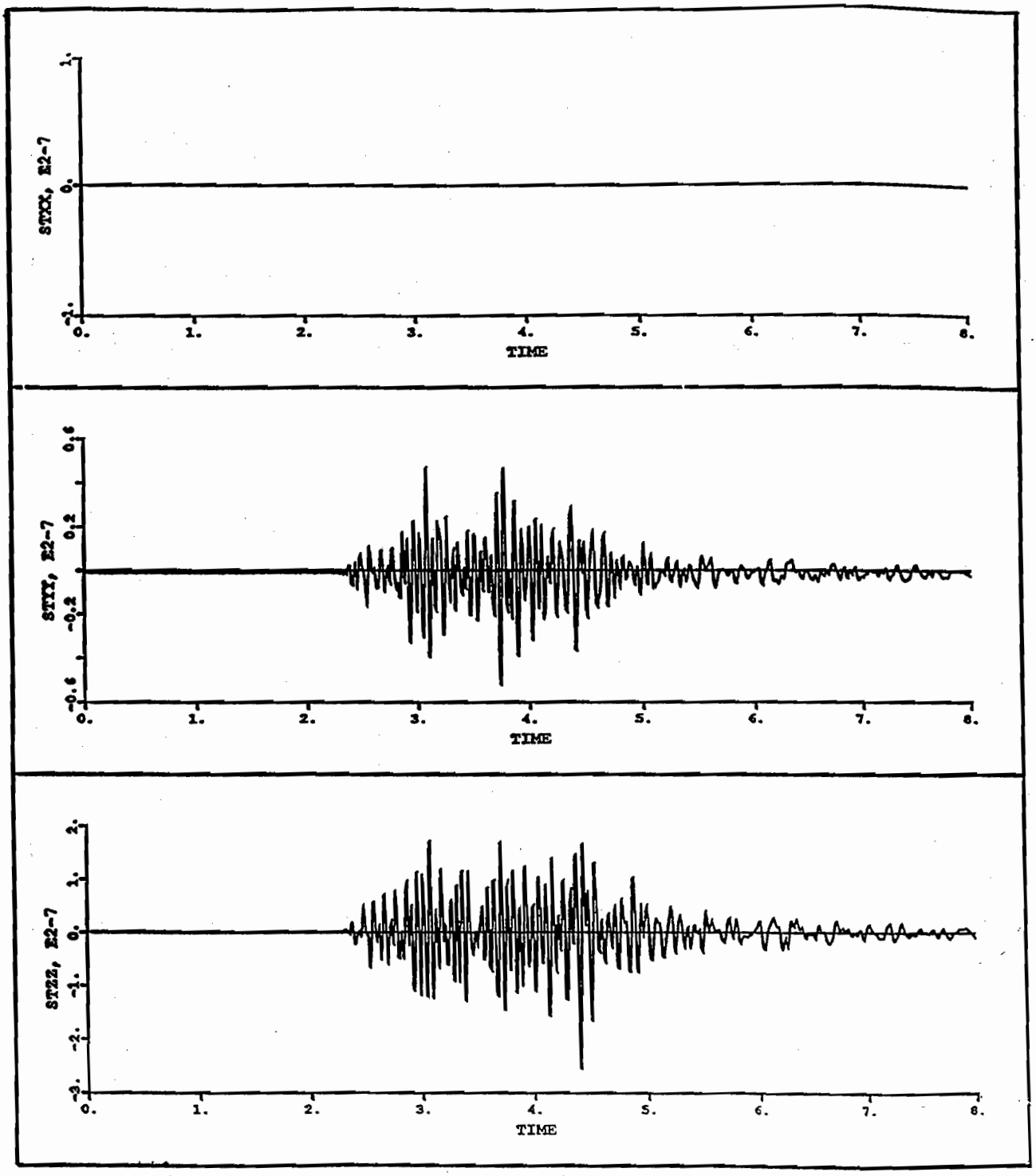

Figure 4.16 Stress time-history in the coordinate axes of the two-story hous
(FE results)

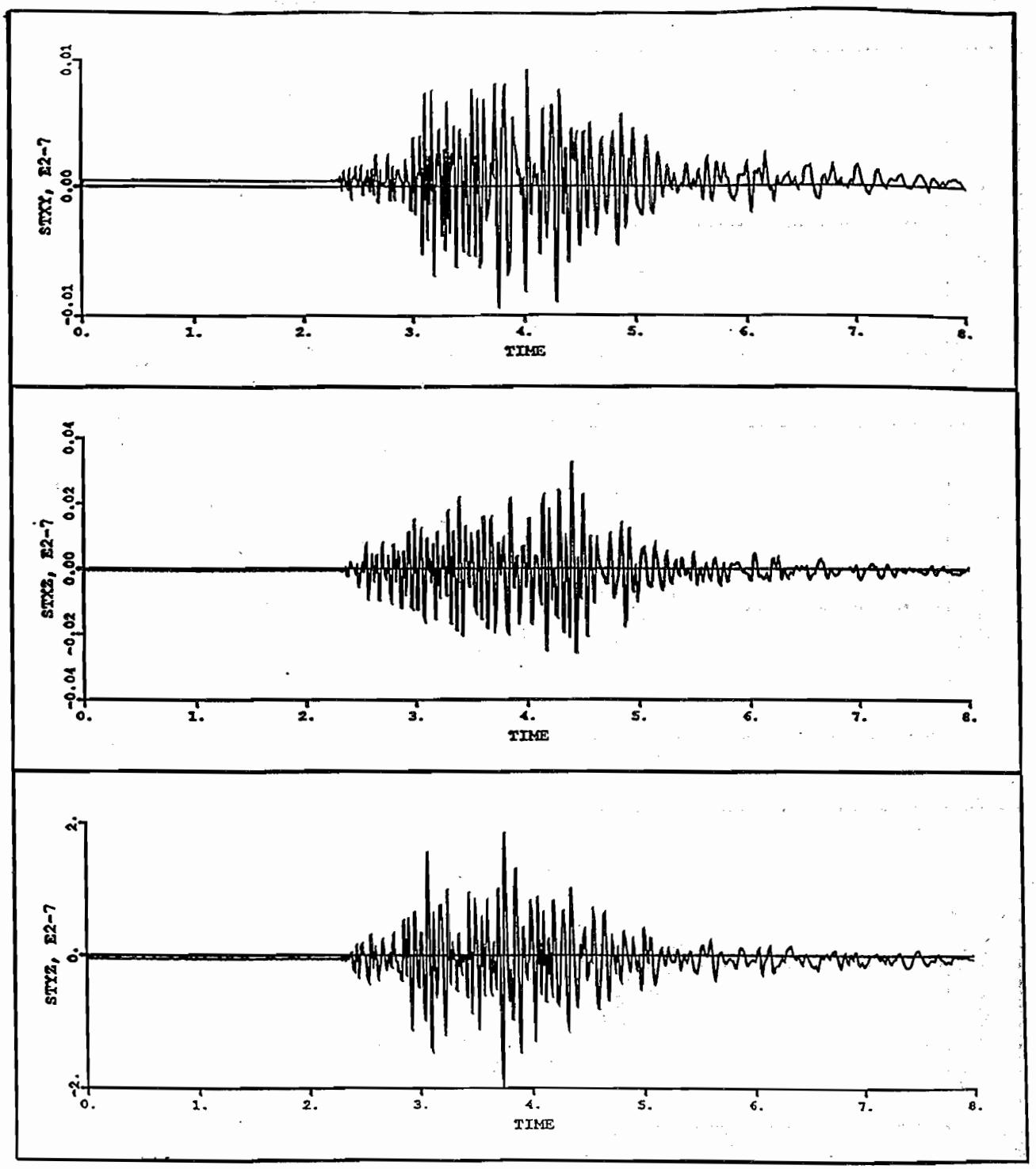

Figure 4.17 Shear stress time-history of the two-story house (FE results)

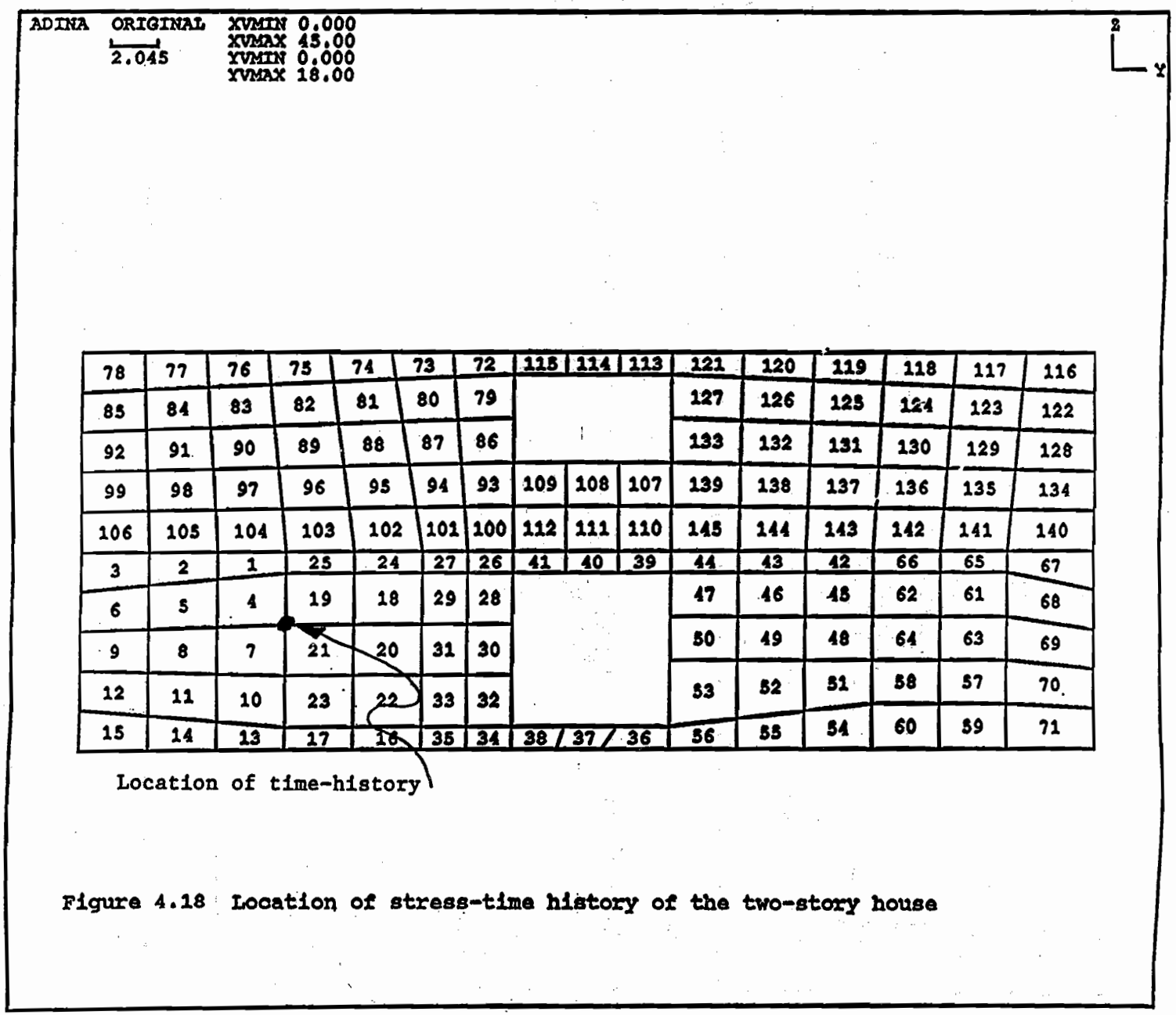

Figure 4.18 Location of stress-time history of the two-story house

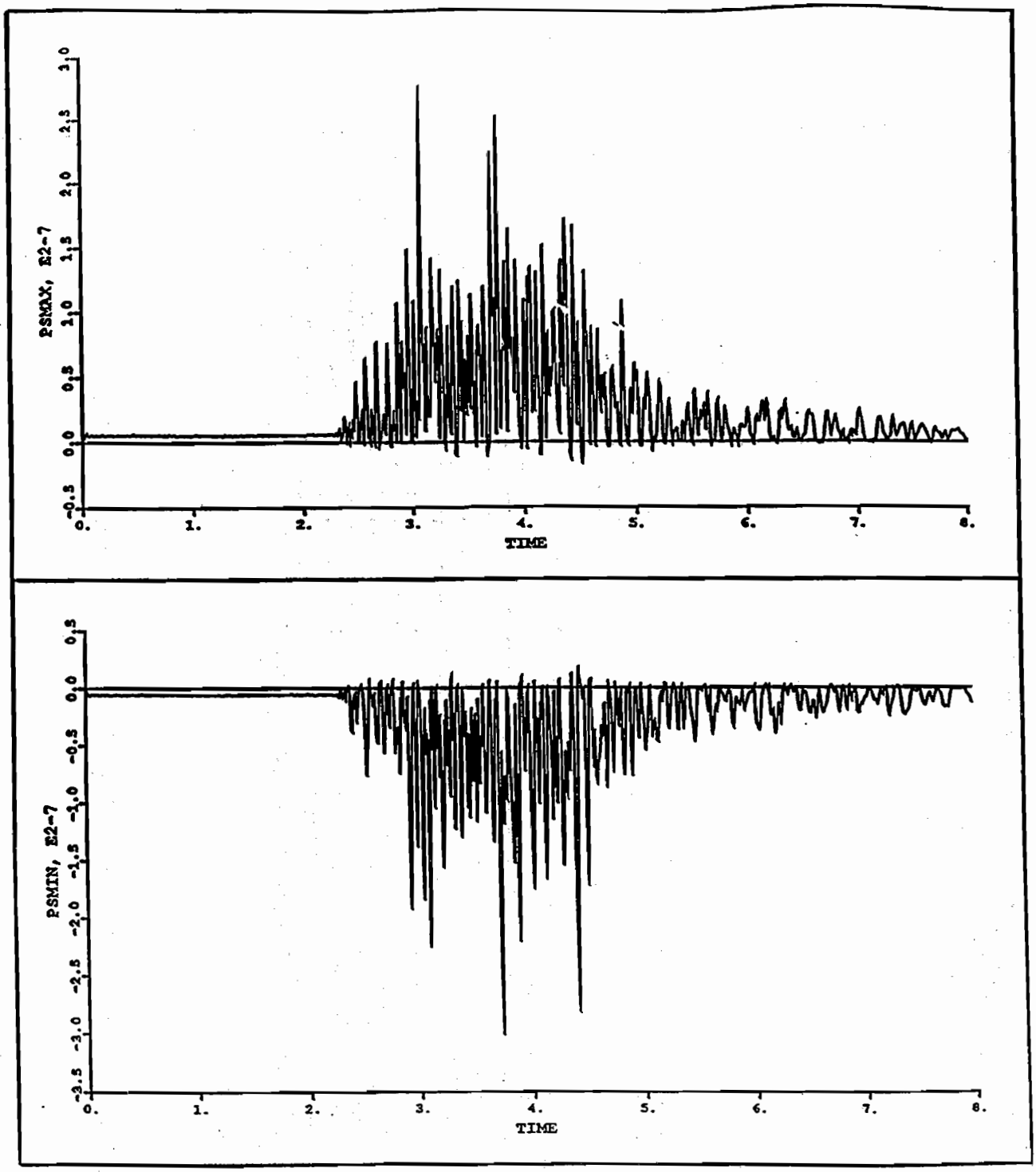

Figure 4.19 Principal stress time-history for the two-story house (FE results)

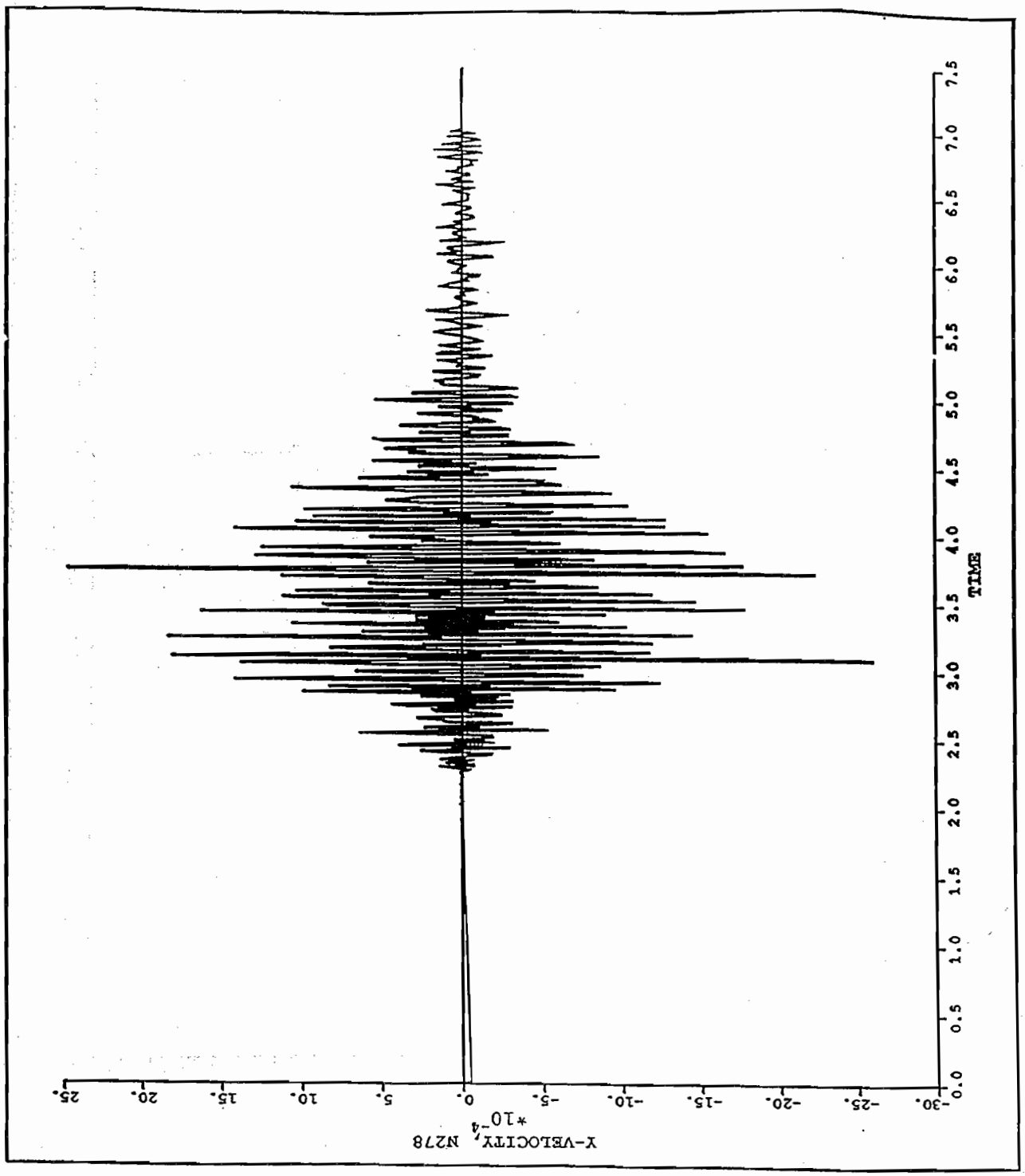

Figure 4.20 Lateral velocity (ft/sec) for two-story house (FE results)

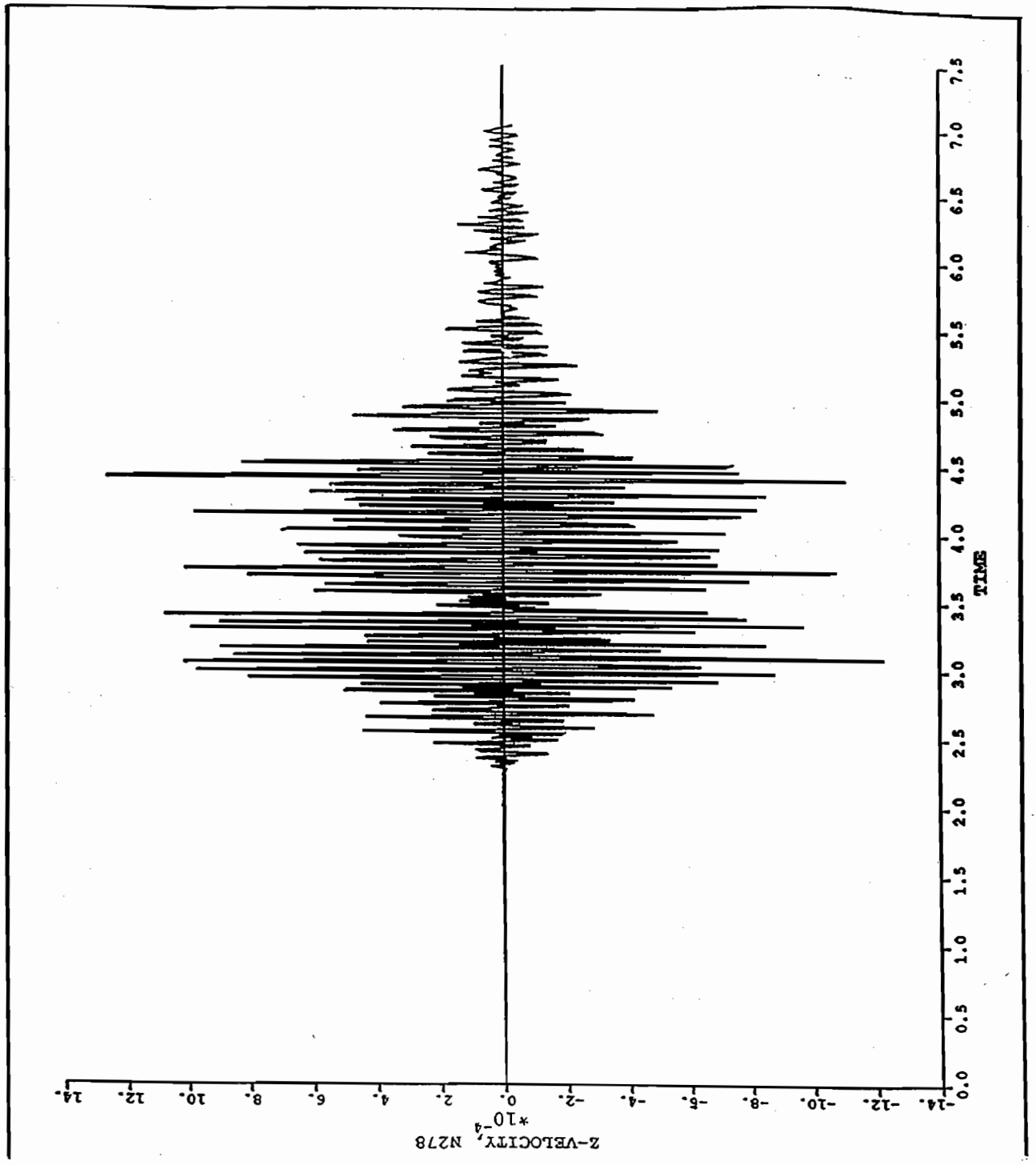

Figure 4.21 Vertical velocity (ft/sec) for two-story house (FE results)

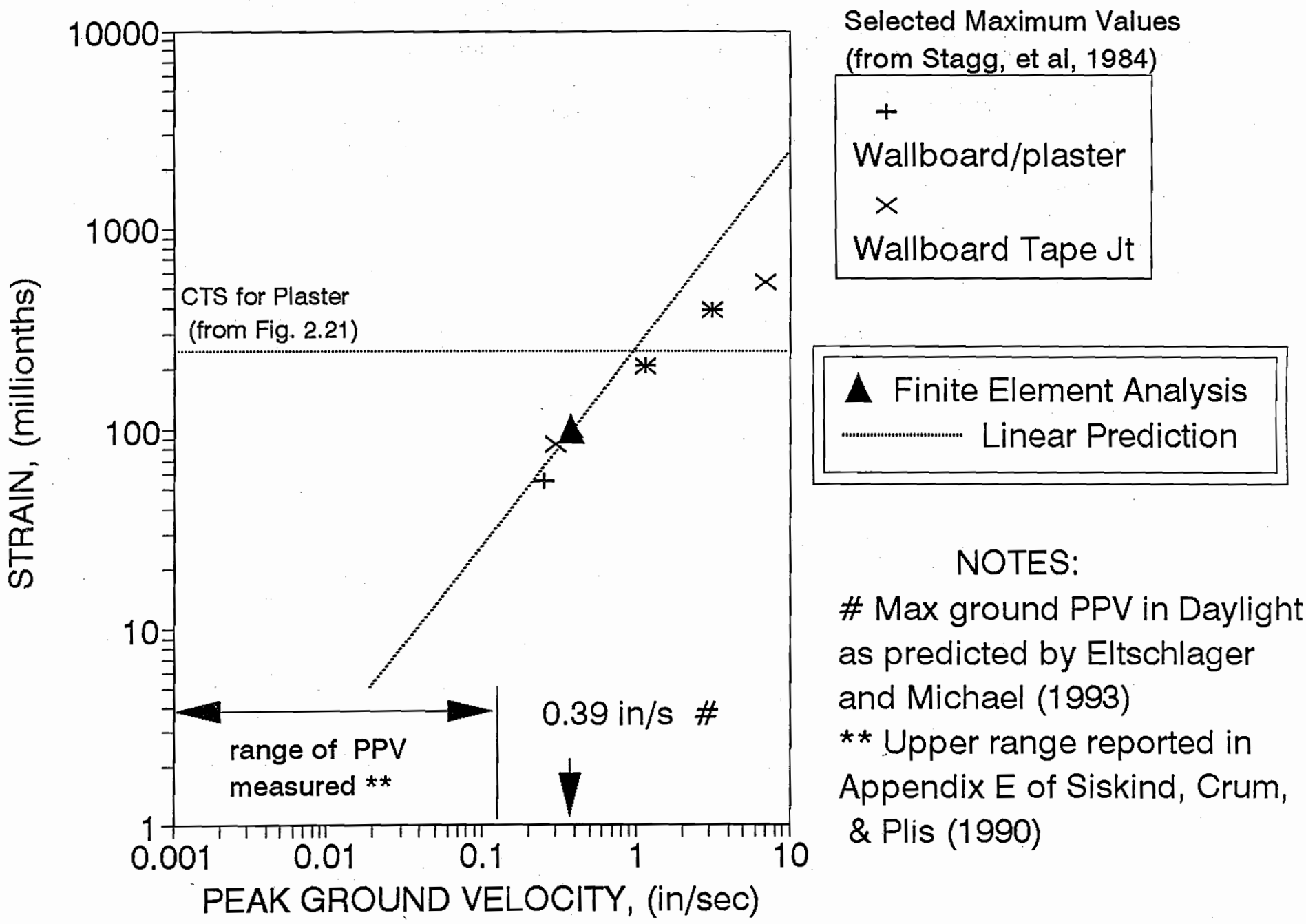

Figure 4.22 Peak ground velocity versus strain

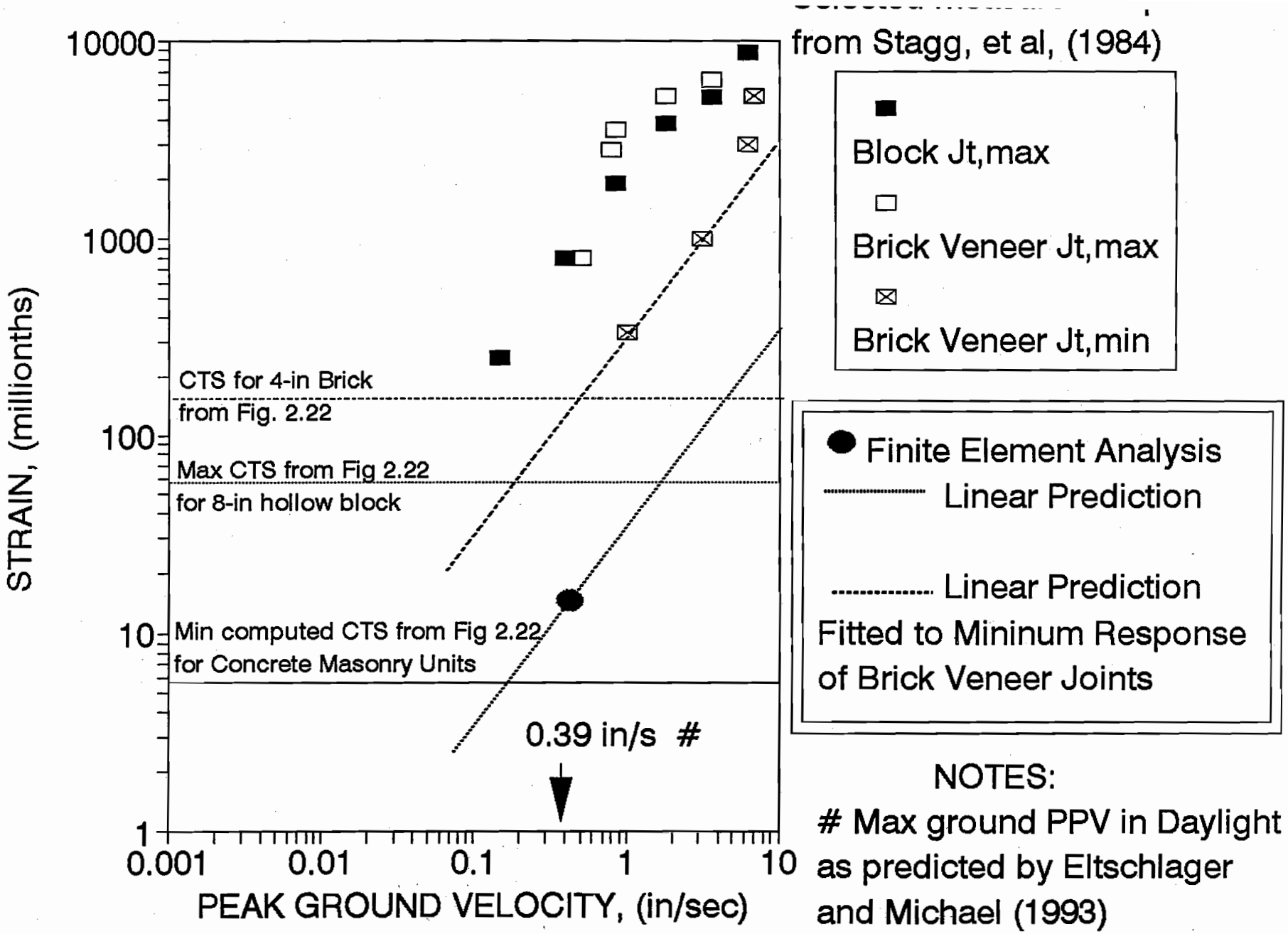

Figure 4.23 **Selected maximum responses of block joints and selected maximum and minimum responses for brick veneer joints measured by Stagg (Stagg, et al., 1984) and fitted linear predictions.**

CHAPTER 5: FATIGUE

General

83. This chapter evaluates whether fatigue is a reasonable threshold damage mechanism. Fatigue is defined as inelastic material response due to repeated application of loads which produce stresses below the elastic limit. Hence, it is important to assess the number of cycles and magnitudes of stress and strain to cause threshold damages in the subject houses and the number of cycles from produced blast-induced vibrations (i.e. by material fatigue) from repetitive vibration events. The cumulative blast-induced vibrations and corresponding magnitudes of stress and strain are compared to existing fatigue test data.

84. Kiger (1992) (Appendix E) reviewed various references dealing with the homes in the subject area and found that Siskind et al. (1990) indicated that a 5- to 10-in./sec PPV blast vibration is the threshold PPV that is required to crack concrete walks, driveways, and foundations, and to cause major superstructure cracks. Siskind et al. (1990) also reported that threshold damage (visible superficial hairline cracks in wall board joints) occurs at 56,000 cycles at a PPV of 0.5 ips. The highest PPV recorded in the referenced study was 0.13 in./sec with the majority of data being 0.01-0.05 ips (Table 2.2). Eltschlager and Michael (1993) predicted that a maximum value of 0.39 in./sec could have occurred in Daylight, and a maximum value of 0.17 in./sec could have occurred in McCutchanville. It is important to note that even these maximum predicted values of PPV are at least an order of magnitude lower than the PPV to cause major damage. At this low level of vibration, it was not believed that the major damage observed, i.e., cracking of basement floors and driveways, could be attributed to material fatigue failure. In any case, those structural elements that are loaded in compression, such as basement walls, will not fail in

fatigue unless tension is induced through other loads (i.e., excessive lateral earth pressures, or other compromising pre-existing load conditions).

85. There are other techniques available for evaluating fatigue such as the deterministic procedure of Palmgren-Miner. Yang (1986) has shown that the Palmgren-Miner deterministic hypothesis is valid to analyze the stress cycle fatigue characteristics of basement walls and other selected structural components of the house if the data show a linear trend when plotted on a Log-Stress vs Log-Number-of-Cycles-to-Failure Curve. However, there are not sufficient data to construct the stress vs number-of-cycles-to-failure curve for wallboard, which eliminates the use of this procedure for these studies. Sufficient data exist to show fatigue of hard wood is not likely here (Stagg et al. 1984) but more data are necessary for evaluation of the fatigue characteristics of brick, wallboard in its installed condition, and plaster coatings on wallboard. The data from Stagg et al. (1984), Leigh (1974), Beck (1978), and this report can assess whether fatigue is a credible damage mechanism.

86. When evaluating material fatigue, it is important to understand that fatigue can occur only from cyclic loads which result in tensile stresses. As Figure 5.1 illustrates, the magnitude of the load as shown by percent of static strength at failure and the number of cycles to failure are the two critical parameters for determining fatigue loads. Figure 5.1 also indicates that for gypsum panels the cyclic load must exceed 70 percent of the yield strength for fatigue to be a problem at 100,000 cycles.

Discussion

87. An estimate of the total possible number of cycles of blast vibrations for a 10-year period, since 1983, is 156,000 cycles. This is based on an average of a predominant house-response frequency of 10 Hz for approximately 5 sec (50 cycles

per blast) at 6 blasts per week (300 cycles per week) times 52 weeks (15,600 cycles per year) times 10 years, which gives 156,000 cycles of vibration at 10 Hz for blasting since 1983. Siskind (1984) states that it would require at least 5 years to produce the necessary number of cycles to cause cracking in new wallboard at continuous sinusoidal shaking at 10 Hz of 0.5 in./sec peak response. In addition, the results of cyclic (cycled at 2 Hz) load tests on 1/2-in.-thick wallboard (Stagg, Siskind, Stevens, and Dowding 1984) show that 475,200 cycles were required to crack the wallboard at 0.5 in./sec peak response. The total number of cycles for a 10-year period at the house is almost a factor of 3 less cycles at lower velocities than that required in a controlled experiment.

88. Examining a typical blast response record as shown in Appendix B, it can be seen that the response decays abruptly, and the number of cycles with the largest responses occur only during the first 2 seconds. This leads to the conclusion that 62,400 is a more realistic value for the number of cycles. Based on this number of cycles and Figure 5.1, the peak acceleration of the records shown in Appendix B must result in strains of almost 70 percent of the static failure strain, which corresponds to a strain level of 182 millionths for fatigue to be a problem. This strain level of 182 millionths results in a stress of 104 psi in the wallboard. This stress level is almost twice as great at the maximum stress of 55 psi determined by the dynamic analysis of the single-story house. The largest reported peak velocity response recorded during any monitoring period of structural response is 0.13 in./sec. It has been determined that ground motion PPV of 0.39 and 0.17 in./sec was predicted as a worst possible case scenario for Daylight and McCutchanville (Eltschlager and Michael 1993), respectively.

89. The information presented by Kiger (1992) showed that a low level of vibration would not contribute to material fatigue failure. Table 5.1 presents data from shaker excitation (Dowding 1985). These data show the brick veneer mortar joint to be the most susceptible to blast vibration and indicate that the

brick veneer mortar joints could have hairline cracks from 15,000 cycles at 0.3 ips. This means that if the worst possible case scenario occurred 6 times a week for 52 weeks, some brick veneer might have some hairline cracks. Also, based on the data in Table 5.1, wallboard is the next weakest link. The required 0.5 ips at 52,000 cycles make mine-blasting operations an unlikely threshold damage mechanism for wall board on any other construction material for houses.

90. Table 5.2 and Figure 5.2 demonstrate the effects of prestrain (or stress) on the material prior to dynamic response. These data indicate that the existance of small prestrain has little effect on fatigue strain level of failure. Therefore, the data from the experiments, static analysis, and dynamic analysis, confirm statements by Stagg et al. (1984) which stated that large prestrain is needed to attain the cyclic failure stress level for house materials and that environmental factors, not blasting, are the major stress/strain producers.

Table 5.1
Cracking Observed from Shaker Excitation

Vibration Equivalency (in./sec)	Crack Observation	Number of Cycles at Cracking
0.5	Entryway tape joint crack.	52,000
	Crack in joint compound over nail head in master bedroom.	52,000
	Fireplace mortar joint crack extension.	52,000
0.3	Brick veneer mortar joint cracks.	15,000
	Four cracks in joint compound over nail heads.	25,000
0.75	Vertical crack through brick veneer mortar.	14,500
	Joint compound over nail heads cracking.	60,000
1.0	Crack in drywall.	22,000

Table 5.2
Summary of Prestrain and Failure Strain Level Versus Cycles*

Material	Strain, Millionths (μ or x 10^{-6} in./in.)				Cycles to Failure
	Prestrain Level		Failure		
	%	μ in./in.	%	μ in./in.	
5/8-in. Gypsum Wallboard (with paper laminate removed)	0	0	62	80	1,000
	0	0	38	50	18,000
	20	26	69	90	330
	20	26	58	76	1,900
	20	26	43	56	8,500

* Excerpted from Table A-1 of Stagg, et al. (1984). Static result (1/4 cycle) was used as 100% level measured on test sample; Stagg, et al.

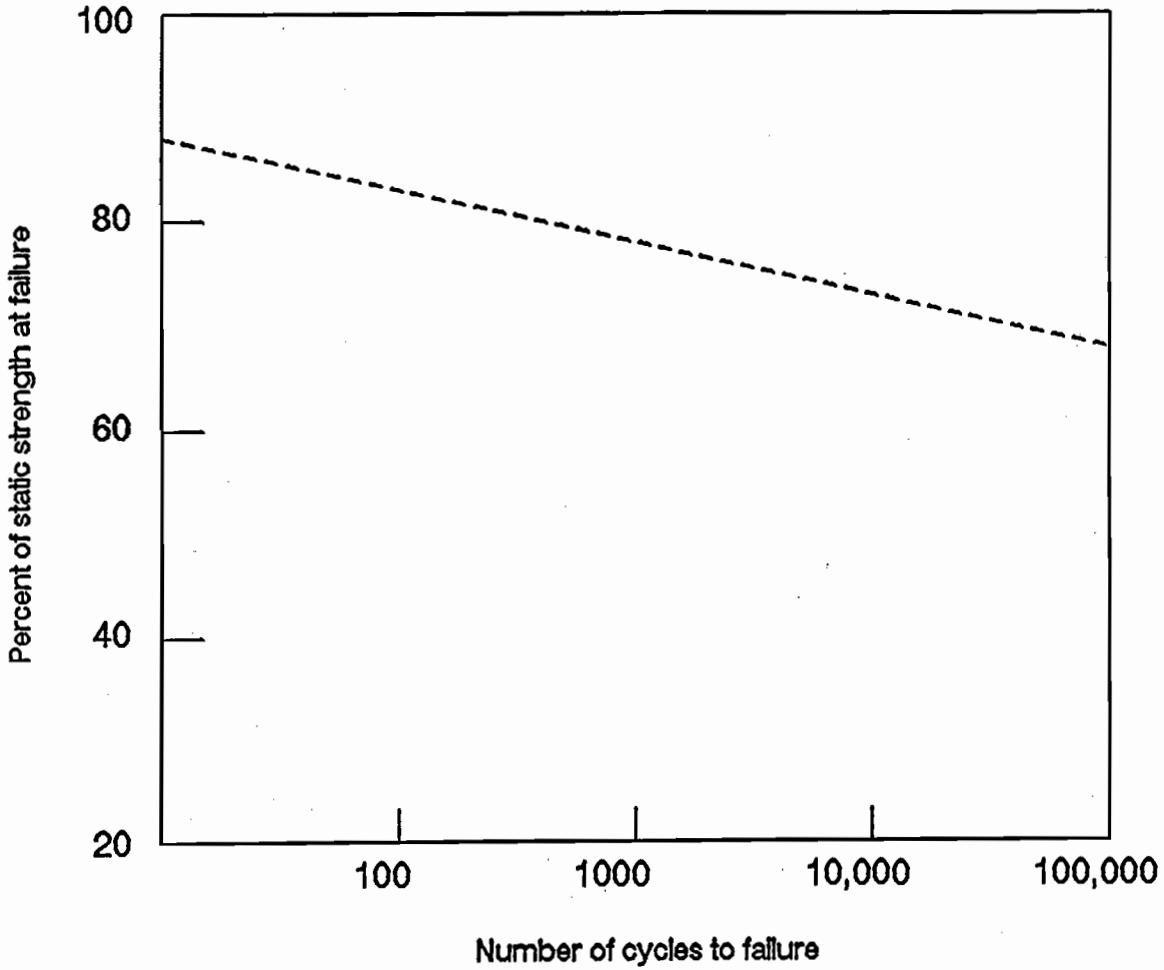

Figure 5.1 Fatigue behavior of gypsum panels (after Leigh, 1974)

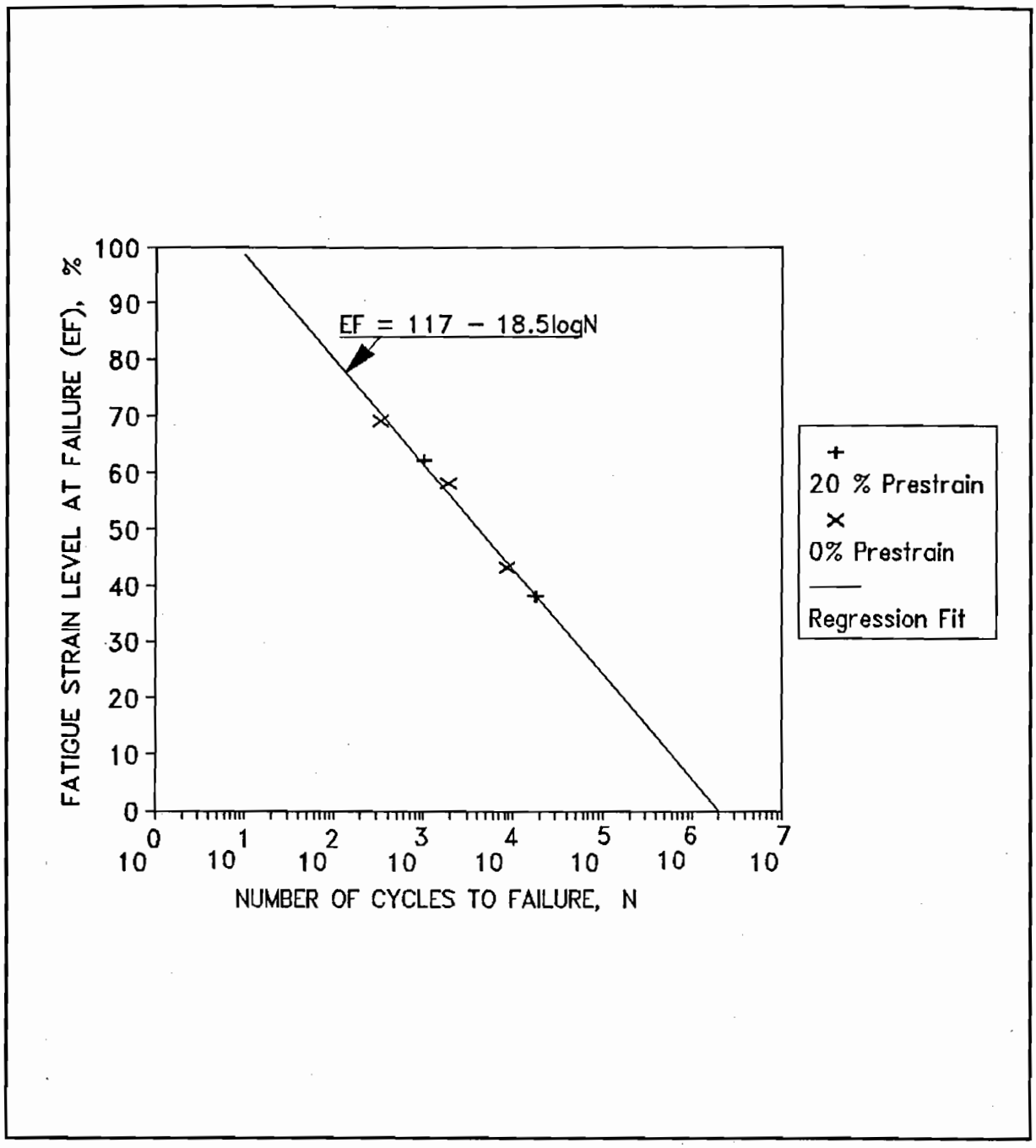

Figure 5.2 Fatigue strain versus failure cycles for 5/8-in. gypsum wallboard. Data were taken from Table A-1 of Stagg, et al. (1984).

CHAPTER 6: CONCLUSIONS

The conclusions address the five issues stated in the objectives in Chapter 1, Paragraph 6, and are based on results from the experimental and analytical investigations presented in this report.

90. Low-frequency ground vibrations below 4 Hz produce no measurable amplified responses in the houses. Above 4 Hz the houses begin to show some amplification of ground motion. The largest, or more significant, amplifications occur at frequency ranges from 7 to 15 Hz. There are isolated cases where amplifications occur above 15 Hz. Therefore, at ground vibrations below 4 Hz, the houses tend to respond as rigid bodies moving with the ground and developing no internal stresses.

91. Within the range of explosive weights used during the period when airblast measurements were made by WES (Table 2.2), recorded pressures were extremely low and would not damage the houses. Even under adverse weather conditions, the airblast pressures would be low enough so that no damage would occur to the houses.

92. Based on measurements made during this investigation, airblasts (when measured) and ground vibrations produce about the same structural response of the houses. Also, for winds occurring during the test period, their contribution to structural response was negligible.

93. Blast monitoring stations in Daylight triggered during the June 10, 1987, Southeast Illinois earthquake, recorded maximum free-field particle velocities of 0.5 in./sec which is near the 0.39 in./sec which represented the worst case scenario for blast as estimated by OSM. This indicates that at least one earthquake has occurred in the vicinity which could have produced as much structural response as the mine blasting.

94. Based on the analysis and discussion presented in Chapter 5, damage observed in the subject houses was not the result of material fatigue failure due to repetitive blast

vibration events. Not enough cycles of vibration above the necessary amplitude were present.

95. Measured settlement in house foundations was large enough to cause potential cracking observed in base slabs of houses in the study area. Static lateral earth pressures, based on realistic assumptions, are large enough to produce potential cracks in the houses' unreinforced masonry block walls.

96. Using the maximum peak ground velocity prediction by Eltschlager and Michael (1993) at 0.39 in./sec and above, and comparing the maximum recorded strain in wallboard, wallboard tape joint, and plaster to the range of computed critical tensile strain capacity of the materials, the maximum reported critical tensile strain capacity is not exceeded for peak ground velocities less than or equal to o.39 in./sec. Therefore, no damage is predicted for wallboard, wallboard tape joints, and plaster for the peak ground motions. This is based on data presented in Figure 2.21 and findings on wallboard and plaster joints by Stagg et al. (1984), and findings from FE calculations.

97. The studies dealing with the block and brick walls indicate the possibility of threshold damage of block and brick veneer joints. The conclusions are based on the occurrence of peak ground velocity of 0.39 in./sec predicted by Eltschlager and Michael (1993), response of block and brick by Stagg et al., and FE studies. As described in Table 1.1, the threshold damage of block and brick wall is small cracks at joints between construction elements. A crack is defined to exist when the tensile capacity of the material has been exceeded. This may result in cracks which are not visible. This level of threshold damage would not affect the ultimate load-carrying capacity of the structure.

98. Induced strains and stresses from settlements and earth pressures produce prestrain/stress which are combined (as tensors are) to the dynamic strains and corresponding stress. The finite-element procedures were used to determine dynamic stresses in selected materials modeled in the house. The dynamic maximum

potential stresses from mine blasting were about 2 psi for the major portion of the walls with peaks of 45 to 55 psi near windows or other abrupt changes in geometry. This leads to the same conclusion as reported by Stagg et al., that a large prestrain is needed to attain the cyclic failure stress level. Foundation settlements, lateral earth pressure, and other uncertainties in loading are potential producers of significant prestrain in all houses.

REFERENCES

ADINA R&D, Inc. 1987a (Dec). "ADINA-IN for ADINA Users Manual; A Program for Pre-Processing and Display of ADINA, ADINA-T, and ADINA-F Input Data," Report ARD 87-4, ADINA R&D, Inc., Watertown, MA.

ADINA R&D, Inc. 1987b (Dec). "ADINA-PLOT for ADINA Users Manual; a Program for Display and Post-Processing of ADINA, ADINA-T, and ADINA-F Input Data," Report ARD 87-7, ADINA R&D, Inc., Watertown, MA.

American Concrete Institute. 1989. Building Code Requirements for Reinforced Concrete, ACI 318-89, Detroit, MI.

American Concrete Institute and American Society of Civil Engineers. 1988. Building Code Requirements for Masonry Structures (ACI 530-88/ASCE 5-88) and Specifications for Masonry Structures (ACI 530.1-88/ASCE 6-88), Detroit, MI; New York, NY.

American Insurance Association. 1972. "Blasting Damage, A Guide for Adjusters and Engineers," Claims Bureau, Engineering and Safety Service and Property Claim Services of American Insurance Association, Washington, DC.

APS Dynamics, Inc. (undated). "Instruction Manual, Electro-Seis®, Model 113 Shaker," Carlsbad, CA.

APS Dynamics, Inc. (undated). "Instruction Manual, Dual-Mode™, Model 113 Shaker," Carlsbad, CA.

American Society of Civil Engineers. 1987. "Use of Vibration Measurements in Structural Evaluation." Proceedings of a session sponsored by the Structural Division of the American Society of Civil Engineers in conjunction with the ASCE Convention in Atlantic City, New Jersey, April 29. John R. Hall, Jr., ed., New York, NY.

Bathe, Klaus-Jürgen. 1982. Finite Element Procedures in Engineering Analysis, Prentice-Hall, Inc., Englewood Cliff, NJ.

Bendat, Julius S., and Piersol, Allan G. 1980. Engineering Applications of Correlation and Spectral Analysis, Wiley, New York, NY.

Chiarito, Vincent P. 1991 (Mar). "Trip Report: Meeting and Field Study on Residential Structural Damages Potentially Related to Surface Mine Blasting in Vanderburgh County, 19-21 Feb 1991, Observations and Recommendations," (unpublished), U.S. Army Engineer Waterways Experiment Station, Vicksburg, MS (Copies may be requested from the U.S. Army Engineer Waterways Experiment

Station, ATTN: CEWES-SS-A, 3909 Halls Ferry Road, Vicksburg, MS 39180-6199).

Chiarito, Vincent P., and Fagerburg, Timothy L. 1988 (Nov). "Vibration Study of the Bloomington Intake Tower," Miscellaneous Paper SL-88-9, U.S. Army Engineer Waterways Experiment Station, Vicksburg, MS.

Clough, Ray W., and Penzien, Joseph. 1975. Dynamics of Structures, McGraw-Hill, New York, NY.

Crawford and Ward. 1965 (Dec). "Dynamic Strains in Concrete and Masonry Walls," Canadian National Research Council, Division of Building Research, National Research Council, Ottawa, Ontairo, Building Research Note 54.

Department of the Army. 1989. "Blasting Vibration Damage and Noise Prediction and Control," Engineer Technical Letter 1110-1-142, Washington, DC.

Dowding, Charles H. 1985. Blast Vibration Monitoring and Control, Prentice-Hall, Inc., Englewood Cliff, NJ.

Duron, Ziyad H. 1987. "Experimental and Finite Element Studies of a Large Arch Dam," Report No. EERL 87-02, Earthquake Engineering Research Laboratory, California Institute of Technology, Pasadena, CA.

Duron, Ziyad H., and Hall, John F. 1988. "Experimental and Finite Element Studies of the Forced Vibration Response of Morrow Point Dam," Earthquake Engineering and Structural Dynamics, Vol 16, pp 1021-1039.

E. I. du Pont de Nemours & Co. 1980. Blasters' Handbook, 175th Anniversary Edition, 16th edition, Wilmington, DE, "Vibration and Air Blast," Chapter 26, pp. 423-446.

Eltschlager, Kenneth K. and Michael, Peter R. 1993. "Surface Mine Blasting Activity and Resultant Ground Vibrations - AMAX Coal Company - Ayrshire Mine January 1, 1986 to April 15, 1992," Draft Report, U.S. Department of the Interior Office of Surface Mining Reclamation and Enforcement, Pittsburgh, PA.

Ewins, D. J. 1984. Modal Testing: Theory and Practice, John Wiley & Sons, Inc. New York, NY.

Hadala, Paul F. and Peterson, Richard W. 1993 (Jan). "Dynamic Soil Property Testing and Analysis of Soil Properties - Daylight and McCutchanville, Indiana," (unpublished) U.S. Army Engineer Waterways Experiment Station, Vicksburg, MS (Copies may be requested from the U.S. Army Engineer Waterways Experiment

Station, ATTN: CEWES-ER-R, 3909 Halls Ferry Road, Vicksburg, MS 39180-6199).

Harris, Cyril M. and Crede, Charles E. 1976. Shock and Vibration Handbook, 2nd ed., McGraw-Hill, New York, NY.

Hewlett Packard. 1986. "The Fundamentals of Modal Testing," Application Note 243, Palo Alto, CA.

Hewlett Packard. 1989. "The Fundamentals of Signal Analysis," Application Note 243, Palo Alto, CA.

King, K., Algermissen, T., Leyendecker, E., and Carver, D. 1993. "Investigation of Building Damage in the McCutchanville-Daylight, Indiana Area," Open-file Report 93-254, U.S. Department of the Interior Geological Survey, Golden, CO.

The MathWorks, Inc. 1990. "386-MATLAB User's Guide," 386-MATLAB™ for 80386-based MS-DOS Personal Computers, Copyright 1985-90, The MathWorks, Inc., Natick, MA.

McKenzie, Cameron. 1990 (Dec). "Quarry Blast Monitoring, Technical and Environmental Perspectives," Quarry Management.

Medearis, Kenneth G. 1975. "Structural Response to Explosion-Induced Ground Motions," American Society of Civil Engineers, New York, NY.

Mlakar, Paul F., Vitaya-Udom, Ken P., and Cole, Robert A. 1984. "Conrete Behavior Under Dynamic Tensile-Compressive Load," Technical Report SL-84-1, U. S. Army Engineer Waterways Experiment Station, Vicksburg, MS.

Naeim, Farzad, ed. Seismic Design Handbook. 1989. Van Nostrand Reinhold, New York, NY,

Newmark, N. and Hall, W. J. 1982. Earthquake Spectra and Design, Earthquake Engineering Research Institute, Berkeley, CA.

Newmark, N M., and Rosenblueth, E. 1971. Fundamentals of Earthquake Engineering, Prentice-Hall, Princeton, NJ.

Paz, Mario. 1985. Structural Dynamics, 2nd ed., Van Nostrand Reinhold, New York, NY.

Peterson, E. L., and Snyder, R. C. 1987 (Mar). "Modal Excitation Made Easy," The Sound and Vibration, Bay Village, OH.

Ramsey, K. A. 1975 (Nov). "Effective Measurements for Structural Dynamics Testing", Part I and Part II , Sound and Vibration, Bay Village, OH.

Rea, Dixon, Liaw, C-Y., and Chopra, Anil K. 1972. "Dynamic Properties of Pine Flat Dam," Report No. EERC 72-7, Earthquake Engineering Research Center, University of California, Berkeley, CA.

Rea, Dixon, Liaw, C-Y., and Chopra, Anil K. 1975 (Feb). "Dynamic Properties of San Bernardino Intake Tower," Report No. EERC 75-7, Earthquake Engineering Research Center, University of California, Berkeley, CA.

Richardson, Mark. 1975 (May). "Modal Testing Using Digital Test Systems," Proceedings of Seminar on Understanding Digital Control and Analysis in Vibration Test Systems, The Shock and Vibration Information Center, NRL, Washington, D.C.

Rossow, E. C., Dowding, C. H., and Mncwango, S. (undated). "High Frequency, Finite Cycle Excitation of SDOF and MDOF Structures," (unpublished).

Siskind, David E., and Stagg, Mark S. 1994. Personal telephonic communication.

Siskind, David E., Crum, Steven V., and, Plis, Matthew N. 1990. "Vibration environment and Damage Characterization for Houses in McCutchanville and Daylight, Indiana," Contract Research Report, Interagency Agreement EC68-IA9-13259, U.S. Department of the Interior, Bureau of Mines, Twin Cities Research Center, Minneapolis, MN.

Shye, Ken, Van Karsen, C., and Richardson, M. 1988. "Modal Testing using Multiple References," Structural Measurement Systems, Inc, San Jose, CA.

Stagg, Mark S., Siskind, David E., Stevens, Michael G., and Dowding, Charles H. 1984. "Effects of Repeated Blasting on a Wood-Frame House," Report of Investigations 8896, U.S. Department of the Interior, Bureau of Mines, Twin Cities Research Center, Minneapolis, MN.

Street, R., Zekulin, A., Jones, D., and Min, G. 1988 (Jul). "A Preliminary Report on the Variability in Particle Velocity Recordings of the June 10, 1987, Southeastern Illinois Earthquake," Seismological Research Letters, Vol. 59, No. 3, pp. 91-97.

Uniform Building Code. 1989. International Conference of Building Officials, 5360 South Workman Mill Road, Whittier, CA.

Vibration Engineering Consultants, Inc. 1990. "PCMAP®, Personal Computer Modal Analysis Program," Ver. 2.04, PCMODAL®, Software Series, Ten State Street, Woburn, MA.

Winter, George, and Nilson, Arthur H. 1972. Design of Concrete Structures, McGraw-Hill, New york, NY.

Wiss, John F. and Nicholls, Harry R. 1974. "A Study to A Residential Structure from Blast Vibrations," American Society of Civil Engineers, New York, NY.

Yang, C. Y. 1986. Random Vibrations of Structures, Wiley, New York, NY.

Appendix A:

Excerpt from
Interagency Agreement between the Office of Surface Mining, Reclamation and Enforcement, U.S. Department of the Interior and the U. S. Army Engineer Waterways Experiment Station, "Field and Laboratory Evaluation of Potential Causative Factors of Structural Damages in Daylight/McCutchanville, Indiana"
Contract No. EF68IA91-13796

Contract No. EF68IA91-13796

INTERAGENCY AGREEMENT

Between

THE OFFICE OF SURFACE MINING, RECLAMATION AND ENFORCEMENT,
U.S. DEPARTMENT OF THE INTERIOR

And

THE U.S. ARMY ENGINEER WATERWAYS EXPERIMENT STATION

FIELD AND LABORATORY EVALUATION OF POTENTIAL CAUSATIVE FACTORS OF STRUCTURAL DAMAGES IN DAYLIGHT/MCCUTCHANVILLE, INDIANA

I. OBJECTIVE

At the request of the Indiana Department of Natural Resources (IDNR), the Office of Surface Mining (OSM), Reclamation and Enforcement, acting through its Eastern Support Center, has undertaken an investigation of citizens' allegations of structural damages from local surface mine blasting in Daylight and McCutchanville, Vanderburgh County, Indiana. The Ayrshire Mine of the AMAX Coal Company is the focal point of blasting complaints in the study area. The mine began operations in 1973 and progressed from the eastern boundary of the permit to within 3.5 miles east of McCutchanville and 2 miles east of Daylight. To date, several phases of investigation have been completed by the IDNR and OSM. Significant and widespread occurrences of structural damage in the study area have been documented. It has also been established that blasting related ground vibrations and/or airblasts from the Aryshire Mine are discernible to the complainants.

A November 1989 through January 1990 study by the U.S. Bureau of Mines (USBM) involved monitoring of ground vibrations, the structural responses to those vibrations, and potential crack development in building materials during ongoing operations at the Ayrshire Mine. This study found no clear correlation between blasting and crack formation or extension in the studied structures. The maximum amplitude of recorded ground vibration and the resulting structure vibration were found to be well below the established thresholds for cosmetic damage. However, in-house and interagency reviews of the OSM investigation up to and including the USBM study identified a number of outstanding technical issues. These issues include the following:

1) Is there a potential for collapse of the structure of unsaturated soils or pore-pressure rise in saturated soils in the study area due to ground vibration?

2) Can observed damage be ascribed to fatigue induced by the repetitive exposure of structures to ground vibrations and/or airblasts?

3) Are there ground vibrations at very low frequencies (down to 0.5 Hz.) that are capable of causing structural damage?

4) Are there comparable damages in a remote area (unaffected by blasting) with similar geology, soils, and topography?

5) Do airblasts produce adverse structural response in the study area?

6) Certain types of structural damages, observed by some investigators, appear to have been caused by lateral forces. If so, what are the relative contributions of blast-induced ground vibrations/airblasts, earthquakes, and wind to this force?

7) Do alternative mechanisms (inadequate foundations, slope/soil movement) contribute to the observed damages?

8) To what degree do geology, soil, and topography influence ground wave propagation, site response amplification, and the amplitude, frequency, and duration of waves?

9) To what extent does blast design (both conventional and cast blasting) alter the effects of blast vibrations in the study area?

II. BACKGROUND

The work to be performed under this Agreement will be an integral part of an interagency study aimed at resolving the above issues. Other agencies participating in this study are the USBM and the U.S. Geological Survey (USGS). The tasks to be performed specifically by the U.S. Army Engineer Waterways Experiment Station (WES) are designed to address Issues 1, 2, 3, 5, 6, and 7. Technical support to this Agreement will be provided by the IDNR and OSM.

Authority to enter into this Interagency Agreement (IA) is contained in the Surface Mining Control and Reclamation Act of 1977 (P.L. 95-87) and the Economy Act (P.L. 97-258).

III. TERMS OF AGREEMENT

This Agreement may be amended by mutual consent of both parties in writing. The period of performance of this Agreement shall be for one year from date of acceptance. It shall continue in force unless modified by mutual consent or terminated by either party by written notice to the other party at least 30 days prior to the termination date. Due to the nature of field and analysis tasks being undertaken and the required schedule for completion, it is acknowledged that the Agreement will span portions of fiscal years 1991 and 1992.

IV. STATEMENT OF WORK

A. OSM agrees to:

1. Provide personnel for the purpose of coordinating site selection and other field activities affecting structure analyses and ground vibration, airblast and structure response monitoring.

2. Obtain all rights of entry and all other Government clearances for property access.

3. Provide geophysical and shallow drilling and undisturbed sampling services, through a contractor or Government agency, for the purpose of collecting soil samples from sites in Daylight, McCutchanville, and a "remote" area (unaffected by blasting). Exact sampling procedures and locations and depths will be selected by OSM in consultation with the principal investigator.

4. Provide soil samples to WES for cyclic load testing.

B. The WES agrees to:

1. Perform testing and modeling services in the field and lab as per the following Scope of Work:

IN-FIELD MONITORING AND STRUCTURAL DYNAMICS ANALYSES

a. Select one structure in the study area for load failure analyses. Select one structure in the study area for monitoring ground vibrations, airblasts and structural responses.

b. Conduct engineering analyses on selected structure to: (1) estimate vertical wall loads on footings, (2) determine probable extent of foundation settlement from estimated static wall

loads, and (3) determine differential settlements required to cause yield-line cracking in unreinforced basement floor slabs.

c. Conduct lateral load analyses for unreinforced basement walls in selected structure as follows: (1) Develop realistic bounding values for lateral earth pressures on basement walls to include probable values for confined swell pressures in expansive clays, (2) estimate vertical loads on the walls, (3) estimate structural strength of the walls, and (4) estimate onset of cracking in the walls, using values for lateral earth pressures, vertical wall loads, and wall strength.

d. Monitor free-field and near-structure ground vibrations, airblast distributions on mine-facing side of structure, and structural response during surface mine blasting activity and other sources of cyclic loading. Monitor ground vibrations in the range of 0.5 to 60 Hz. Also, conduct a modal test to identify overall and component dynamic properties of structure. Use data to determine energy levels of very low frequency vibrations and interrelationships between exterior dynamic loadings and structural response.

e. Perform multi-degree-of-freedom and fatigue analyses using a structural model (one-story and two-story) based on information obtained under Task 1.d. Estimate minimum stress levels that could cause cracking and/or other damage based on various scenarios pertaining to dynamic loading parameters, material prestrain levels, and fatigue. Determine whether a relationship exists between common crack patterns in the study area and cyclic loading.

LABORATORY SOIL TESTING

f. Test soil samples for consolidation under induced cyclic loading by applying cyclic loading tests to 12 samples obtained by OSM from Daylight, McCutchanville, and the remote area. Between 12 and 24 tests shall be conducted using a Drnevich resonant column loading device. Each tested sample shall be drained and subjected to 30,000 cyclic loadings in a frequency range of 4 to 20 Hz. All 12 samples shall initially be

tested at two separate shear strain levels, the largest of which shall be based on the highest observed peak particle velocity measured in the study area. Further testing at 1/10 the original shear strain level shall be performed only if consolidation is detected in the initial results.

g. If consolidation occurs in testing under Task 1.f., evaluate potential damaging effects of soil consolidation beneath structural foundations. The evaluation shall be based on available site-specific soil data as well as the test results.

h. Conduct two pilot undrained cyclic triaxial tests and two companion static undrained triaxial tests to failure on saturated specimens from the study area. Use a vertical strain level equal to twice the maximum shear strain level used under Task 1.f. Assess whether significant strength degradation occurs as a result of low level cyclic loading. If significant strength degradation is determined, recommend further testing not funded under this IA.

i. If significant strength degradation is determined under Task 1.h., develop a chart showing effect of degradation on slope stability.

2. Attend meetings with other interagency team members from USGS, USBM, OSM and IDNR. Present preliminary findings, recommend project modifications where appropriate, and identify support/coordination requirements for remaining activities. The exact time and place of the meetings shall be agreed upon by all project participants.

APPENDIX B

Data Acquisition Setup and Data Reduction

Dr. Cary Cox
Instrumentation Services Division (ISD),
U.S. Army Engineer Waterways Experiment Station (WES)

Data Acquisition Setup and Data Reduction

1. The data from all vibration responses were digitized and analyzed using an IBM compatible 386, 25 MHz portable computer. This system is equipped with 8 Mbytes of extended memory, a 80387 co-processor, a 3.25-in., high-density floppy disk drive and an 88 Mbyte hard disk drive. Alternatively, a 386, 16 MHz laptop with a 100 Mbyte hard disk drive was available for the remote data acquisition setup. This provided the storage and processing speed required to acquire and analyze large quantities of data at the field site. The system was also configured with an Analog Devices RTI-815-F analog-to-digital converter (ADC). This ADC accepted 32 single-ended channels of analog input over a range of +/- 5 volts. The ADC provided 12-bit resolution with a linearity of +/- 1/2 LSB. The ADC could sample at a maximum aggregate rate of 100,000 samples per second. The RTI-815-F also provided two 12-bit digital-to-analog (DAC) channels and a programmable clock to trigger the ADC or DAC. A diagram of the system is shown in Figure B1.

2. In order to acquire the data a custom digitizing program was written to perform three tasks: (a) calibrate the data, (b) digitize the data, and (c) archive the data.

3. The calibration module digitizes an AC or DC calibration signal on each analog channel. The engineering units that are equivalent to each of these voltages are entered into the program and the ratio of engineering units to ADC units is calculated in order to scale the data accurately.

4. The digitizing module was designed to acquire data at rates of up to 500 samples per second per channel and store the acquired data in extended memory. The programmable clock provides a pulse at the desired digitizing rate. When this pulse is detected, all analog channels are scanned at the maximum digitizing rate (100,000 samples/sec) in order to minimize the skew between channels. The maximum skew between adjacent channels is 10 microseconds.

5. After data are acquired to the extended memory, the archive module saves the data on either the hard disk or high-density floppy disk. The data can be saved in either of two formats. The first format is a compact integer format that allows an entire 240-second test to be placed on one floppy disk. The second format is one that is compatible with the digital signal processing software package, MATLAB. MATLAB is a product of The MathWorks, Inc., and provides the user with tools to manipulate matrices, perform frequency analysis, plot graphs, or use many other mathematical functions.

6. The basic test procedure was as follows: (1) adjust the gains on the signal conditioning equipment to provide the expected outputs, (2) calibrate the system to provide the scaling values used in the digitizing program, (3) digitize a sample test, (4) archive the data in MATLAB format, (5) display the data and observe how close the data's peak values are to the expected peak values, (6) readjust the signal conditioning gains to a more optimum level, (7) start the vibrator and digitize the test. (8) archive the data, (9) periodically analyze a test to assure that the data is within the calibration range, and (10) repeat steps 7 through 9 until testing is complete.

7. The MATLAB software was used to provide the following analysis of the data: (1) time-history plots, (2) power spectral density plots (applying a Hanning window for random data processing), (3) cross-spectral density plots (with Hanning window), (4) coherence plots, (5) Phase difference plots, (6) Discrete Fourier Transform plots, (7) peak detection, and (8) data reduction.

8. Tests were recorded from different stimuli applied to the structure. These include an electrodynamic, inertial mass exciter, instrumented hammer for impacting, blast events, and other ambient excitations.

9. A frequency sweep signal provided by a signal generator was used to control the shaker through a predefined sweep rate over a frequency range of 1 to 25 Hz.

10. The vibration tests were recorded at 500 samples per

second per channel. This was adequate to prevent aliasing since the analog signal was low-pass filtered at 50 Hz. The impact tests were digitized at 500 samples per second per channel.

11. Two copies of all the test were archived on floppy disk to ensure against media defects and safe transportation back to WES.

12. Acceleration measurements were acquired using the following type of instrumentation equipment: PCB Model 393C and Wilcoxon Model 731 seismic accelerometers with an output of 1.075 to 1.173 and 7.23 to 7.49 v per g output at a gain of 1.0, respectively. The calibration of the PCB and Wilcoxon accelerometers was conducted at ISD, WES, on an Unholtz/Dickey shaker table capable of controlled amplitude vibrations of 0.1 to 10.0 g's peak from 2.0 to 2000 Hz. The actual seismic accelerometer calibration was conducted from 2.0 to 50.0 Hz at a controlled amplitude of 0.1 g peak, at a sweep rate of 0.5 decades per minute. X/Y plots were collected on each PCB accelerometer. The signal conditioning was a PCB Model 483A11 (6 channel) and a 483A10 (12 channel) power unit capable of variable gains of .001 to 100.0. All 18 channels had an internal plug-in, low-pass filter module set at 25 Hz single pole, low pass. The seismic accelerometers were powered by a PCB 12-channel AC power amplifier. The model 731 seismic accelerometer had a frequency response of 0.1 to 300 Hz and has an output of 7.23 to 7.49 v per g at a gain of 1.0. The type P31 power unit had selectable gains of 1.0, 10.0, and 100.0 labeled as 10v/g, 100v/g, and 1000v/g, respectively.

13. A data acquisition log indicated any gage location changes, amplifier gain changes, gage sensitivity settings, and other pertinent information concerning channel listings.

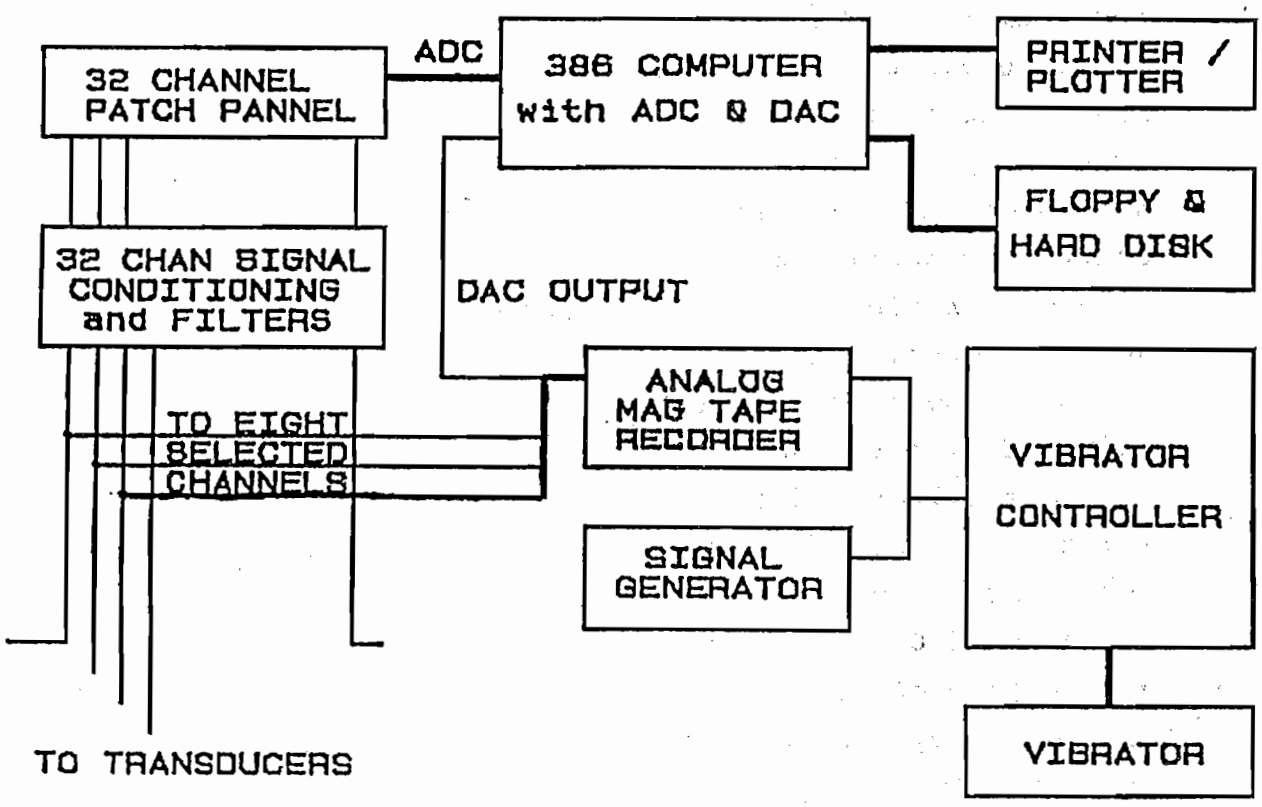

Figure B-1. Diagram of the data acquisition system.

Table B-1

List of Experimental Equipment and Instrumentation

PCB Model 393C seismic accelerometers with an output of 1.075 to 1.173 v/g output at a gain of 1.0.

PCB 393C's used with: PCB Model 483A11 (6 channel) and a 483A10 (12 channel) power unit capable of variable gains of .001 to 100.0. All 18 channels have an internal plug in low pass filter module set at 25 Hz, double pole, low pass.

Wilcoxon model 731 seismic accelerometer/(used with PCB Amplifier) with output of 7.23 and 7.49 volts per g output at a gain of 1.0.

Spectral Dynamics Model 104A-1 Sweep Oscillator constant sine output.

Six-channel Trig-Tek Model 530W Tracking Filter System.

IBM-compatible 25 MHz, 386 computer, with 8 Mb of extended memory.

Tektronix Model 5111A four-channel storage oscilloscope and a Fluke 8050A Digital Multimeter.

Analog Devices RTI-815-F analog-to-digital converter (ADC).

PC-MATLAB for 80386-based MS-DOS personal computer.

APPENDIX C

FIELD TEST DATA

PART 1: Free-field and one-story house response time-histories for conventional blast

PART 2: Free-field and one-story house response for cast blast

PART 3: Free-field airblast from conventional and cast blast at distant and near locations to one-story house

PART 4: Free-field and one-story house response as a function of frequency (average of nine shots)

PART 5: Free-field and one-story house response as a function of frequency (average of 20 shots conducted during March and April)

PART 6: Forced vibration data for one-story house

PART 7: Hammer test data for two-story house

PART 1

(See Figure 2.10 for locations)

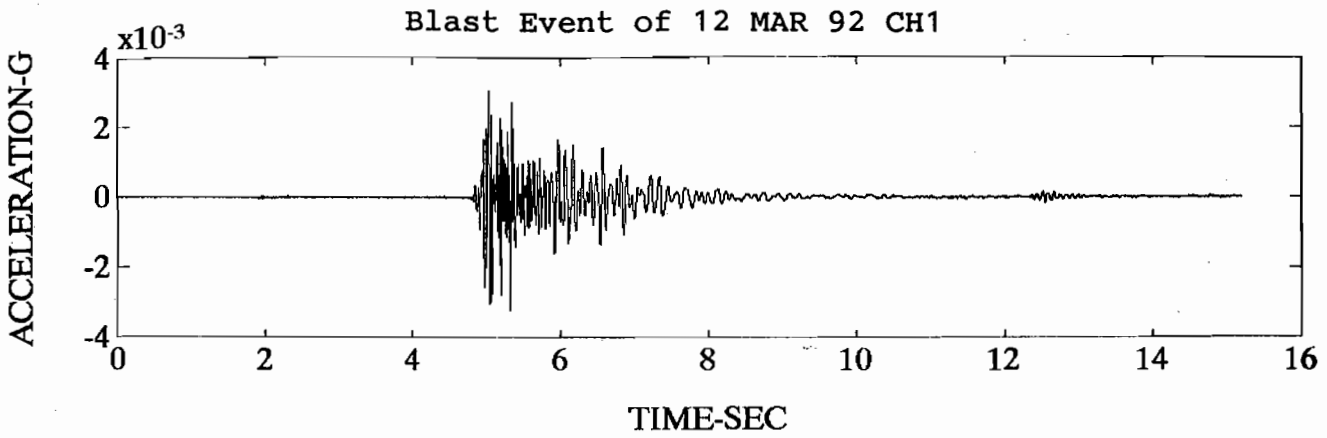
Blast Event of 12 MAR 92 CH1
x10-3
ACCELERATION-G
4
2
0
-2
-4
0
2
4
6
8
10
12
14
16
TIME-SEC

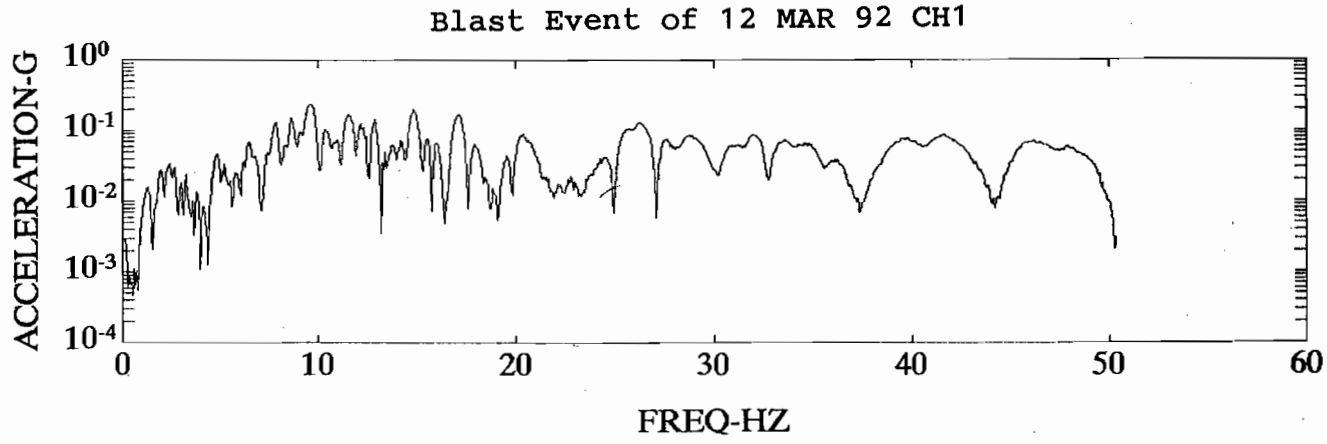
Blast Event of 12 MAR 92 CH1
ACCELERATION-G
10^0
10^-1
10^-2
10^-3
10^-4
0
10
20
30
40
50
60
FREQ-HZ

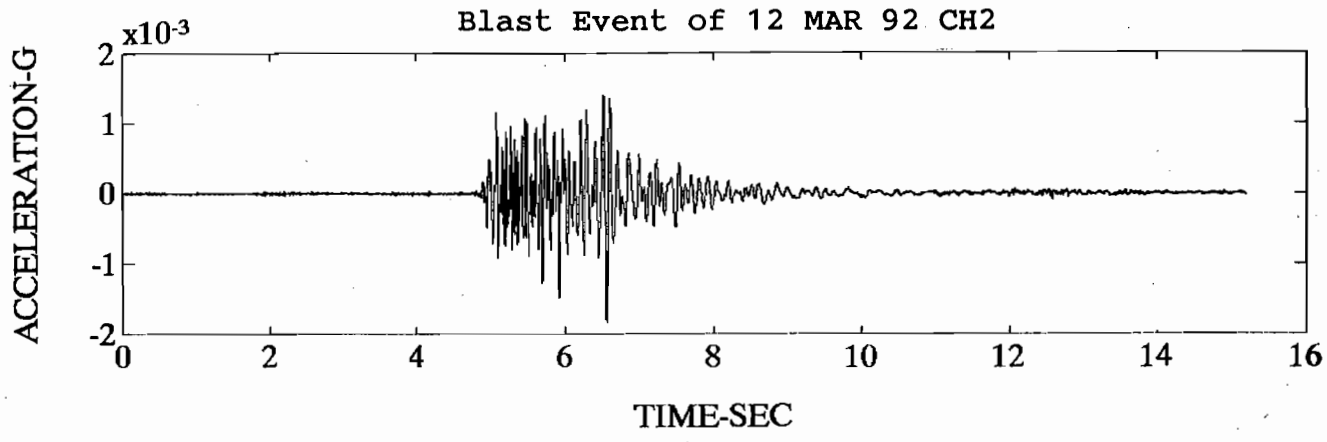
Blast Event of 12 MAR 92 CH2
x10-3
ACCELERATION-G
2
1
0
-1
-2
0
2
4
6
8
10
12
14
16
TIME-SEC

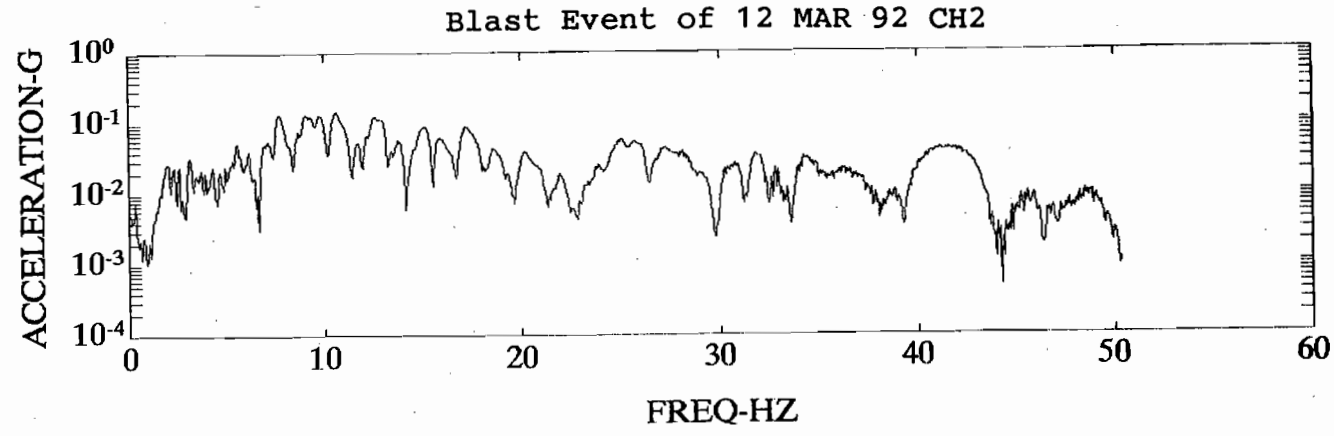
Blast Event of 12 MAR 92 CH2
ACCELERATION-G
10^0
10^-1
10^-2
10^-3
10^-4
0
10
20
30
40
50
60
FREQ-HZ

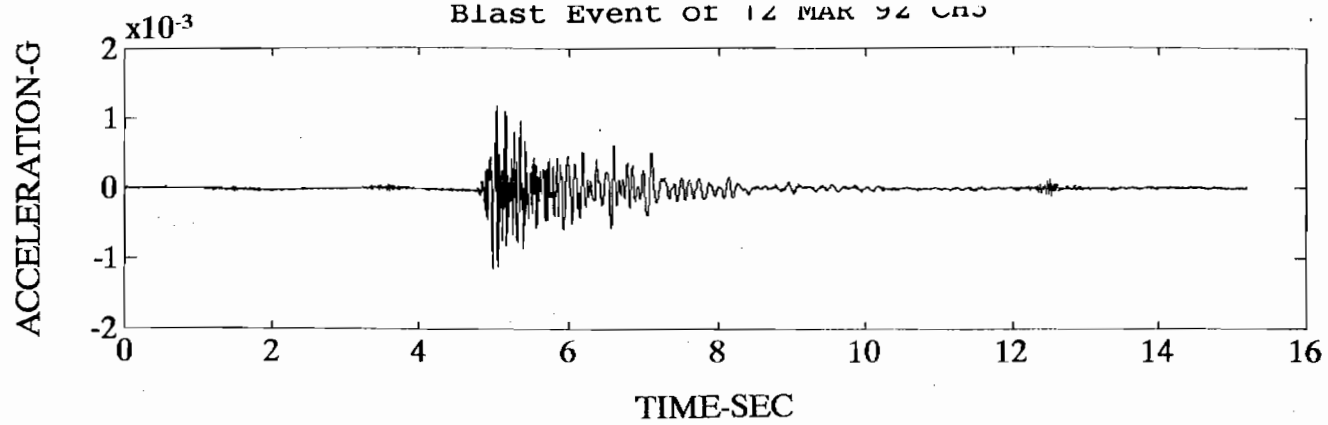
Blast Event of 12 MAR 92 CH3
x10-3
ACCELERATION-G
TIME-SEC

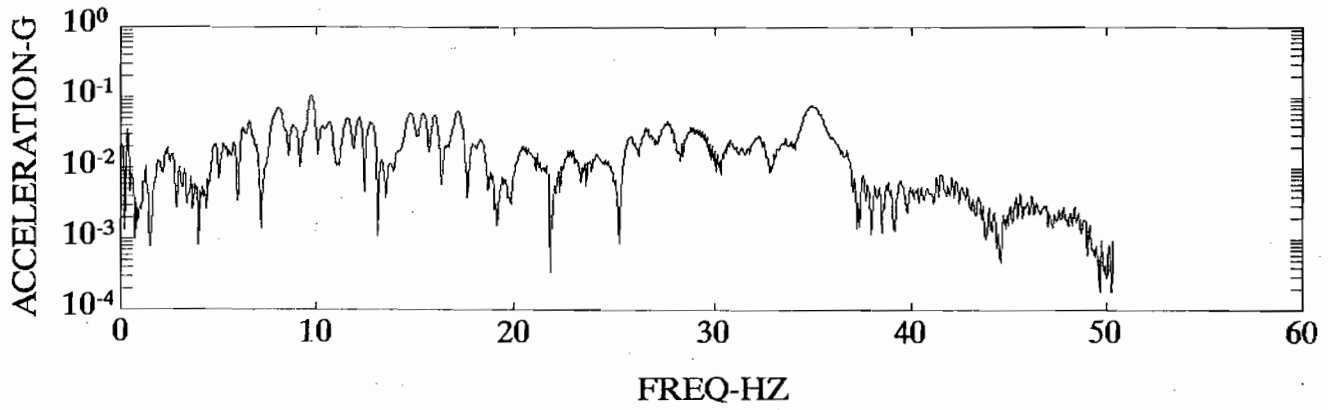
Blast Event of 12 MAR 92 CH3
ACCELERATION-G
FREQ-HZ

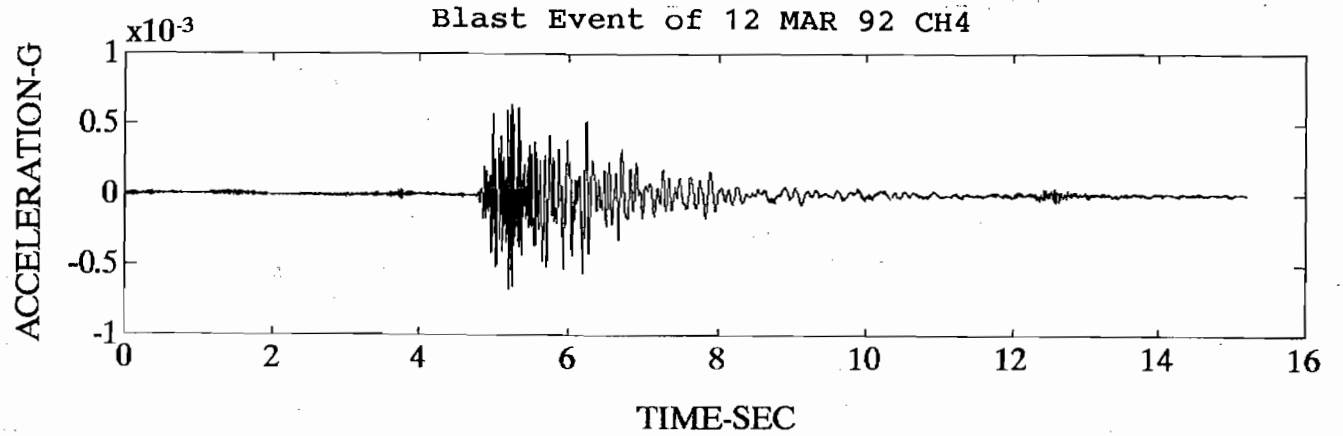
Blast Event of 12 MAR 92 CH4
x10-3
ACCELERATION-G
TIME-SEC

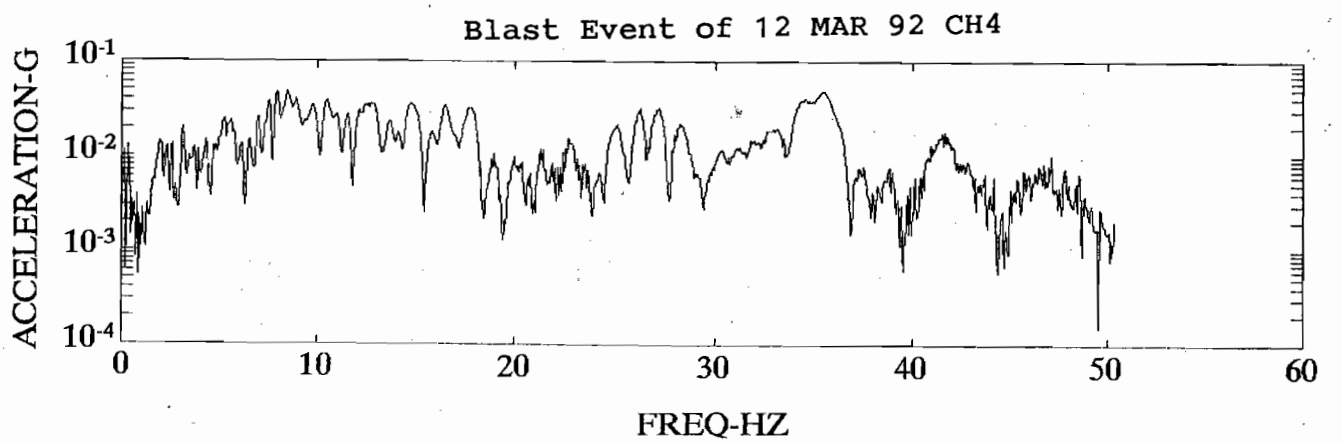
Blast Event of 12 MAR 92 CH4
ACCELERATION-G
FREQ-HZ

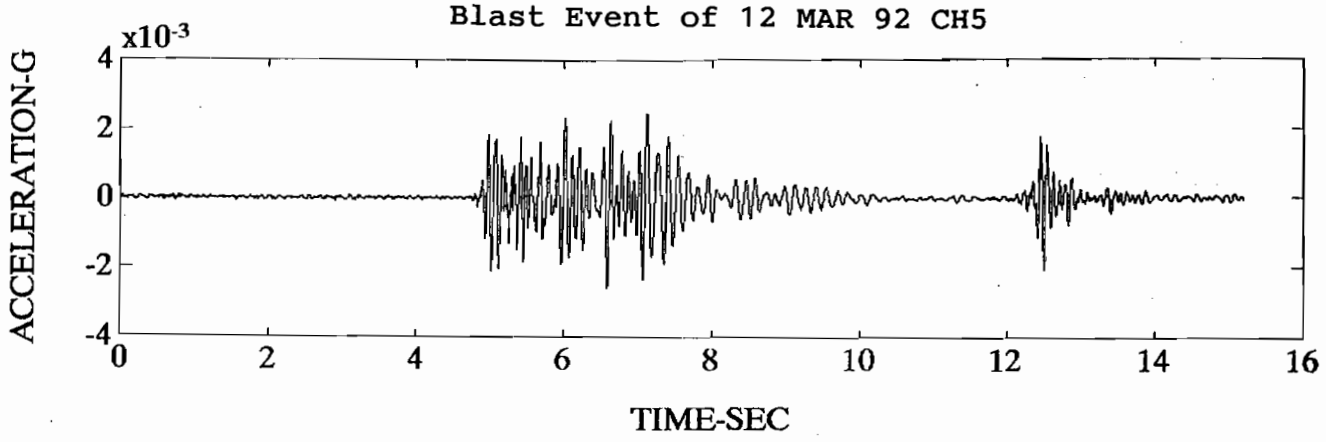
Blast Event of 12 MAR 92 CH5
x10-3
ACCELERATION-G
TIME-SEC

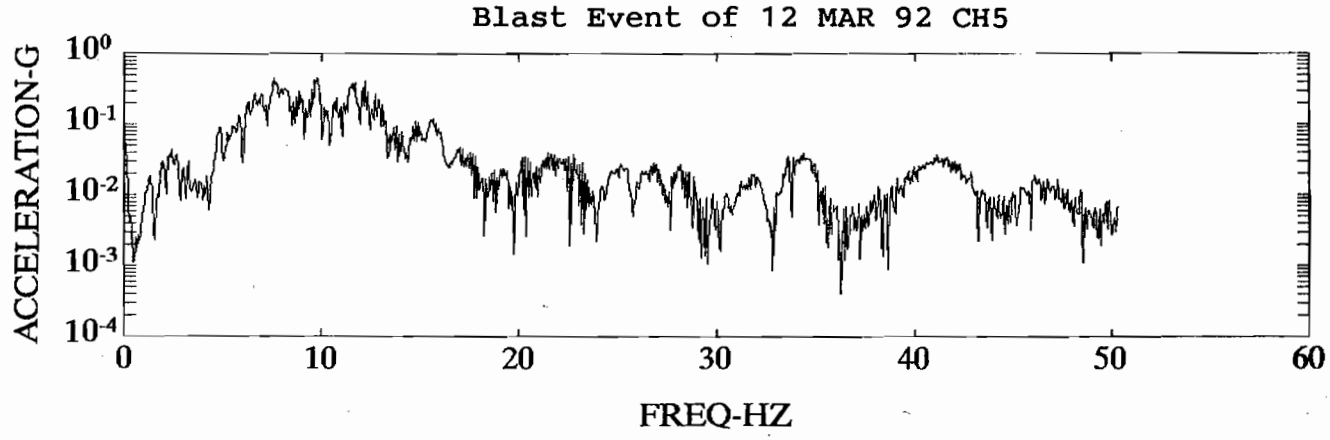
Blast Event of 12 MAR 92 CH5
ACCELERATION-G
FREQ-HZ

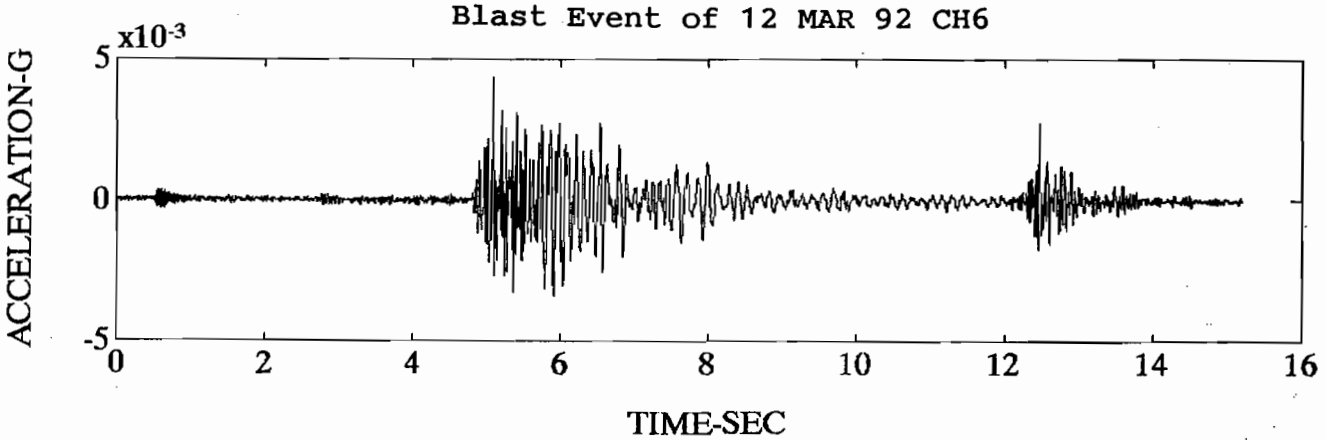
Blast Event of 12 MAR 92 CH6
x10-3
ACCELERATION-G
TIME-SEC

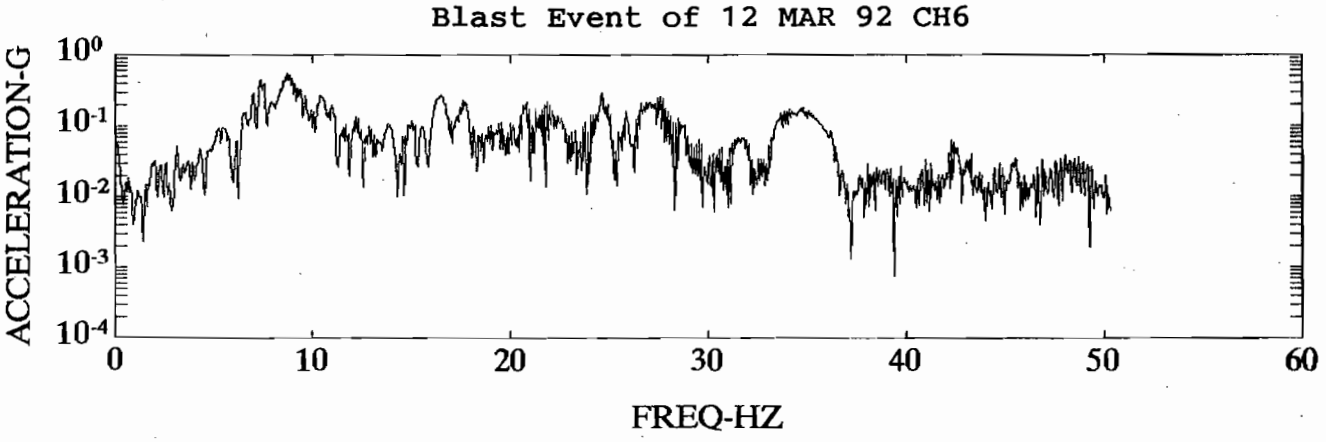
Blast Event of 12 MAR 92 CH6
ACCELERATION-G
FREQ-HZ

PART 2

(See Figure 2.10 for locations)

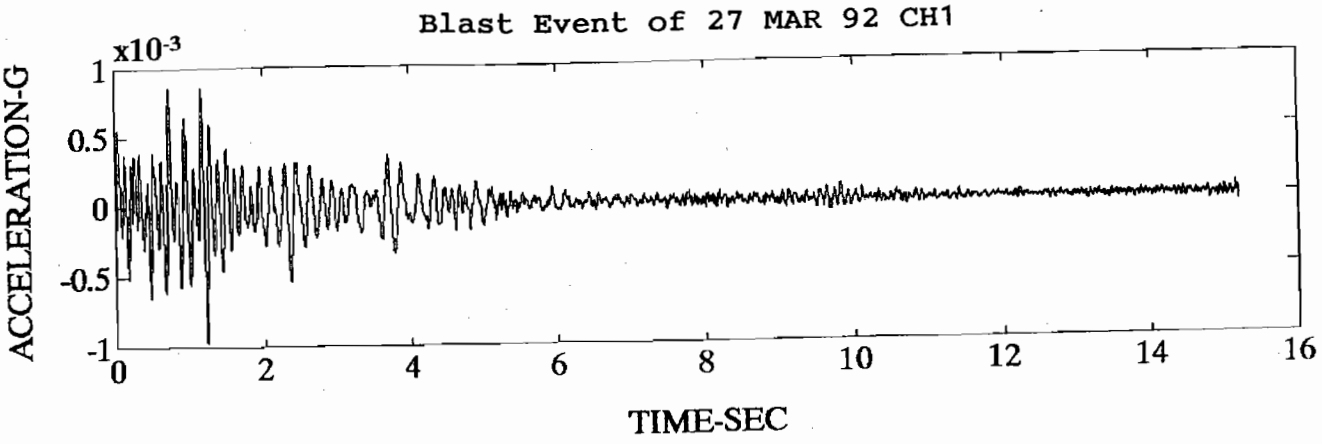
Blast Event of 27 MAR 92 CH1
x10-3
ACCELERATION-G
TIME-SEC

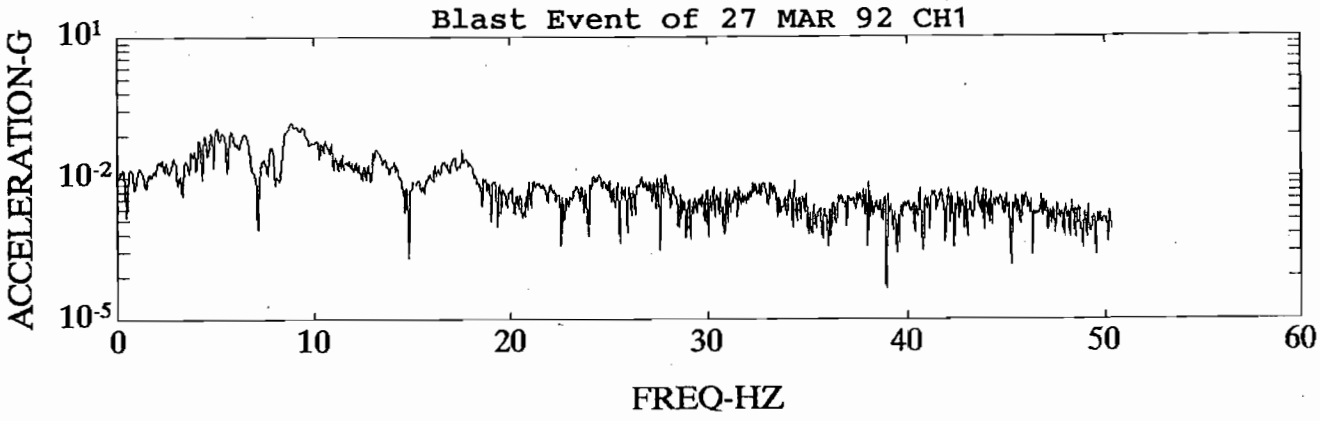
Blast Event of 27 MAR 92 CH1
ACCELERATION-G
FREQ-HZ

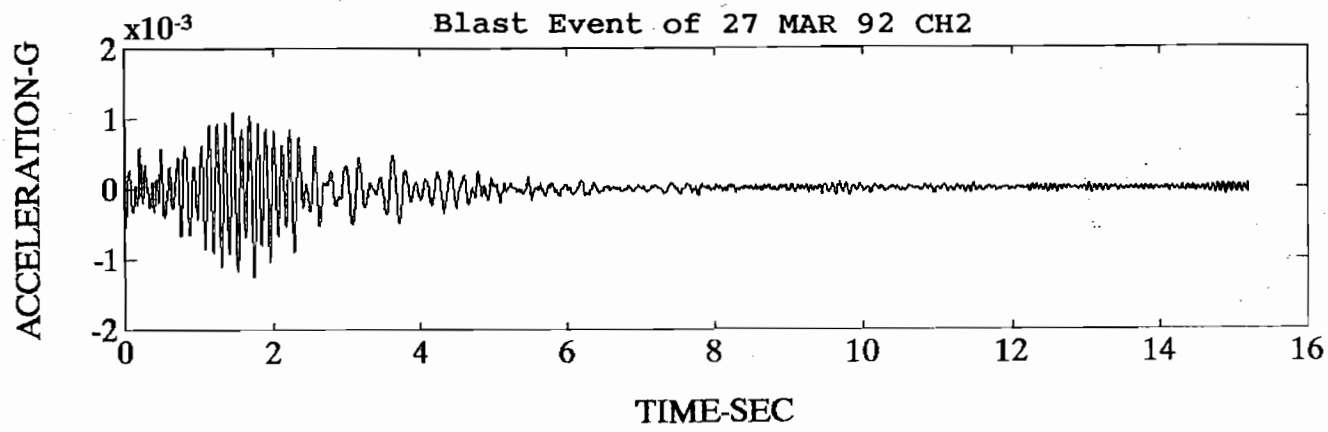
Blast Event of 27 MAR 92 CH2
x10-3
ACCELERATION-G
TIME-SEC

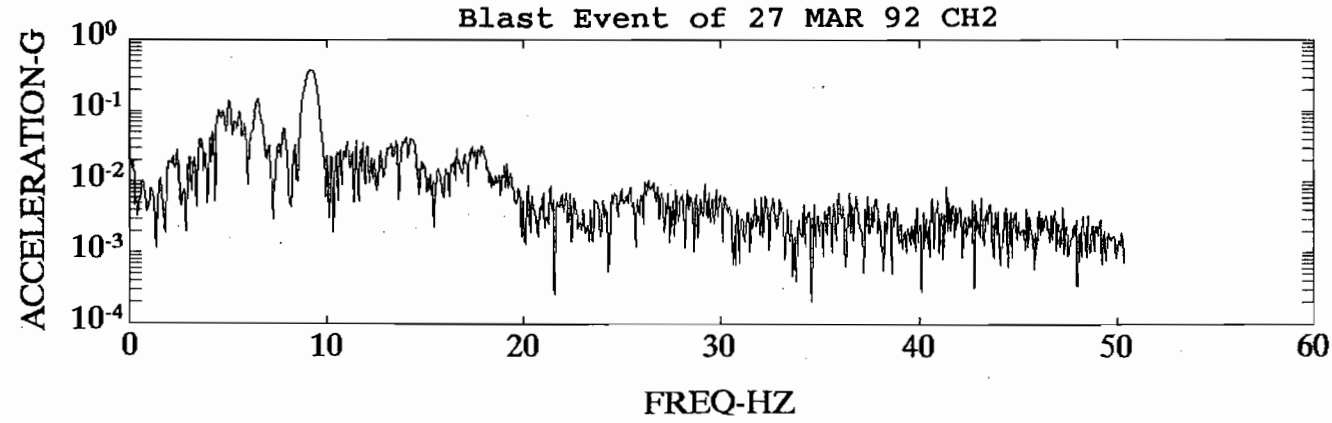
Blast Event of 27 MAR 92 CH2
ACCELERATION-G
FREQ-HZ

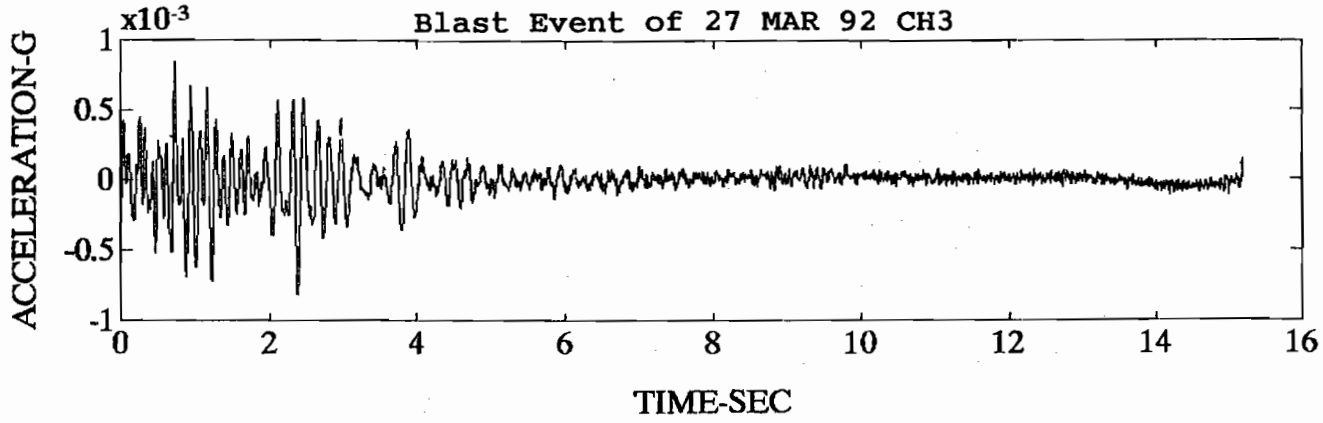
Blast Event of 27 MAR 92 CH3
x10-3
ACCELERATION-G
TIME-SEC

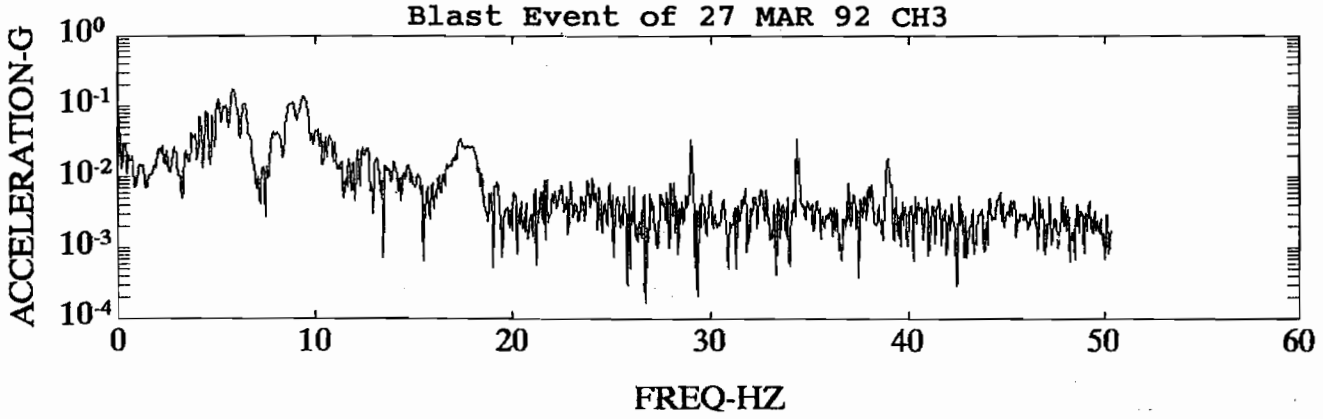
Blast Event of 27 MAR 92 CH3
ACCELERATION-G
FREQ-HZ

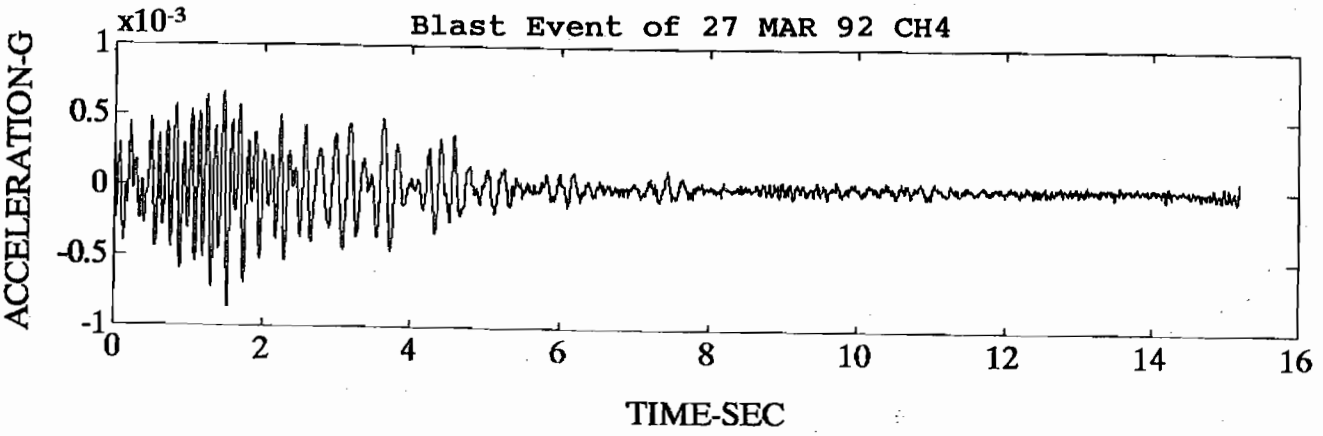
Blast Event of 27 MAR 92 CH4
x10-3
ACCELERATION-G
TIME-SEC

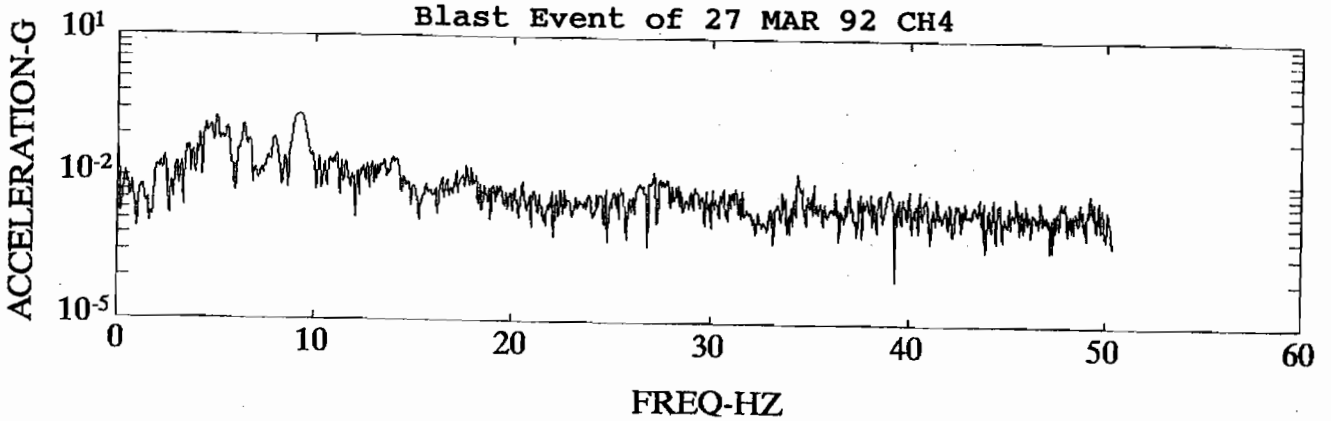
Blast Event of 27 MAR 92 CH4
ACCELERATION-G
FREQ-HZ

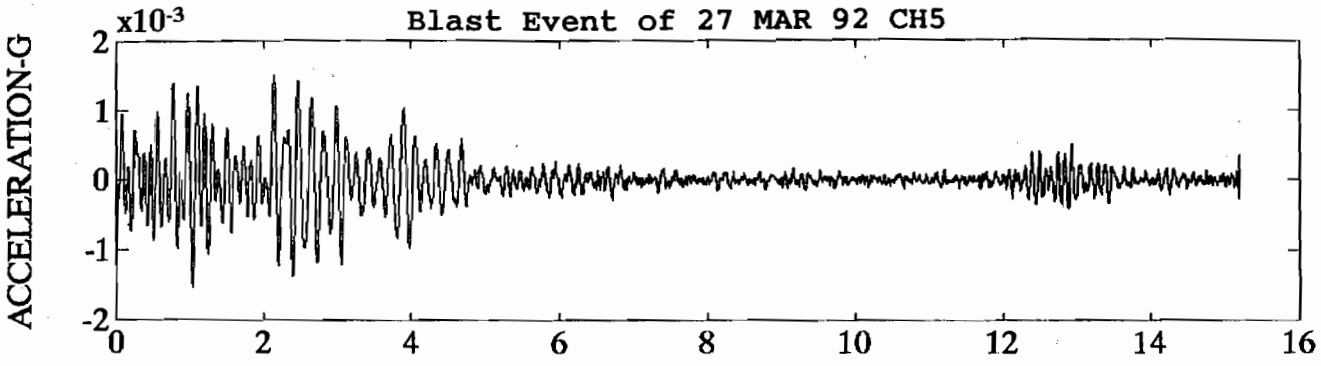
Blast Event of 27 MAR 92 CH5
x10-3
ACCELERATION-G
TIME-SEC

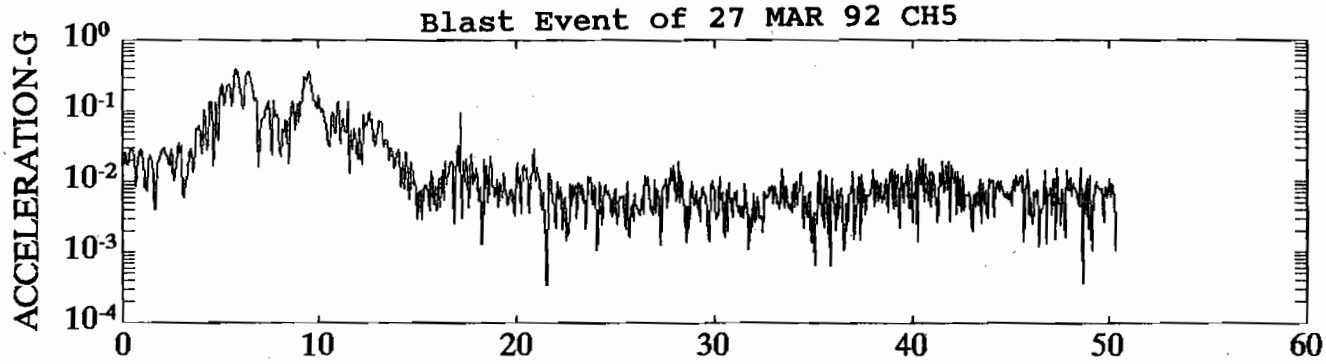
Blast Event of 27 MAR 92 CH5
ACCELERATION-G
FREQ-HZ

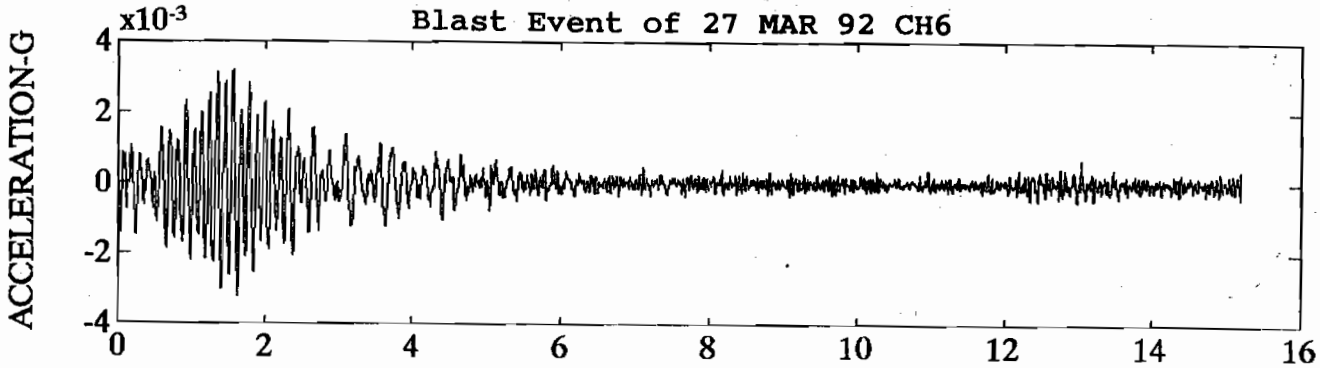
Blast Event of 27 MAR 92 CH6
x10-3
ACCELERATION-G
TIME-SEC

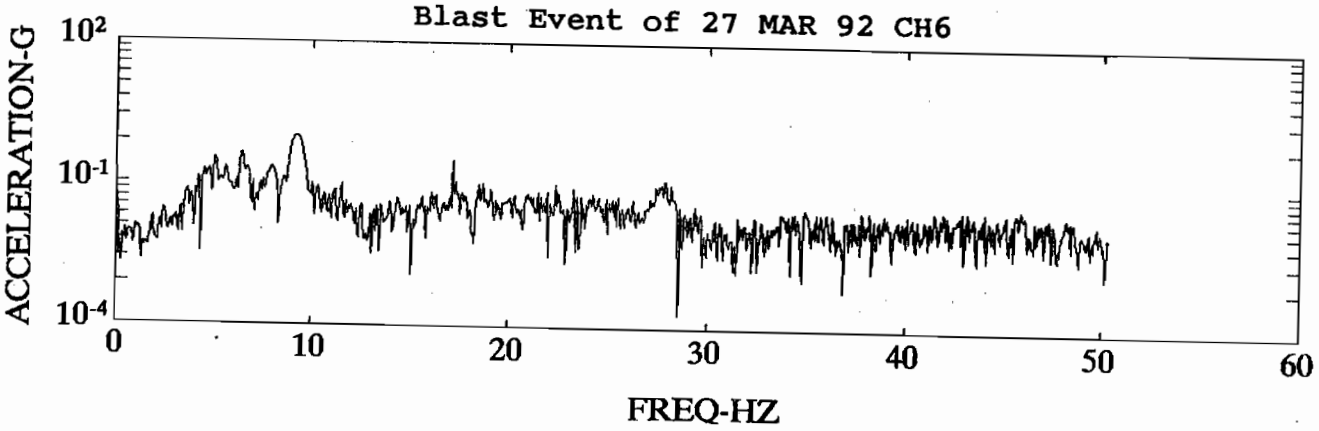
Blast Event of 27 MAR 92 CH6
ACCELERATION-G
FREQ-HZ

PART 3

(See Figure 2.10 for locations)

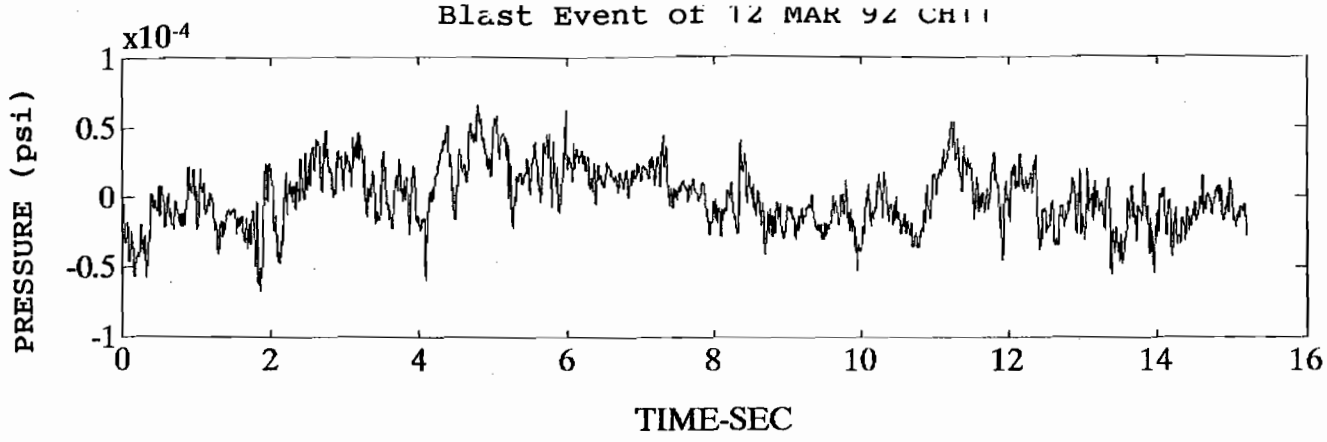
Blast Event of 12 MAR 92 CH11
x10-4
PRESSURE (psi)
TIME-SEC

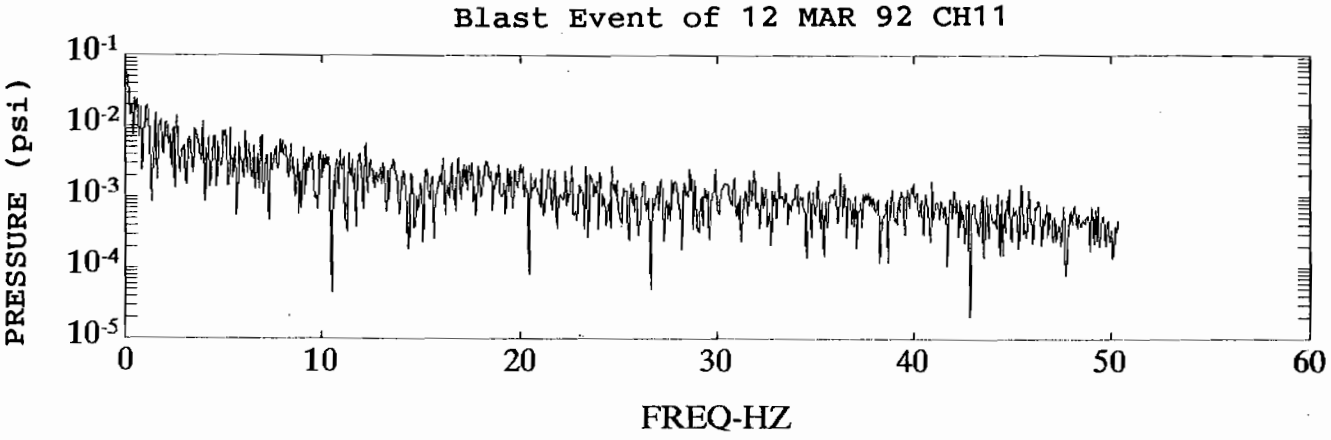
Blast Event of 12 MAR 92 CH11
PRESSURE (psi)
FREQ-HZ

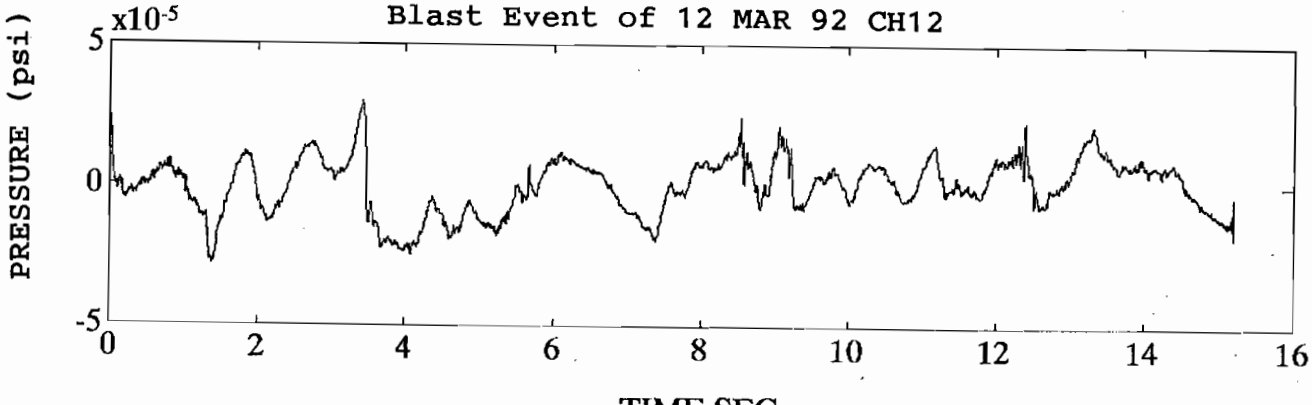
x10-5
Blast Event of 12 MAR 92 CH12
PRESSURE (psi)
TIME-SEC

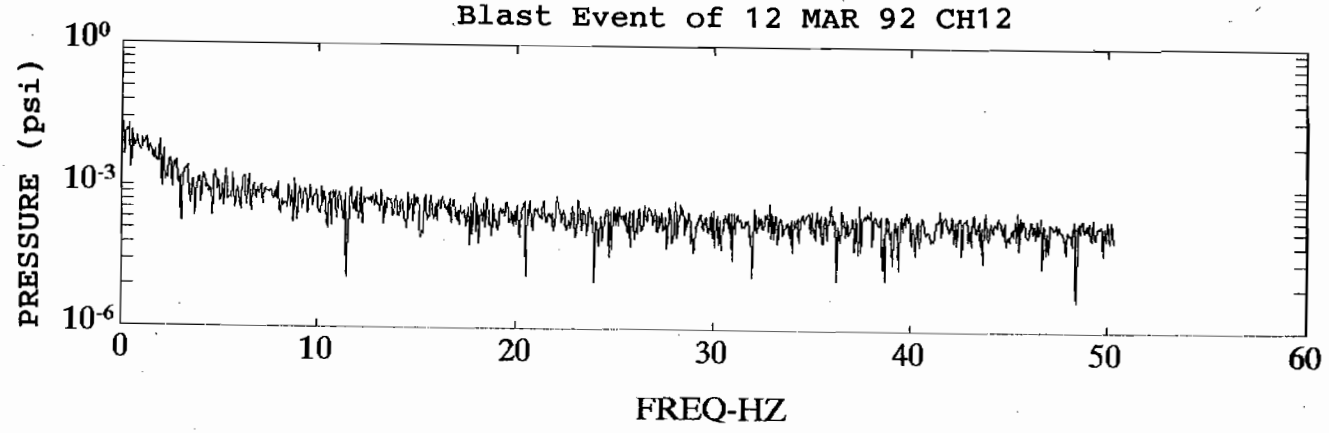
Blast Event of 12 MAR 92 CH12
PRESSURE (psi)
FREQ-HZ

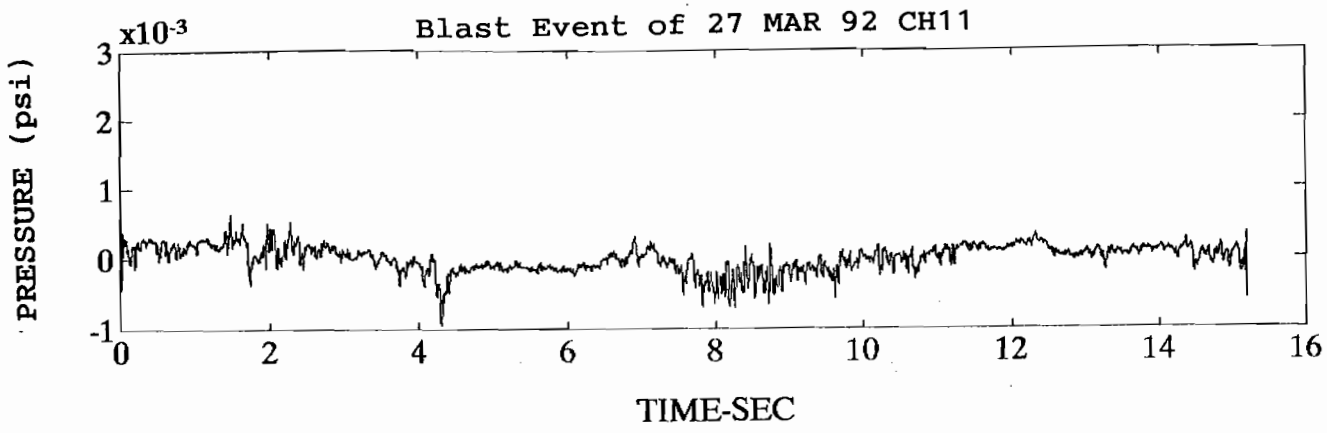
Blast Event of 27 MAR 92 CH11
x10-3
PRESSURE (psi)
TIME-SEC

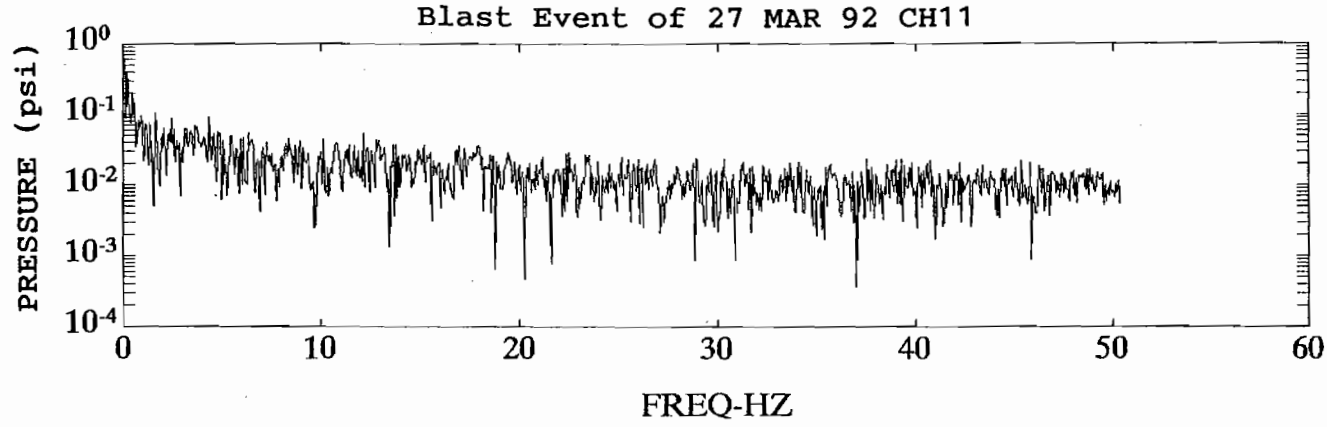
Blast Event of 27 MAR 92 CH11
PRESSURE (psi)
FREQ-HZ

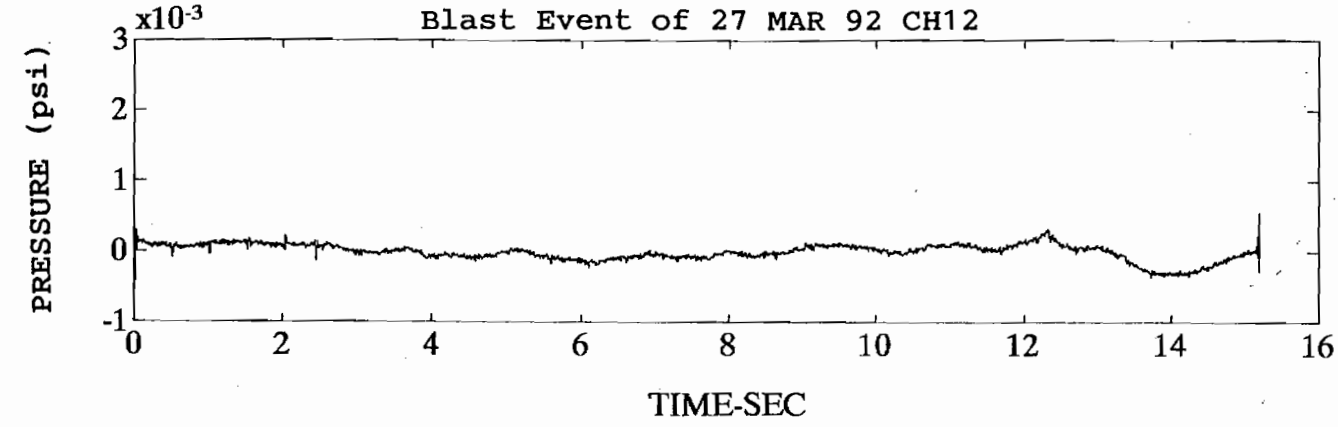
Blast Event of 27 MAR 92 CH12
x10-3
PRESSURE (psi)
TIME-SEC

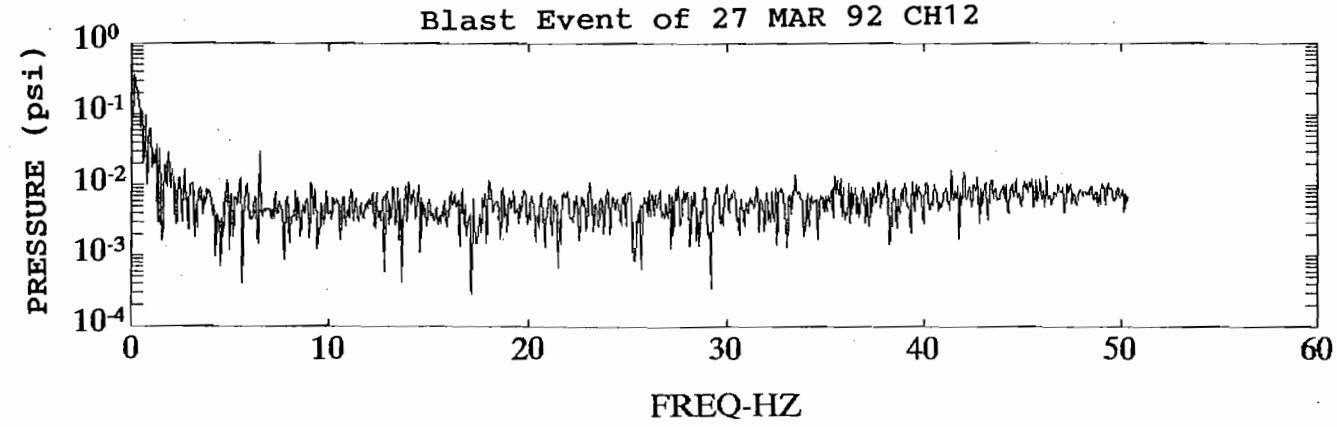
Blast Event of 27 MAR 92 CH12
PRESSURE (psi)
FREQ-HZ

PART 4

PSD: Power Spectral Density

CSD: Cross Spectral Density

Transfer Function: $\frac{CSD}{PSD}$

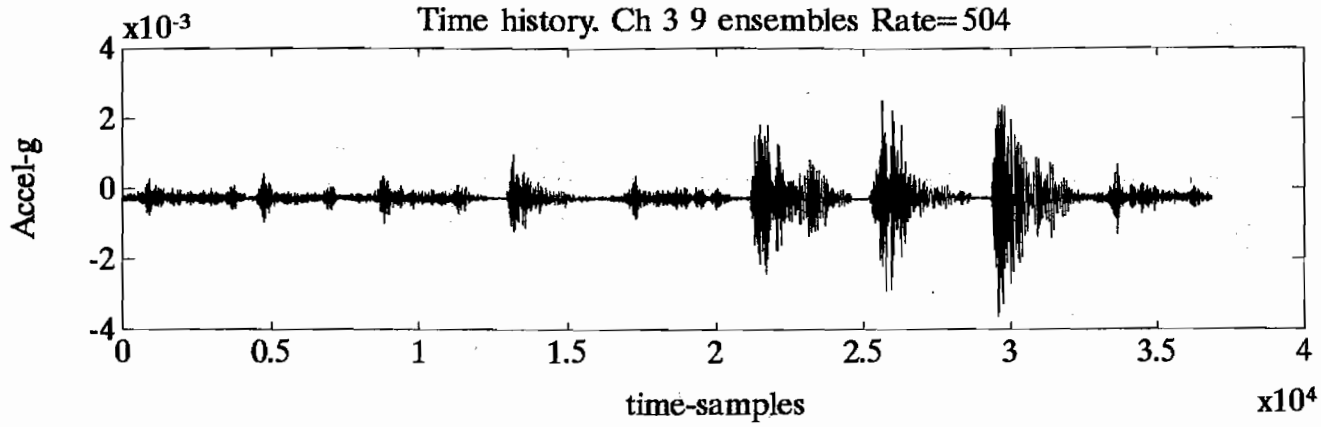
Time history. Ch 3 9 ensembles Rate=504
x10-3
Accel-g
time-samples
x10^4

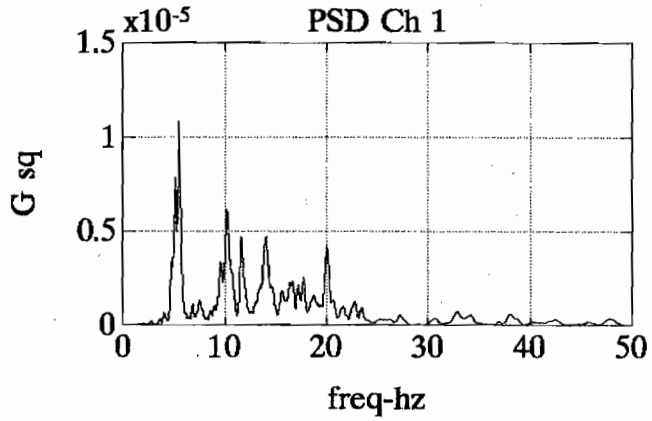
PSD Ch 1
x10-5
G sq
freq-hz

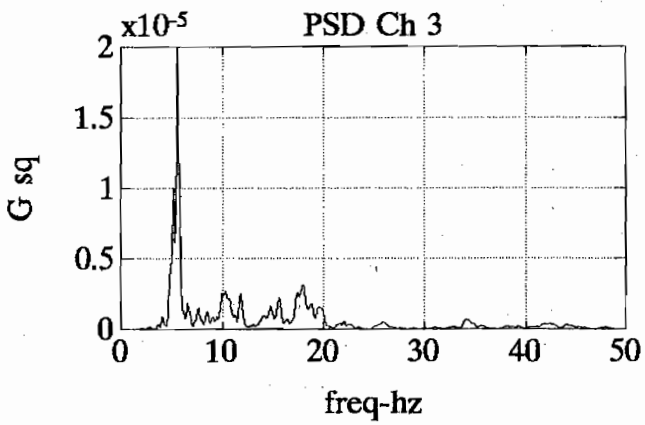
PSD Ch 3
x10-5
G sq
freq-hz

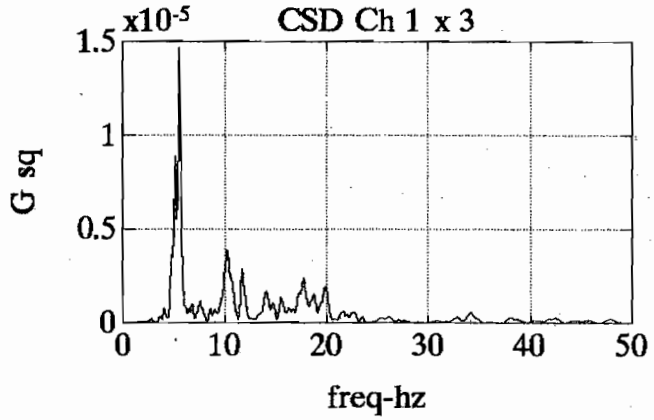
CSD Ch 1 x 3
x10-5
G sq
freq-hz

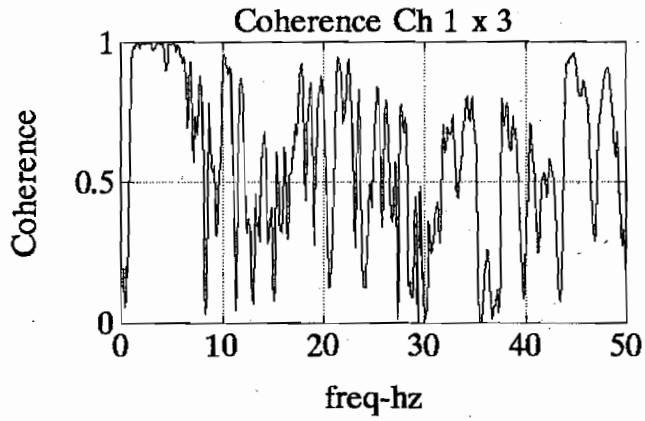
Coherence Ch 1 x 3
Coherence
freq-hz

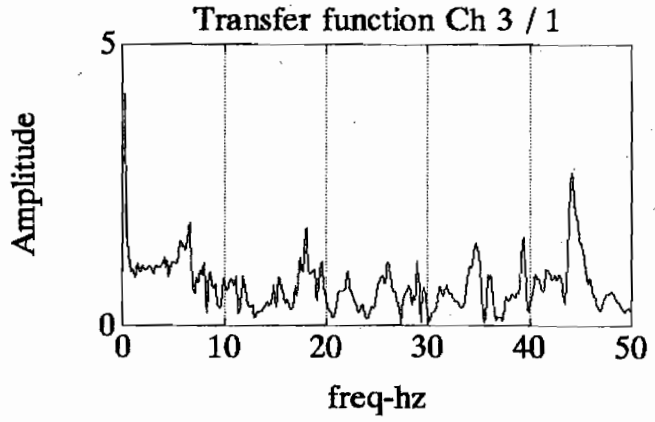
Transfer function Ch 3 / 1
Amplitude
freq-hz

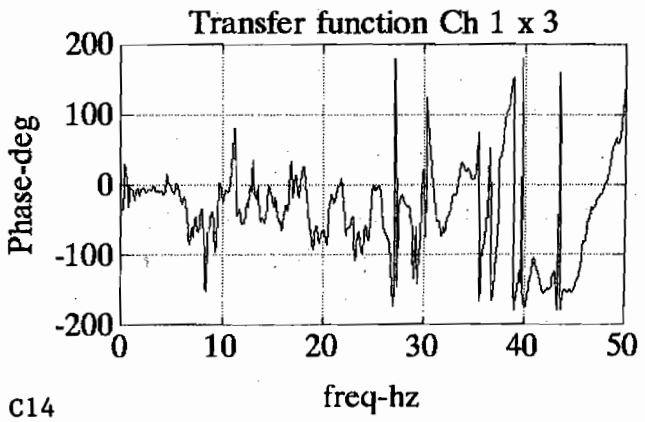
Transfer function Ch 1 x 3
Phase-deg
freq-hz

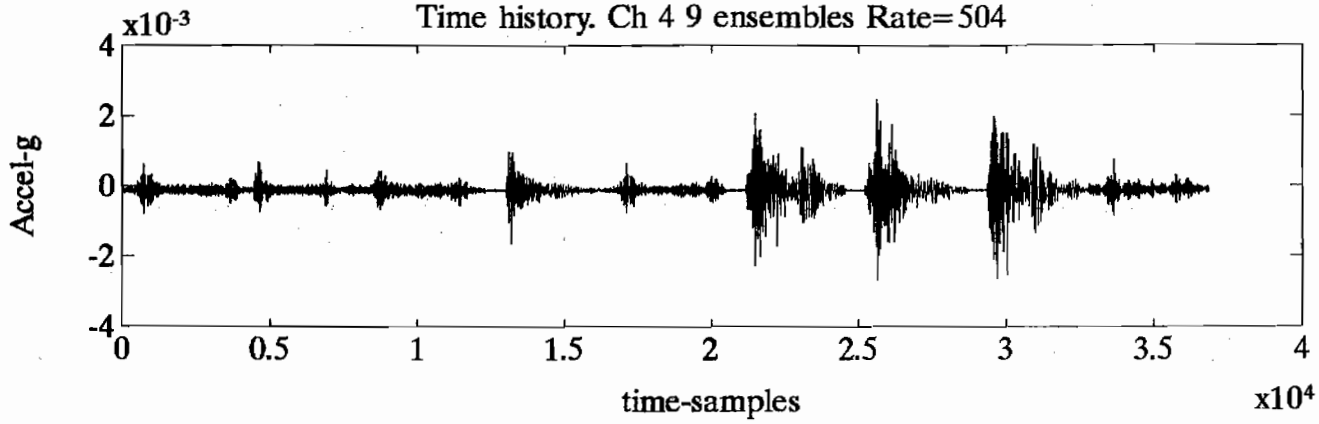
Time history. Ch 4 9 ensembles Rate=504
x10-3
Accel-g
time-samples
x10^4

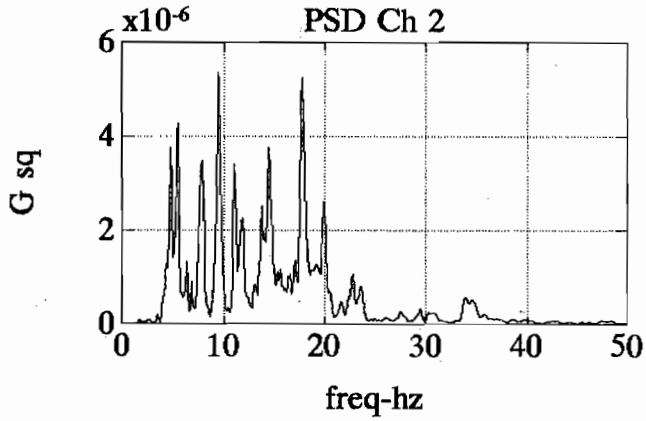
PSD Ch 2
x10-6
G sq
freq-hz

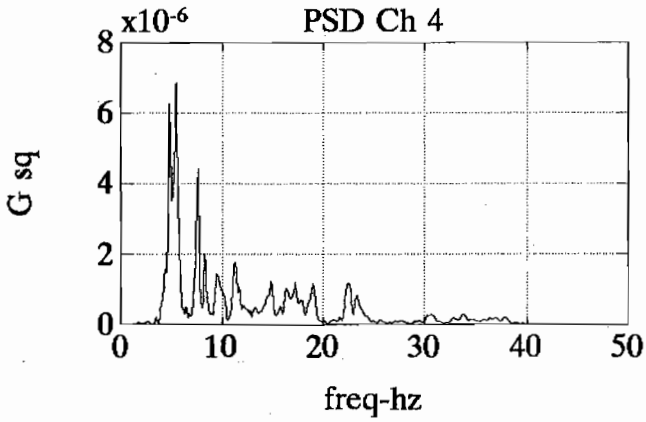
PSD Ch 4
x10-6
G sq
freq-hz

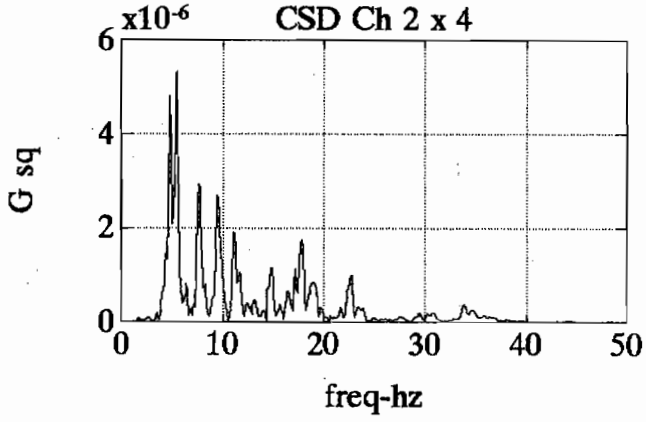
CSD Ch 2 x 4
x10-6
G sq
freq-hz

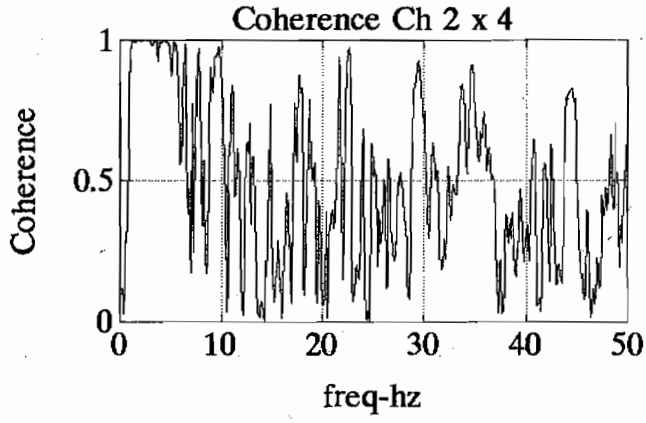
Coherence Ch 2 x 4
Coherence
freq-hz

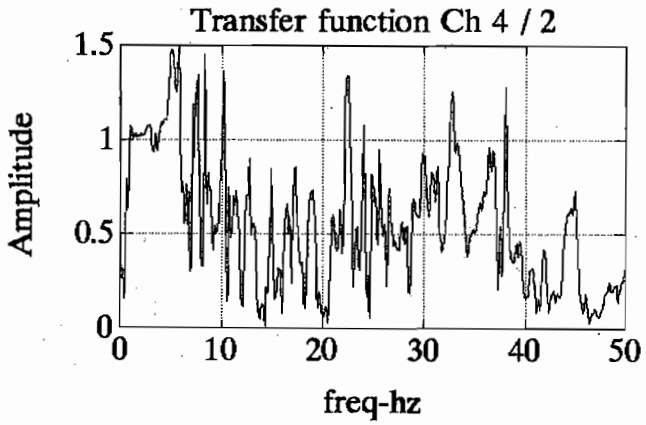
Transfer function Ch 4 / 2
Amplitude
freq-hz

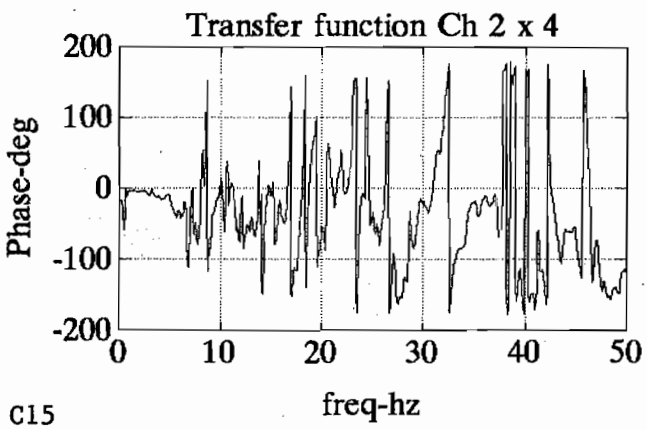
Transfer function Ch 2 x 4
Phase-deg
freq-hz

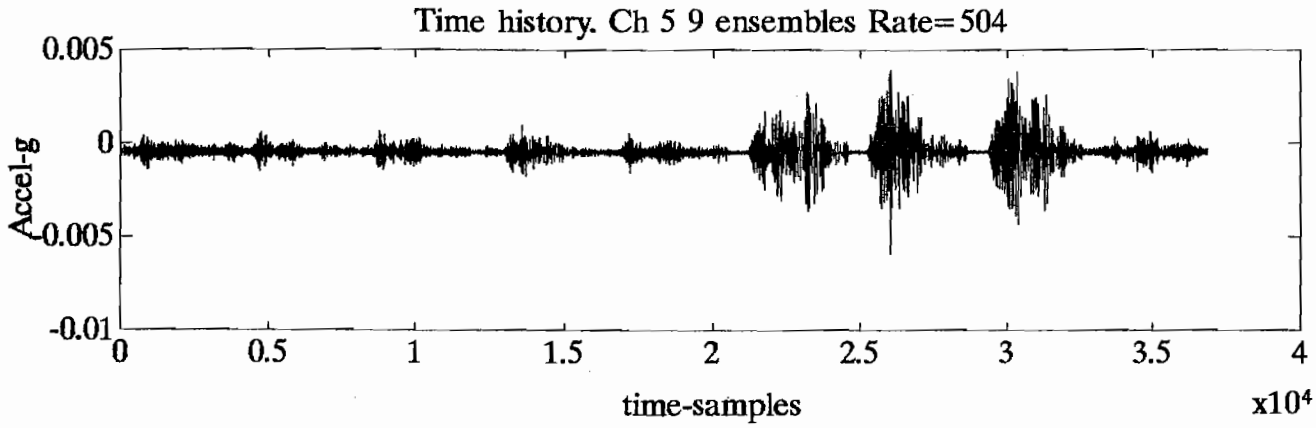
Time history. Ch 5 9 ensembles Rate=504
Accel-g
0.005
0
-0.005
-0.01
0
0.5
1
1.5
2
2.5
3
3.5
4
time-samples
x10^4

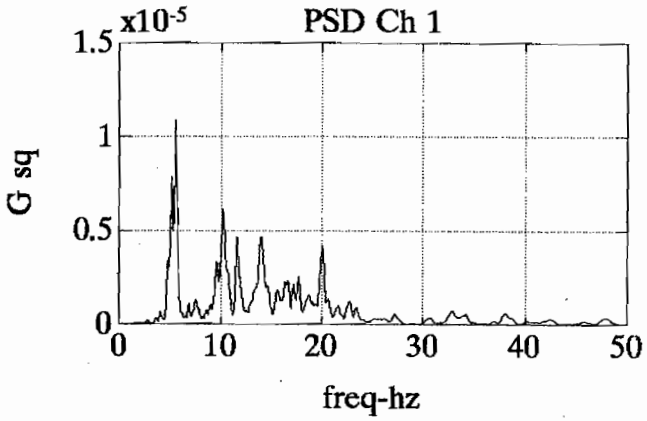
x10^-5
PSD Ch 1
G sq
1.5
1
0.5
0
0
10
20
30
40
50
freq-hz

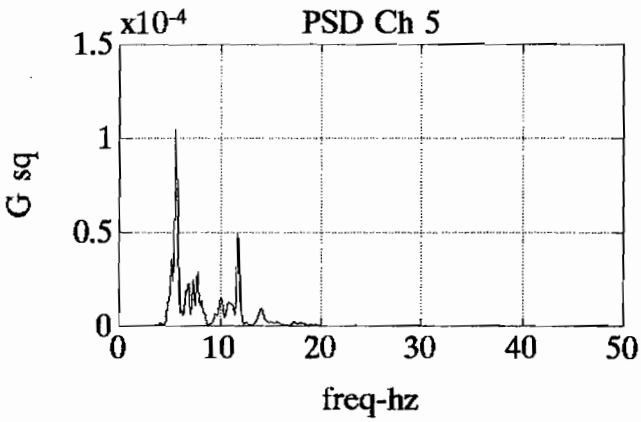
x10^-4
PSD Ch 5
G sq
1.5
1
0.5
0
0
10
20
30
40
50
freq-hz

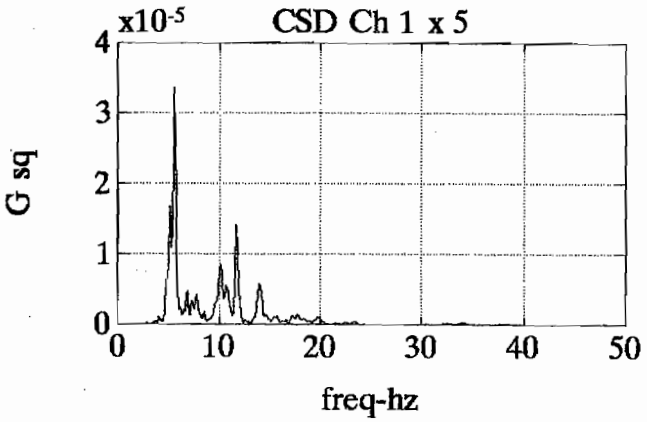
x10^-5
CSD Ch 1 x 5
G sq
4
3
2
1
0
0
10
20
30
40
50
freq-hz

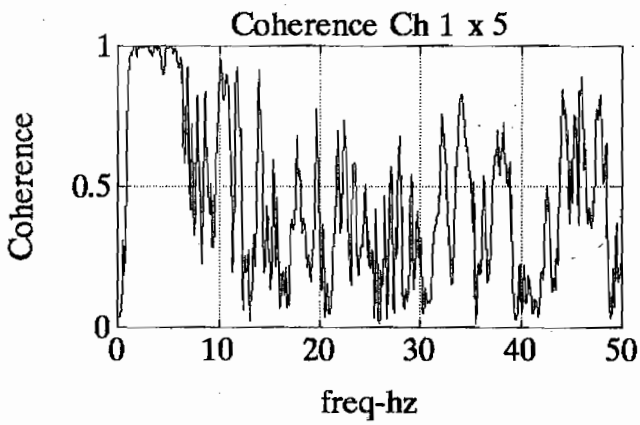
Coherence Ch 1 x 5
Coherence
1
0.5
0
0
10
20
30
40
50
freq-hz

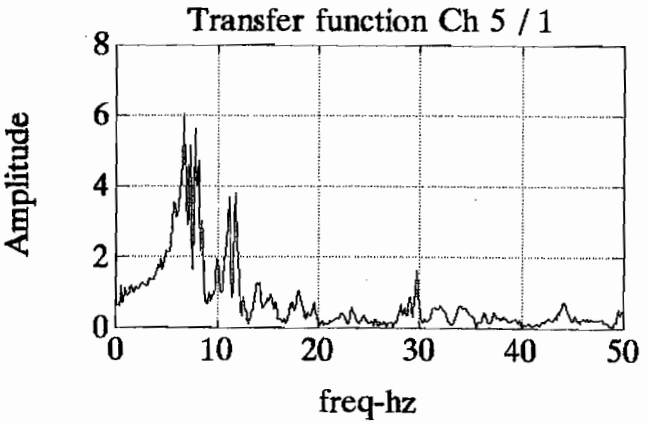
Transfer function Ch 5 / 1
Amplitude
8
6
4
2
0
0
10
20
30
40
50
freq-hz

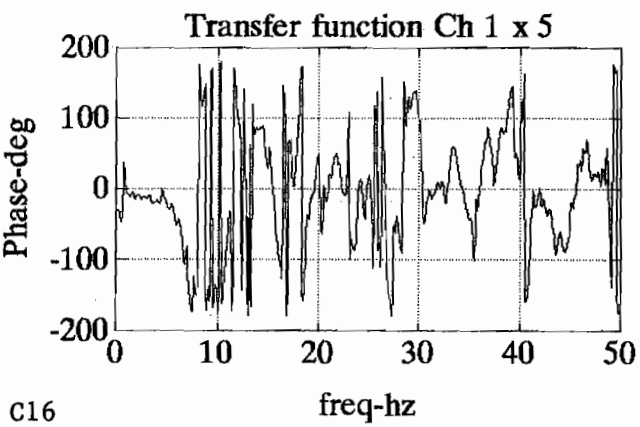
Transfer function Ch 1 x 5
Phase-deg
200
100
0
-100
-200
0
10
20
30
40
50
freq-hz

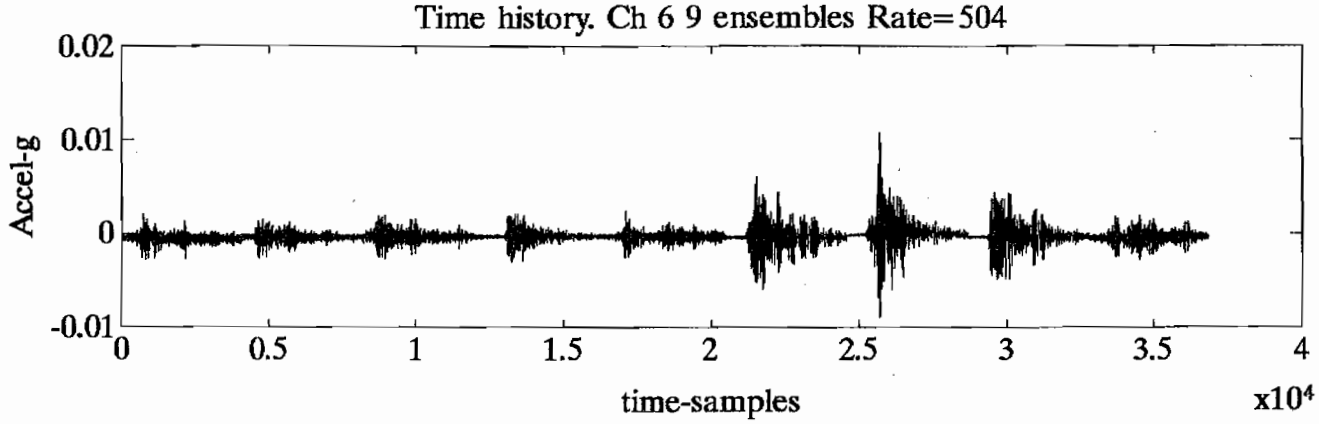
Time history. Ch 6 9 ensembles Rate=504
Accel-g
0.02
0.01
0
-0.01
0
0.5
1
1.5
2
2.5
3
3.5
4
time-samples
x10^4

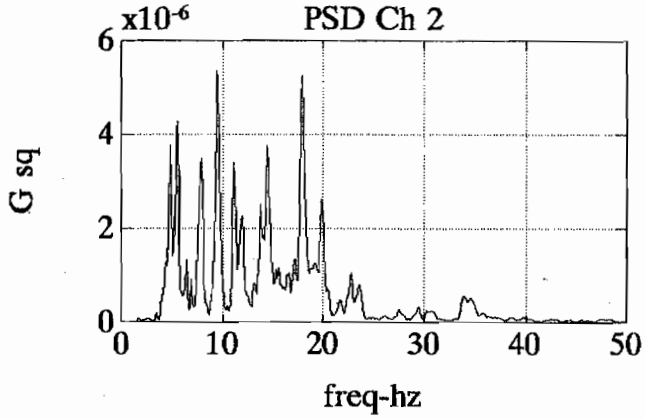
x10^-6
PSD Ch 2
G sq
6
4
2
0
0
10
20
30
40
50
freq-hz

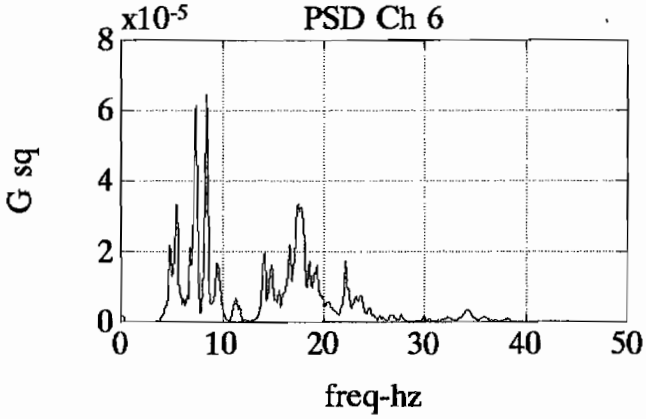
x10^-5
PSD Ch 6
G sq
8
6
4
2
0
0
10
20
30
40
50
freq-hz

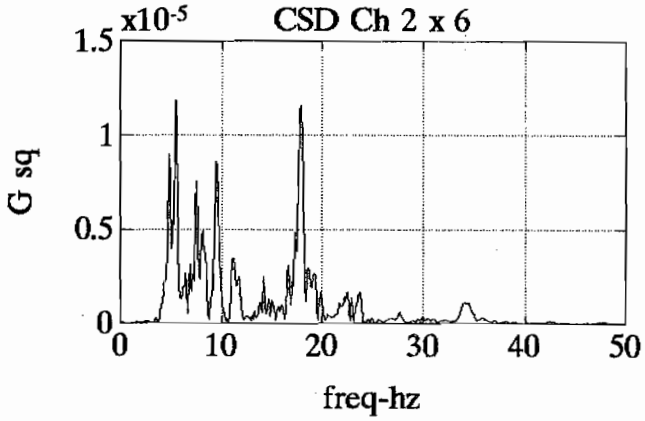
x10^-5
CSD Ch 2 x 6
G sq
1.5
1
0.5
0
0
10
20
30
40
50
freq-hz

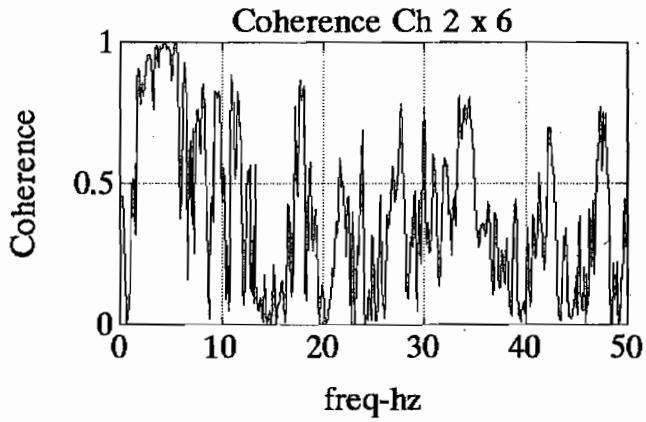
Coherence Ch 2 x 6
Coherence
1
0.5
0
0
10
20
30
40
50
freq-hz

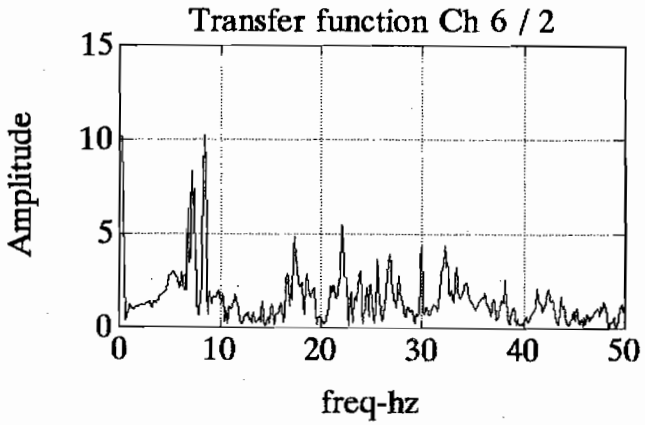
Transfer function Ch 6 / 2
Amplitude
15
10
5
0
0
10
20
30
40
50
freq-hz

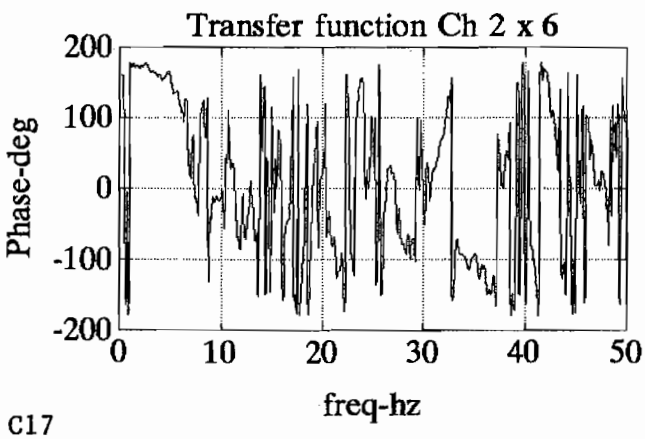
Transfer function Ch 2 x 6
Phase-deg
200
100
0
-100
-200
0
10
20
30
40
50
freq-hz

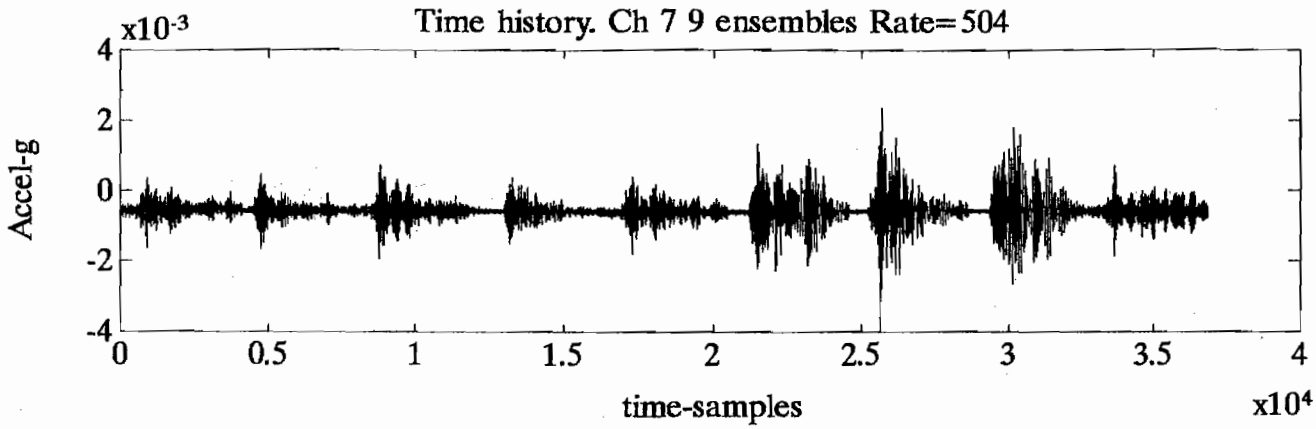
Time history. Ch 7 9 ensembles Rate=504
x10-3
Accel-g
time-samples
x10⁴

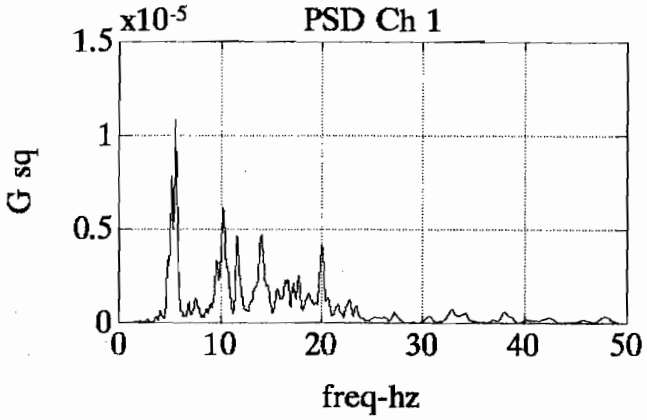
PSD Ch 1
x10-5
G sq
freq-hz

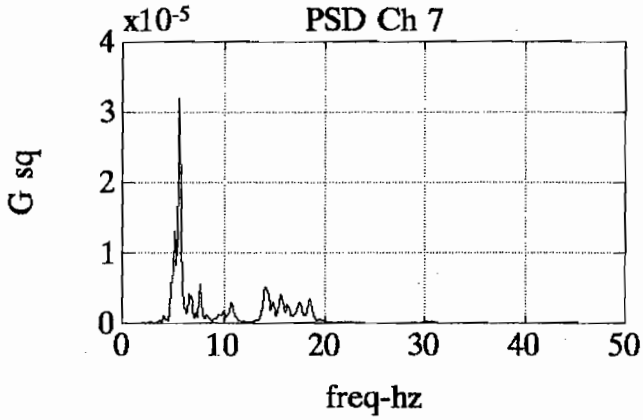
PSD Ch 7
x10-5
G sq
freq-hz

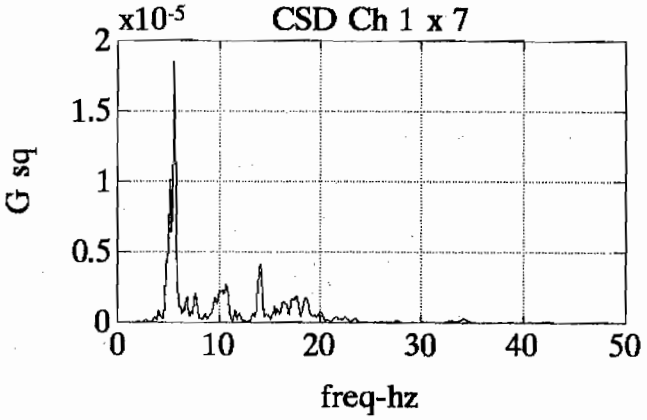
CSD Ch 1 x 7
x10-5
G sq
freq-hz

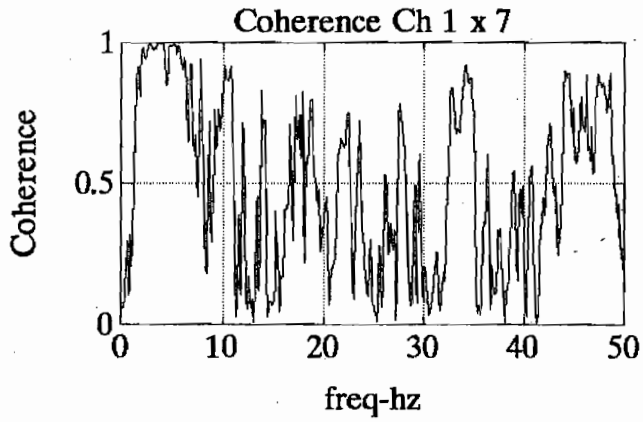
Coherence Ch 1 x 7
Coherence
freq-hz

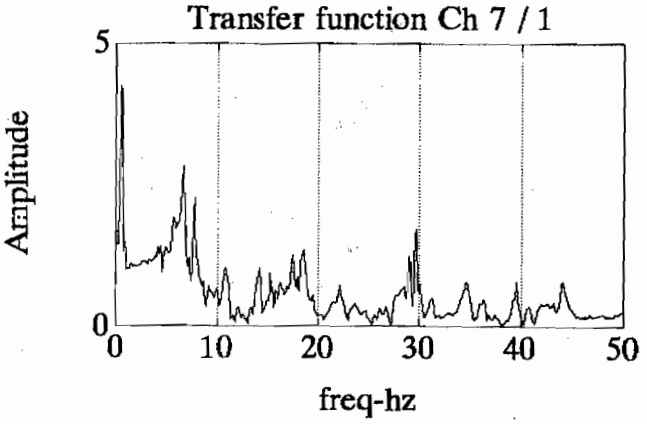
Transfer function Ch 7 / 1
Amplitude
freq-hz

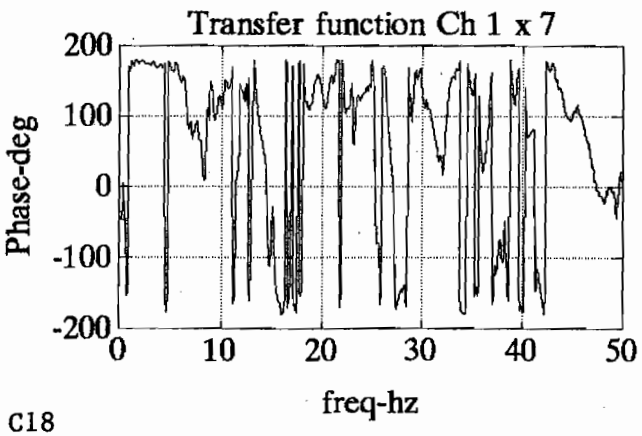
Transfer function Ch 1 x 7
Phase-deg
freq-hz

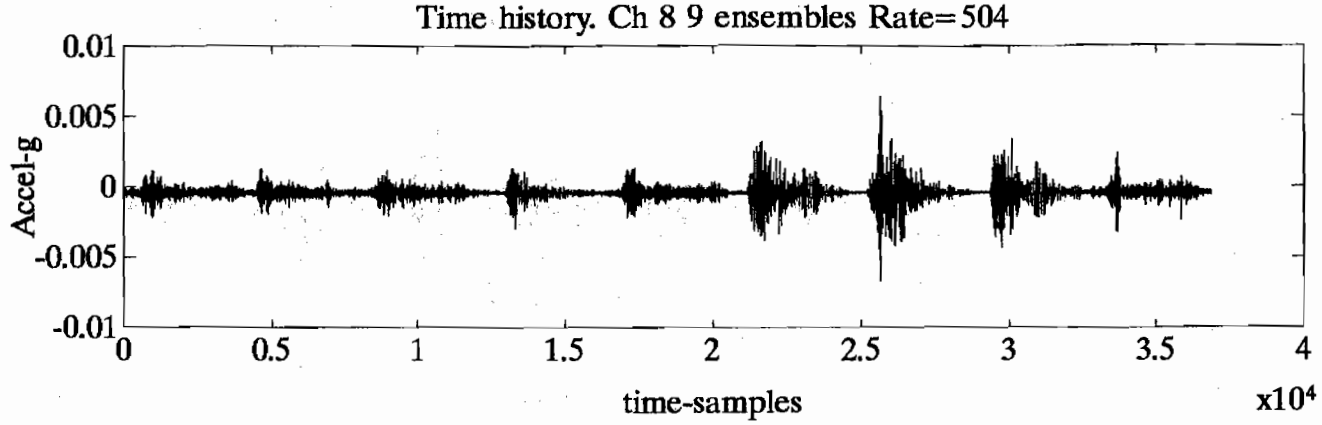
Time history. Ch 8 9 ensembles Rate=504
Accel-g
0.01
0.005
0
-0.005
-0.01
0
0.5
1
1.5
2
2.5
3
3.5
4
time-samples
x10^4

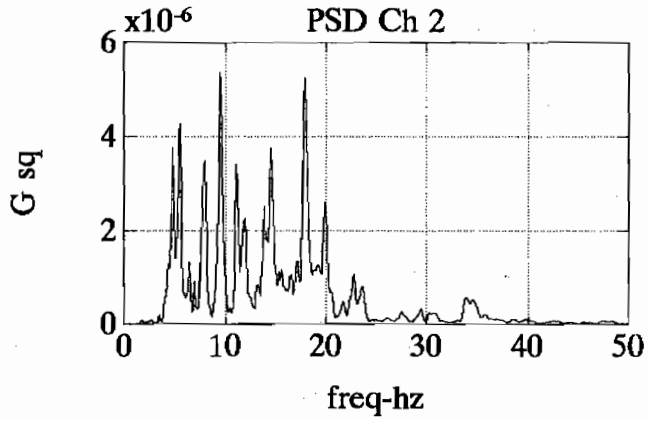
x10^-6
PSD Ch 2
G sq
6
4
2
0
0
10
20
30
40
50
freq-hz

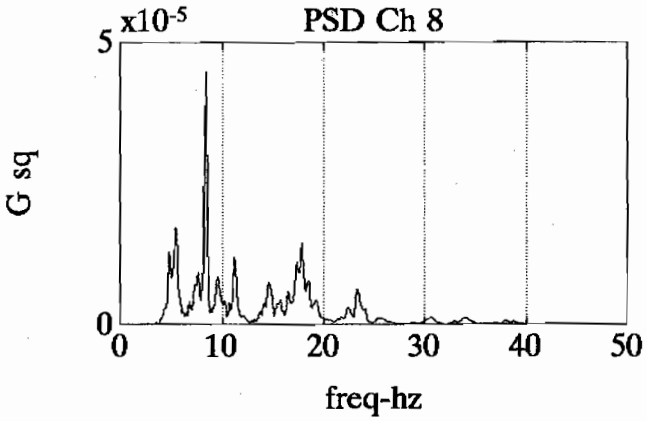
x10^-5
PSD Ch 8
G sq
5
0
0
10
20
30
40
50
freq-hz

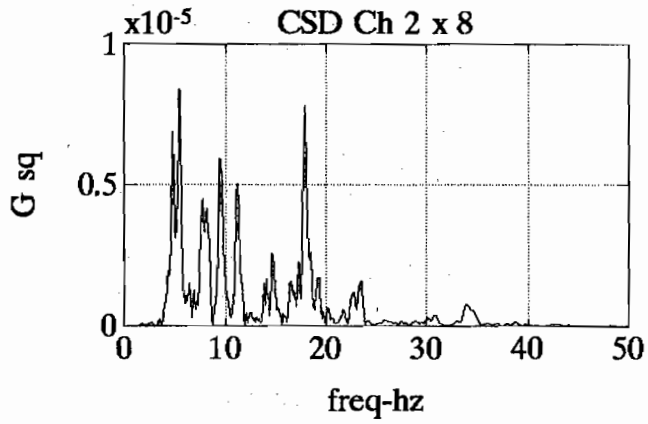
x10^-5
CSD Ch 2 x 8
G sq
1
0.5
0
0
10
20
30
40
50
freq-hz

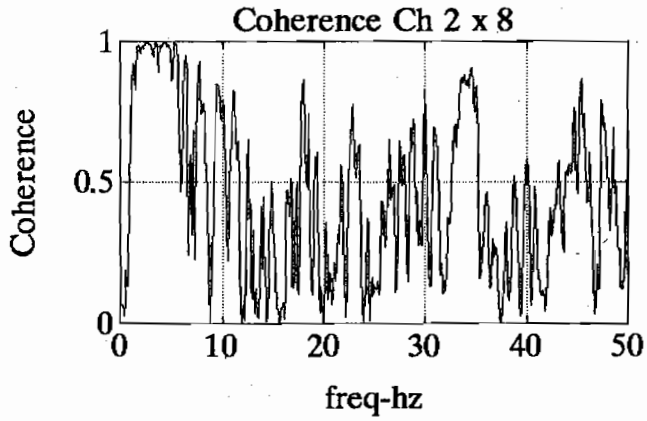
Coherence Ch 2 x 8
Coherence
1
0.5
0
0
10
20
30
40
50
freq-hz

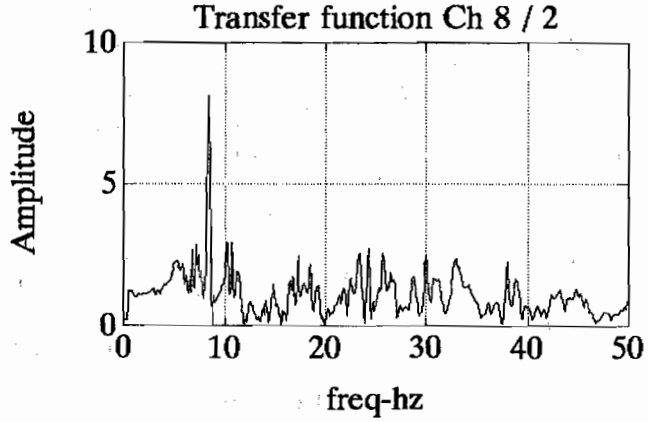
Transfer function Ch 8 / 2
Amplitude
10
5
0
0
10
20
30
40
50
freq-hz

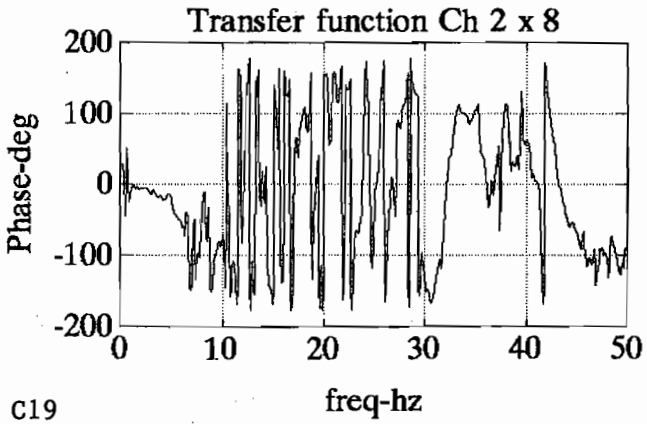
Transfer function Ch 2 x 8
Phase-deg
200
100
0
-100
-200
0
10
20
30
40
50
freq-hz

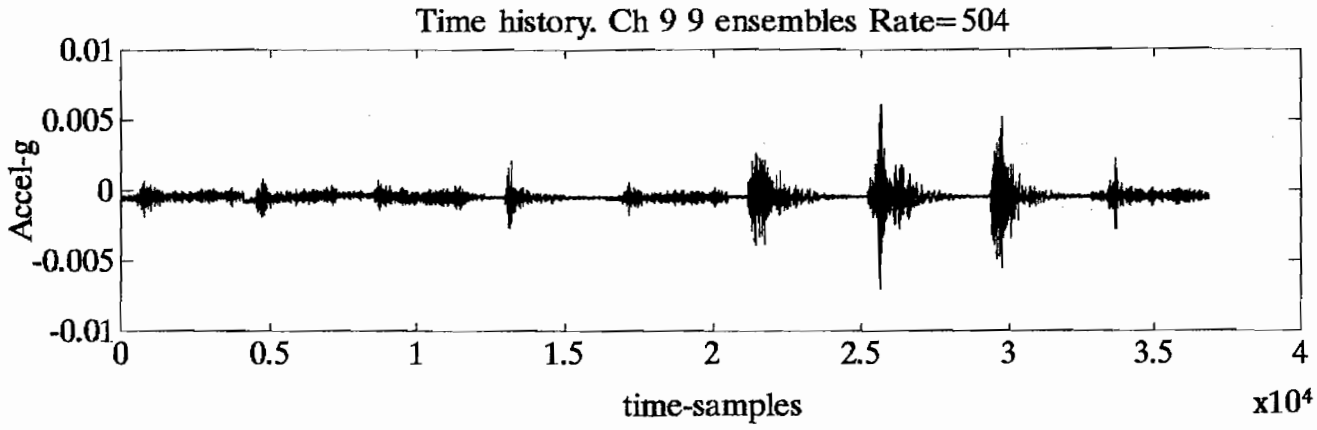
Time history. Ch 9 9 ensembles Rate=504
Accel-g
0.01
0.005
0
-0.005
-0.01
0
0.5
1
1.5
2
2.5
3
3.5
4
time-samples
x10^4

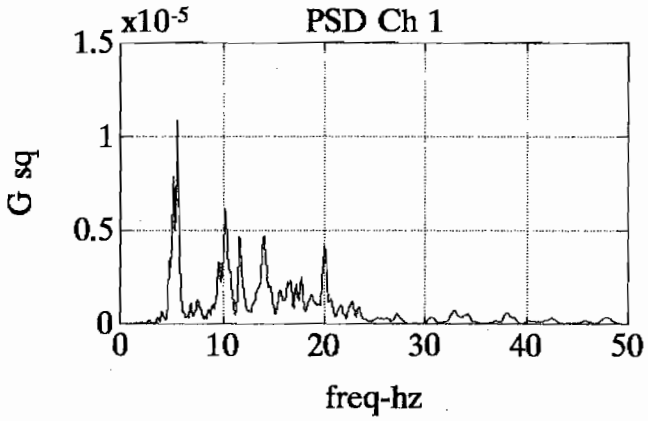
x10^-5
PSD Ch 1
G sq
1.5
1
0.5
0
0
10
20
30
40
50
freq-hz

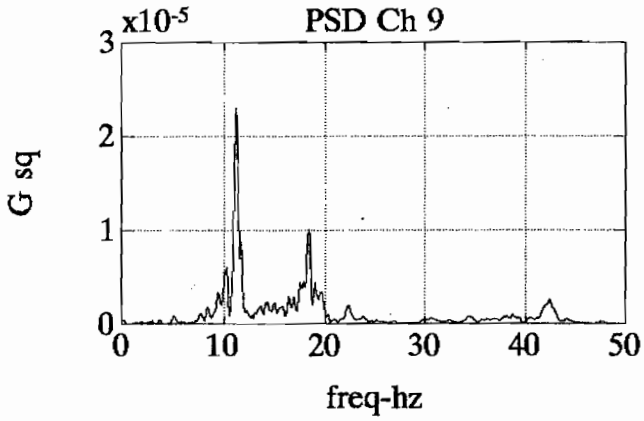
x10^-5
PSD Ch 9
G sq
3
2
1
0
0
10
20
30
40
50
freq-hz

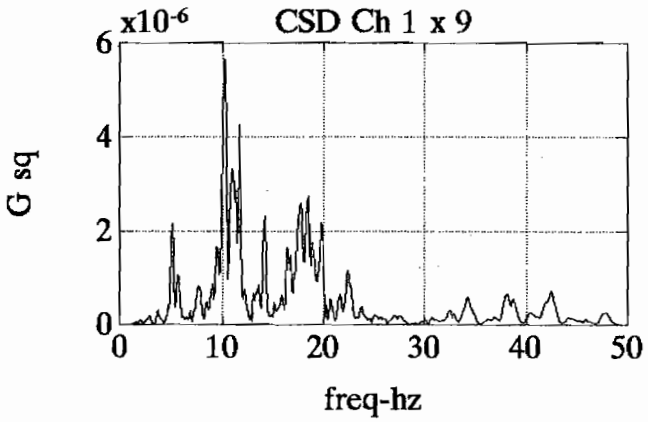
x10^-6
CSD Ch 1 x 9
G sq
6
4
2
0
0
10
20
30
40
50
freq-hz

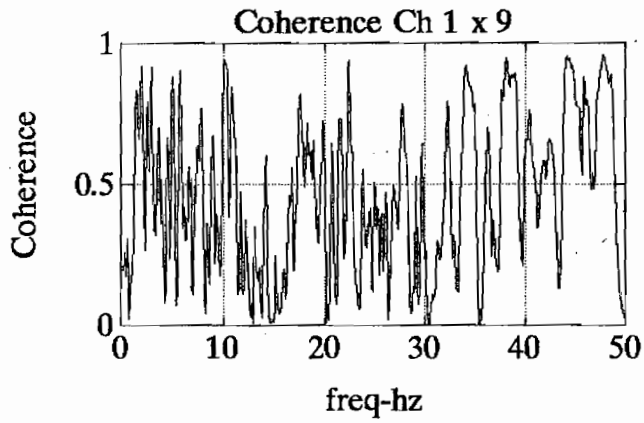
Coherence Ch 1 x 9
Coherence
1
0.5
0
0
10
20
30
40
50
freq-hz

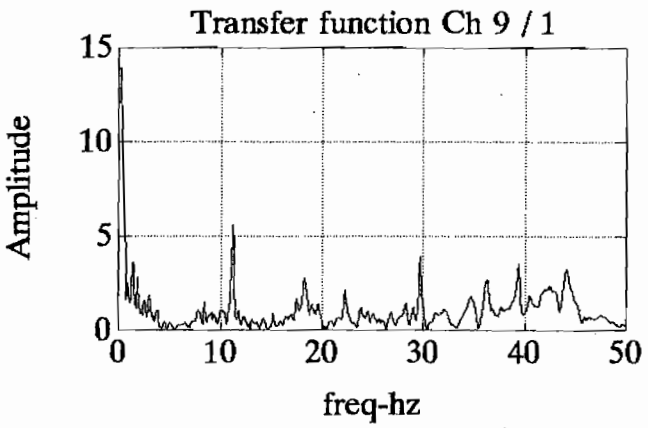
Transfer function Ch 9 / 1
Amplitude
15
10
5
0
0
10
20
30
40
50
freq-hz

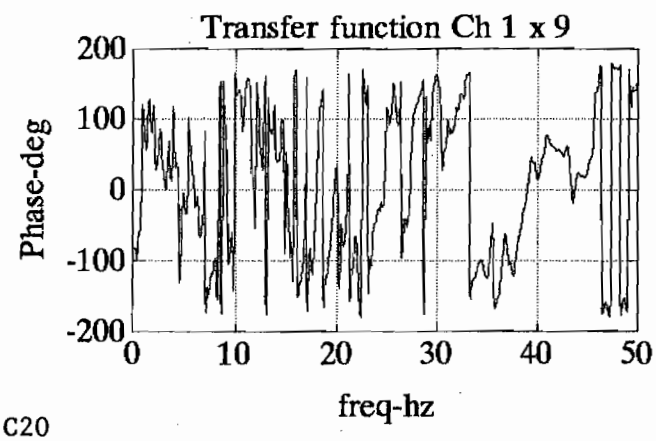
Transfer function Ch 1 x 9
Phase-deg
200
100
0
-100
-200
0
10
20
30
40
50
freq-hz

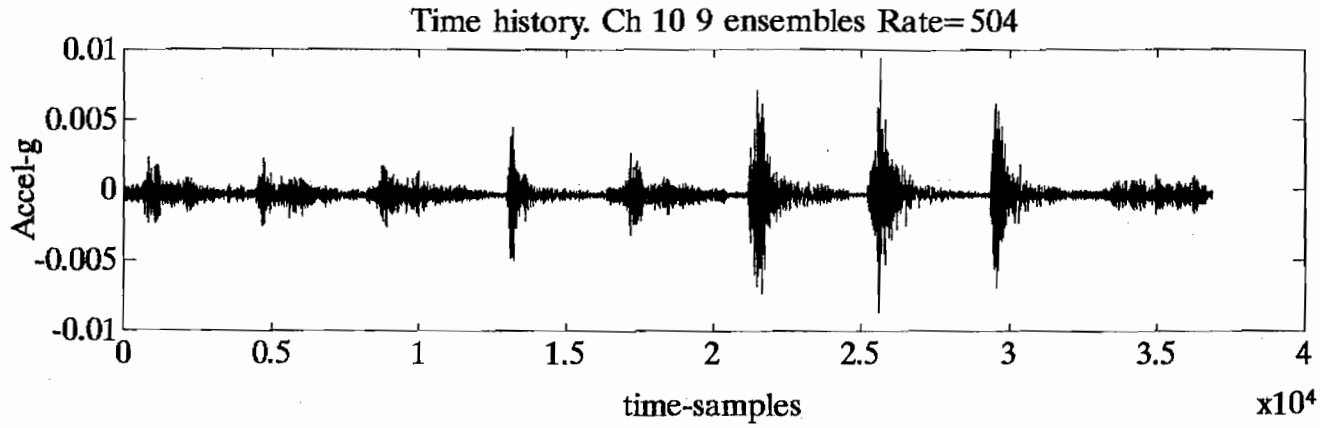
Time history. Ch 10 9 ensembles Rate= 504
Accel-g
0.01
0.005
0
-0.005
-0.01
0
0.5
1
1.5
2
2.5
3
3.5
4
time-samples
x10^4

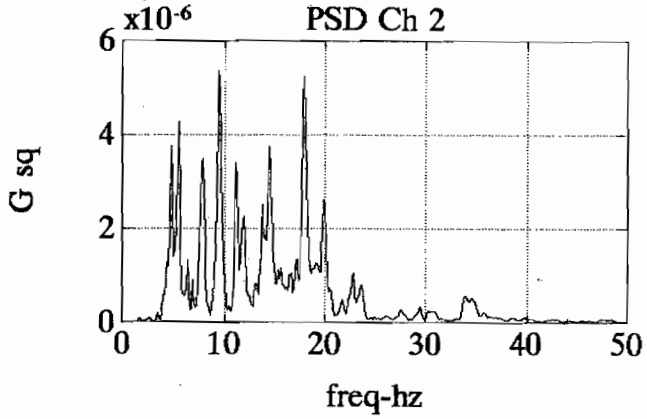
x10^-6
PSD Ch 2
G sq
6
4
2
0
0
10
20
30
40
50
freq-hz

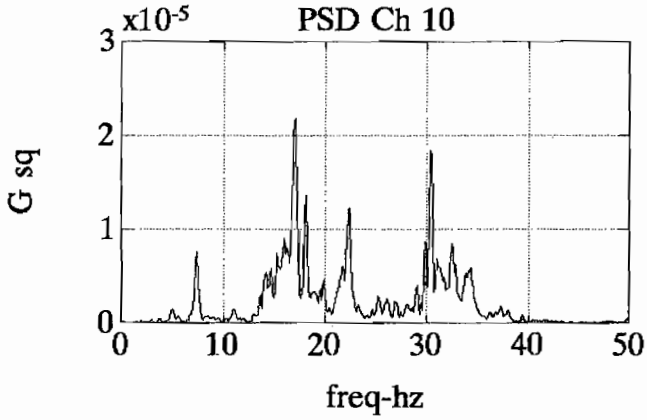
x10^-5
PSD Ch 10
G sq
3
2
1
0
0
10
20
30
40
50
freq-hz

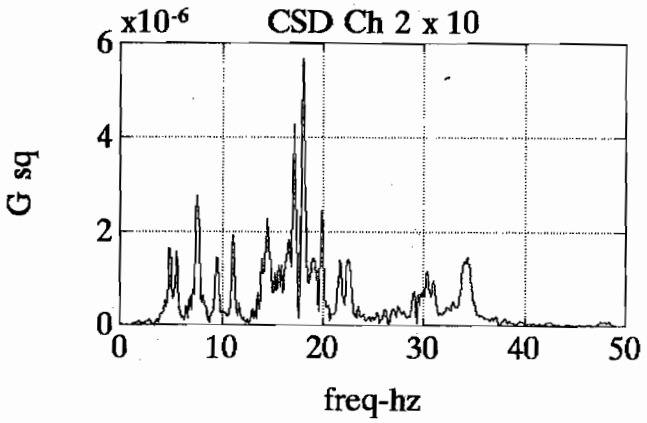
x10^-6
CSD Ch 2 x 10
G sq
6
4
2
0
0
10
20
30
40
50
freq-hz

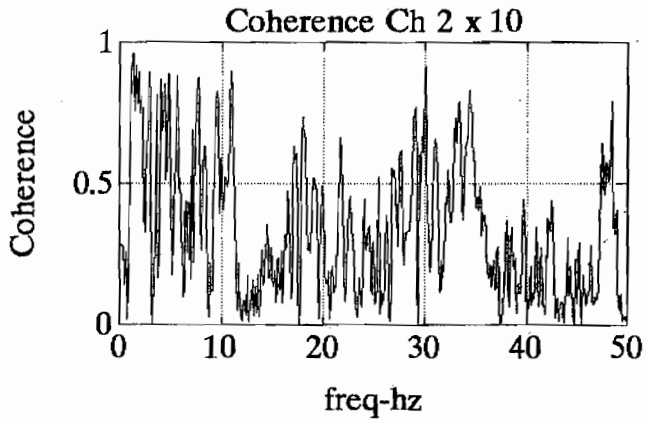
Coherence Ch 2 x 10
Coherence
1
0.5
0
0
10
20
30
40
50
freq-hz

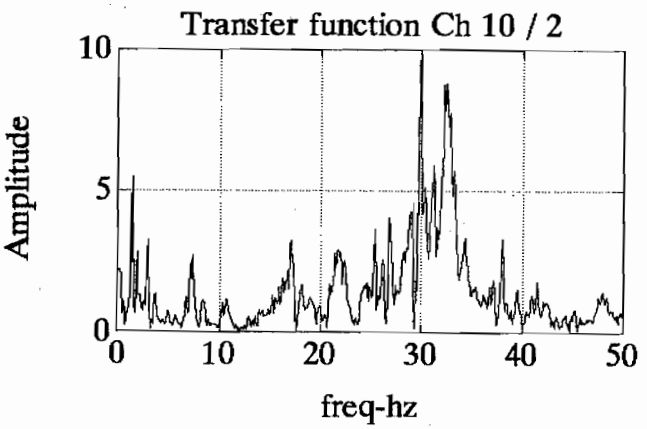
Transfer function Ch 10 / 2
Amplitude
10
5
0
0
10
20
30
40
50
freq-hz

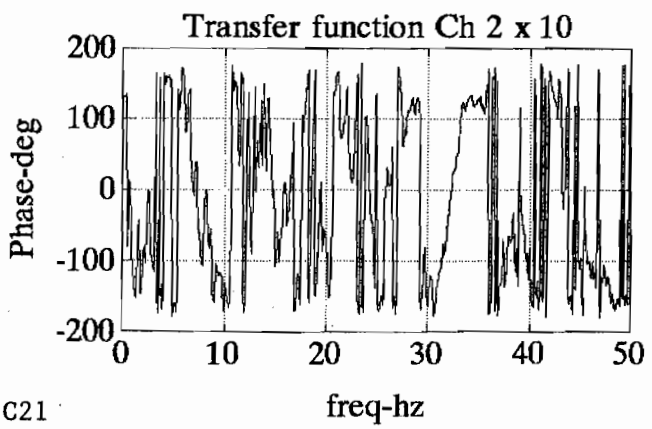
Transfer function Ch 2 x 10
Phase-deg
200
100
0
-100
-200
0
10
20
30
40
50
freq-hz

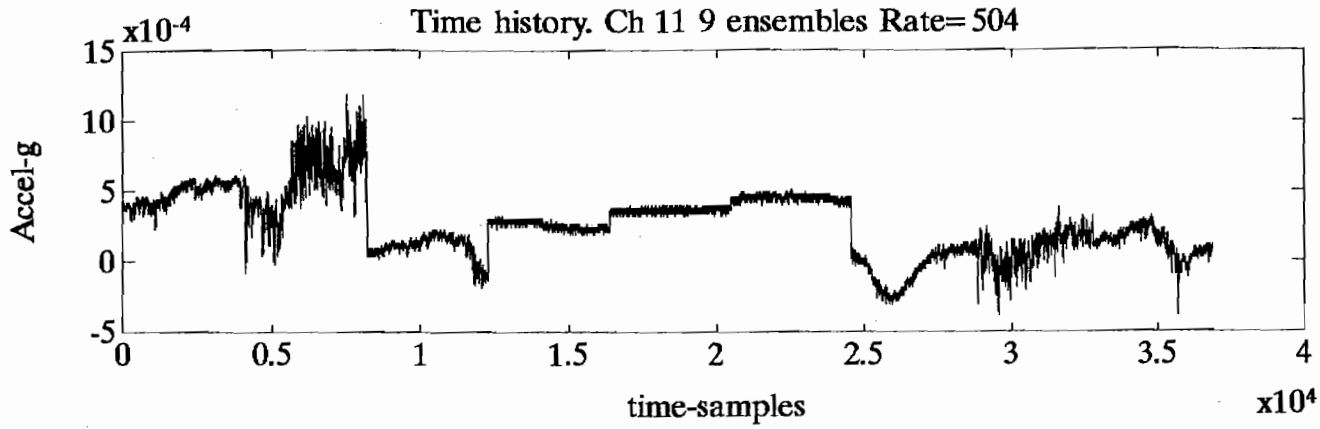
Time history. Ch 11 9 ensembles Rate= 504
x10-4
Accel-g
time-samples
x10⁴

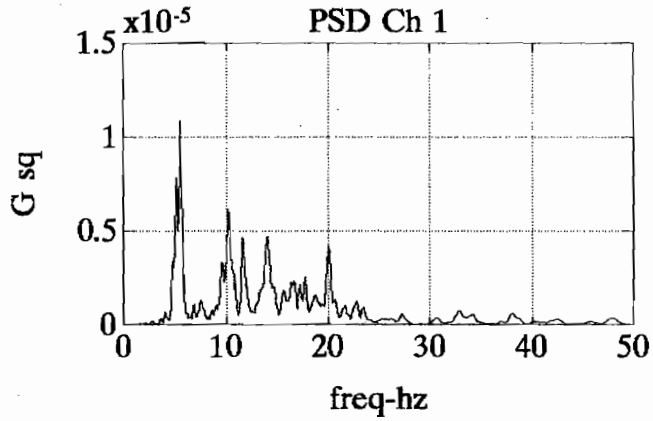
PSD Ch 1
x10-5
G sq
freq-hz

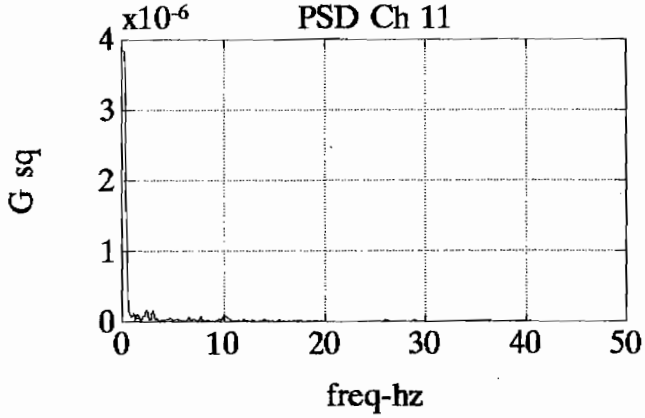
PSD Ch 11
x10-6
G sq
freq-hz

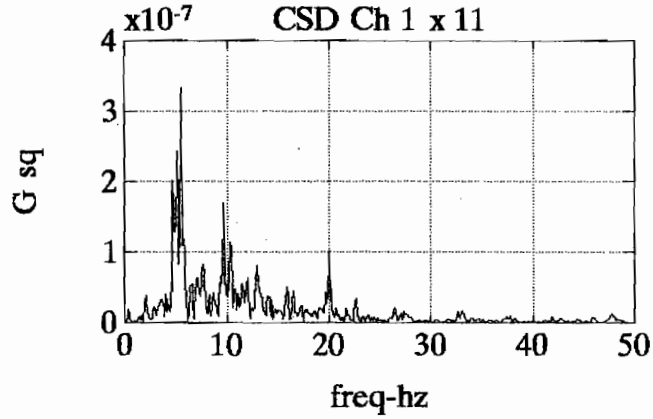
CSD Ch 1 x 11
x10-7
G sq
freq-hz

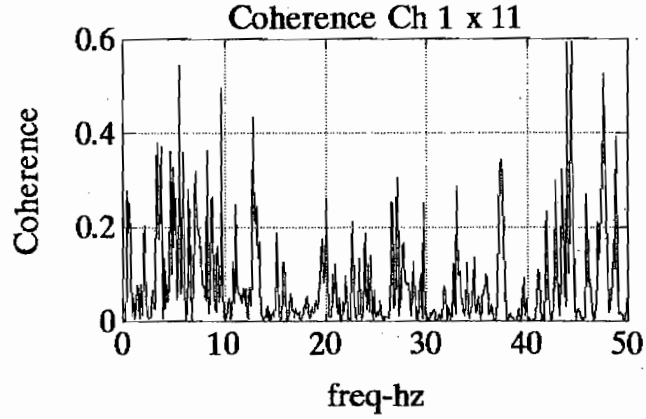
Coherence Ch 1 x 11
Coherence
freq-hz

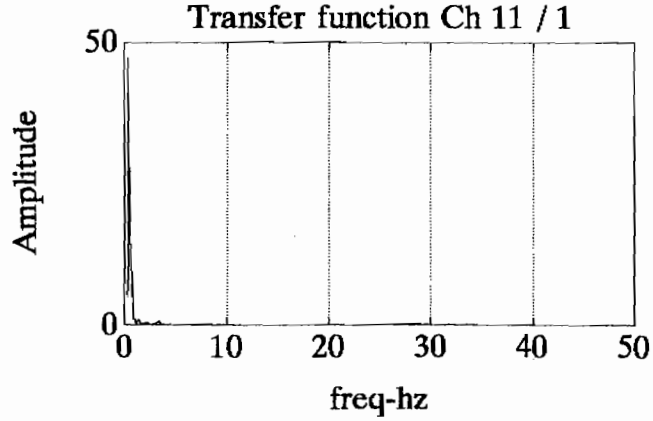
Transfer function Ch 11 / 1
Amplitude
freq-hz

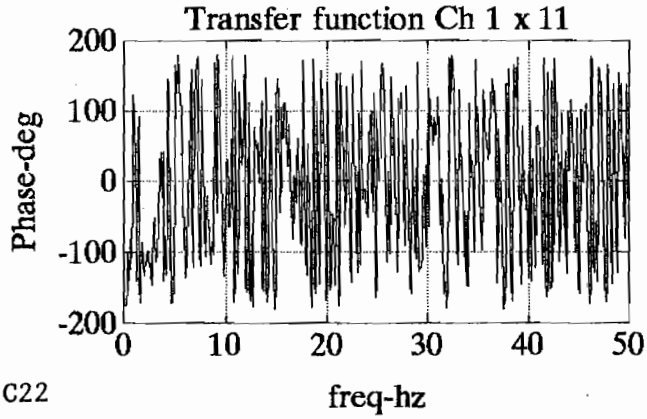
Transfer function Ch 1 x 11
Phase-deg
freq-hz

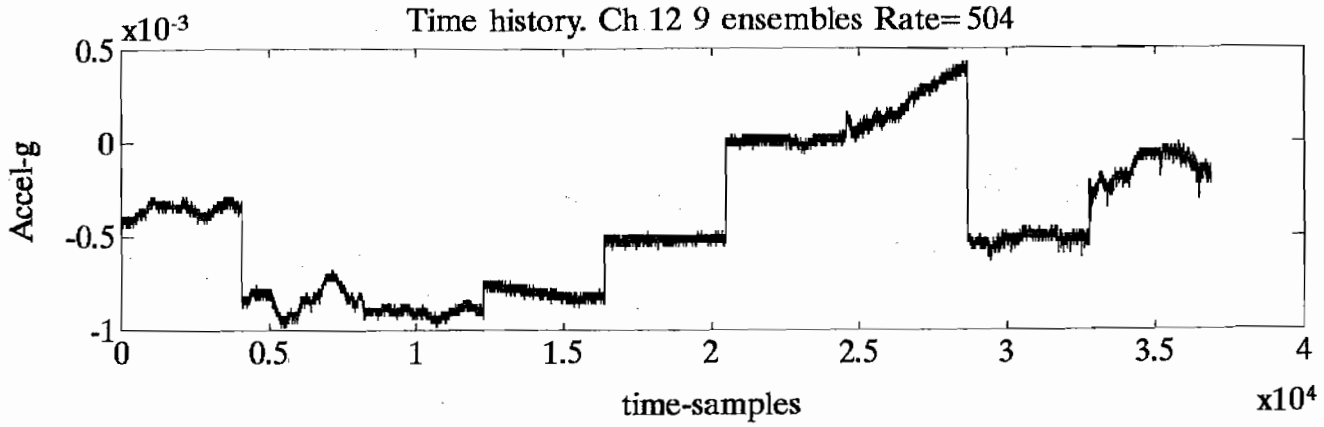
Time history. Ch 12 9 ensembles Rate= 504
x10-3
0.5
0
-0.5
-1
Accel-g
0
0.5
1
1.5
2
2.5
3
3.5
4
time-samples
x10^4

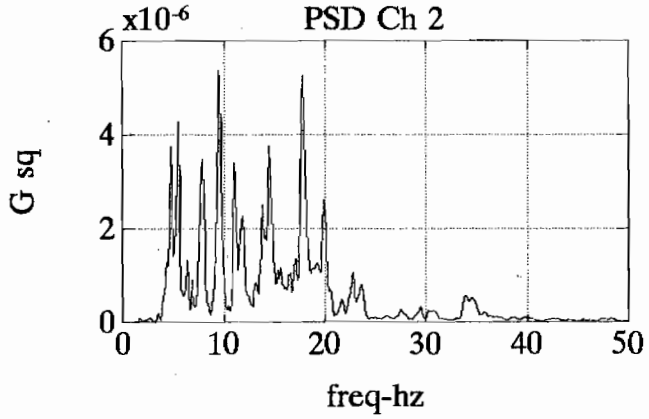
x10-6
PSD Ch 2
6
4
2
0
G sq
0
10
20
30
40
50
freq-hz

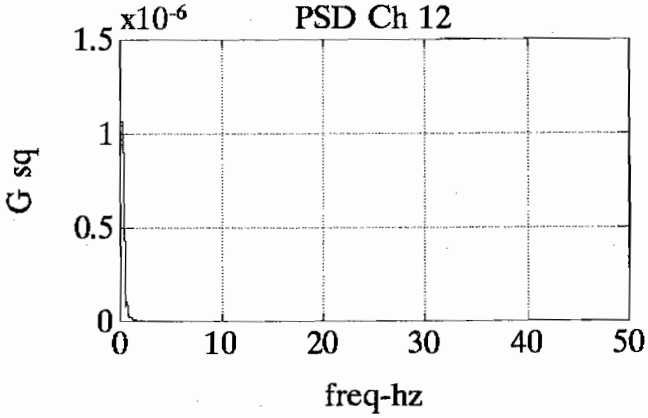
x10-6
PSD Ch 12
1.5
1
0.5
0
G sq
0
10
20
30
40
50
freq-hz

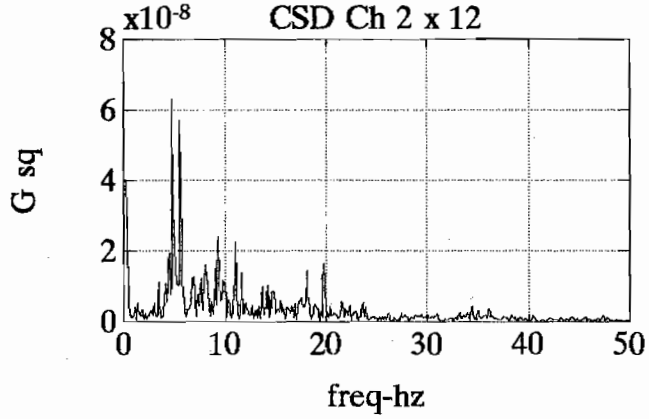
x10-8
CSD Ch 2 x 12
8
6
4
2
0
G sq
0
10
20
30
40
50
freq-hz

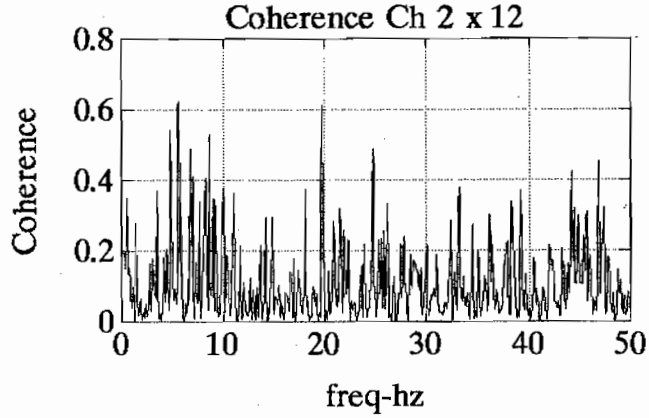
Coherence Ch 2 x 12
0.8
0.6
0.4
0.2
0
Coherence
0
10
20
30
40
50
freq-hz

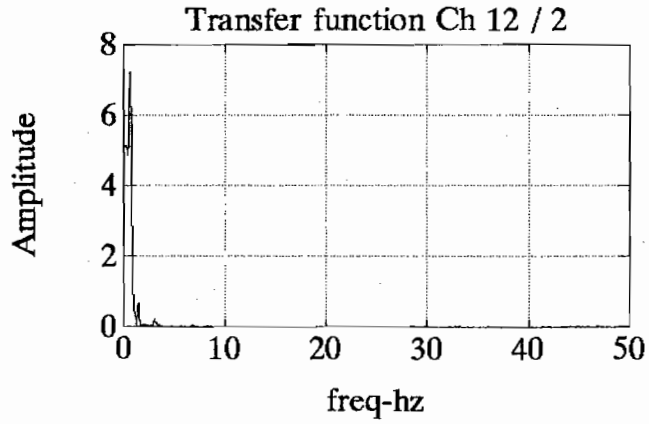
Transfer function Ch 12 / 2
8
6
4
2
0
Amplitude
0
10
20
30
40
50
freq-hz

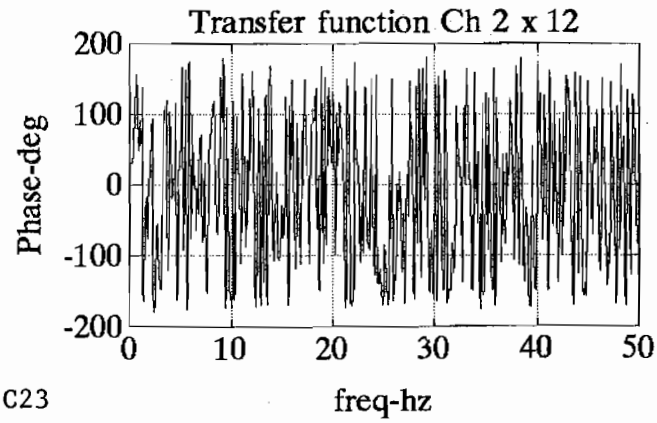
Transfer function Ch 2 x 12
200
100
0
-100
-200
Phase-deg
0
10
20
30
40
50
freq-hz

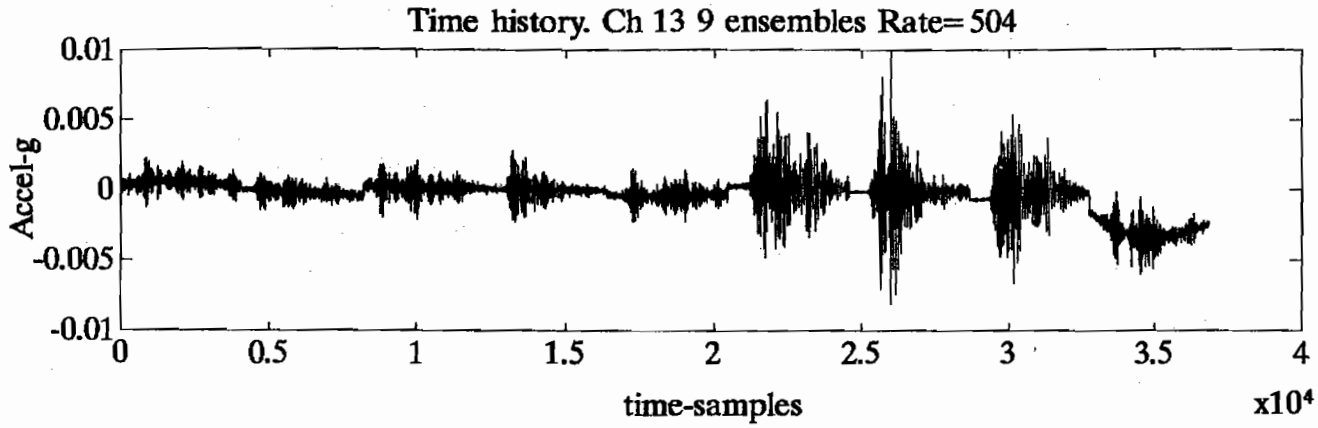
Time history. Ch 13 9 ensembles Rate= 504
Accel-g
0.01
0.005
0
-0.005
-0.01
0
0.5
1
1.5
2
2.5
3
3.5
4
time-samples
x10⁴

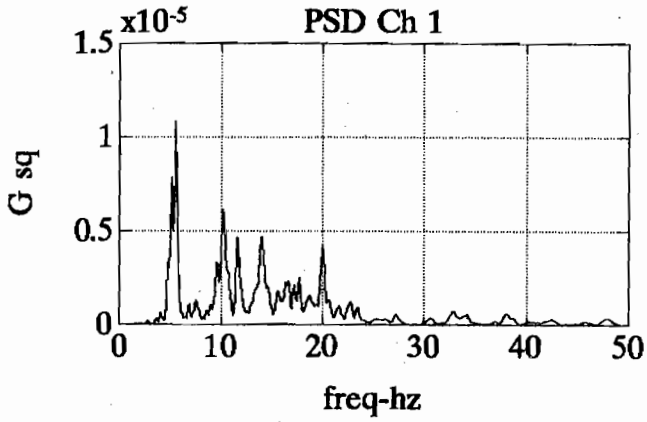
x10-5
PSD Ch 1
G sq
1.5
1
0.5
0
0
10
20
30
40
50
freq-hz

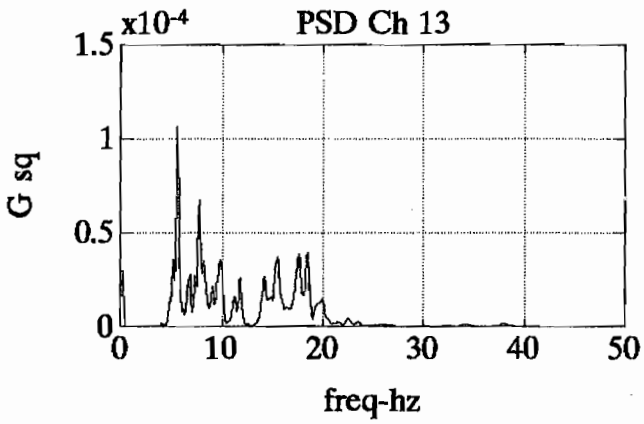
x10-4
PSD Ch 13
G sq
1.5
1
0.5
0
0
10
20
30
40
50
freq-hz

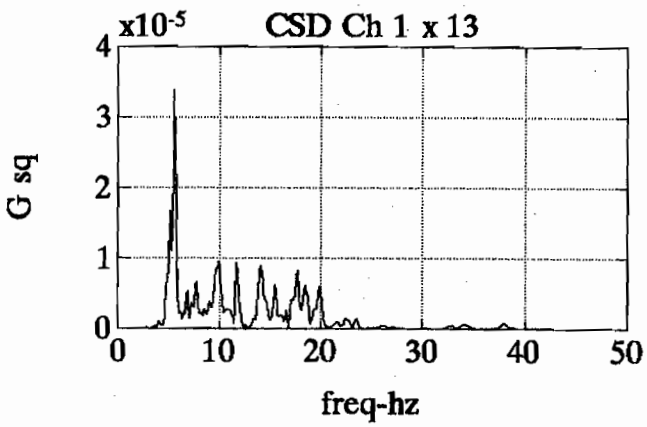
x10-5
CSD Ch 1 x 13
G sq
4
3
2
1
0
0
10
20
30
40
50
freq-hz

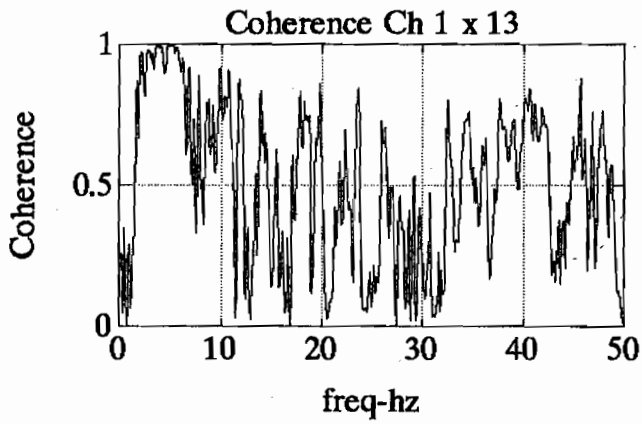
Coherence Ch 1 x 13
Coherence
1
0.5
0
0
10
20
30
40
50
freq-hz

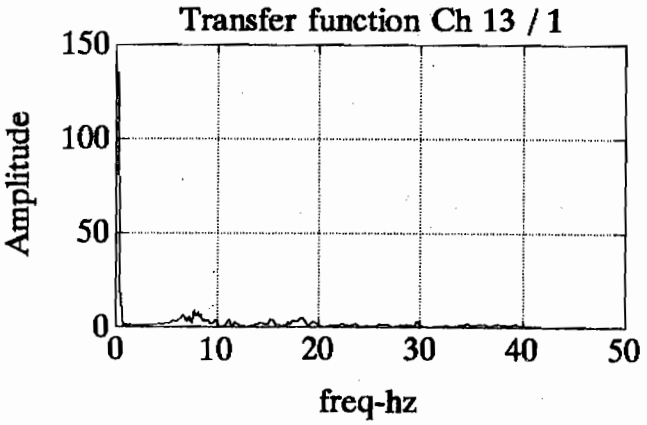
Transfer function Ch 13 / 1
Amplitude
150
100
50
0
0
10
20
30
40
50
freq-hz

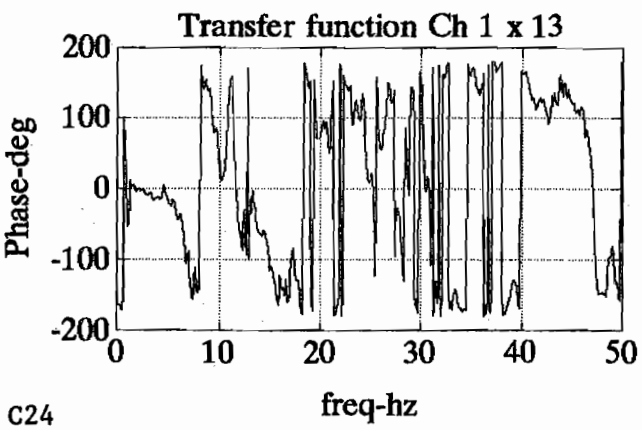
Transfer function Ch 1 x 13
Phase-deg
200
100
0
-100
-200
0
10
20
30
40
50
freq-hz

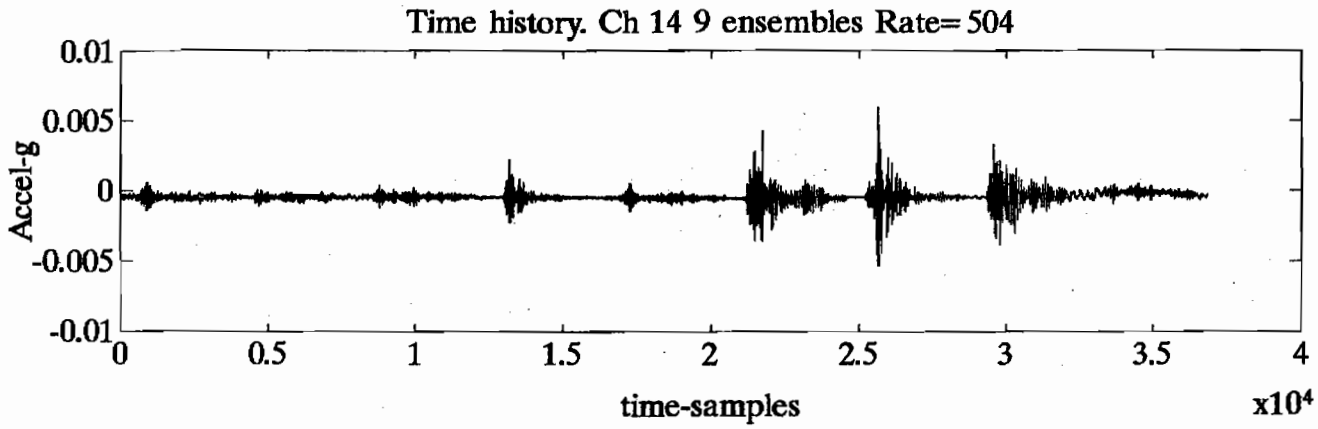
Time history. Ch 14 9 ensembles Rate= 504
Accel-g
0.01
0.005
0
-0.005
-0.01
0
0.5
1
1.5
2
2.5
3
3.5
4
time-samples
x10^4

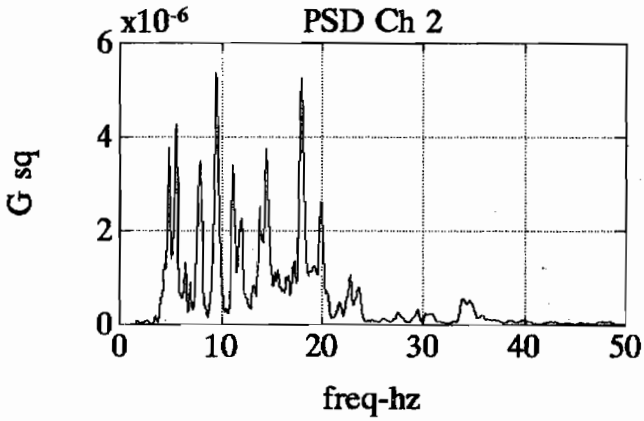
x10^-6
PSD Ch 2
G sq
6
4
2
0
0
10
20
30
40
50
freq-hz

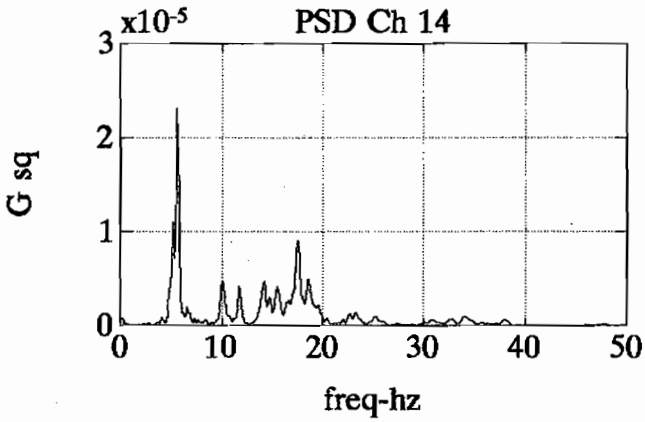
x10^-5
PSD Ch 14
G sq
3
2
1
0
0
10
20
30
40
50
freq-hz

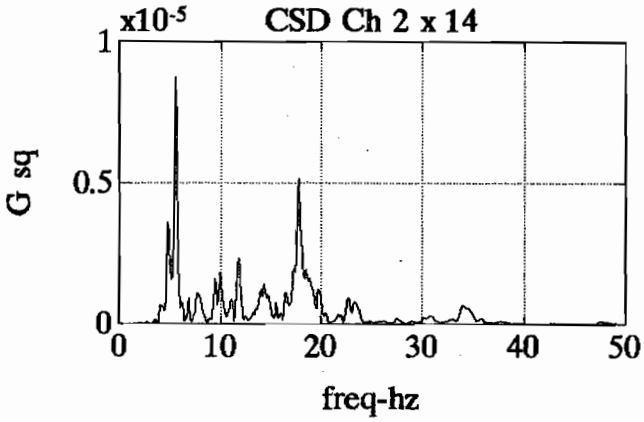
x10^-5
CSD Ch 2 x 14
G sq
1
0.5
0
0
10
20
30
40
50
freq-hz

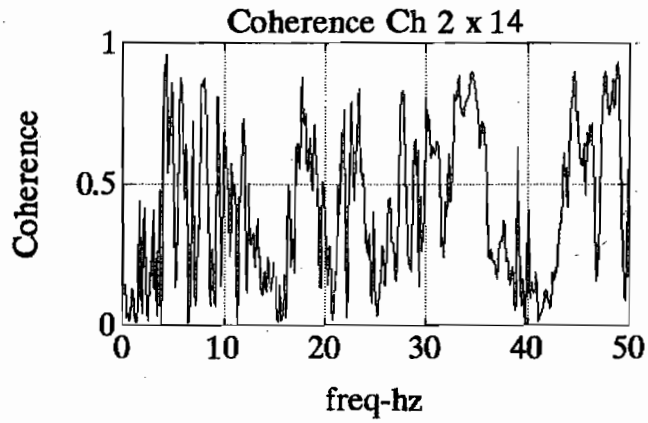
Coherence Ch 2 x 14
Coherence
1
0.5
0
0
10
20
30
40
50
freq-hz

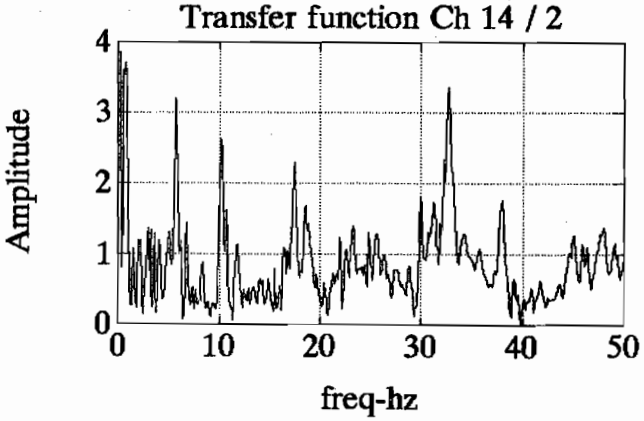
Transfer function Ch 14 / 2
Amplitude
4
3
2
1
0
0
10
20
30
40
50
freq-hz

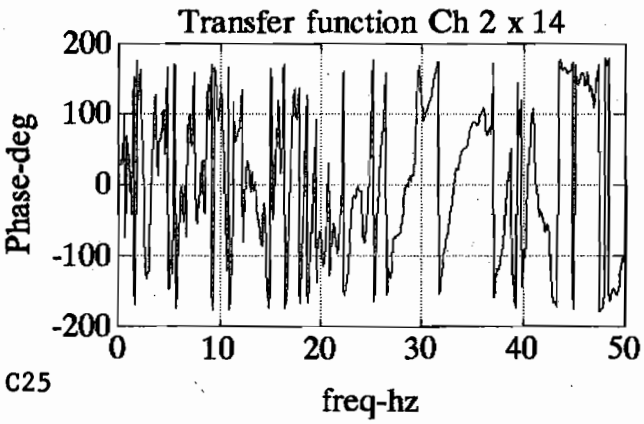
Transfer function Ch 2 x 14
Phase-deg
200
100
0
-100
-200
0
10
20
30
40
50
freq-hz

PART 5

PSD: Power Spectral Density

CSD: Cross Spectral Density

Transfer Function: $\frac{CSD}{PSD}$

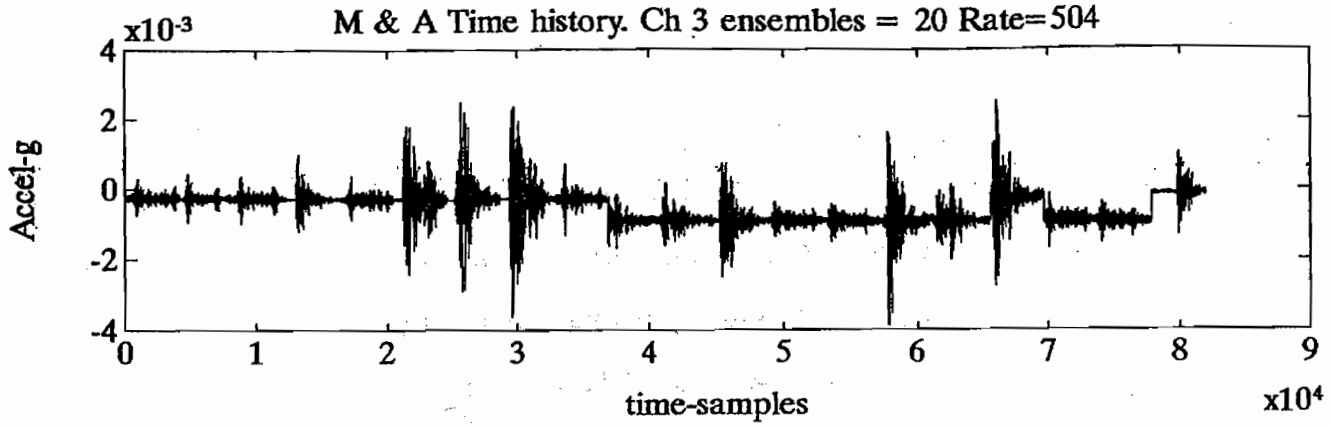
M & A Time history. Ch 3 ensembles = 20 Rate=504
x10-3
Accel-g
time-samples
x10⁴

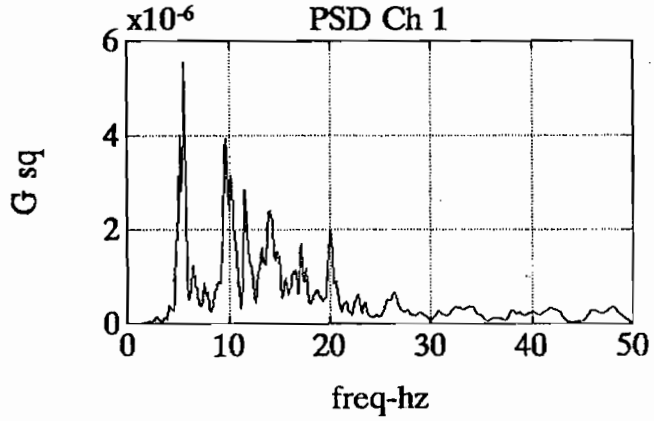
x10-6
PSD Ch 1
G sq
freq-hz

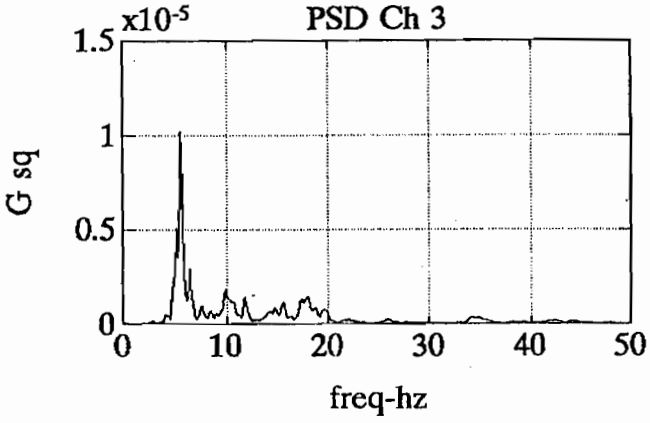
x10-5
PSD Ch 3
G sq
freq-hz

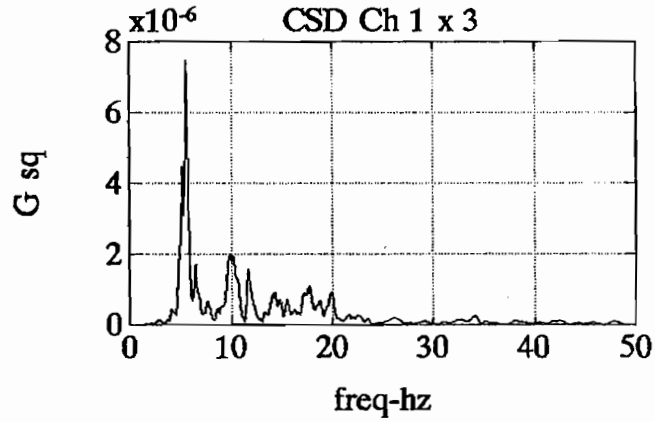
x10-6
CSD Ch 1 x 3
G sq
freq-hz

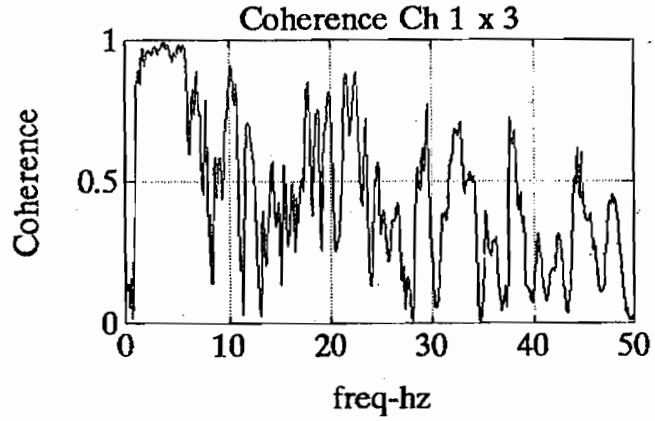
Coherence Ch 1 x 3
Coherence
freq-hz

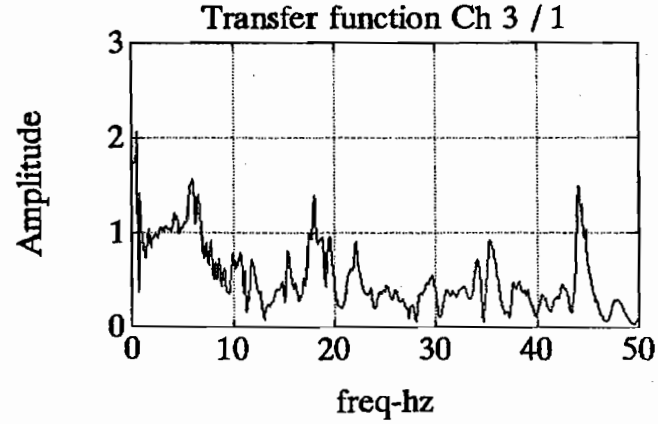
Transfer function Ch 3 / 1
Amplitude
freq-hz

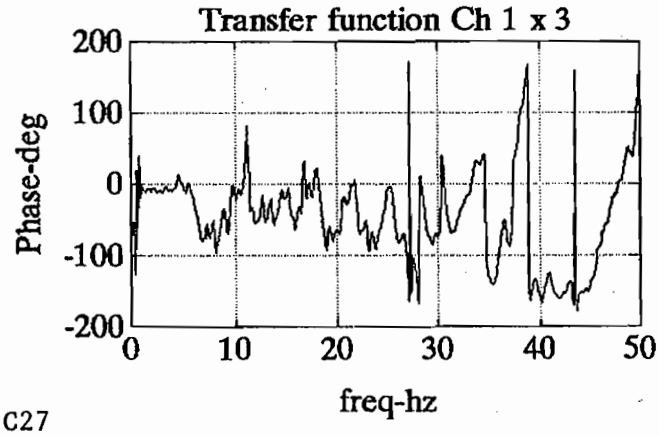
Transfer function Ch 1 x 3
Phase-deg
freq-hz

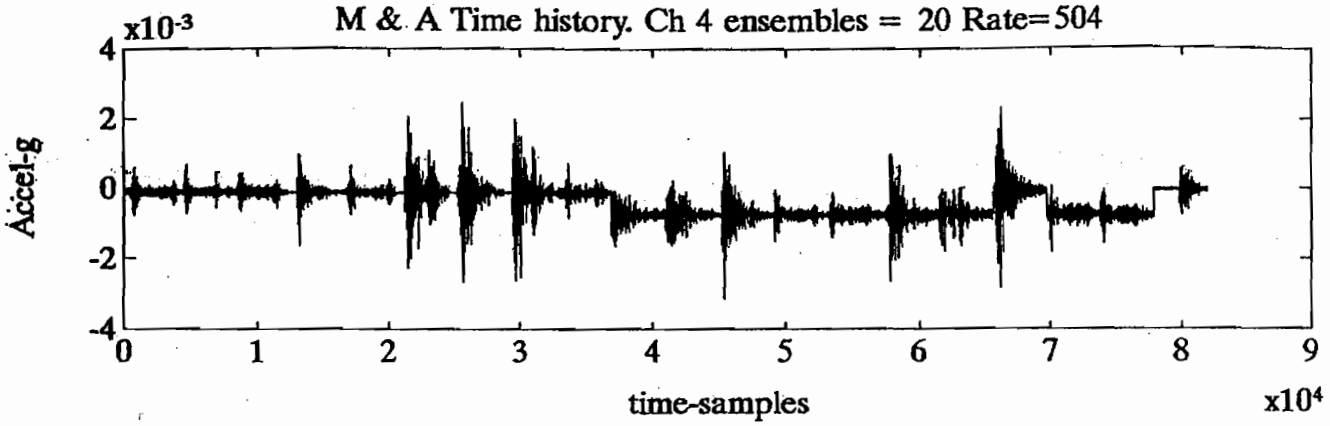
M & A Time history. Ch 4 ensembles = 20 Rate=504
x10-3
Accel-g
time-samples
x10⁴

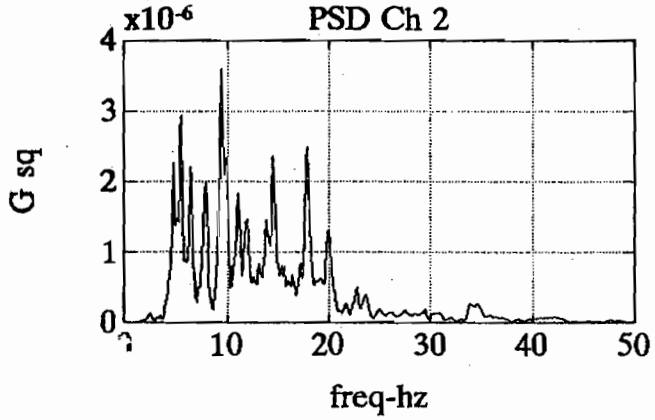
x10-6
PSD Ch 2
G sq
freq-hz

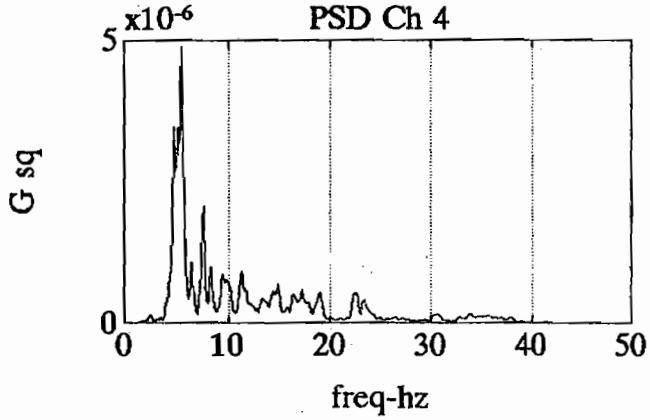
x10-6
PSD Ch 4
G sq
freq-hz

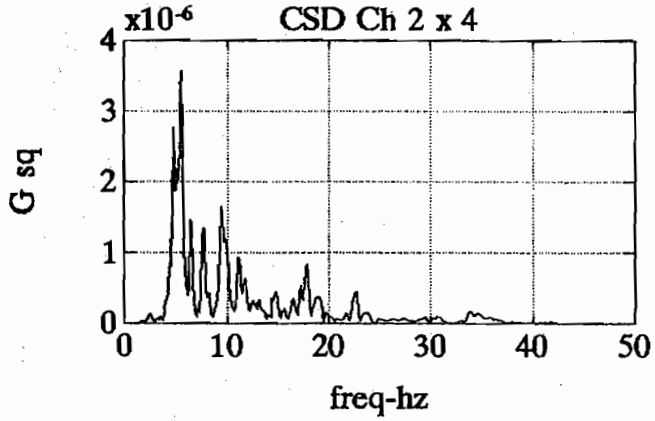
x10-6
CSD Ch 2 x 4
G sq
freq-hz

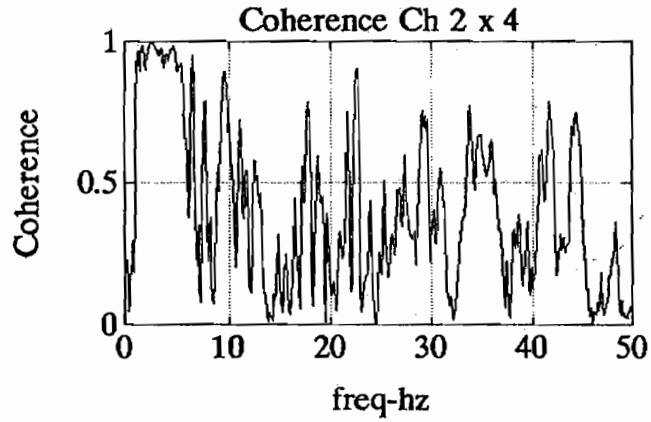
Coherence Ch 2 x 4
Coherence
freq-hz

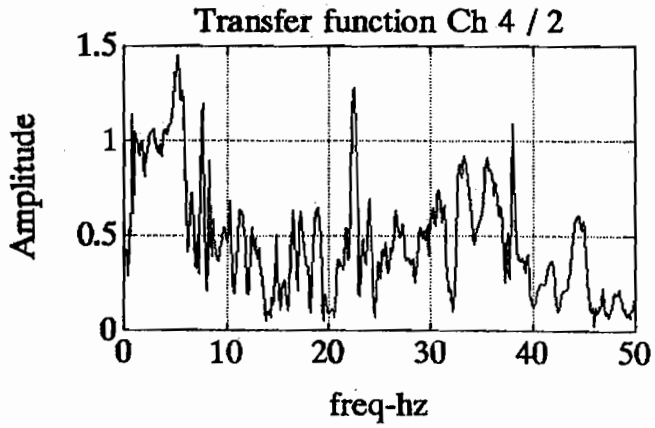
Transfer function Ch 4 / 2
Amplitude
freq-hz

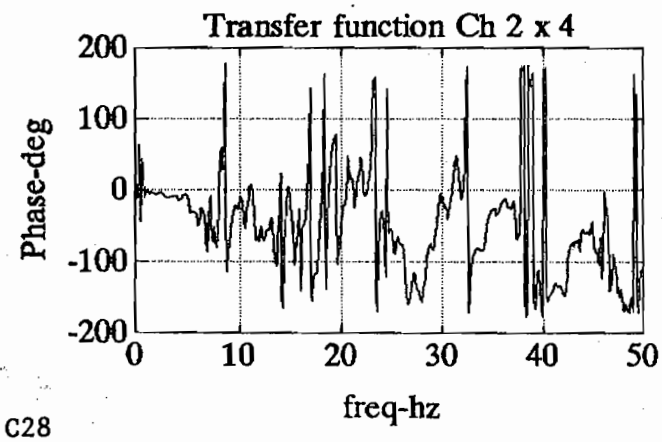
Transfer function Ch 2 x 4
Phase-deg
freq-hz

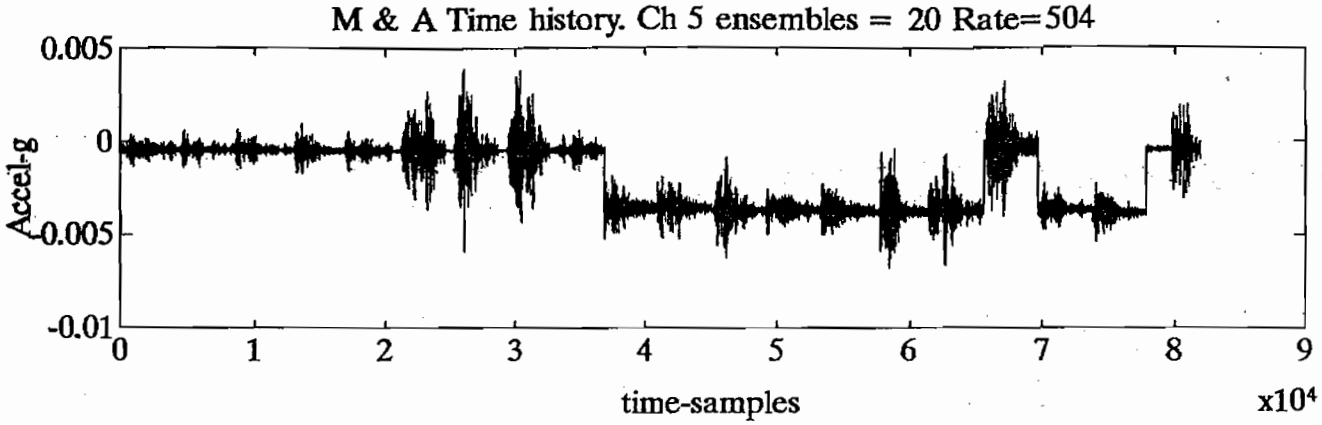
M & A Time history. Ch 5 ensembles = 20 Rate=504
Accel-g
0.005
0
-0.005
-0.01
0 1 2 3 4 5 6 7 8 9
time-samples
x10^4

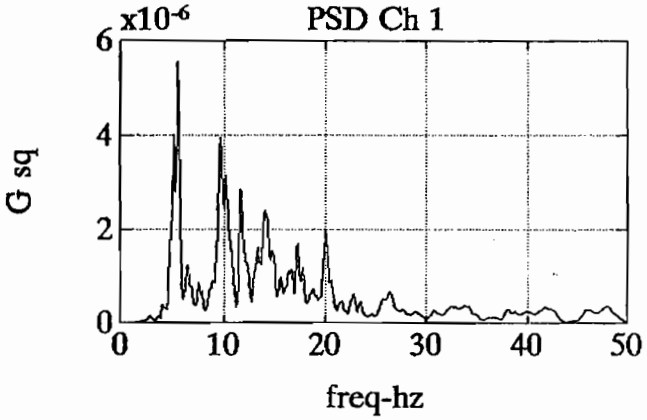
x10^-6
PSD Ch 1
G sq
6
4
2
0
0 10 20 30 40 50
freq-hz

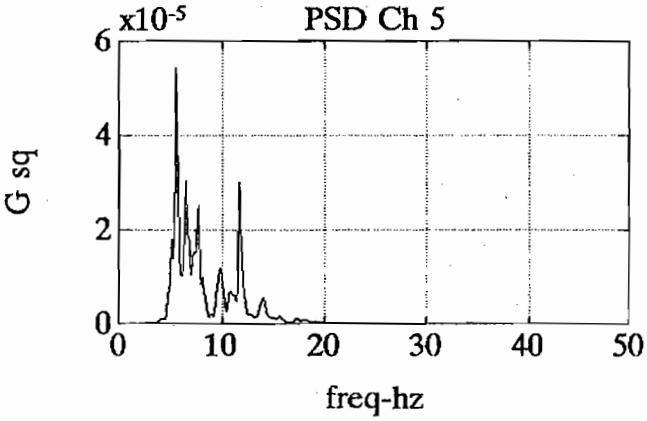
x10^-5
PSD Ch 5
G sq
6
4
2
0
0 10 20 30 40 50
freq-hz

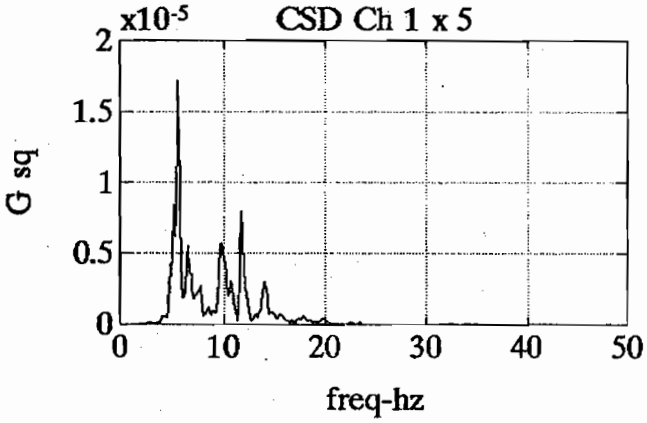
x10^-5
CSD Ch 1 x 5
G sq
2
1.5
1
0.5
0
0 10 20 30 40 50
freq-hz

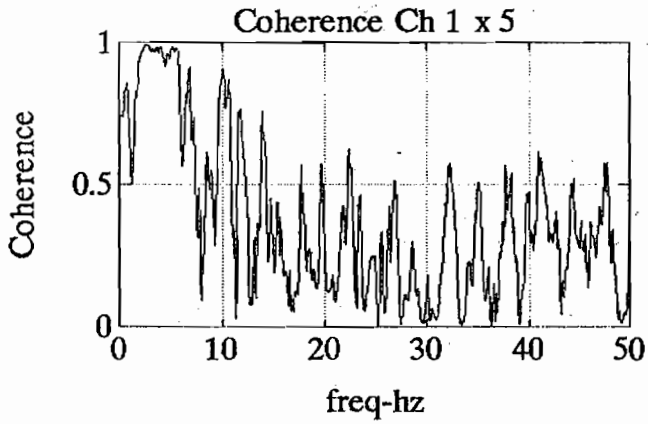
Coherence Ch 1 x 5
Coherence
1
0.5
0
0 10 20 30 40 50
freq-hz

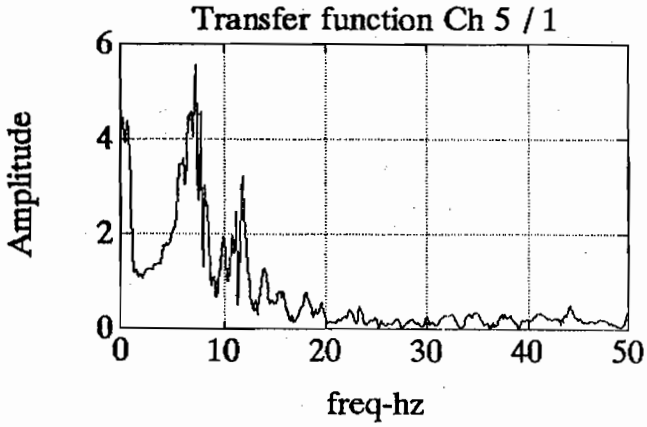
Transfer function Ch 5 / 1
Amplitude
6
4
2
0
0 10 20 30 40 50
freq-hz

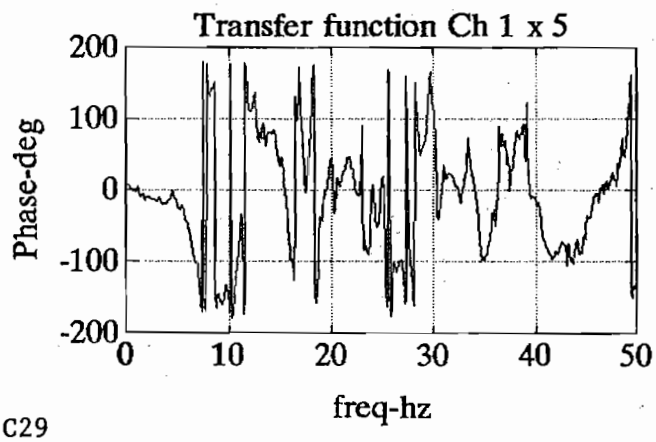
Transfer function Ch 1 x 5
Phase-deg
200
100
0
-100
-200
0 10 20 30 40 50
freq-hz

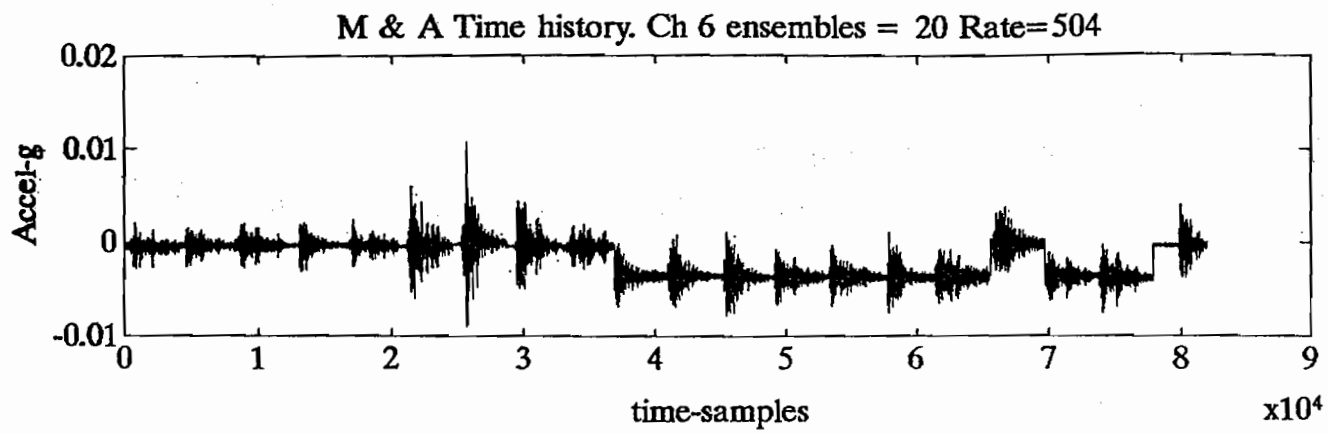
M & A Time history. Ch 6 ensembles = 20 Rate=504
Accel-g
0.02
0.01
0
-0.01
0 1 2 3 4 5 6 7 8 9
time-samples
x10⁴

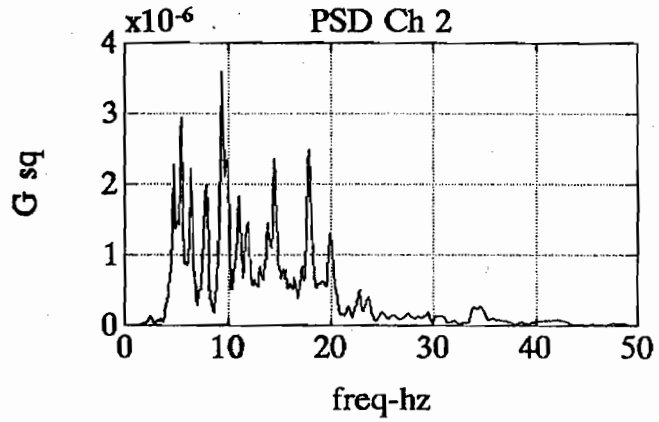
x10⁻⁶
PSD Ch 2
G sq
0 1 2 3 4
0 10 20 30 40 50
freq-hz

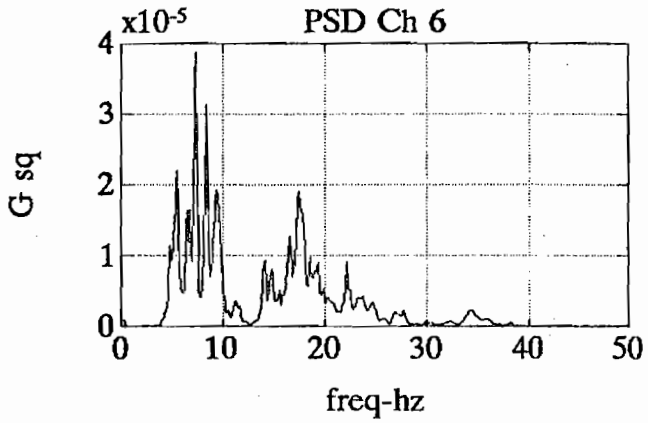
x10⁻⁵
PSD Ch 6
G sq
0 1 2 3 4
0 10 20 30 40 50
freq-hz

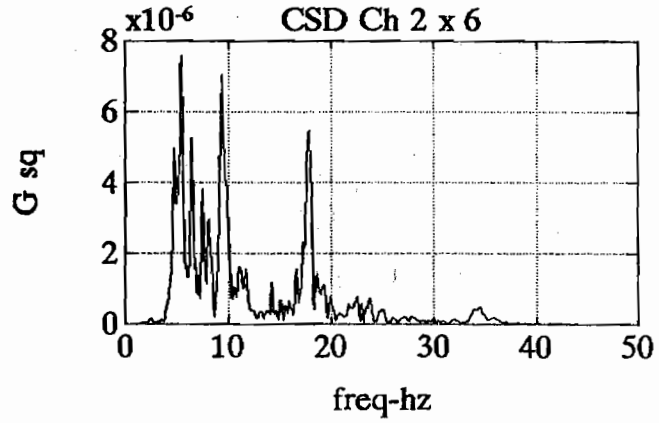
x10⁻⁶
CSD Ch 2 x 6
G sq
0 2 4 6 8
0 10 20 30 40 50
freq-hz

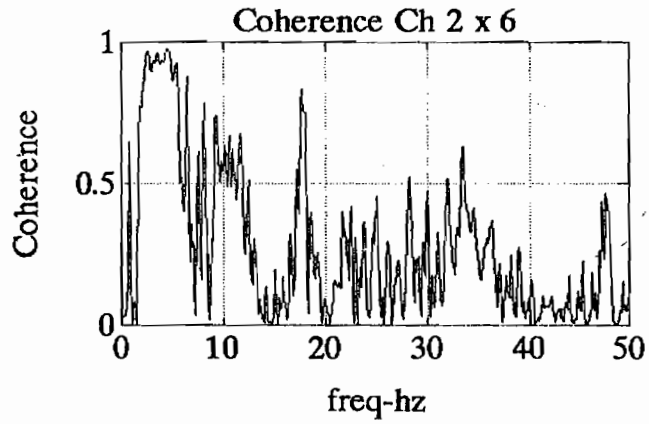
Coherence Ch 2 x 6
Coherence
0 0.5 1
0 10 20 30 40 50
freq-hz

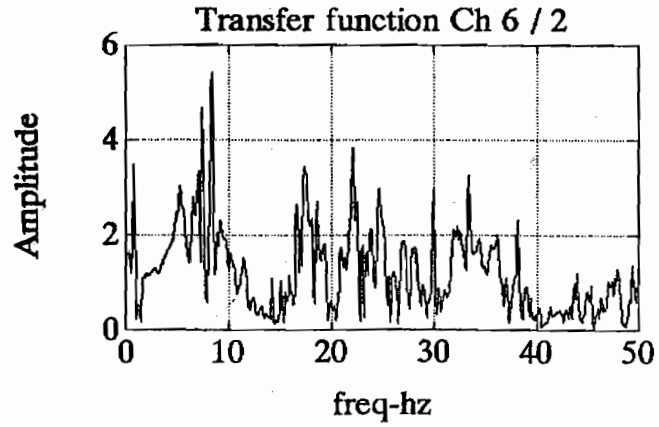
Transfer function Ch 6 / 2
Amplitude
0 2 4 6
0 10 20 30 40 50
freq-hz

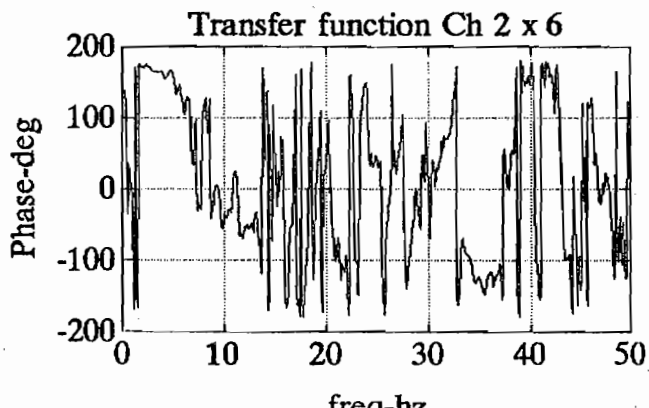
Transfer function Ch 2 x 6
Phase-deg
200
100
0
-100
-200
0 10 20 30 40 50
freq-hz

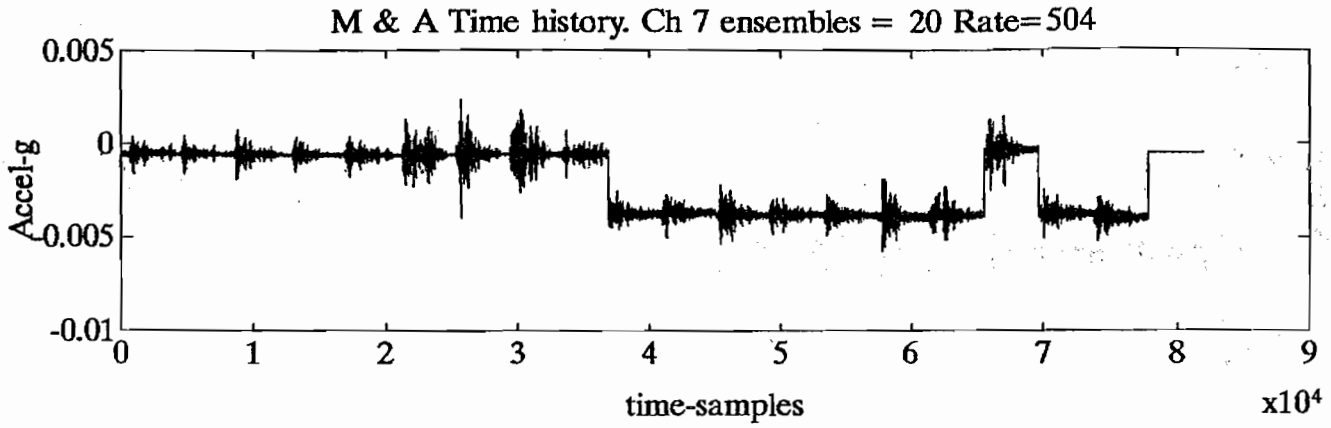
M & A Time history. Ch 7 ensembles = 20 Rate=504
Accel-g
0.005
0
-0.005
-0.01
0 1 2 3 4 5 6 7 8 9
time-samples
x10^4

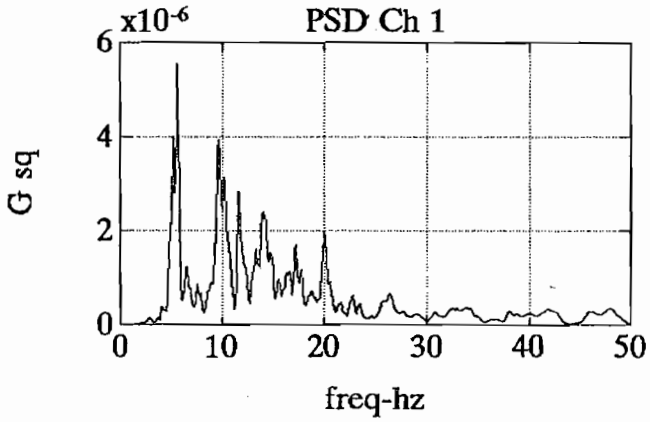
x10^-6
PSD Ch 1
G sq
6
4
2
0
0 10 20 30 40 50
freq-hz

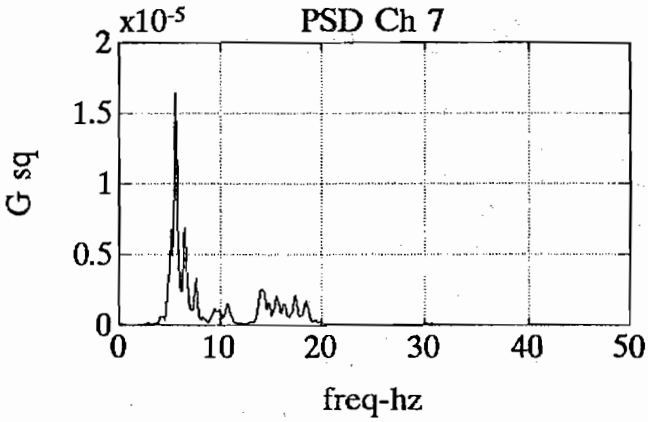
x10^-5
PSD Ch 7
G sq
2
1.5
1
0.5
0
0 10 20 30 40 50
freq-hz

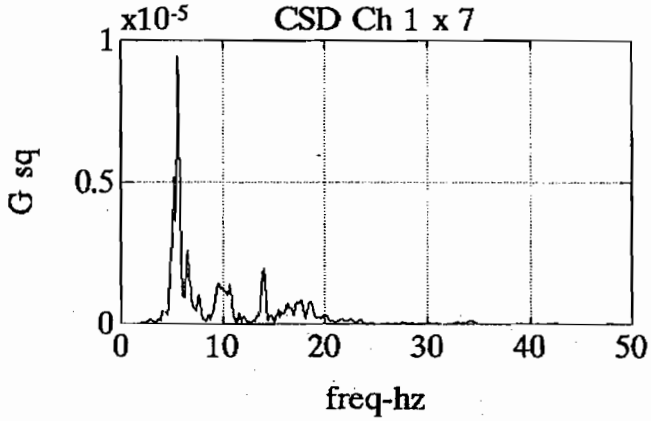
x10^-5
CSD Ch 1 x 7
G sq
1
0.5
0
0 10 20 30 40 50
freq-hz

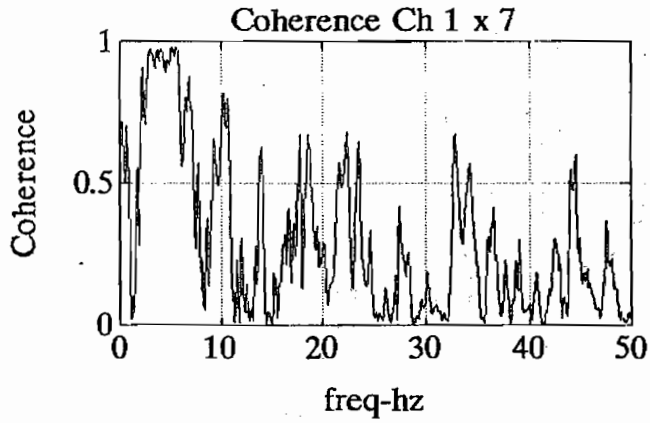
Coherence Ch 1 x 7
Coherence
1
0.5
0
0 10 20 30 40 50
freq-hz

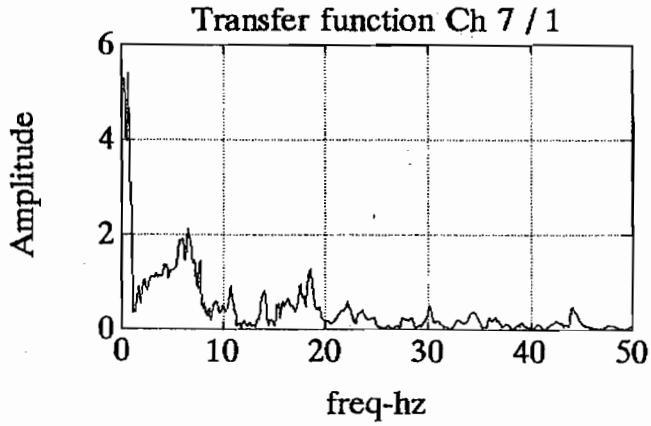
Transfer function Ch 7 / 1
Amplitude
6
4
2
0
0 10 20 30 40 50
freq-hz

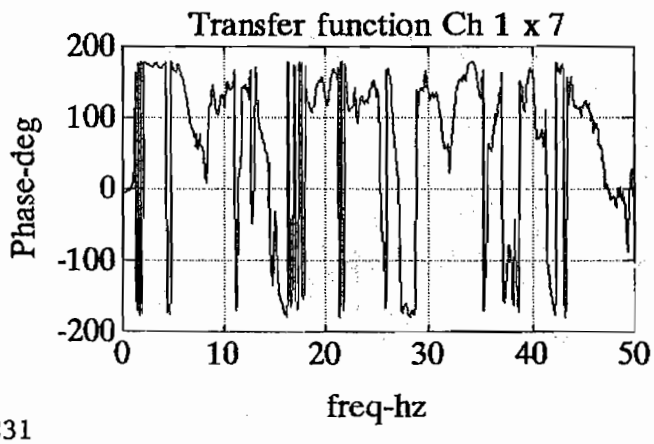
Transfer function Ch 1 x 7
Phase-deg
200
100
0
-100
-200
0 10 20 30 40 50
freq-hz

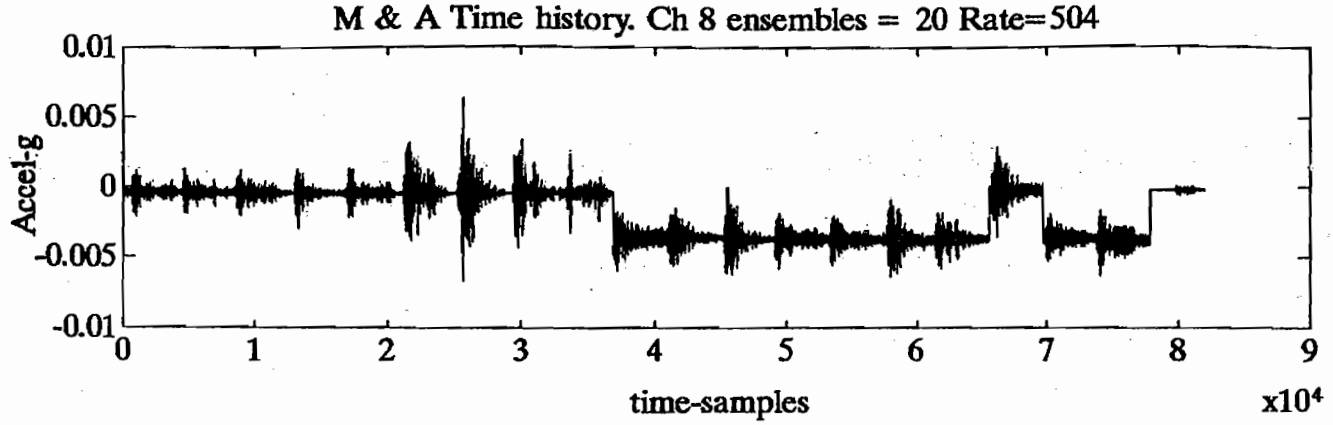
M & A Time history. Ch 8 ensembles = 20 Rate=504
Accel-g
0.01
0.005
0
-0.005
-0.01
0
1
2
3
4
5
6
7
8
9
time-samples
x10^4

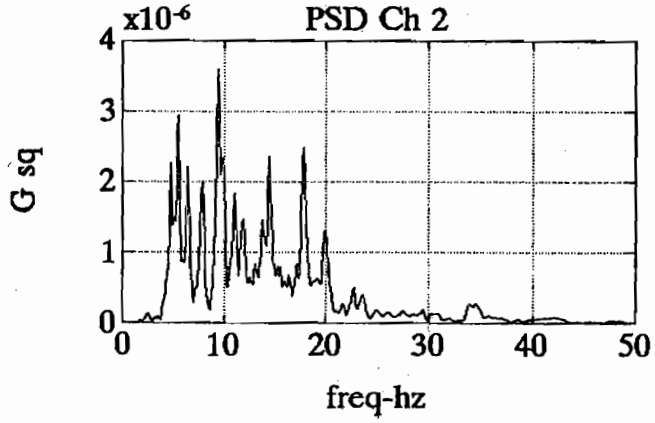
x10^-6
PSD Ch 2
G sq
4
3
2
1
0
0
10
20
30
40
50
freq-hz

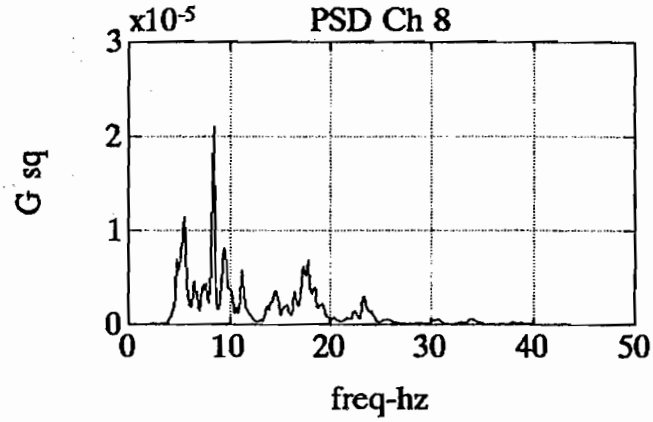
x10^-5
PSD Ch 8
G sq
3
2
1
0
0
10
20
30
40
50
freq-hz

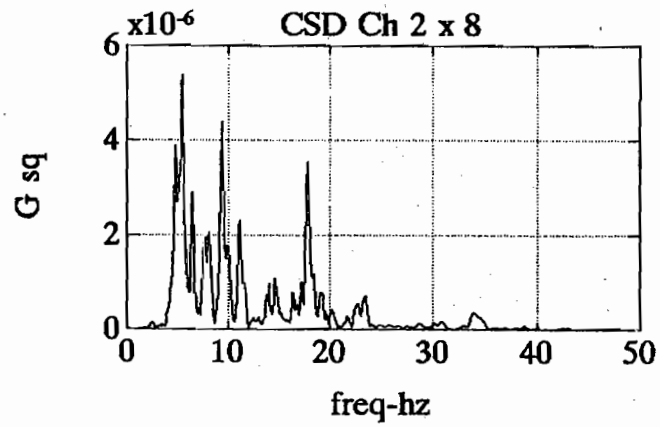
x10^-6
CSD Ch 2 x 8
G sq
6
4
2
0
0
10
20
30
40
50
freq-hz

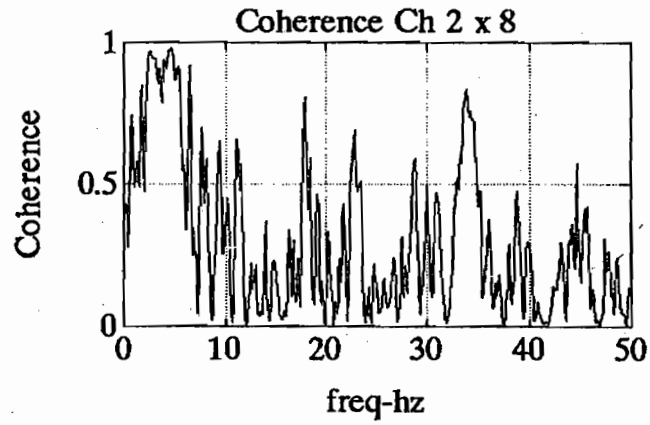
Coherence Ch 2 x 8
Coherence
1
0.5
0
0
10
20
30
40
50
freq-hz

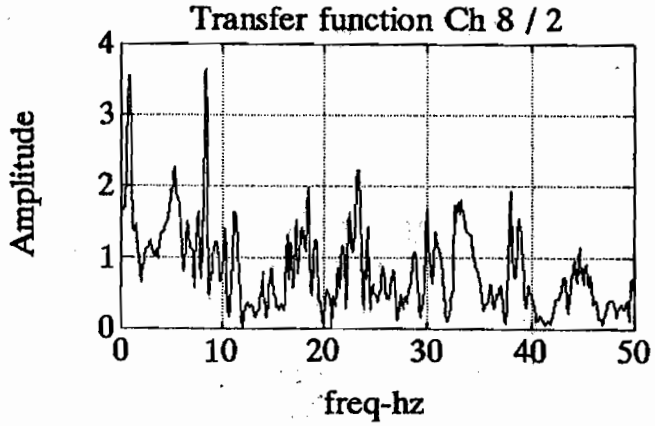
Transfer function Ch 8 / 2
Amplitude
4
3
2
1
0
0
10
20
30
40
50
freq-hz

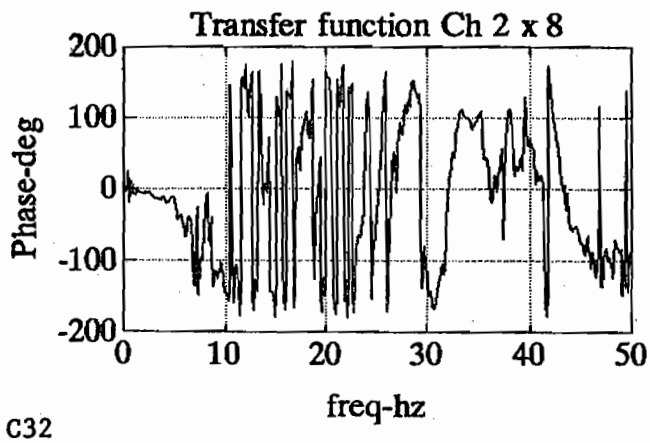
Transfer function Ch 2 x 8
Phase-deg
200
100
0
-100
-200
0
10
20
30
40
50
freq-hz

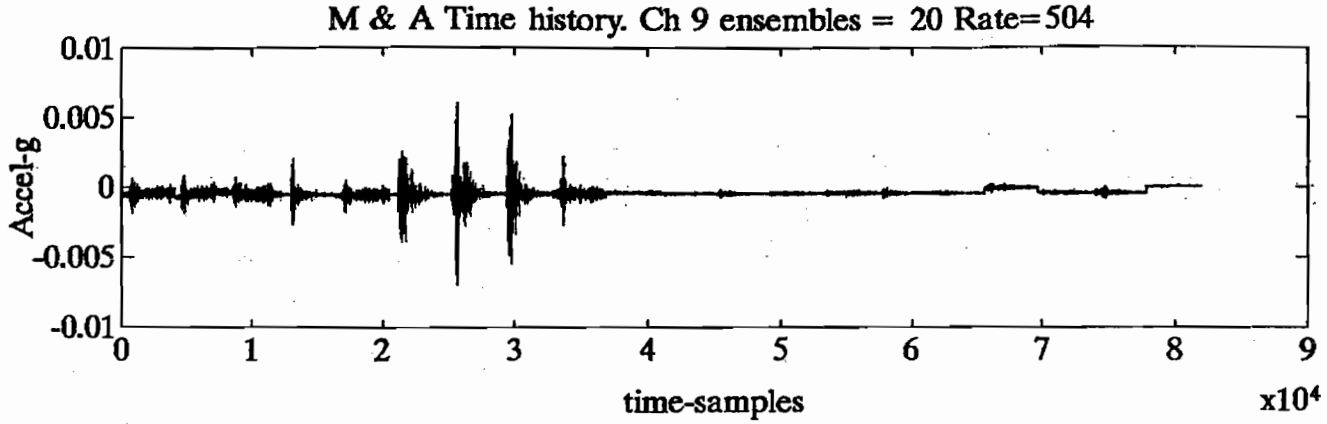
M & A Time history. Ch 9 ensembles = 20 Rate=504
Accel-g
0.01
0.005
0
-0.005
-0.01
0
1
2
3
4
5
6
7
8
9
time-samples
x10⁴

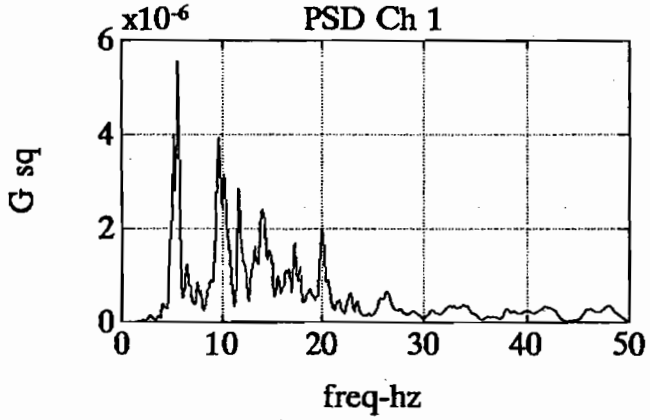
x10⁻⁶
PSD Ch 1
G sq
6
4
2
0
0
10
20
30
40
50
freq-hz

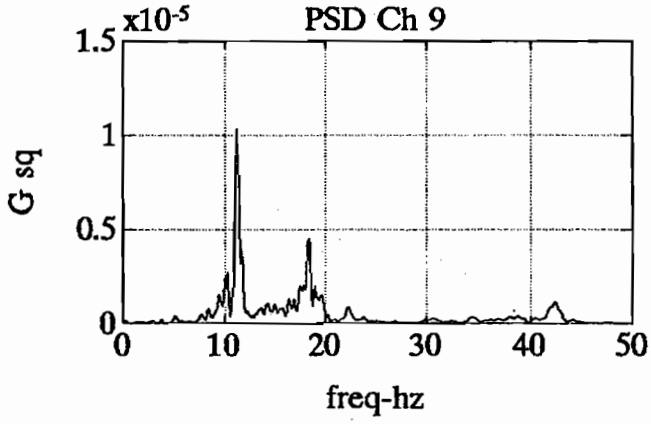
x10⁻⁵
PSD Ch 9
G sq
1.5
1
0.5
0
0
10
20
30
40
50
freq-hz

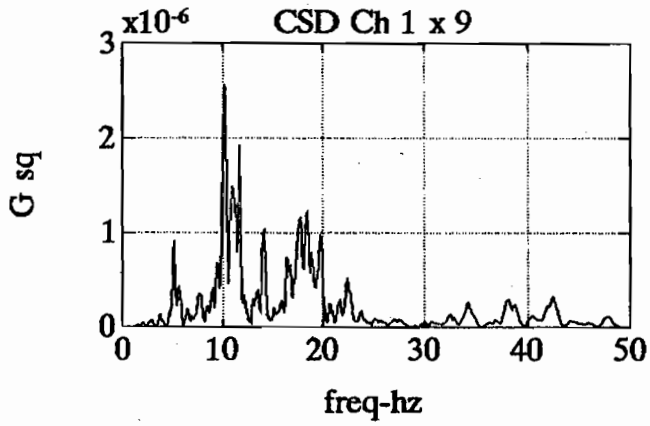
x10⁻⁶
CSD Ch 1 x 9
G sq
3
2
1
0
0
10
20
30
40
50
freq-hz

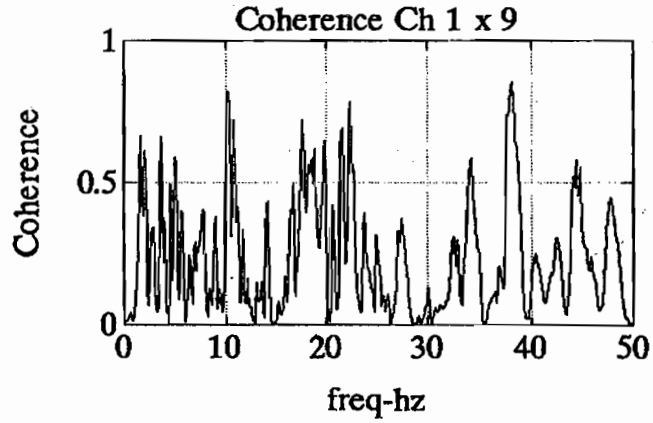
Coherence Ch 1 x 9
Coherence
1
0.5
0
0
10
20
30
40
50
freq-hz

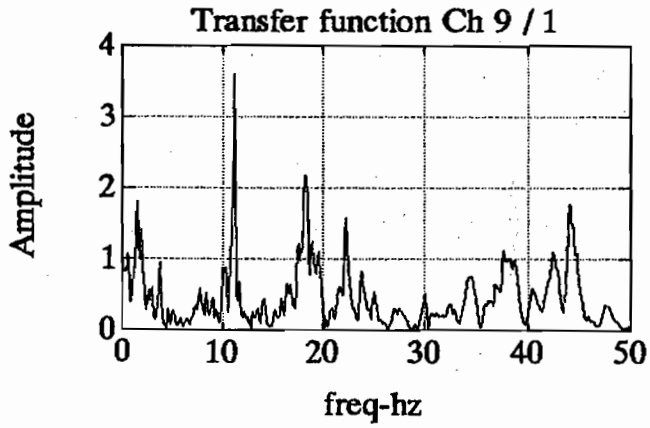
Transfer function Ch 9 / 1
Amplitude
4
3
2
1
0
0
10
20
30
40
50
freq-hz

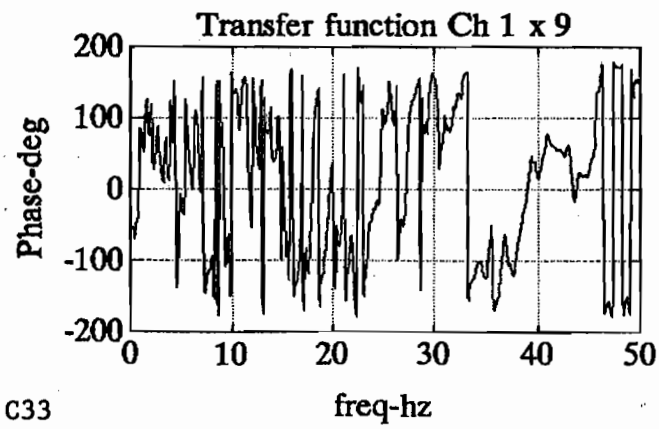
Transfer function Ch 1 x 9
Phase-deg
200
100
0
-100
-200
0
10
20
30
40
50
freq-hz

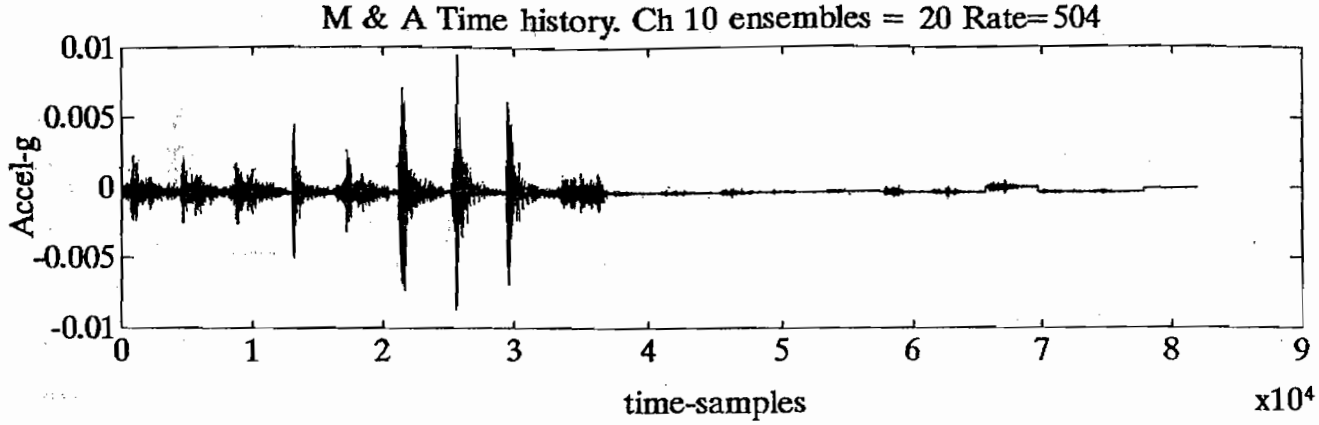
M & A Time history. Ch 10 ensembles = 20 Rate=504
Accel-g
0.01
0.005
0
-0.005
-0.01
0
1
2
3
4
5
6
7
8
9
time-samples
x10^4

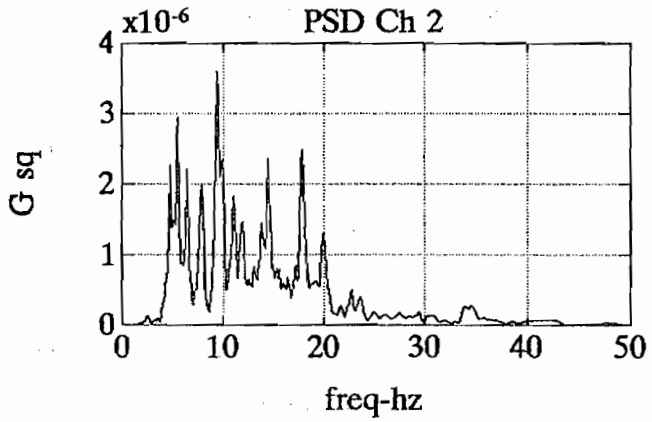
x10^-6
PSD Ch 2
G sq
4
3
2
1
0
0
10
20
30
40
50
freq-hz

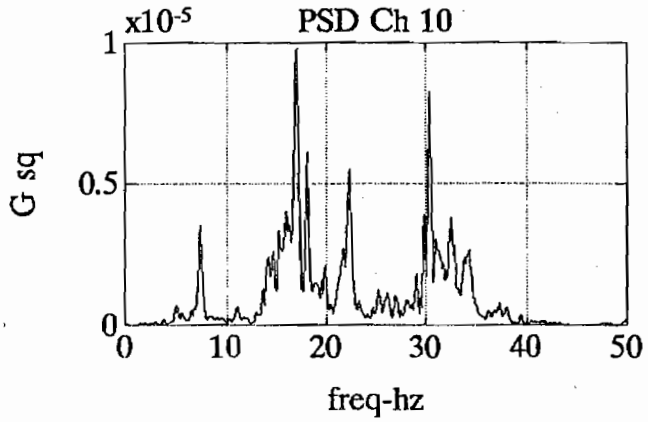
x10^-5
PSD Ch 10
G sq
1
0.5
0
0
10
20
30
40
50
freq-hz

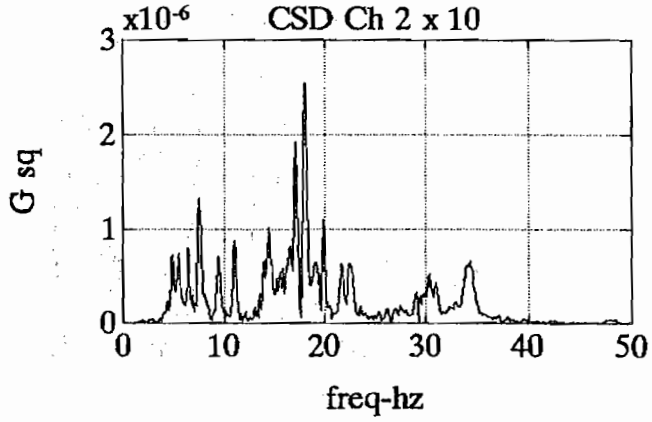
x10^-6
CSD Ch 2 x 10
G sq
3
2
1
0
0
10
20
30
40
50
freq-hz

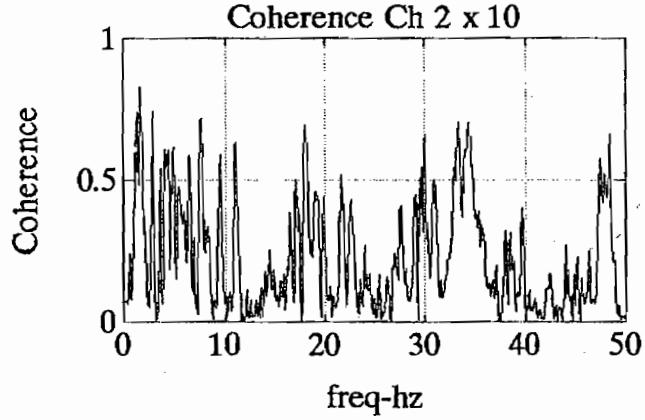
Coherence Ch 2 x 10
Coherence
1
0.5
0
0
10
20
30
40
50
freq-hz

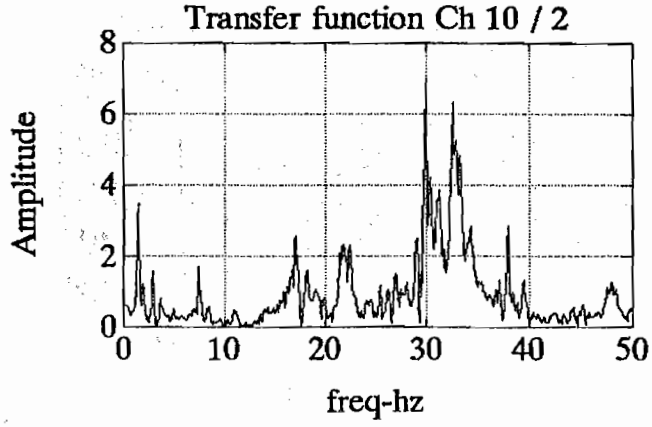
Transfer function Ch 10 / 2
Amplitude
8
6
4
2
0
0
10
20
30
40
50
freq-hz

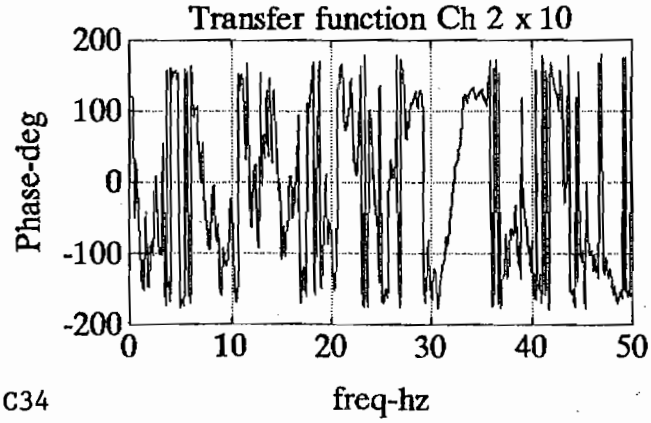
Transfer function Ch 2 x 10
Phase-deg
200
100
0
-100
-200
0
10
20
30
40
50
freq-hz

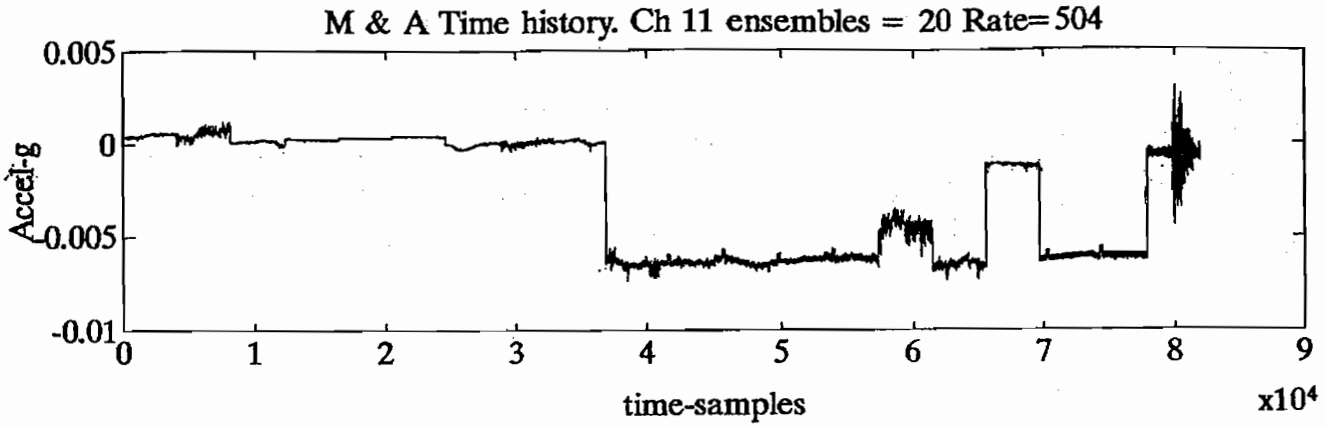
M & A Time history. Ch 11 ensembles = 20 Rate=504
Accel-g
0.005
0
-0.005
-0.01
0
1
2
3
4
5
6
7
8
9
time-samples
x10^4

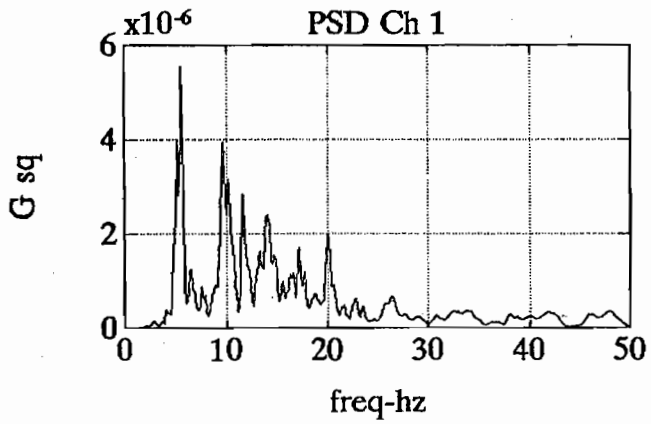
x10^-6
PSD Ch 1
G sq
6
4
2
0
0
10
20
30
40
50
freq-hz

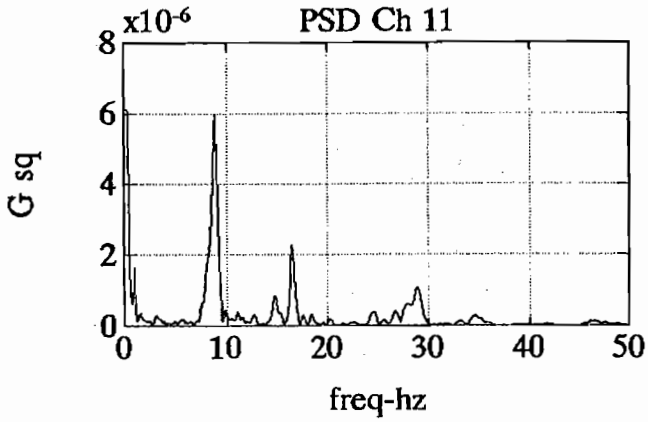
x10^-6
PSD Ch 11
G sq
8
6
4
2
0
0
10
20
30
40
50
freq-hz

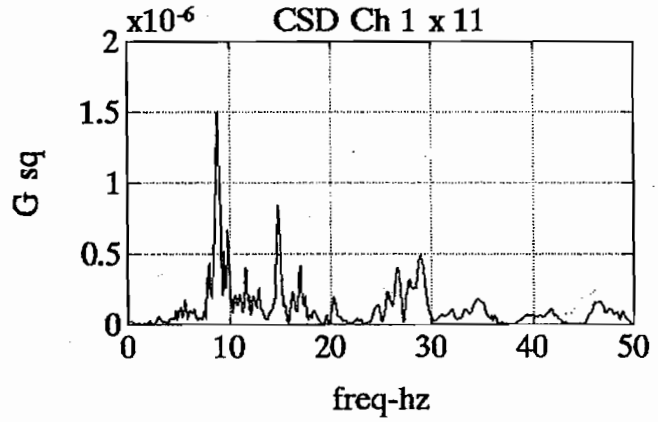
x10^-6
CSD Ch 1 x 11
G sq
2
1.5
1
0.5
0
0
10
20
30
40
50
freq-hz

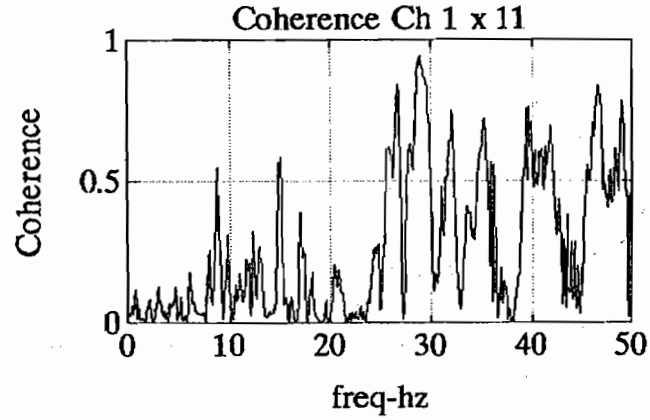
Coherence Ch 1 x 11
Coherence
1
0.5
0
0
10
20
30
40
50
freq-hz

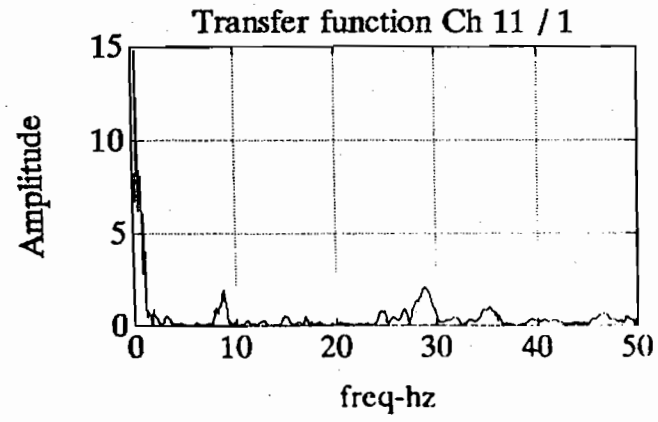
Transfer function Ch 11 / 1
Amplitude
15
10
5
0
0
10
20
30
40
50
freq-hz

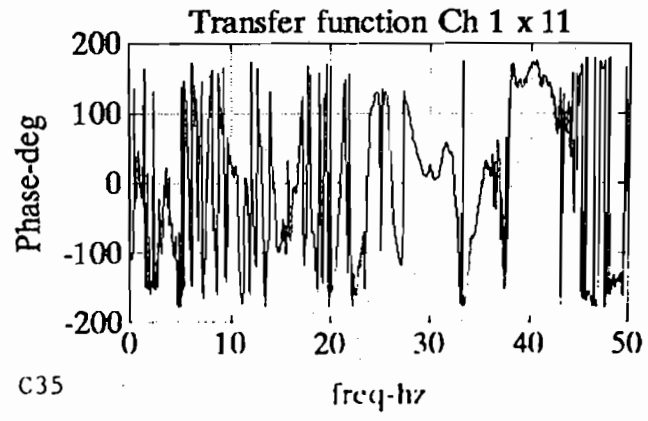
Transfer function Ch 1 x 11
Phase-deg
200
100
0
-100
-200
0
10
20
30
40
50
freq-hz

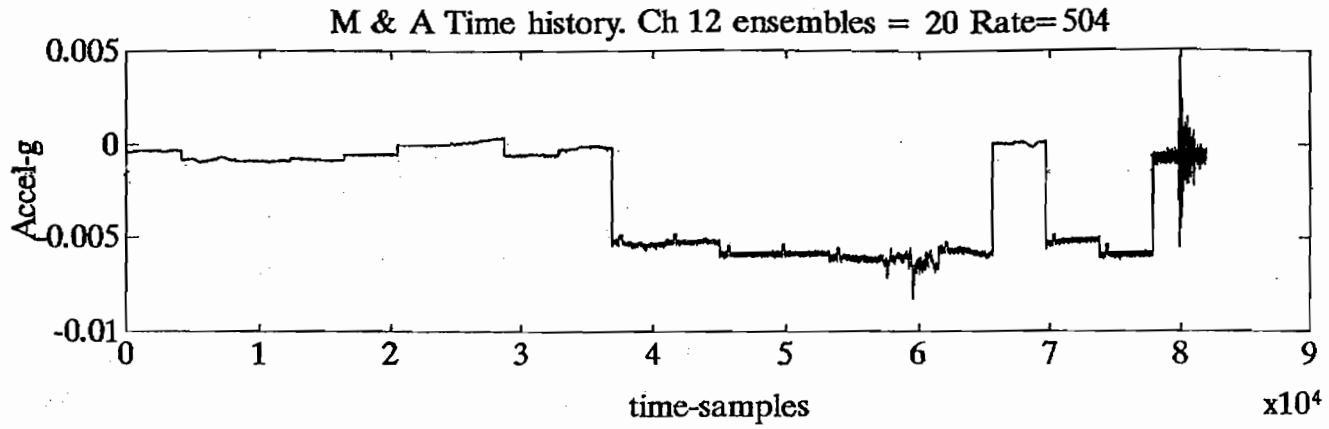
M & A Time history. Ch 12 ensembles = 20 Rate=504
Accel-g
0.005
0
-0.005
-0.01
0 1 2 3 4 5 6 7 8 9
time-samples
x10^4

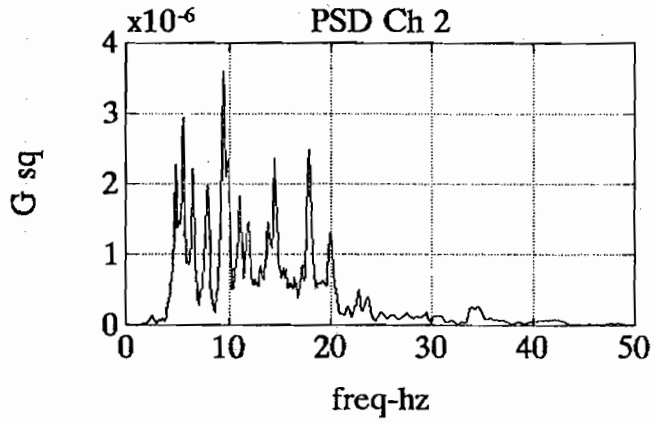
x10^-6
PSD Ch 2
G sq
4 3 2 1 0
0 10 20 30 40 50
freq-hz

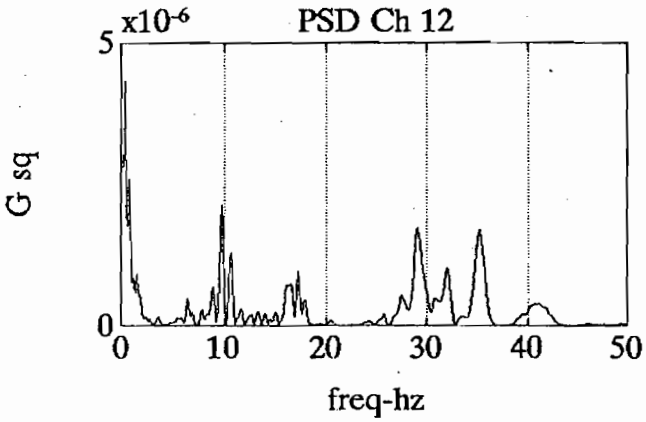
x10^-6
PSD Ch 12
G sq
5 0
0 10 20 30 40 50
freq-hz

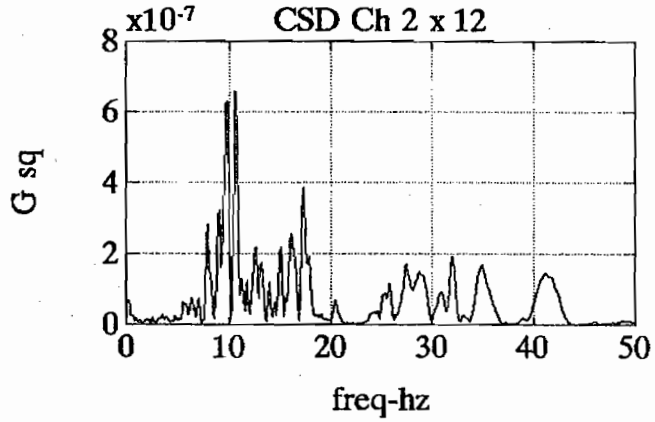
x10^-7
CSD Ch 2 x 12
G sq
8 6 4 2 0
0 10 20 30 40 50
freq-hz

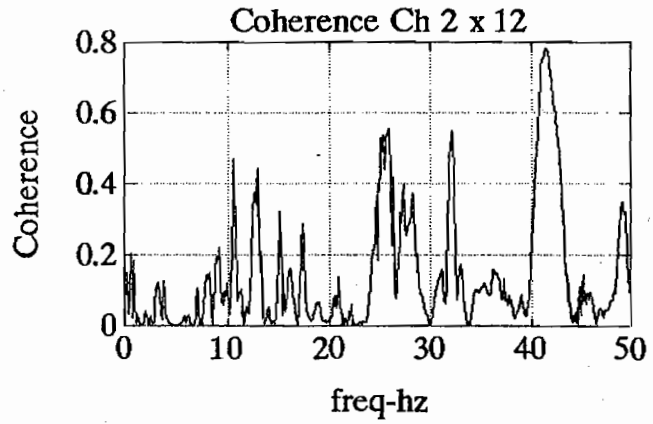
Coherence Ch 2 x 12
Coherence
0.8 0.6 0.4 0.2 0
0 10 20 30 40 50
freq-hz

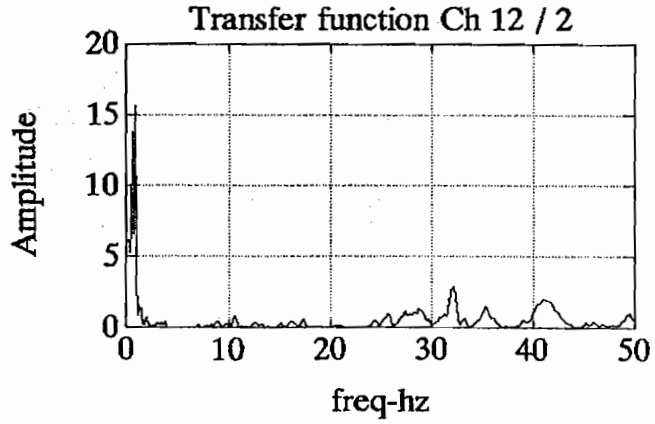
Transfer function Ch 12 / 2
Amplitude
20 15 10 5 0
0 10 20 30 40 50
freq-hz

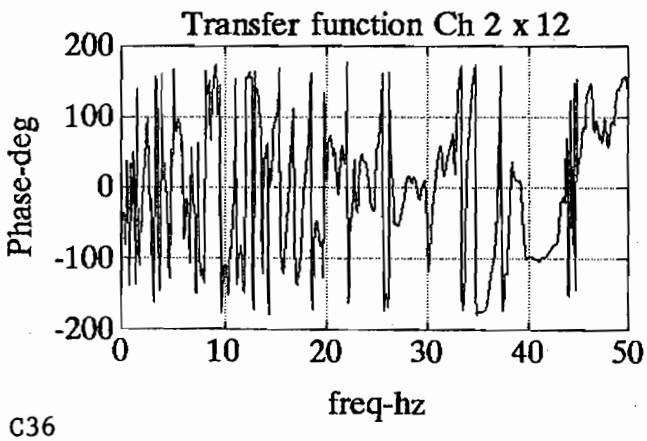
Transfer function Ch 2 x 12
Phase-deg
200 100 0 -100 -200
0 10 20 30 40 50
freq-hz

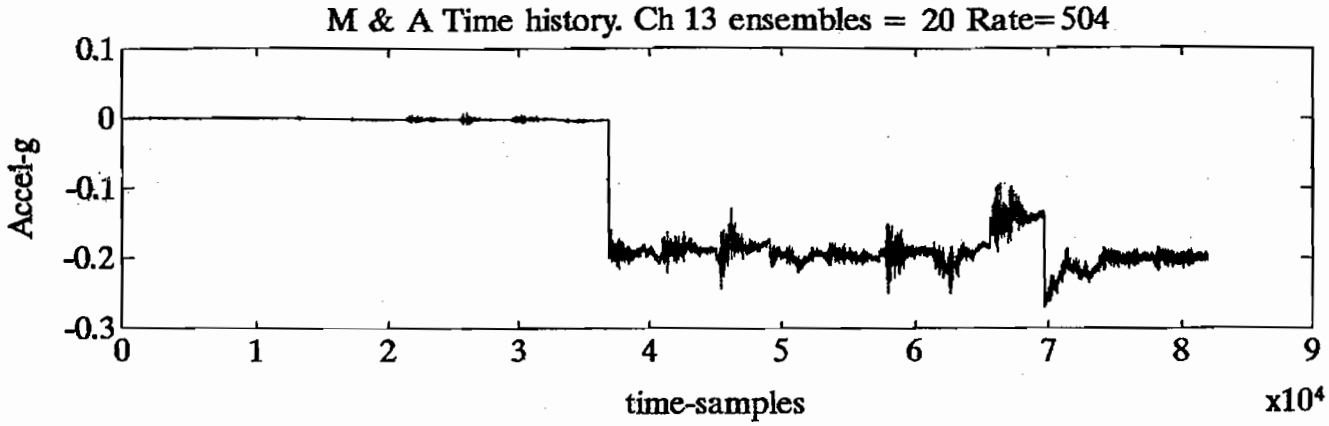
M & A Time history. Ch 13 ensembles = 20 Rate=504
Accel-g
0.1
0
-0.1
-0.2
-0.3
0 1 2 3 4 5 6 7 8 9
time-samples
x10⁴

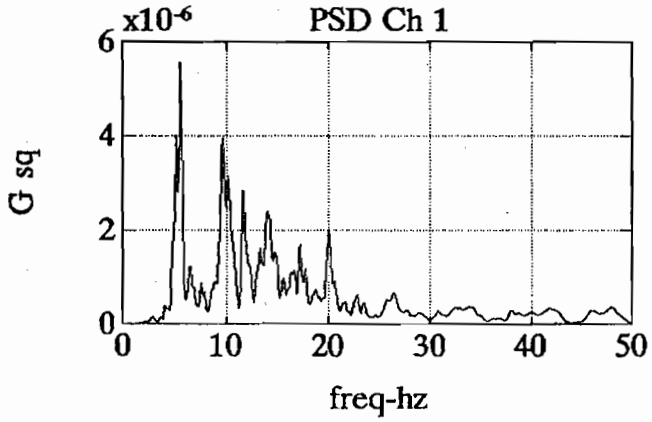
x10⁻⁶
PSD Ch 1
G sq
6
4
2
0
0 10 20 30 40 50
freq-hz

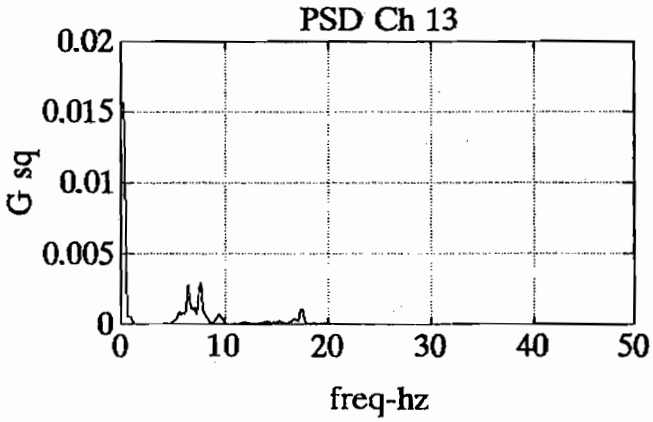
PSD Ch 13
G sq
0.02
0.015
0.01
0.005
0
0 10 20 30 40 50
freq-hz

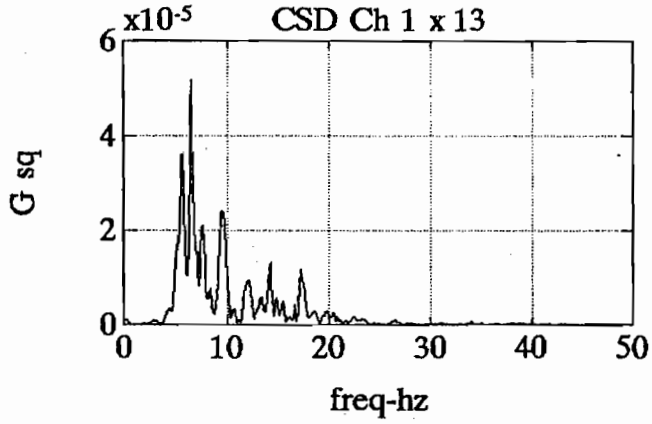
x10⁻⁵
CSD Ch 1 x 13
G sq
6
4
2
0
0 10 20 30 40 50
freq-hz

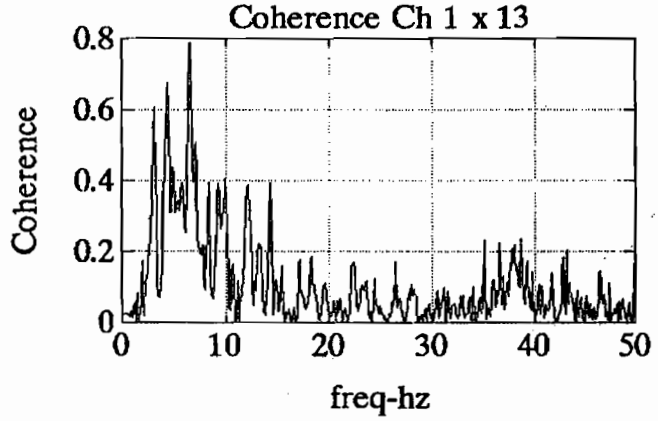
Coherence Ch 1 x 13
Coherence
0.8
0.6
0.4
0.2
0
0 10 20 30 40 50
freq-hz

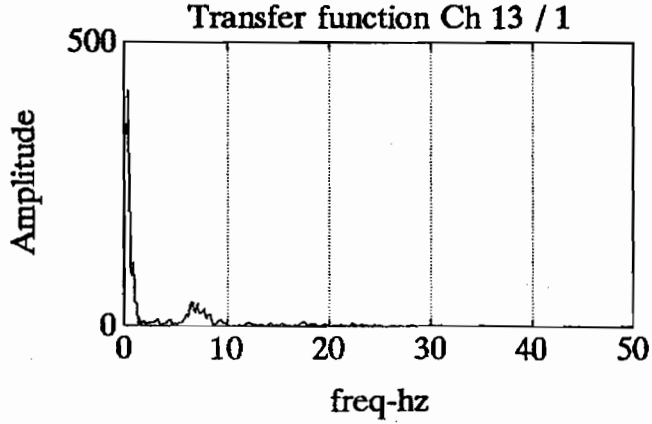
Transfer function Ch 13 / 1
Amplitude
500
0
0 10 20 30 40 50
freq-hz

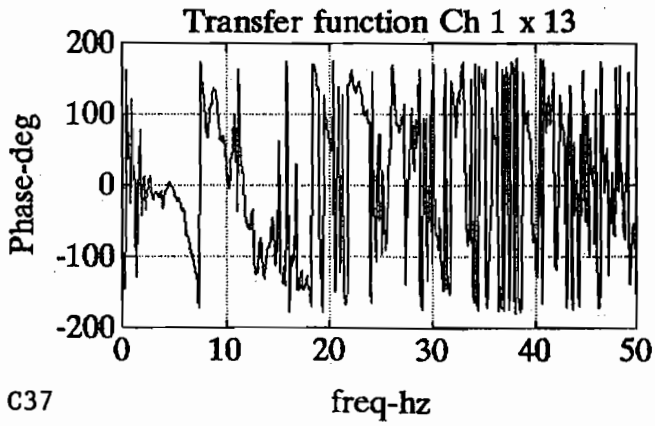
Transfer function Ch 1 x 13
Phase-deg
200
100
0
-100
-200
0 10 20 30 40 50
freq-hz

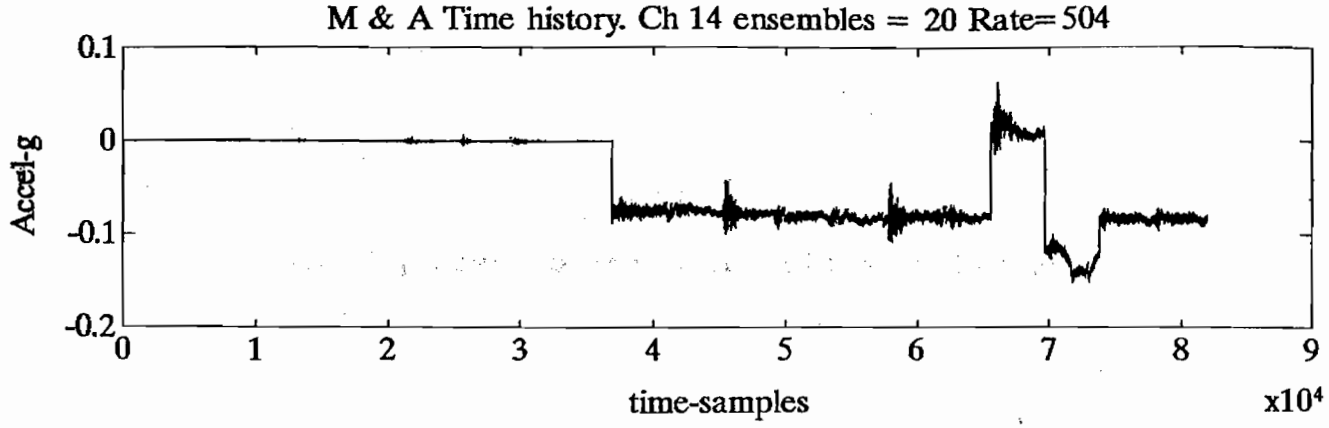
M & A Time history. Ch 14 ensembles = 20 Rate= 504
Accel-g
0.1
0
-0.1
-0.2
0 1 2 3 4 5 6 7 8 9
time-samples
x10^4

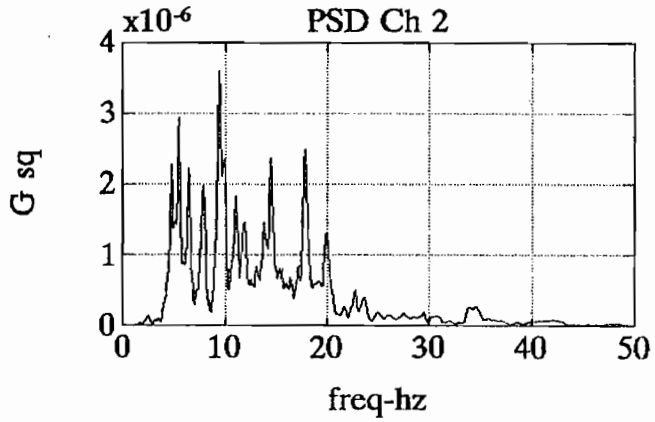
x10^-6
PSD Ch 2
G sq
4 3 2 1 0
0 10 20 30 40 50
freq-hz

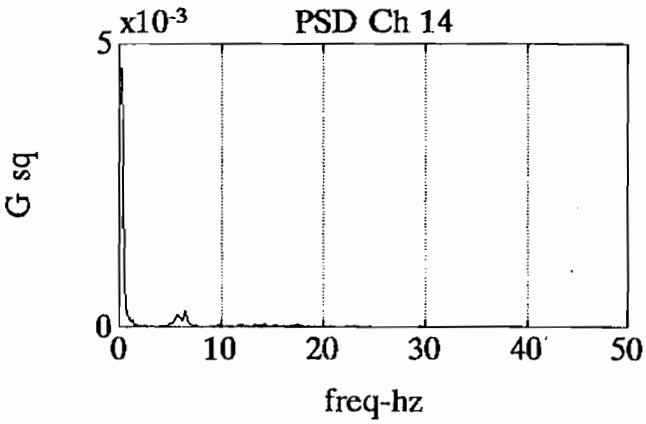
x10^-3
PSD Ch 14
G sq
5 0
0 10 20 30 40 50
freq-hz

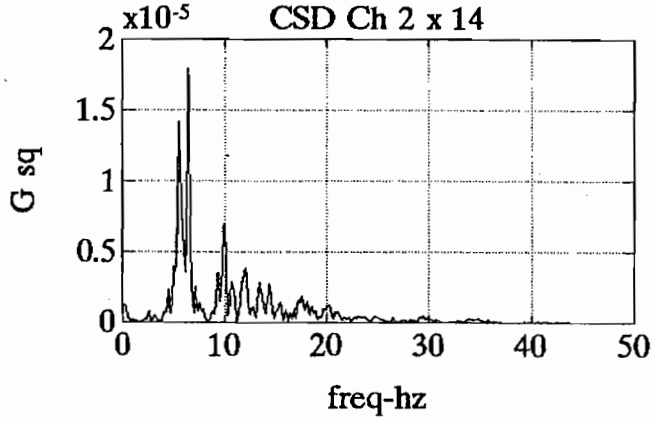
x10^-5
CSD Ch 2 x 14
G sq
2 1.5 1 0.5 0
0 10 20 30 40 50
freq-hz

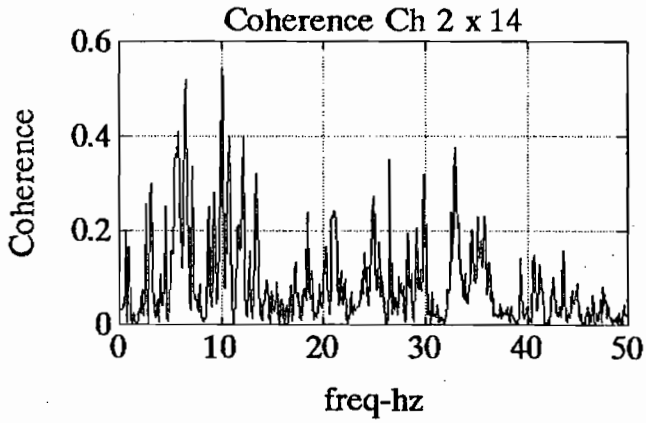
Coherence Ch 2 x 14
Coherence
0.6 0.4 0.2 0
0 10 20 30 40 50
freq-hz

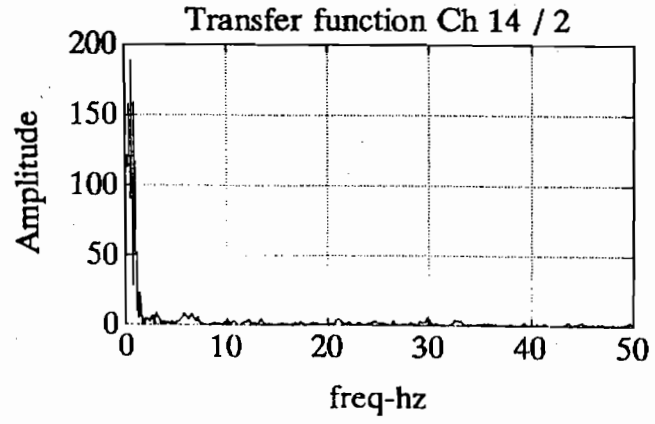
Transfer function Ch 14 / 2
Amplitude
200 150 100 50 0
0 10 20 30 40 50
freq-hz

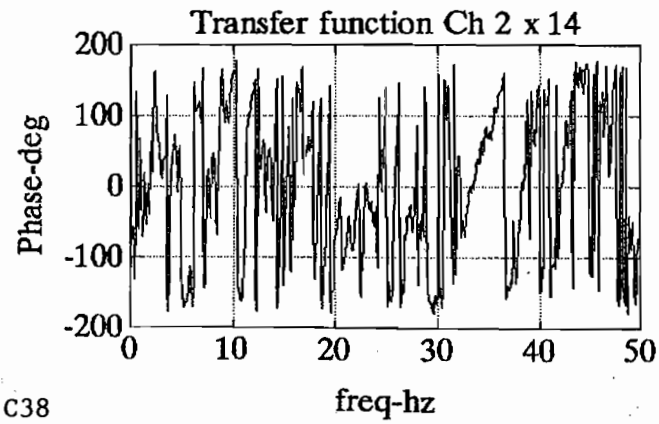
Transfer function Ch 2 x 14
Phase-deg
200 100 0 -100 -200
0 10 20 30 40 50
freq-hz

PART 6

Forced vibration data for one-story house

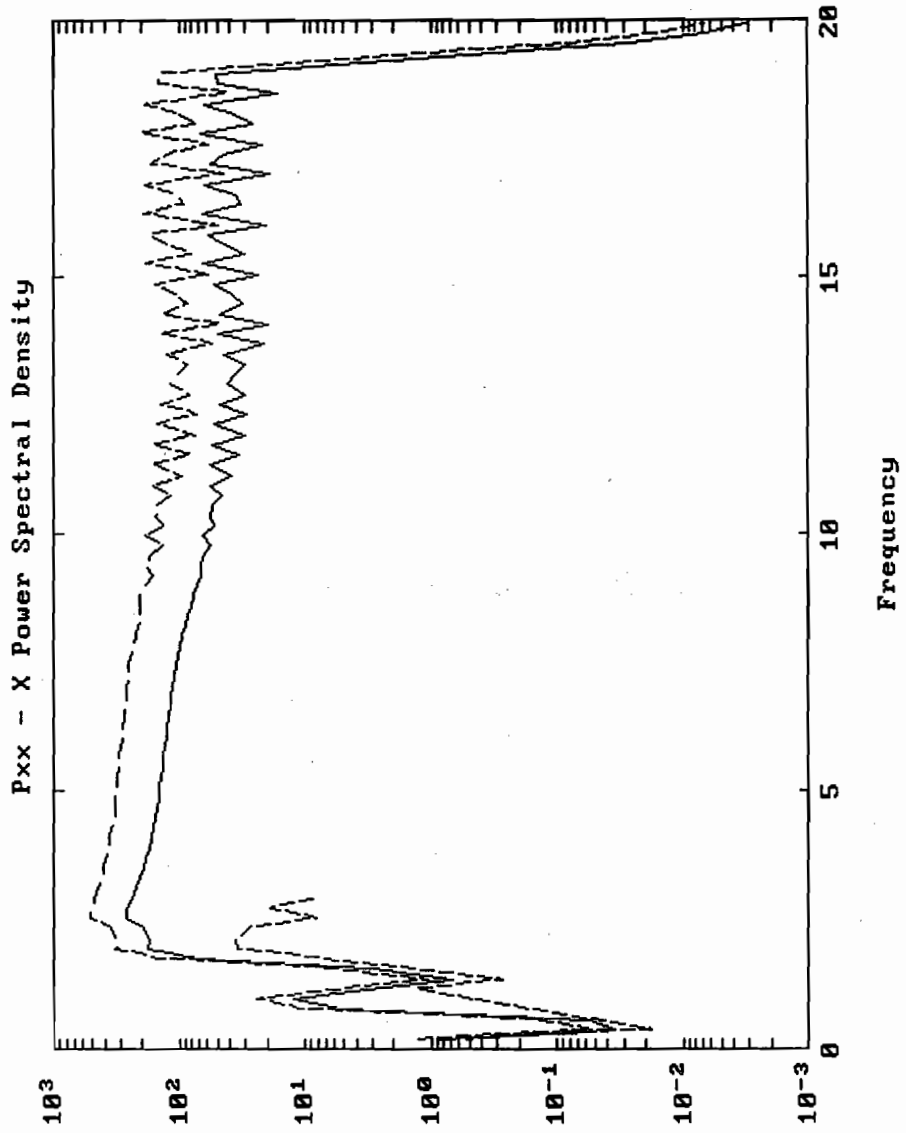
Pxx - X Power Spectral Density
10^3
10^2
10^1
10^0
10^{-1}
10^{-2}
10^{-3}
0
5
10
15
20
Frequency

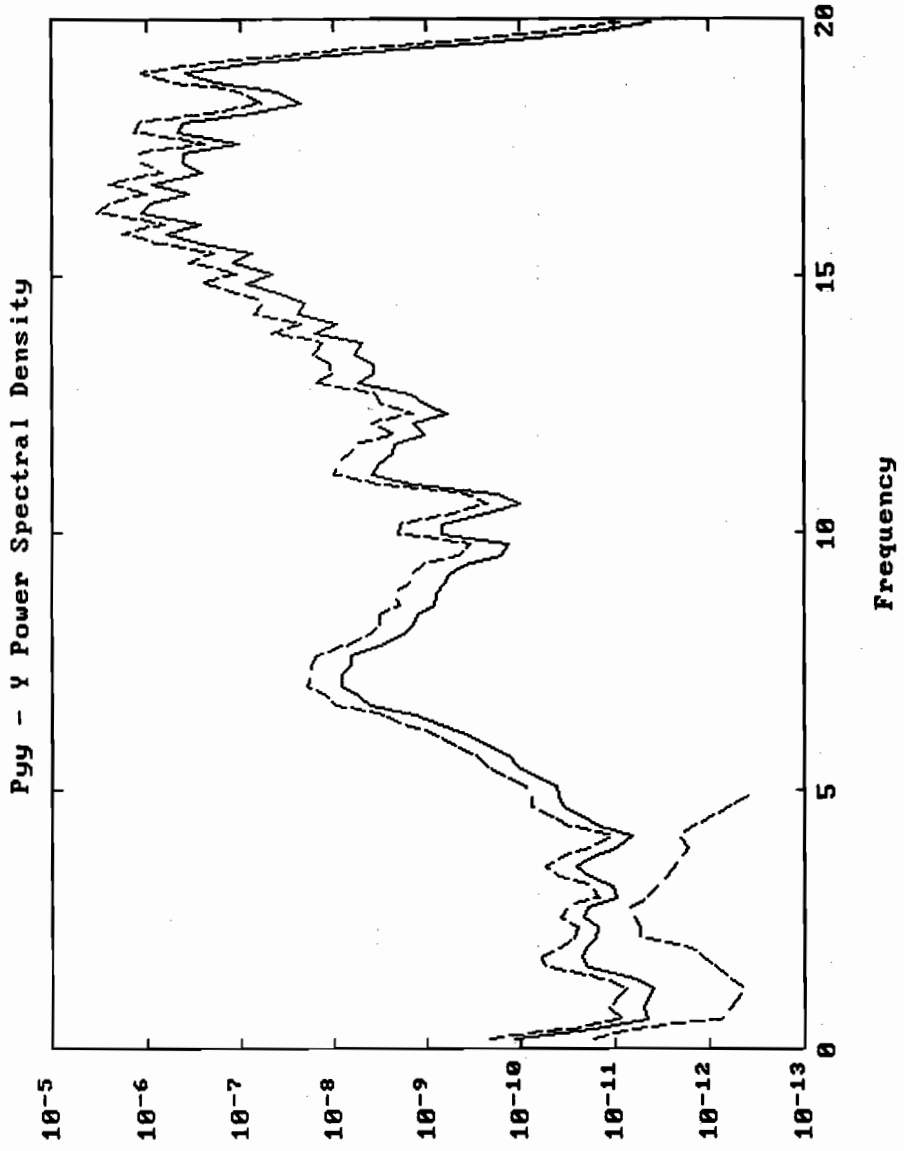
Pyy - Y Power Spectral Density
10-5
10-6
10-7
10-8
10-9
10-10
10-11
10-12
10-13
0
5
10
15
20
Frequency

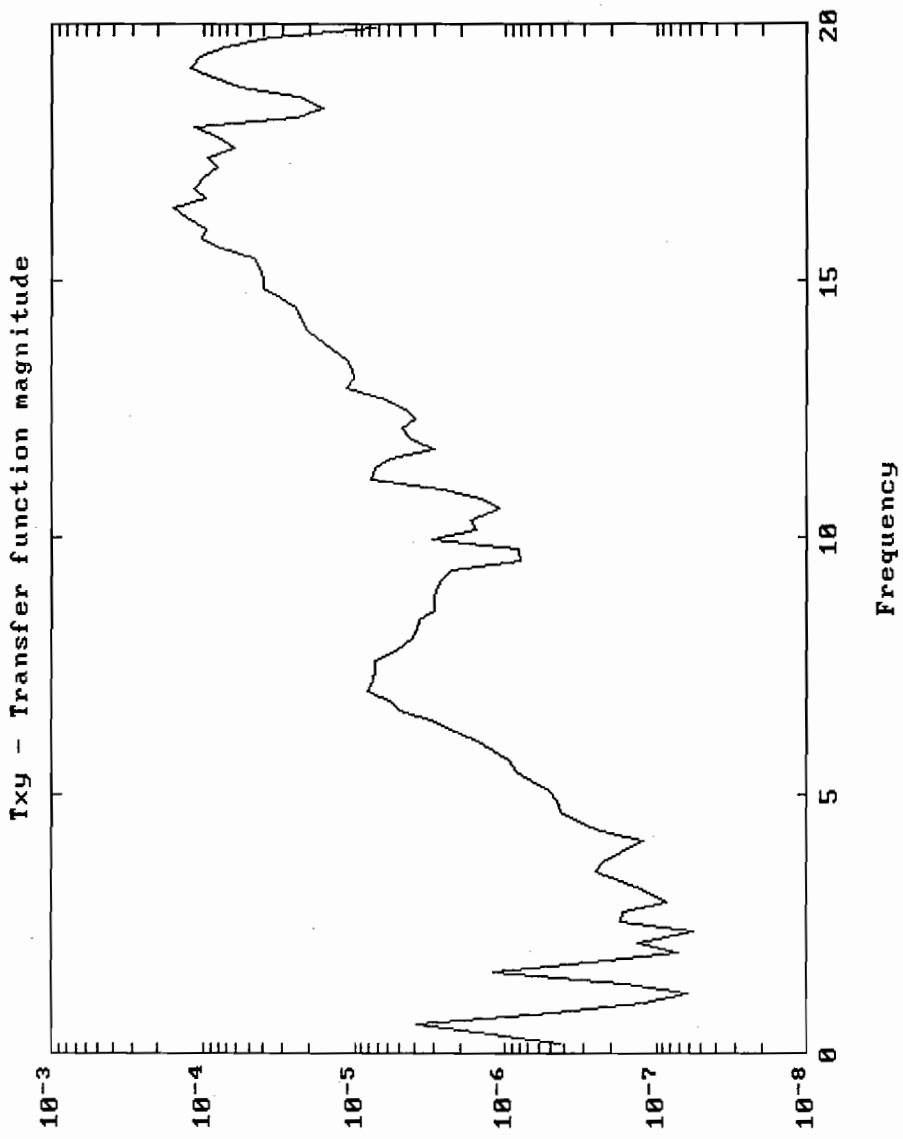
Txy - Transfer function magnitude
10-3
10-4
10-5
10-6
10-7
10-8
0
5
10
15
20
Frequency

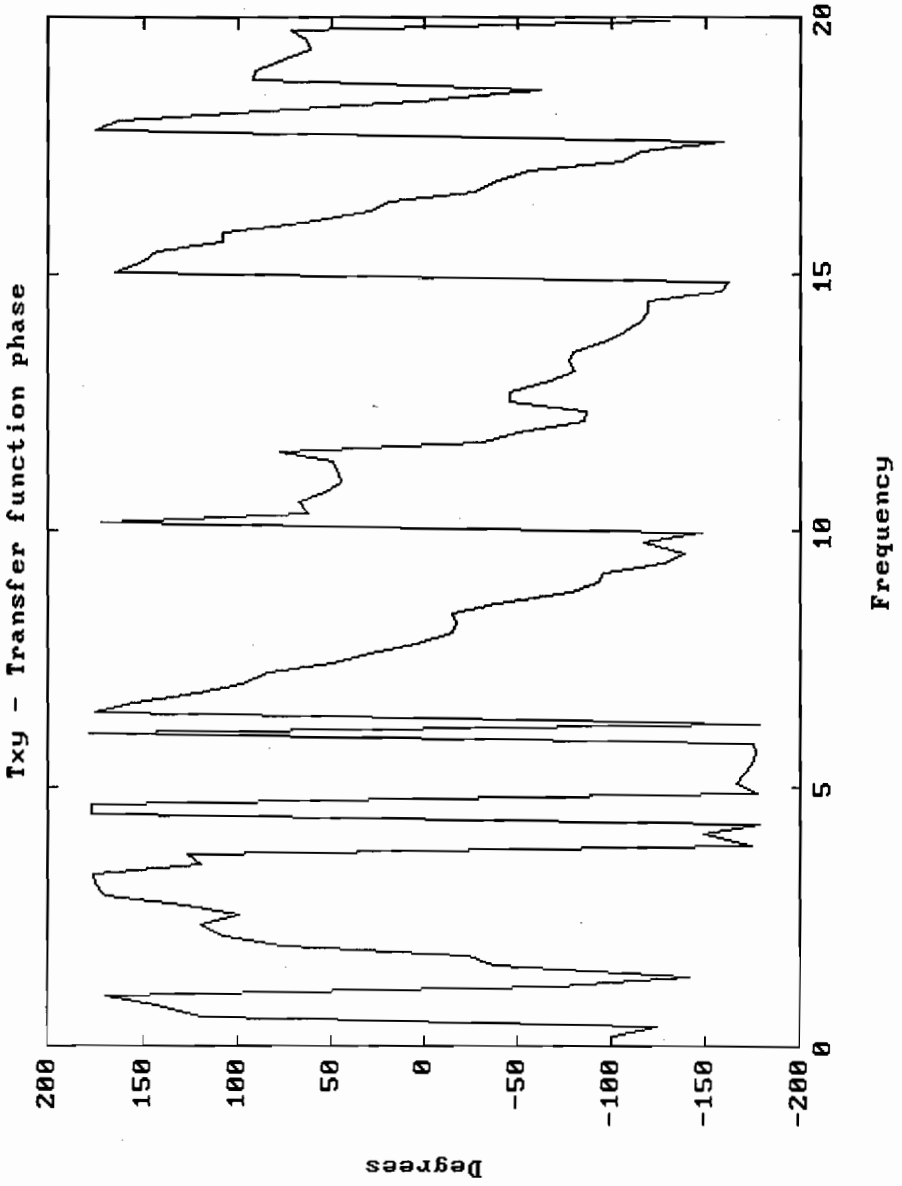
Txy - Transfer function phase
Degrees
200
150
100
50
0
-50
-100
-150
-200
0
5
10
15
20
Frequency

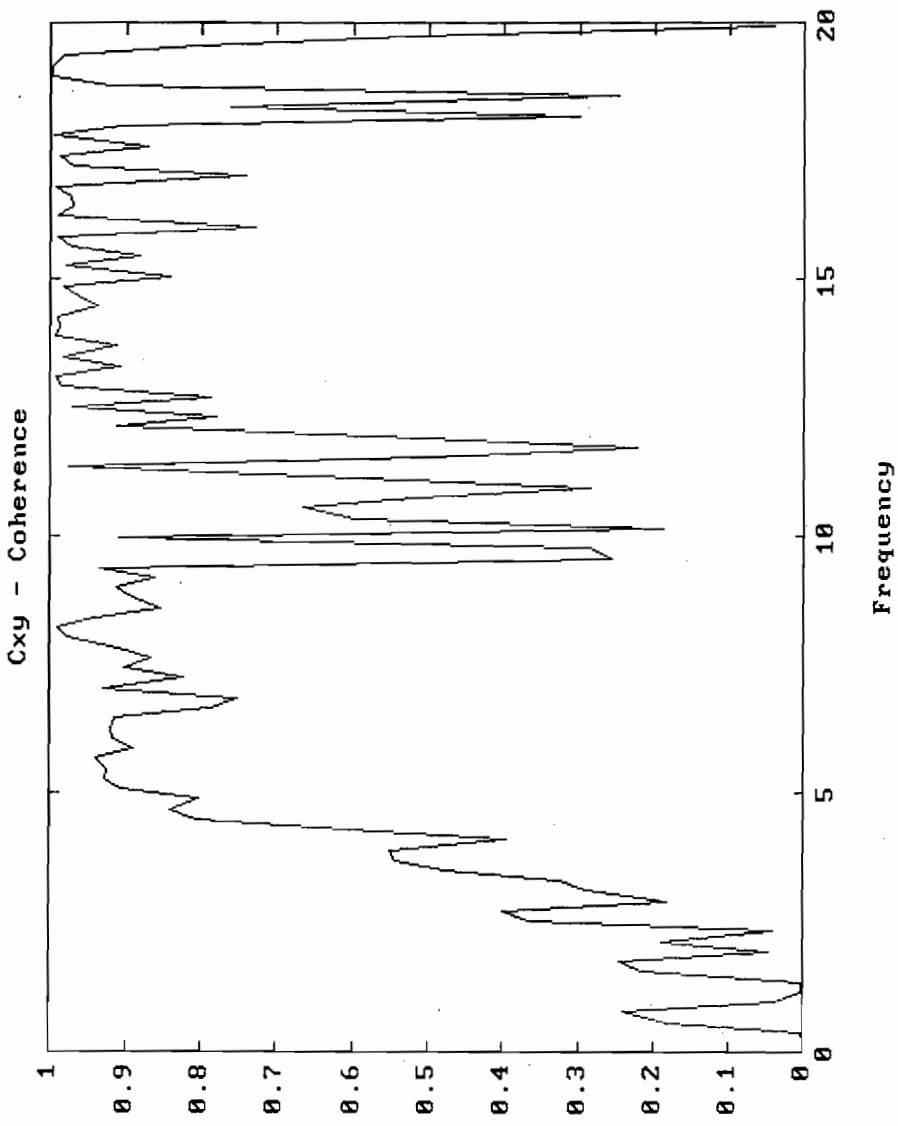
Cxy - Coherence
1
0.9
0.8
0.7
0.6
0.5
0.4
0.3
0.2
0.1
0
0
5
10
15
20
Frequency

PART 7

Hammer test data for two-story house

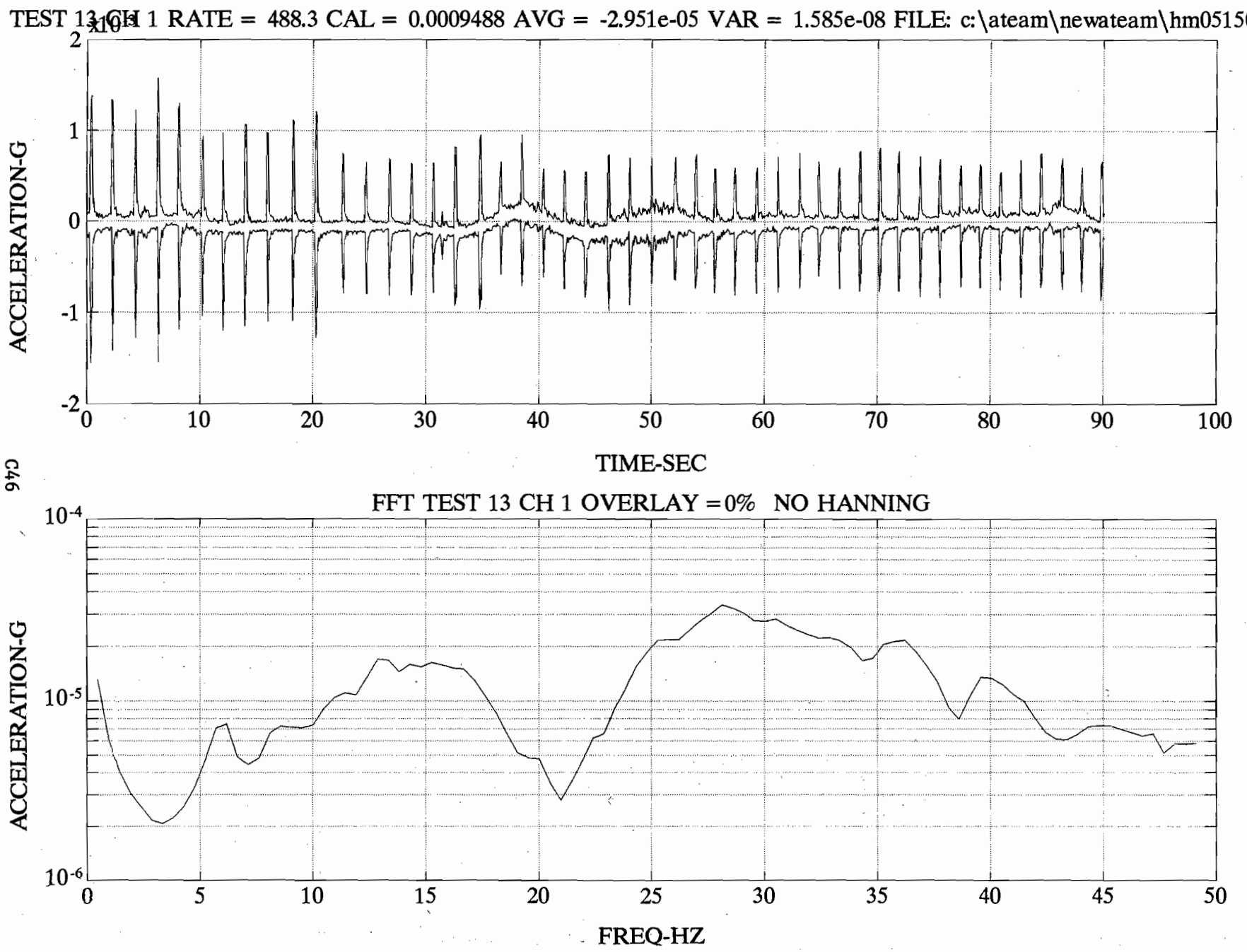
TEST 13 CH 1 RATE = 488.3 CAL = 0.0009488 AVG = -2.951e-05 VAR = 1.585e-08 FILE: c:\ateam\newateam\hm05150
x10^-5
2
1
0
-1
-2
ACCELERATION-G
0
10
20
30
40
50
60
70
80
90
100
TIME-SEC
C46
FFT TEST 13 CH 1 OVERLAY =0% NO HANNING
10^-4
10^-5
10^-6
ACCELERATION-G
0
5
10
15
20
25
30
35
40
45
50
FREQ-HZ

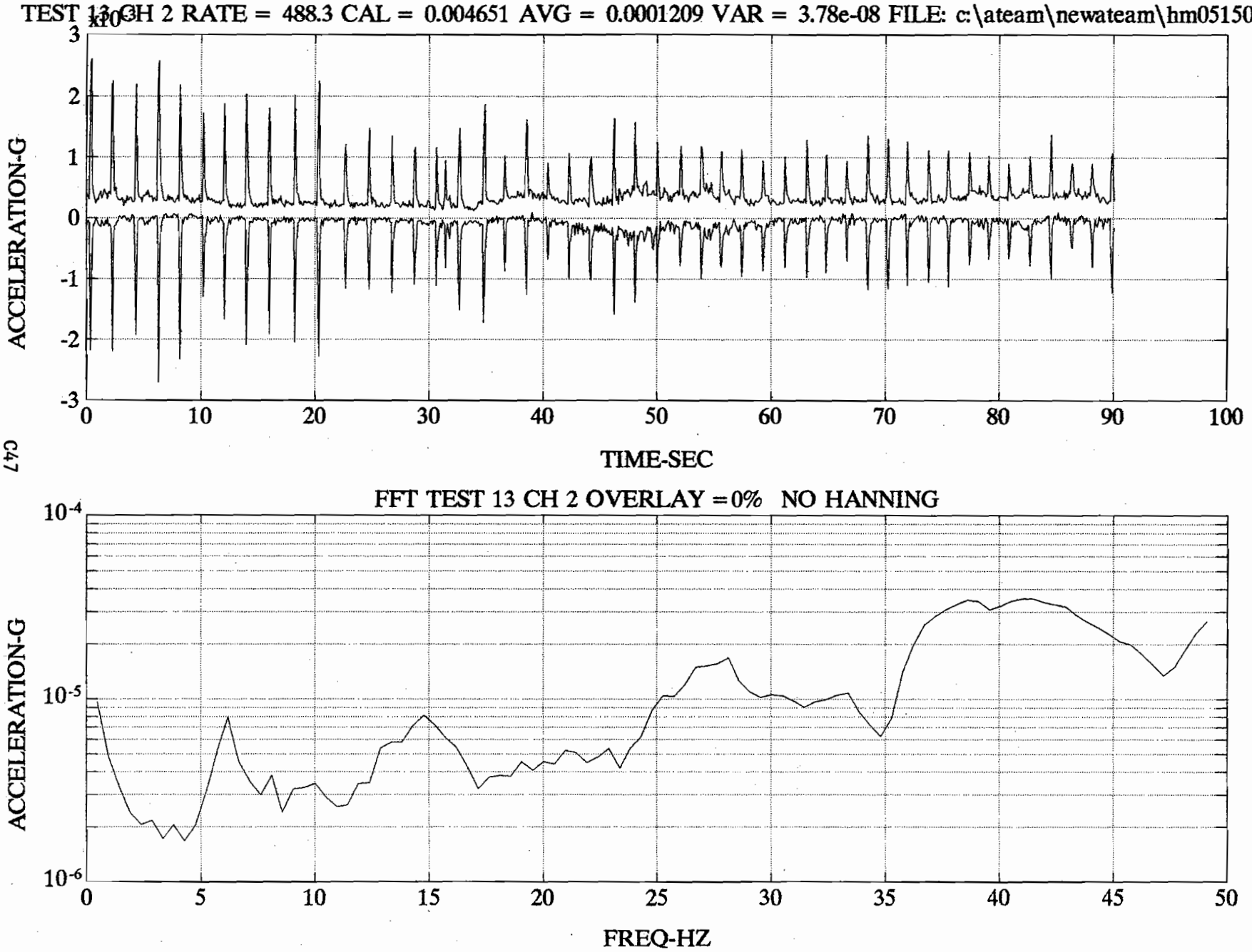
TEST 13 CH 2 RATE = 488.3 CAL = 0.004651 AVG = 0.0001209 VAR = 3.78e-08 FILE: c:\ateam\newateam\hm051500
x10^3
3
2
1
0
-1
-2
-3
ACCELERATION-G
0
10
20
30
40
50
60
70
80
90
100
TIME-SEC
FFT TEST 13 CH 2 OVERLAY =0% NO HANNING
10^-4
10^-5
10^-6
ACCELERATION-G
0
5
10
15
20
25
30
35
40
45
50
FREQ-HZ

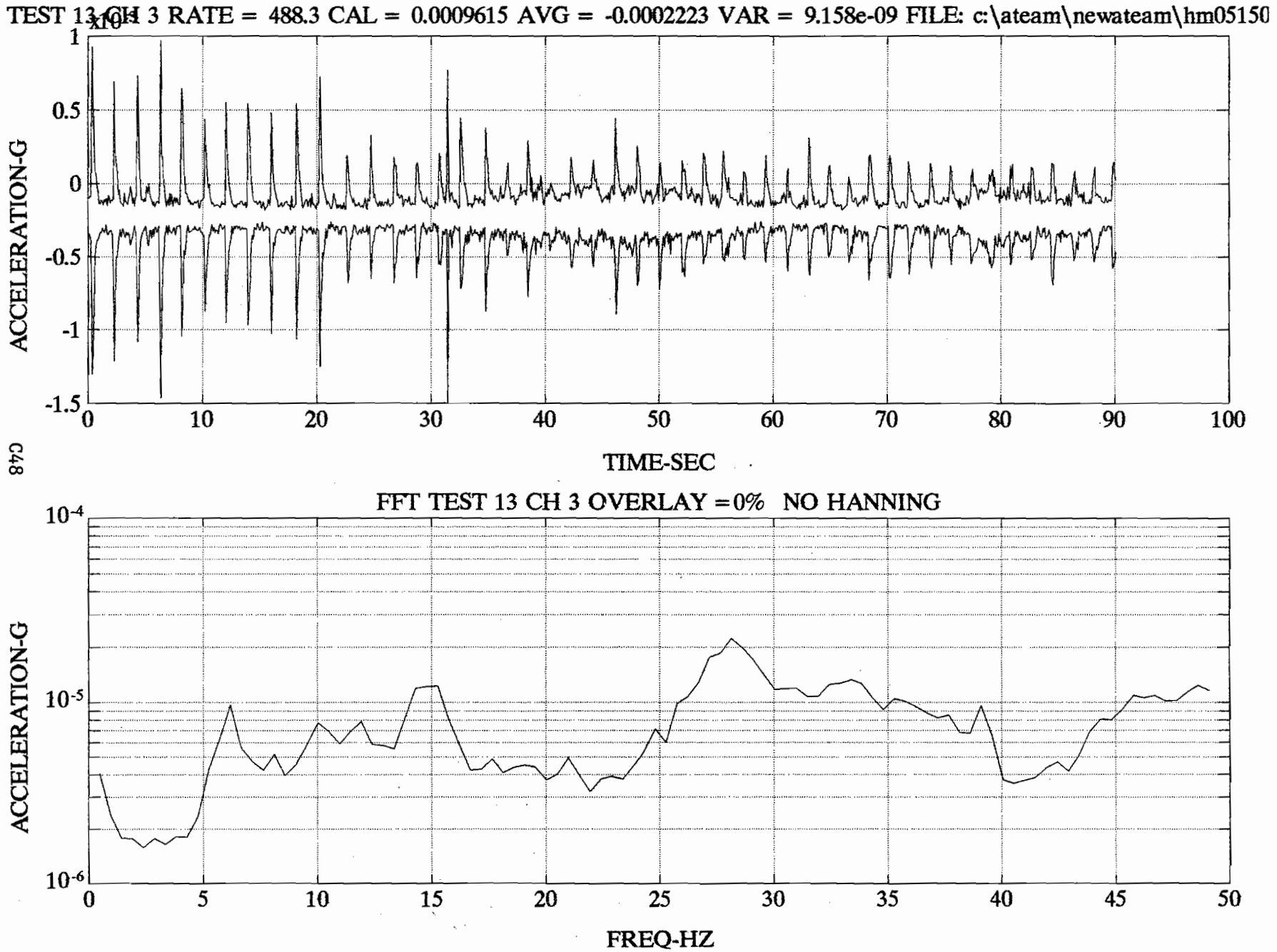
TEST 13 CH 3 RATE = 488.3 CAL = 0.0009615 AVG = -0.0002223 VAR = 9.158e-09 FILE: c:\ateam\newateam\hm05150
x10^-1
1
0.5
0
-0.5
-1
-1.5
ACCELERATION-G
0
10
20
30
40
50
60
70
80
90
100
TIME-SEC
C48
FFT TEST 13 CH 3 OVERLAY =0% NO HANNING
10^-4
10^-5
10^-6
ACCELERATION-G
0
5
10
15
20
25
30
35
40
45
50
FREQ-HZ

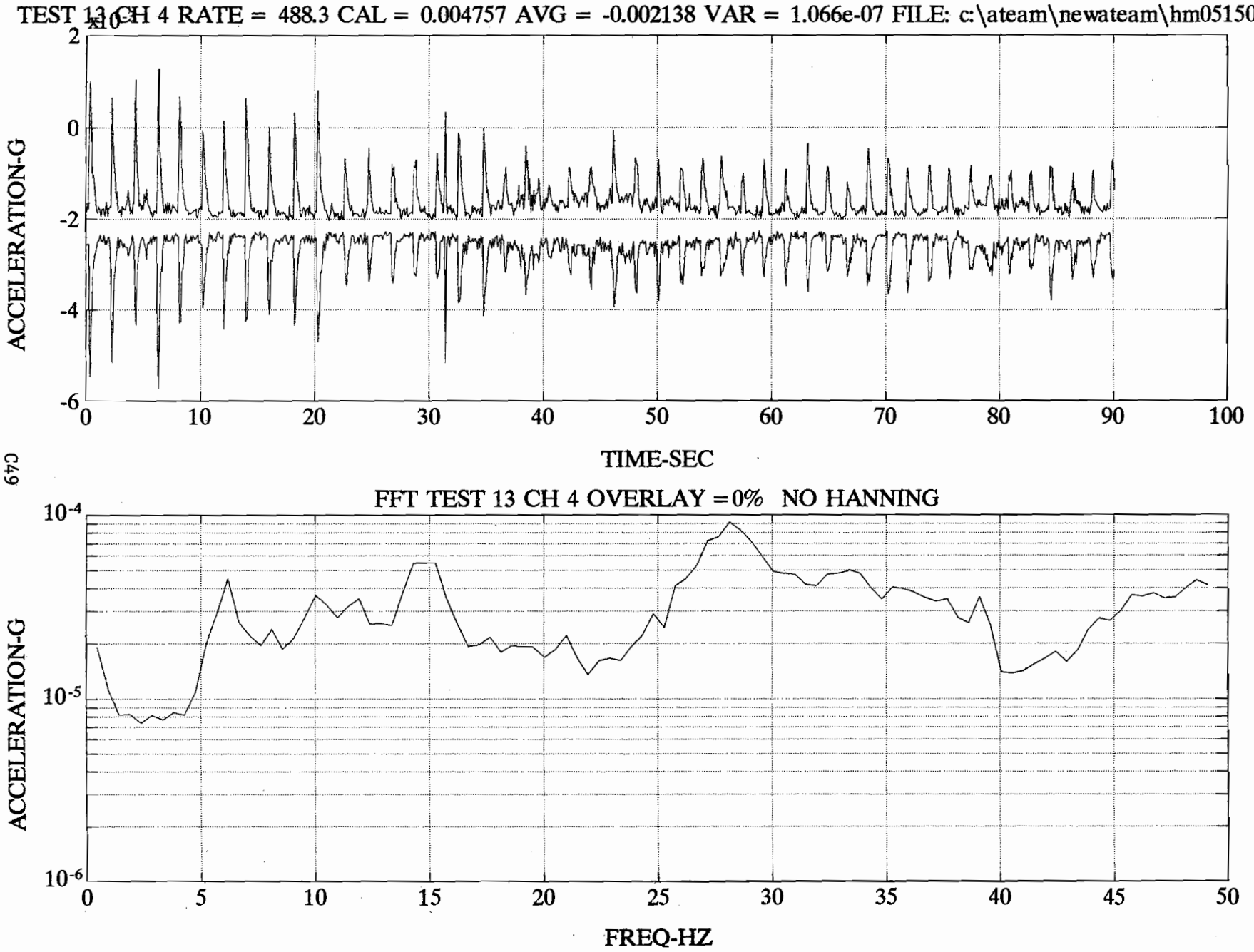
TEST 13 CH 4 RATE = 488.3 CAL = 0.004757 AVG = -0.002138 VAR = 1.066e-07 FILE: c:\ateam\newateam\hm051500
x10^-4
2
0
-2
-4
-6
ACCELERATION-G
0
10
20
30
40
50
60
70
80
90
100
TIME-SEC
FFT TEST 13 CH 4 OVERLAY =0% NO HANNING
10^-4
10^-5
10^-6
ACCELERATION-G
0
5
10
15
20
25
30
35
40
45
50
FREQ-HZ

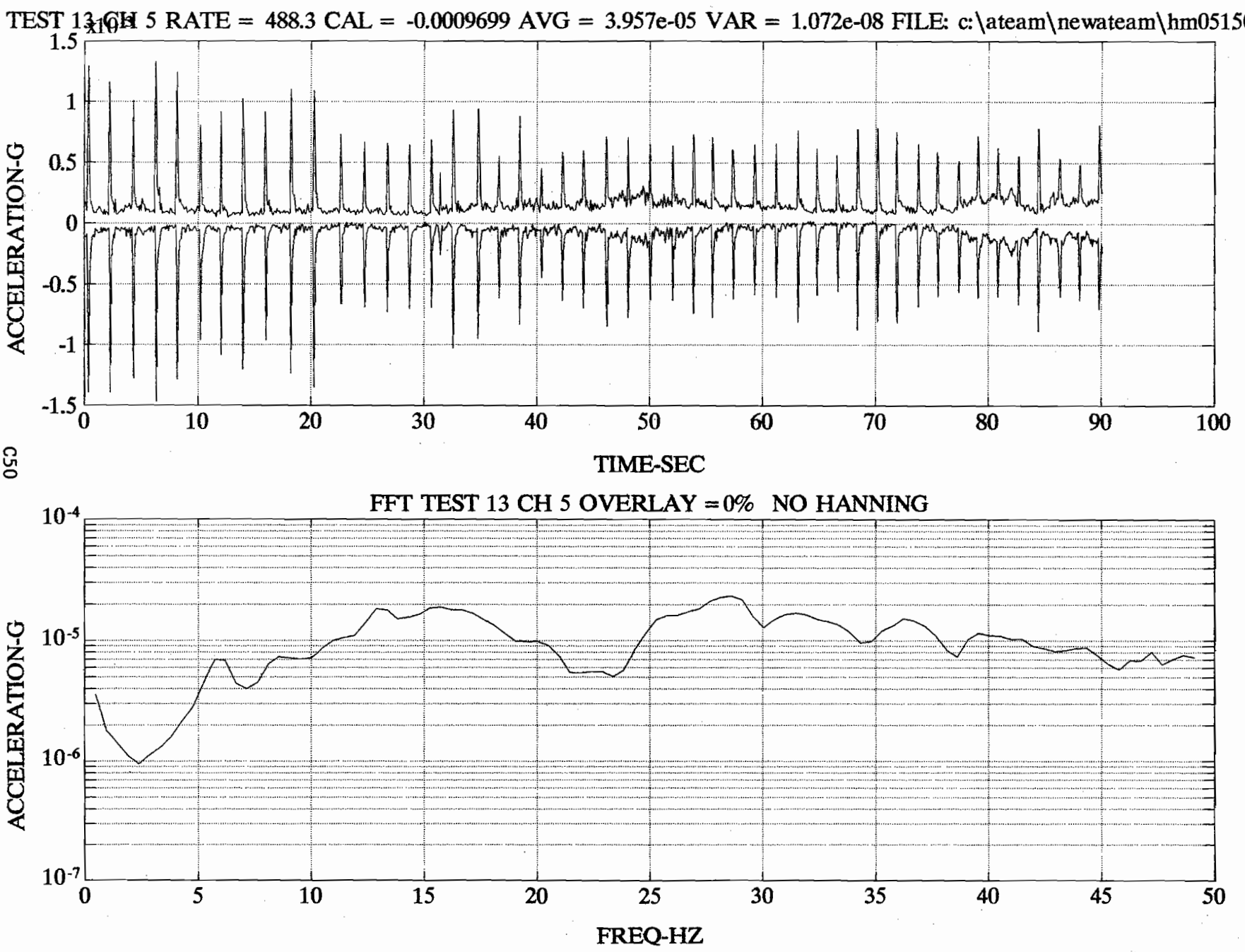
TEST 13 CH 5 RATE = 488.3 CAL = -0.0009699 AVG = 3.957e-05 VAR = 1.072e-08 FILE: c:\ateam\newateam\hm05150
x10^1
1.5
1
0.5
0
-0.5
-1
-1.5
ACCELERATION-G
0
10
20
30
40
50
60
70
80
90
100
TIME-SEC
FFT TEST 13 CH 5 OVERLAY =0% NO HANNING
10^-4
10^-5
10^-6
10^-7
ACCELERATION-G
0
5
10
15
20
25
30
35
40
45
50
FREQ-HZ

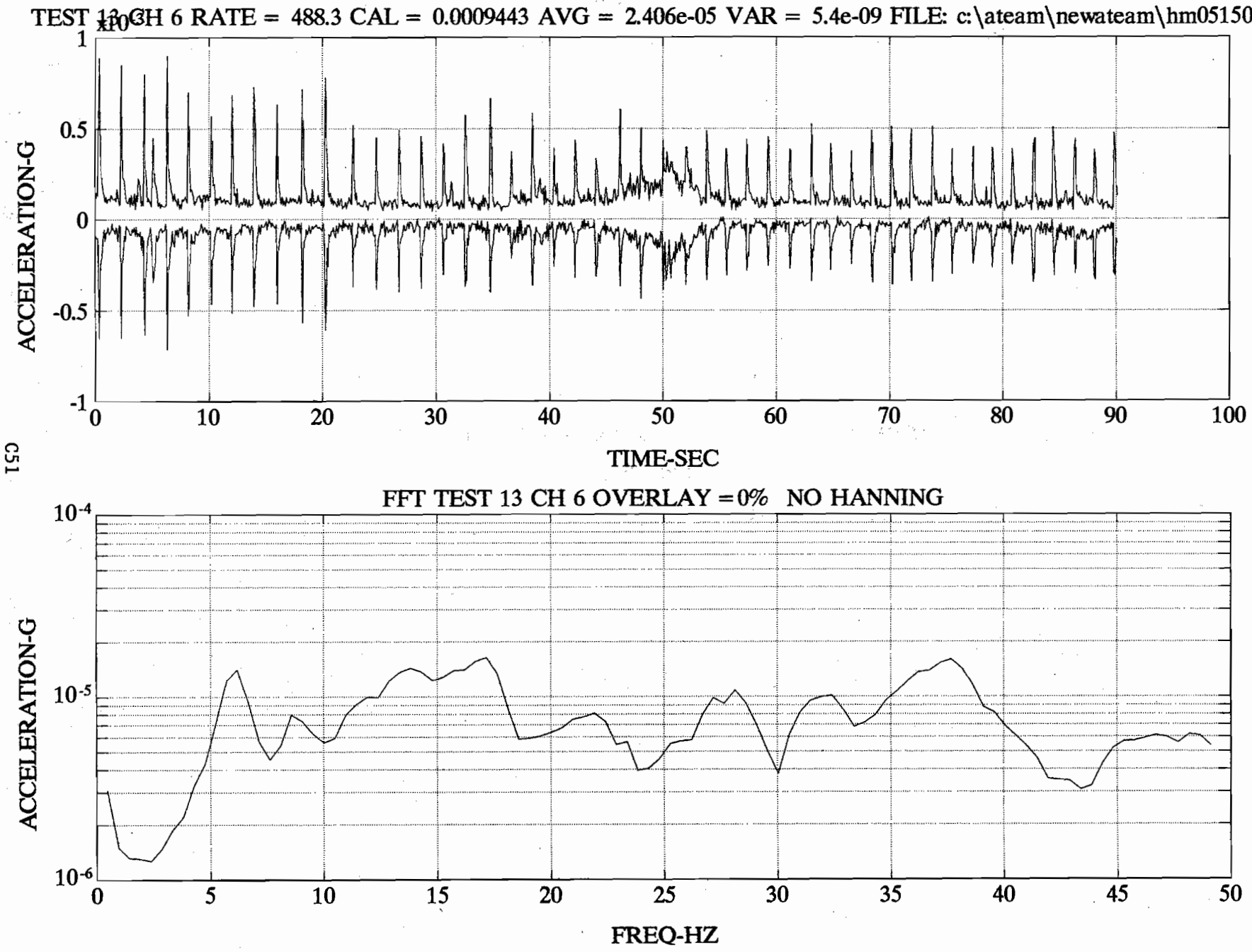
TEST 13 CH 6 RATE = 488.3 CAL = 0.0009443 AVG = 2.406e-05 VAR = 5.4e-09 FILE: c:\ateam\newateam\hm051500.
x10^3
ACCELERATION-G
TIME-SEC
FFT TEST 13 CH 6 OVERLAY =0% NO HANNING
ACCELERATION-G
FREQ-HZ

C51

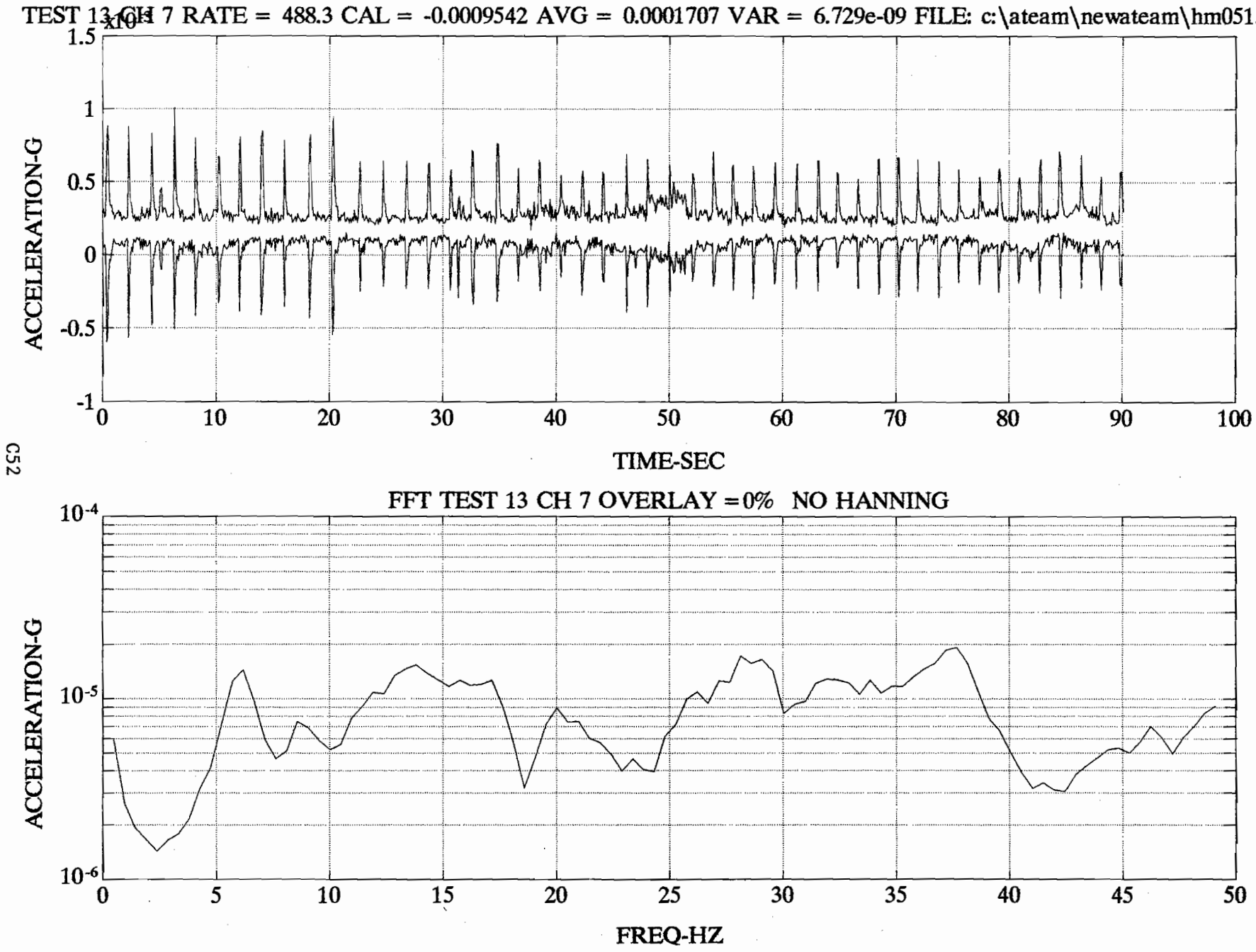
TEST 13 CH 7 RATE = 488.3 CAL = -0.0009542 AVG = 0.0001707 VAR = 6.729e-09 FILE: c:\ateam\newateam\hm05150
x10^1
1.5
1
0.5
0
-0.5
-1
ACCELERATION-G
0
10
20
30
40
50
60
70
80
90
100
TIME-SEC
FFT TEST 13 CH 7 OVERLAY =0% NO HANNING
10^-4
10^-5
10^-6
ACCELERATION-G
0
5
10
15
20
25
30
35
40
45
50
FREQ-HZ

C52